Assessing the Effects of Disruptive Events on Spatiotemporal Networks

Devesh Aggarwal[1], Caglar Koylu, Ph.D.[2]

[1]Interlake High School, Bellevue, WA; [2]Department of Geographical and Sustainability Sciences, University of Iowa, Iowa City, IA

Introduction

Background

- Disruptive events (such as COVID-19) affect human mobility and communication, **changing physical and virtual community structures**.
- To assess these changes, **community detection** within **spatiotemporal networks** must be performed, detecting changes within communities over space and time.

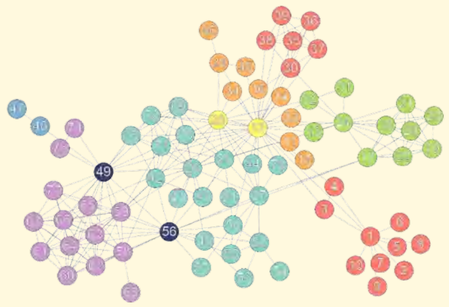

*Community structures are visualized as a **network with nodes and edges**. Nodes represent counties and edges represent **weighted, directional connections** between nodes. Weights are assigned according to the strength of physical/virtual connections. Different colors represent distinct communities (Kuikka, 2021).*

Data

We capture **flow data** from **two sources** to form both **physical and virtual** flow datasets. Both sources aggregate data at a **county level** and have discrete **snapshots** of data during individual periods.

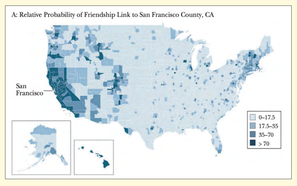

*Virtual: Facebook **Social Connectedness Index**, calculated using friend counts across counties (Bailey et al. 2018)*

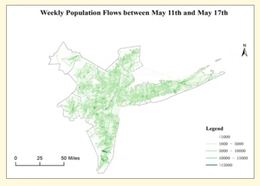

*Physical: **Safegraph data**, created using anonymized cellphone location tracking. (Kang et al., 2020)*

Purpose

Research Question

How do disruptive events, such as COVID-19, change physical and virtual community structures?

Objectives

- Develop a **methodology** to **track physical and virtual communities** over time AND **assess structural changes** during disruptive events.
- Conduct a **case study** on COVID-19

Methods

Data Preparation
Remove noise by smoothing snapshots within the flow dataset
Part 1

Temporal Comparison
Detect communities and compare between snapshots
Part 2

Time Series Periodization
Decompose similarity metrics and segment into periods
Part 3

Evolution Analysis
Aggregate periodized communities to visualize changes
Part 4

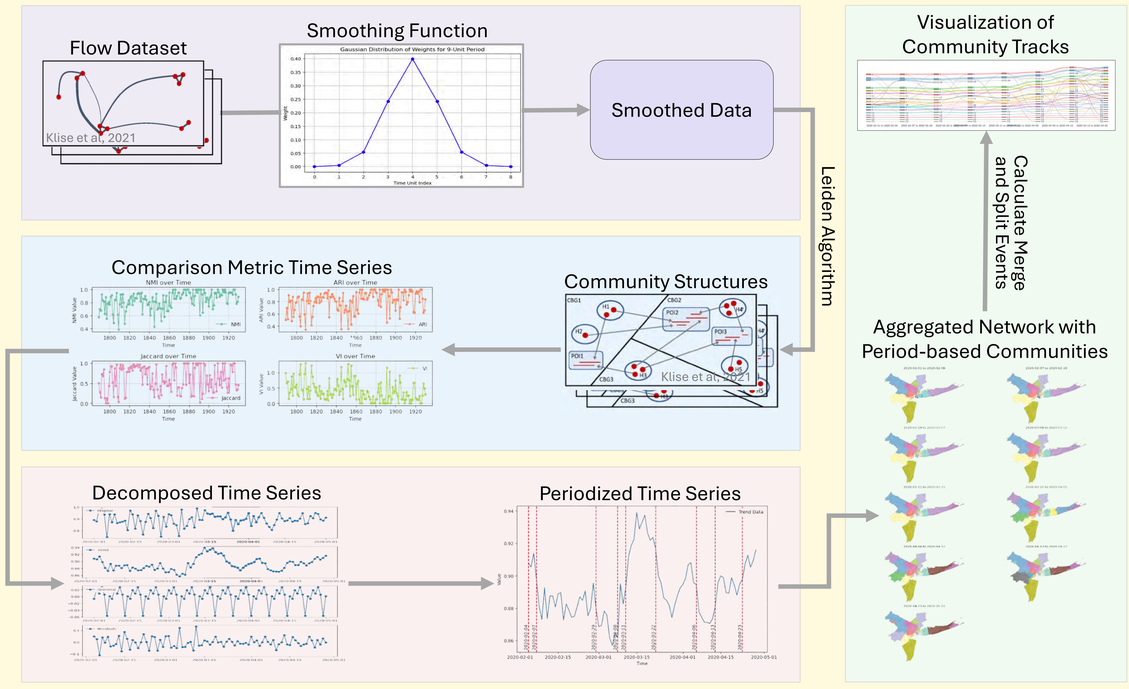

Results

Network	Pre-Period	Post-Period	Adj. Rand	Jaccard	NMI
SafeGraph	2019/3 – 2020/3	2020/4 – 2021/4	0.82	0.70	0.93
Facebook	2015	2021	0.67	0.52	0.83

Various similarity metrics indicating community similarity pre- and post-covid. Higher values indicate greater similarity.

Primary Results

- **Online connections were intensified** (decrease in modularity and number of regions)
- **Long-distance physical travel decreased** (increase in modularity and number of regions)
- **Virtual communities changed more drastically than physical communities** (smaller community similarity metric values)
- We detected many interesting **regional community events,** such as growth, merge, and split events.

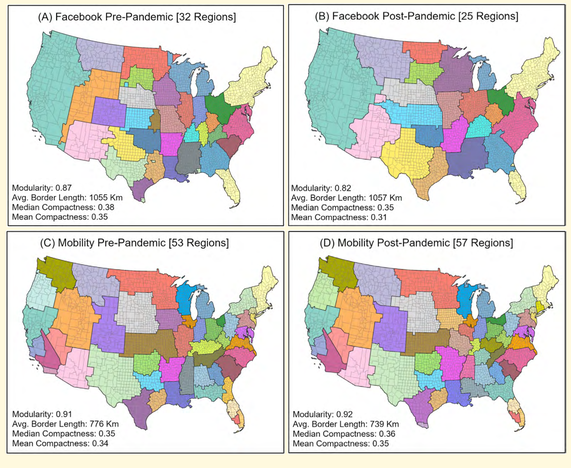

Conclusions

Primary Conclusion

Physical interactions became shorter, resulting in more localized geographic communities and greater modularity. Virtual interactions became longer, resulting in larger communities with less modularity.

Impact

- **Novel methodology** quantitively assesses community evolution, applicable on **wide spatial and temporal scales.**
- **Developed understanding** of how disruptive events affect communities.

Limitations

- We have not proven that the trends found are **specific to the COVID-19 pandemic**, as opposed to being a symptom of global virtualization.

Future Work

- Enhancing **techniques for visualizing** community evolution, e.g. improving Sankey diagrams.
- **Further case studies** on different spatial and temporal scales. We are currently working on studying community evolution during the **Civil War** using **family tree data.**

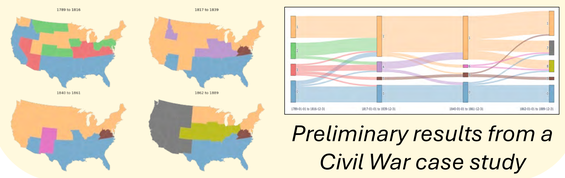

Preliminary results from a Civil War case study

Acknowledgements

Thank you to my mentors at the Geo-Social Lab: Dr. Koylu, Jinyi, Maryam, and Henry—you have each been extremely helpful and supportive, and I have learned so much here.

References

Bailey, M., Cao, R., Kuchler, T., Stroebel, J., & Wong, A. (2018). Social connectedness: measurement, determinants, and effects. *Journal of Economic Perspectives*, *32*(3), 259–280. https://doi.org/10.1257/jep.32.3.259

Kang, Y., Gao, S., Liang, Y., Li, M., Rao, J., & Kruse, J. (2020). Multiscale dynamic human mobility flow dataset in the U.S. during the COVID-19 epidemic. *Scientific Data*, *7*(1), 390. https://doi.org/10.1038/s41597-020-00734-5

Klise, K., Beyeler, W., Finley, P., & Makvandi, M. (2021). Analysis of mobility data to build contact networks for COVID-19. *PLOS ONE*, *16*(4). https://doi.org/10.1371/journal.pone.0249726

Koylu, C., & Torkashvand, M. (2023). *The effect of disruptive events on spatial and social interactions: An assessment of structural changes in pre-and post-COVID-19 pandemic networks*. arXiv. https://doi.org/10.48550/arXiv.2311.01559

Kuikka, V. (2021). Modelling community structure and temporal spreading on complex networks. *Computational Social Networks*, *8*(1). https://doi.org/10.1186/s40649-021-00094-z

Exploring the Relationship Between Social Vulnerability and Well Nitrate Concentration in Iowa Through Interpretable Machine Learning

Sumin Bae[1]; Jinyi Cai[2]; Caglar Koylu, PhD[2]

American Community School of Abu Dhabi[1], Department of Geographical and Sustainability Sciences, University of Iowa[2]

Geo-Social

Belin-Blank Center
College of Education
The University of Iowa

Introduction

Background Information

Climate change increases the frequency and severity of **extreme weather events**, such as droughts and floods, leading to higher **nitrate concentrations** in water

An estimated **12-14%** of the US population relies on **unregulated private wells**, primarily in rural areas, putting these populations at greater risk of nitrate contamination

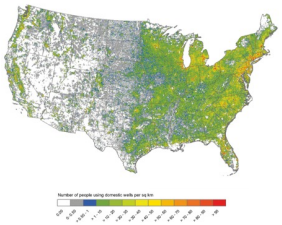

(Source: Johnson TD, etc. 2018)

Problem

Private wells are particularly vulnerable to contamination because they are not covered by the federal **Safe Drinking Water Act**

Nitrate contamination in drinking water has been linked to serious health issues, including **methemoglobinemia** (blue baby syndrome) in infants and various types of **cancers** in adults

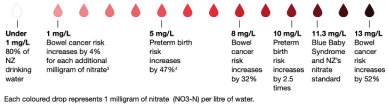

(Source: Greenpeace, 2022)

Previous Research

Nationwide studies link **public water contaminants** to **vulnerable populations**, but data on **private wells** is limited

Surveys found no link between **private well contamination** and **population characteristics**

Objectives

Analyze the spatial distribution of nitrate contamination and socio-demographic factors

Apply an **advanced interpretable machine learning model** to study these relationships

Data and Methodology

Data Collection

Nitrate Test Results:

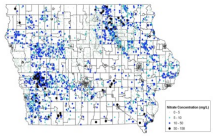

(Source: Iowa Department of Natural Resources, 2018)

Socio-Demographic Factors:

Socio-demographic data were obtained from the American Community Survey (2014-2018). The variables included:

- **Racial and ethnic minority** percentage
- Percentage of individuals **with less than a college degree**
- **Unemployment rate**

	Mean	Std	Min	Median	Max
% Racial & Ethnic Minority	13.55	14.37	0.00	8.18	88.02
% less than college degree (25+)	41.54	12.50	4.57	42.98	76.92
% unemployed civilian labor force	16.60	5.83	4.80	15.63	40.81

Data Preparation

Regression Analysis Models

Compared several **regression models** to analyze the **relationship** between **socio-demographic characteristics** and **nitrate contamination levels**

	Spatial Lag & Error Model (SLM)	Multi-scale geographically weighted regression (MGWR)	Generalized Additive Models (GAMs)	Extreme Gradient Boosting Model (XGBoost)
Spatial Effects	✓	✓	✓ (GeoAdditive Model)	✓ (With Location Variables)
Spatial Non-Stationary		✓		✓ (With Location Variables)
Non-linearity			✓	✓
Interaction Effects				✓
Interpretability	✓	✓	✓ (Less Interpretability with the Smooth Functions)	✓ (With Variable Contribution Analysis (SHAP Values))

Variables Contribution Analysis

SHapley Additive Explanations (SHAP) Values:

$$\phi_i(f) = \sum_{S \subseteq N \setminus \{i\}} \frac{|S|!\,(n - |S| - 1)!}{n!} \left[f(S \cup \{i\}) - f(S) \right]$$

marginal contribution of feature i

change of predicted value before and after adding the new feature i

n : total number of features,
$N \setminus \{i\}$: all the combinations of features excluding feature i,
S : one of the subsets of $N \setminus \{i\}$,
$f(S)$: model prediction with feature values in S,
$f(S \cup \{i\})$: model prediction with feature values in S and feature value of i.

Positive SHAP Value: feature i contributes to increasing the predicted outcome value

Negative SHAP Value: feature i contributes to decreasing the predicted outcome value

Results

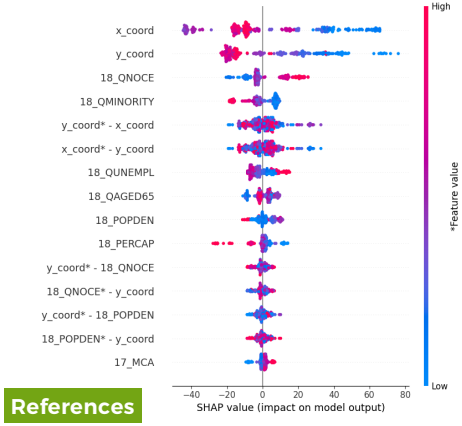

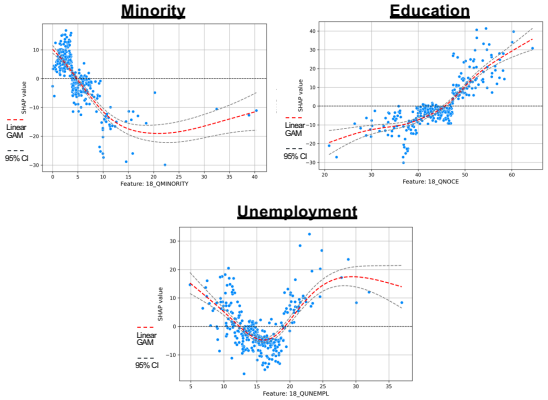

- **X-Axis:** Percentage of population with no college education / unemployed / minority status
- **Y-Axis:** SHAP value indicating the impact on nitrate levels
- **Red dashed line:** Linear relationship
- **Solid line:** Generalized Additive Model (GAM) fit
- **Dashed black line:** 95% confidence interval

References

- **Base Value** (nitrate concentration): **4.87 mg/L**
- **X-Axis: Percentage change** in **nitrate concentration** based on **4.87 mg/L**
- **Y-Axis: Analyzed features**

Discussion

Model Evaluation

Use of **SHAP values** enhances the interpretability of the model, providing insights into the relative importance of different features, such as **unemployment rate, educational attainment, and minority status**

Socio-Demographic Factors

Unemployment and **low educational attainment** emerged as significant predictors of risk

- Areas with **high unemployment** (greater than 16%) have a **25% higher risk** of nitrate contamination
- Areas with **low education levels** (less than a college degree) have a **20% higher risk**

SHAP values also highlight the importance of considering **minority status**

- **Hispanic populations** face a **15% higher risk** of nitrate contamination
- **Minority populations** from **0 to 10%** contribute to a **20% decrease** in predicted nitrate levels, indicating less exposure to elevated nitrate well water

Spatial Effects

SHAP values indicate that **location** has the most crucial effect on contributing to nitrate levels prediction, with lower values towards the **west and south areas** relating to an **up to 80% increase** in nitrate concentration

Conclusion

Findings

Understand population disparities in exposure to high nitrate well water pollution

- Communities with **low college degree attainment**, **high number of population with minority status**, **high unemployment**

Underscore **non-linear relationships** in social vulnerability analysis

Future Work

Measure the uncertainty for the SHAP values

- Use **non-parametric inference approaches** to derive confidence intervals

Acknowledgements

I firstly am grateful to God for His love, provision, and grace through Christ. I also want to thank my mentors in the Geo-Social Lab, Dr. Caglar Koylu and Jinyi Cai, for their meticulous and exceptional mentorship and invaluable support, inspiring me to go above and beyond with my research. Moreover, I am thankful for my lab mates, Ariana and Devesh, who supported me throughout this experience. Finally, I would also like to extend my gratitude to my parents and the Belin-Blank Center for this incredible opportunity.

Silken Strength

Exploring the Mechanical Properties of Bio-Fabricated Silk Fibroin Structures

Anik Banerji[1], Harjeevan Singh[2], Milad Arzani[3], and Xuan Mu[3]*

[1]St. John's School, TX; [2]Pleasant Valley High School, IA; [3]Roy J. Carver Department of Biomedical Engineering, University of Iowa. Email: xuan-mu@uiowa.edu

IOWA
Roy J. Carver Department of Biomedical Engineering

Introduction

Silk Fibroin Beyond Textiles & Sutures

- **Silk fibroin (SF)** is a natural protein-based biopolymer
- SF possesses unique strength, softness, and biocompatibility, suitable for bio-fabrication
- We seek to characterize this material's qualities

Silk Fibroin as Feedstock

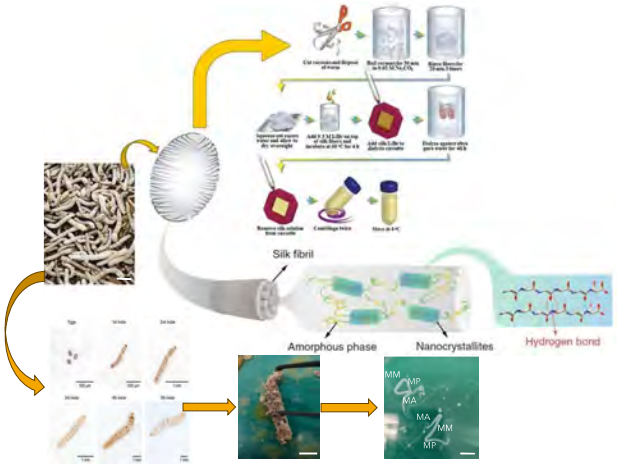

Figure 1. Processes for obtaining native silk structure and regenerative silk fibroin (RSF) [1, 5] (scale bars: 1 cm)

SF Casting Techniques

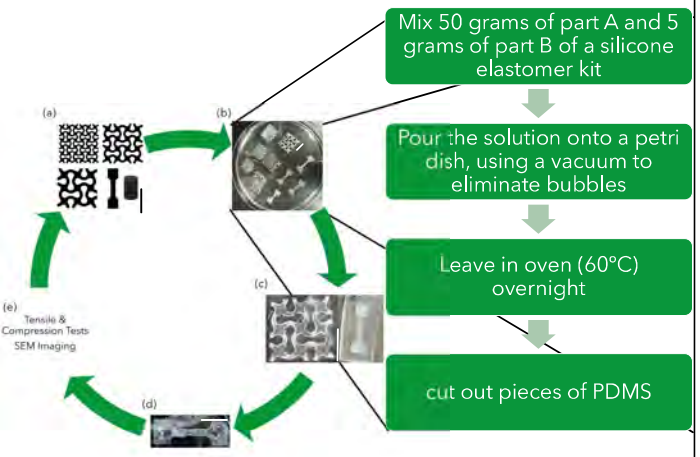

Figure 2. Casting of silk fibroin structures. (a) versatile mold designs with different geometries and shapes; (b) mold manufacturing process; (c) casting of silk fibroin solution followed by salt treatment; and finally (d) extracting the structures to (e) perform characterizations. (Scale bars: 1 cm)

Results & Discussion

Re-entrant Sinusoidal Silk Structures

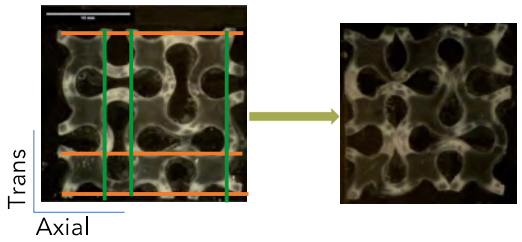

Figure 3. When an auxetic structure undergoes axial compression, it also compresses transversely

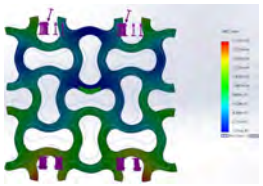

Figure 4. A simulation of the deformation of a re-entrant sinusoidal auxetic structure, made in SolidWorks

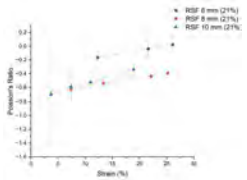

Figure 5. A graph of the changes in Poisson's ratios of different auxetic structures as strain increases

Mechanical Properties

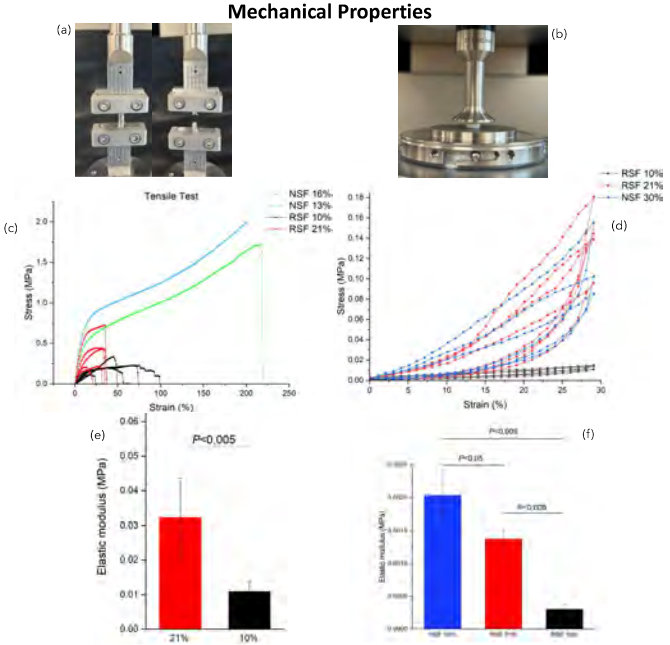

Figure 6. Tensile (a, c, e) and compression (b, d, f) testing (pictured in a, b) generated stress-strain curves (c, e) that show that dog bones made with native silk fibroin had a higher Young's modulus, or resistance to elastic deformation, than those made with regenerated silk fibroin, while among structures of RSF, dog bones with higher concentrations of silk fibroin had a higher Young's modulus (d, f)

pH Variation in Silk Glands

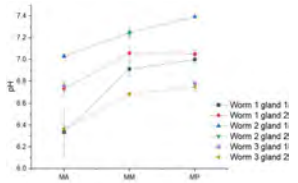

Figure 7. PH values were lower in the anterior regions of the silk glands than in the posterior, but pH often varied between different glands even in the same worm.

SEM Images

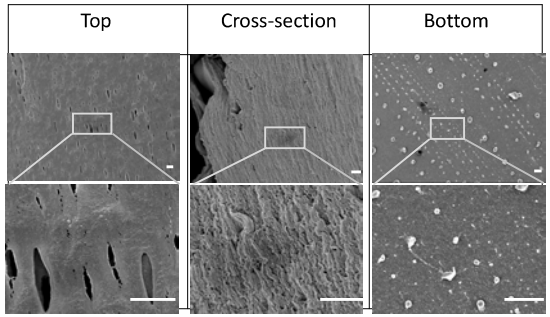

Figure 8. SEM images of dog bone 10 (w/w)% regenerative silk fibroin molded structures after tensile test. (scale bars: 1 μm). The elongation of structures on each surface, caused by the tensile force, is visible.

Conclusions

- Molded structures were successfully created and characterized
- **Natural silk fibroin (NSF)** - extracted from living silkworm glands - used instead of RSF as the feedstock for molding
- Using NSF eliminates additional processing, making it more environmentally friendly and cost effective
- Preliminary data also suggest that NSF structures perform better mechanically

Future applications

- Silk patches compatible with human organs
- Softer, eco-friendly components in robotic devices

Acknowledgement

Special thanks to SSTP and the Belin-Blank Center for giving me this amazing opportunity.

References:

[1] Guo, C. et al. Thermoplastic moulding of regenerated silk. Nat Mater 19, 102-108 (2020). https://doi.org/10.1038/s41563-019-0560-8

[2] Koh, L.-D. et al. Structures, mechanical properties and applications of silk fibroin materials, Progress in Polymer Science, 46, 86-110 (2015). https://doi.org/10.1016/j.progpolymsci.2015.02.001

[3] Lee, J., Park, S., Seo, I. H., Lee, K. J., & Ryu, W. (2015). Rapid and repeatable fabrication of high A/R silk fibroin microneedles using thermally-drawn micromolds, European Journal of Pharmaceutics and Biopharmaceutics, 94, 11-19. https://doi.org/10.1016/j.ejpb.2015.04.024

[4] McNamara, S. L., McCarthy, E. M., Schmidt, D. F., Johnston, S. P., & Kaplan, D. L. (2021). Rheological characterization, compression, and injection molding of hydroxyapatite-silk fibroin composites, Biomaterials, 269. https://doi.org/10.1016/j.biomaterials.2020.120643

[5] Sun, W., Gregory, D. A., Tomeh, M. A. & Zhao, X. Silk Fibroin as a Functional Biomaterial for Tissue Engineering. Int J Mol Sci 22 (2021). https://doi.org/10.3390/ijms22031499

Effects of Surgery on Brain Structure and Language Skills Among Children with Isolated Cleft of the Lip and/or Palate

Julianna Blackman[1], Amy L. Conrad, PhD, LP, HSP[2]

[1]Harrison High School, Harrison, NY, USA [2]Stead Family Department of Pediatrics, University of Iowa Roy J and Lucille A Carver College of Medicine, Iowa City, IA, USA

INTRODUCTION

1 in every 1,563 babies born in the U.S. has cleft lip and cleft palate
(Mai et al., 2019)

Reading Skills

- Isolated cleft of the lip and/or palate (iCL/P) significantly elevates risk of reading impairment -- dependent on type (Conrad, 2018)

Brain Structure

- Differences for oral clefts:
  - Increased frontal gray matter volume -- associated with better reading skills
  - Increased posterior occipital volume -- associated with worse reading skills (Conrad et al., 2021)
- Differences in interhemispheric and cerebellar white matter integrity

Speech/Language

- Quality of speech in males with cleft is associated to structural differences in the cerebellum (Conrad et al., 2010)
- Presence of oral cleft causes differences in speech input skills (Southby et al., 2021)

QUESTION

How does **surgery exposure** impact the **brain structure** and **language skills** of children with oral clefts?

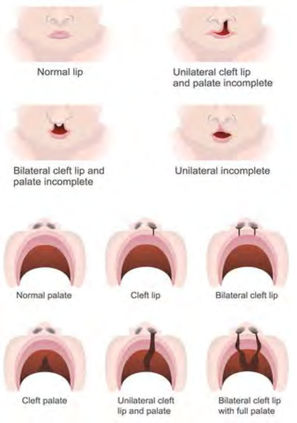

PURPOSE

- Investigate the **neurological impacts** of **surgery** on patients with isolated cleft of the lip and/or palate
- Examine the role of **cleft type** (lip only, lip *and* palate, palate only) on pediatric neuropsychology

(Ameri Surgical Instruments, 2023)

VARIABLES

Independent: Type of oral cleft, number of surgeries

Dependent: Language skills, brain structure

DATA ANALYSIS

1. Divided data into 3 groups based on cleft type
2. Univariate Analysis of Variance (ANOVA)
3. Group difference statistics for those with significant F-values
4. Pearson Correlations (r)
5. Z-score transformation to evaluate significant differences in correlation strengths

RESULTS

Table 1. Univariate Analysis of Variance and Group Difference Statistics		iCLO N = 6 Mean (SD)	iCLP N = 11 Mean (SD)	iCPO N = 10 Mean (SD)	F	Sig.
Age		10.21 (1.06)	10.06 (1.23)	11.01 (.85)	.785	.465
Surgeries	Total Number	3.00 (1.67)#	6.08 (3.53)	2.70 (1.77)^#	**5.146**	**.013**
Language Skills	Expressive	107.33 (9.16)	101.17 (15.37)	101.46 (13.47)	.470	.630
	Receptive	111.00 (8.83)	107.08 (14.70)	98.57 (13.28)	1.574	.230
Brain Data: Global	Intracranial Volume (cc^3)	1533511.50 (178891.86)	1523356.75 (120815.30)	1474080.71 (129848.02)	0.598	.557
	Whole Brain (cc^3)	1279909.71 (110351.16)	1380139.46 (92985.82)	1350161.84 (102787.26)	1.991	.155
Brain Data: Regional	Cerebrum†	0.88 (0.04)	0.89 (0.02)	0.87 (0.03)	1.476	.245
	Cerebellum †	0.11 (0.01)	0.10 (0.01)	0.11 (0.01)	2.406	.108
	Frontal †	0.38 (0.03)	0.37 (0.03)	0.37 (0.03)	0.205	.816
	Parietal †	0.20 (0.01)	0.20 (0.01)	0.19 (0.02)	0.990	.384
	Temporal †	0.17 (0.01)	0.17 (0.02)	0.17 (0.02)	0.234	.793
	Occipital †	0.10 (0.01)	0.10 (0.01)	0.10 (0.01)	1.251	.301
Brain Data: Language-Specific ROIs	Broca's Area †	0.02 (0.00)	0.02 (0.00)	0.02 (0.00)	0.194	.824
	Wernicke's Area †	0.01 (0.00)	0.01 (0.00)	0.02 (0.00)	0.013	.987
	Angular Gyrus †	0.04 (0.01)	0.03 (0.00)	0.03 (0.00)	0.478	.625

†Ratio to whole brain volume; #< iCLP; ^< iCLO

Table 2. Pearson Correlations (r) and Differences between Groups		iCLO			iCLP			iCPO			Sig. Group Differences			
		Surgeries	Exp.	Rec.	Surgeries	Exp.	Rec.	Surgeries	Exp.	Rec.	Var.	Groups	Z	*p*
Language Skills	Expressive	.091	-	-	.542	-	-	-.511	-	-	#S	iCLP > iCPO	2.26	.024
	Receptive	.000	-	-	.494	-	-	-.217	-	-	-	-	-	-
Brain Data: Global	ICV (cc^3)	-.639	-.142	.117	-.026	**.781****	**.725***	.207	.081	-.374	-	-	-	-
	Whole Brain (cc^3)	.474	.500	.360	-.065	**.875*****	**.819****	-.137	.121	-.498	Exp.	iCLP > iCPO	2.38	.017
											Rec.	iCLP > iCPO	2.51	.012
Brain Data: Regional	Cerebrum	-.167	.042	.421	-.043	.487	.450	.641	.034	.355	-	-	-	-
	Cerebellum	-.290	-.502	-.626	-.020	**-.831****	**-.787****	-.483	-.300	-.540	-	-	-	-
	Frontal	.193	-.121	.180	.261	.425	.457	.322	.159	-.246	-	-	-	-
	Parietal	-.737	-.118	-.009	-.149	-.513	-.595	.149	-.343	.717	Rec.	iCPO > iCLP	2.34	.019
	Temporal	-.074	-.513	-.255	-.101	**-.738****	**-.714***	.138	.054	.560	Rec.	iCLP > iCPO	2.26	.024
	Occipital	-.654	-.213	-.035	-.178	-.248	-.170	**.694***	.024	.143	#S	iCPO > iCLO	2.32	.021
Brain Data: Language-Specific ROIs	Broca's	-.212	-.288	.102	.388	-.386	-.384	.280	.114	-.213	-	-	-	-
	Wernicke's	-.365	**-.859***	-.705	-.007	-.561	-.442	.277	.124	.485	Exp.	iCLO > iCPO	2.05	.040
	Ang. Gyrus	-.569	-.259	-.156	.250	.165	.114	.000	-.139	-.120	-	-	-	-

*p < .05; **p < .01; ***p < .001

DISCUSSION

Conclusions

- Number of surgeries did **not** have a strong impact on language skills or brain structure
- There was **not** a strong relationship between language skills and brain structure in participants with iCLO and iCPO
- Significant relationships between language skills and global/regional brain data among iCLP participants

Limitations

- Small sample size
- Did not use Bonferroni correction
- Only one variable for surgery – might have been overshadowed by other surgery variables or not the most accurate predictor

FUTURE RESEARCH

- Larger sample size
- Different method for classifying the cleft type (unilateral vs bilateral cleft)
- Impact of sex on neurological effects
- Prevention methods

ACKNOWLEDGEMENTS

Special thanks to Dr. Amy Conrad for her mentorship and support, the Conrad Neurodevelopment Lab for making this research possible, and the Secondary Student Training Program and Belin-Blank Center at the University of Iowa for providing this research opportunity.

This study was supported by K23DE024511 (NIH/NIDCR).

REFERENCES

Ameri Surgical Instruments. (2023). *Understanding cleft lip and palate: what to expect before, during, and after the procedure* [Illustration]. Ameri Surgical Instruments Inc. https://www.amerisurgicalinstruments.com/blogs/news/understanding-cleft-lip-and-palate-what-to-expect-before-during-and-after-the-procedure

Conrad, A. L. (2018). Are predictors of reading impairment in isolated cleft similar to those in idiopathic dyslexia? *Annals of Dyslexia, 69*(2), 153-165. https://doi.org/10.1007/s11881-018-00166-2

Conrad, A.L., Dailey, S., Richman, L., Canady, J., Karnell, M.P., Axelson, E., & Nopoulos, P. (2010) Cerebellum structure differences and relationship to speech in boys and girls with nonsyndromic cleft of the lip and/or palate. *The Cleft Palate-Craniofacial Journal: Official Publication of the American Cleft Palate-Craniofacial Association, 47*(5), 469–475. https://doi.org/10.1597/08-228

Conrad, A. L., Kuhlmann, E., van der Plas, E., & Axelson, E. (2021). Brain structure and neural activity related to reading in boys with isolated oral clefts. *Child Neuropsychology, 27*(5), 621–640. https://doi.org/10.1080/09297049.2021.1879765

Mai, C. T., Isenberg, J. L., Canfield, M. A., Meyer, R. E., Correa, A., Alverson, C. J., Lupo, P. J., Riehle-Colarusso, T., Cho, S. J., Aggarwal, D., & Kirby, R. S. (2019). National population-based estimates for major birth defects, 2010–2014. *Birth Defects Research, 111*(18), 1321-1447. https://doi.org/10.1002/bdr2.1589

Southby, L., Harding, S., Phillips, V., Wren, Y., & Joinson, C. (2021). Speech input processing in children born with cleft palate: A systematic literature review with narrative synthesis. *International Journal of Language & Communication Disorders, 56*(4), 668-693. https://doi.org/10.1111/1460-6984.12633

Gene Profiling of Left Ventricles from Ts65Dn Mice in Anthracycline-Induced Cardiotoxicity Model

Michelle Chen[1], Michelle Buckman[2], Mikhail Vasilyev MD[2,3], Anastasiia Vasileva MD[2,4], Michael H. Tomasson MD[2,3,4]

Department of Biology, Phillips Academy, Andover, MA[1]; Department of Internal Medicine[2], Division of Hematology, Oncology, and Bone Marrow Transplantation[3], Health and Human Physiology[4], University of Iowa, Iowa City, Iowa, USA

Introduction

- People with Down syndrome have a higher risk of acute leukemia[1].
- Chemotherapy regime for acute leukemia involves anthracycline-based treatment[1].
- Trisomy 21 is a risk factor for anthracycline-induced cardiotoxicity[1] .
- Cardiotoxicity leads to cardiac remodeling[2] and results in systolic heart failure[3].
- To better understand the molecular mechanisms involved in increased susceptibility to anthracyclines in Down syndrome, it is important to identify genes involved in the physiological mechanisms underlying anthracycline-induced damage.
- The Ts65Dn mouse is a model of Down syndrome that resembles the cardiovascular phenotype observed in this population[4].
- Our study aims to investigate the gene profiling of the left ventricles in the Ts65Dn mouse model.

Hypothesis

RNA from the left ventricle of Ts65Dn mice will have nucleic acid purity parameters (A260/A280; A260/A230) and RNA Integrity Number (RIN) greater than 2 and 8 respectively when extracted with TRIzol compared to the Qiagen RNeasy Fibrous Tissue Mini Kit.

Methods

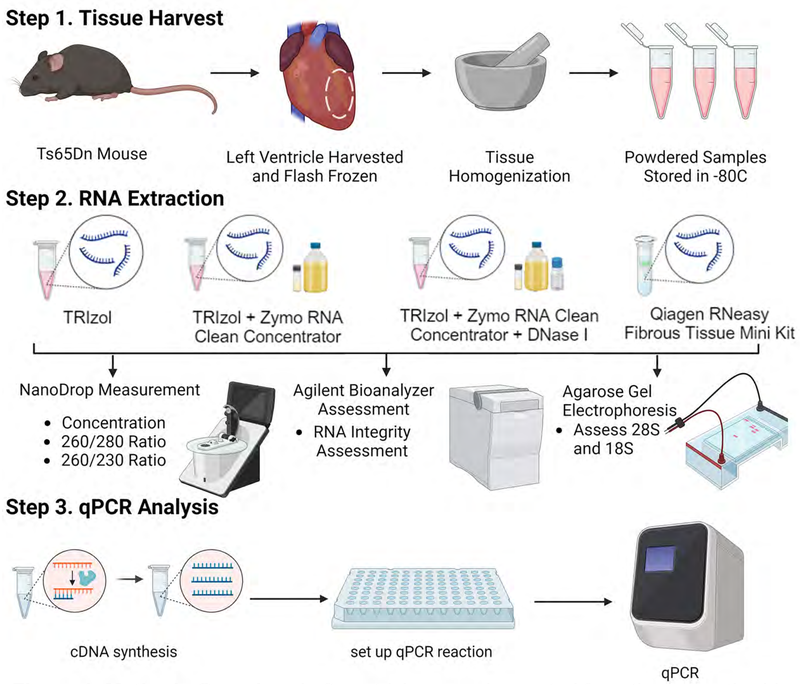

Figure 1. Methods Overview. Left ventricles were harvested from three-month-old male Ts65Dn mice (n=3) and immediately frozen in liquid nitrogen. The tissue was homogenized, and RNA extraction was performed using four different protocols to access the highest-quality RNA . Quality of RNA was assessed using NanoDrop and bioanalyzer Agilent 2100. RNA was then used for the subsequent qPCR analysis.

Results

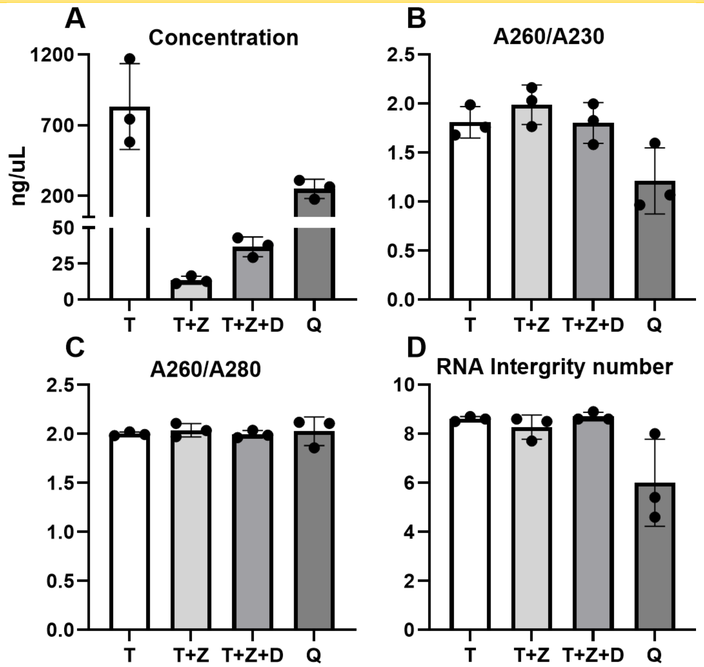

Figure 2. RNA quality assessment. (A) RNA concentration of samples was measured with a NanoDrop using TRIzol (T); TRIzol + Zymo column cleanup (T+Z); TRIzol + Zymo column cleanup + DNAse I (T+Z+D) and Qiagen RNeasy Fibrous Tissue Mini Kit (Q).(p<0.001) **(B)** The A260/230 ratio of RNA samples was measured with a NanoDrop. (p=0.018) **(C))** The A260/280 ratio of RNA was measured with a NanoDrop. (p=0.9) **(D)** The RIN was measured with a bioanalyzer. An RIN greater than 7 indicates quality and non-degraded RNA. (p=0.02) n=3 for all groups. ANOVA statistical analysis was used to determine significance.

Figure 3. Representative agarose RNA gel. Two distinguished bands demonstrate 28S and 18S, respectively.

Conclusions

- RNA extracted with TRIzol was higher in concentration compared to other methods.
- Qiagen RNeasy Mini Kit yielded the lowest A260/A230 ratio.
- A260/A280 ratio was not significantly changed across methods.
- RIN was lower in Qiagen RNeasy Mini Kit .

Future Directions

- We will complete qPCR analysis for genes listed in Table 1.
- The next step will be to investigate the expression of genes involved in left ventricular dysfunction in anthracycline-induced cardiotoxicity by performing single-cell sequencing.

Table 1. Candidate Genes for qPCR analysis of left ventricles in Ts65Dn mice

Gene	Involvement in:
DYRK1a	impacts the splicing of cardiac troponin in the whole heart of Ts65Dn mice resulting in decreased myocardial contractility[5] anthracyclines decrease beating frequency in Human iPSC cardiomyocytes overexpressing *DYRK1A*.[6]
RCAN1	expression was significantly reduced in the hearts of B6.129 mice in response to anthracycline treatment[7]
Sh3bgr	overexpression causing abnormal sarcomere formation[8]
ATP5J	early biomarkers of anthracycline-induced chronic cardiotoxicity in B6C3F1 mice[9]
GART	diminished expression by doxorubicin[10]
ATP5O	regulates the contractile function of the heart (*SIRT3* substrate) [11]
KCNE1	presence in pathologies cased by anthracycline-induced cardiotoxicity[12]
Tiam1	required for α1-adrenoceptor induced neonatal rat cardiomyocyte hypertrophy[13]
ETS2	promotes cardiomyocyte apoptosis and autophagy in heart failure[14]
SOD1	defense against oxidative stress[15]
NDUFV3	mitochondrial impairment in cardiac tissue[16]
Genes triplicated in Ts65Dn mice.	

Figure 4. Single – cell sequencing analysis. (A) UMAP of C57BL/6 murine cardiomyocytes resourced from UCSC cell browser. **(B)** Dyrk1a gene expression in murine heart. Each dot represents a single cell, with cells that are closer together having a more similar gene expression profile.

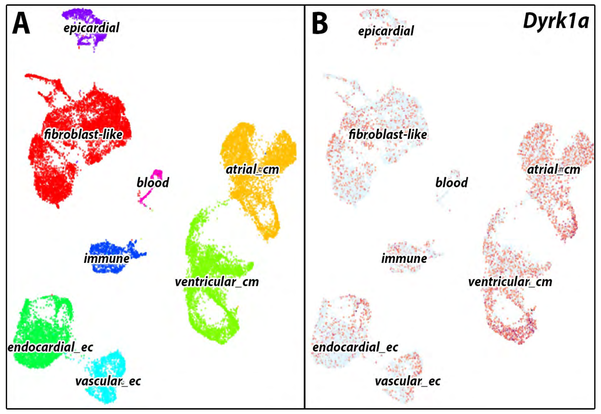

Acknowledgements

I would like to thank Michelle Buckman, Dr. Vasilyev, Dr. Vasileva, Dr. Tomasson, Dr. Bates, and everyone at the IPG lab for the amazing learning opportunity. Thank you SSTP for the experience. This work was supported with R21HD099573

References

Effects of prenatal chronic unpredictable stress on the levels of the enzyme for telomere maintenance, telomerase reverse transcriptase (TERT), in the embryonic mouse brain

Liuqing Chen, Maya M. Evans, Sara V. Maurer, Benjamin A. Kelvington, Hanna E. Stevens

Dept. of Psychiatry, University of Iowa

Introduction

- **Telomeres** are the protective caps on the end of eukaryotic chromosomes that prevent the end of the chromosomes from degradation. During each cell division process, the length of the telomere shortens, which thus limits the total number of cell divisions[1].
- **Telomerase** is an enzyme that counteracts the shortening of telomeres by adding repeated nucleotide sequences to the end of telomeres[2].
- The **telomerase reverse transcriptase (TERT)** is a catalytic component that reactivates the telomerase and modulates its activity, maintaining the stability of the chromosome[3].

Many studies have shown that prenatal stress alters the development of the embryonic brain, even having an impact on telomere length and TERT[4]. For example, data from the Stevens lab shows that there is a higher level of TERT in male mice brains but not in females after prenatal stress induced by a restraint stress paradigm. **Our study asks whether a different model of stress, chronic unpredictable stress (CUS), similarly affects the TERT levels in embryonic mouse brains. We hypothesize that prenatal CUS will increase TERT levels in the male embryonic brains but have no effect on the female embryonic brains.**

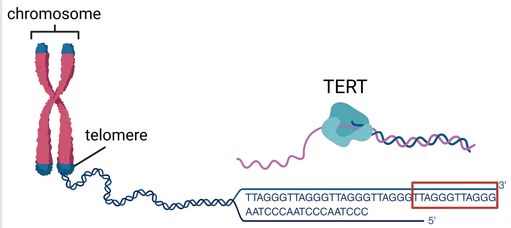

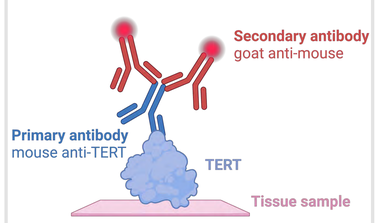

Methods

1 Animal Model

The pregnant female mice were divided into two groups, with one group receiving no stress exposure and the other receiving chronic unpredictable stress starting at embryonic day 12 (E12). Stress exposure continued until tissue collection. The chronic unpredictable stress used in this experiment included cage shaking, wet bedding, and colder temperatures. The three treatments were randomized and applied in three 45-minute sessions each day.

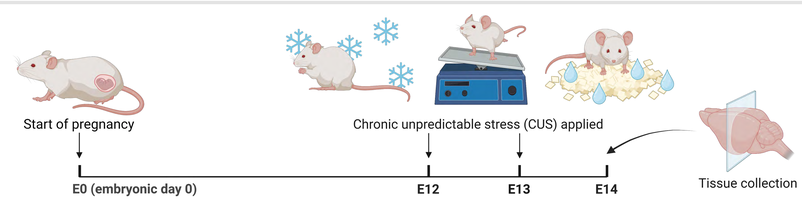

2 Sample Collection & Tissue Preparation

Samples of offspring brain tissues were collected on E14. Our sample included 20 offspring, with 5 males and 5 females from both the stress and control groups. Whole heads were fixed in paraformaldehyde, switched to 30% sucrose solution for cryoprotection two days later, and frozen in O.C.T. They were sectioned on a cryostat at 25um.

3 Immunohistochemistry (IHC)

1. Block solution applied
2. 1:50 mouse anti-TERT (Santa Cruz) as primary antibody applied, incubated overnight
3. 1:500 goat anti-mouse 594nm (Alexa Fluor) as secondary antibody applied, incubated for one hour
4. Mounted in DAPI

4 Microscopy

Images were captured using Zeiss Axioskope at 20x magnification using consistent light intensity, exposure time, and gain.

5 ImageJ Analysis

Integrated density was measured in both proliferative and non-proliferative zones of dorsal and ventral forebrain. Values were averaged from two locations, bilaterally, from three serial sections for each following zone: dorsal proliferative, dorsal non-proliferative, ventral proliferative, and ventral non-proliferative zones. Values were normalized to ventral proliferative zones in control samples from the same staining batch. Males and females were analyzed separately.

Results

Coronal section of mouse brain at E14, stained in DAPI

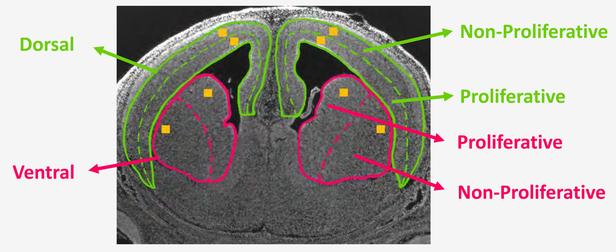

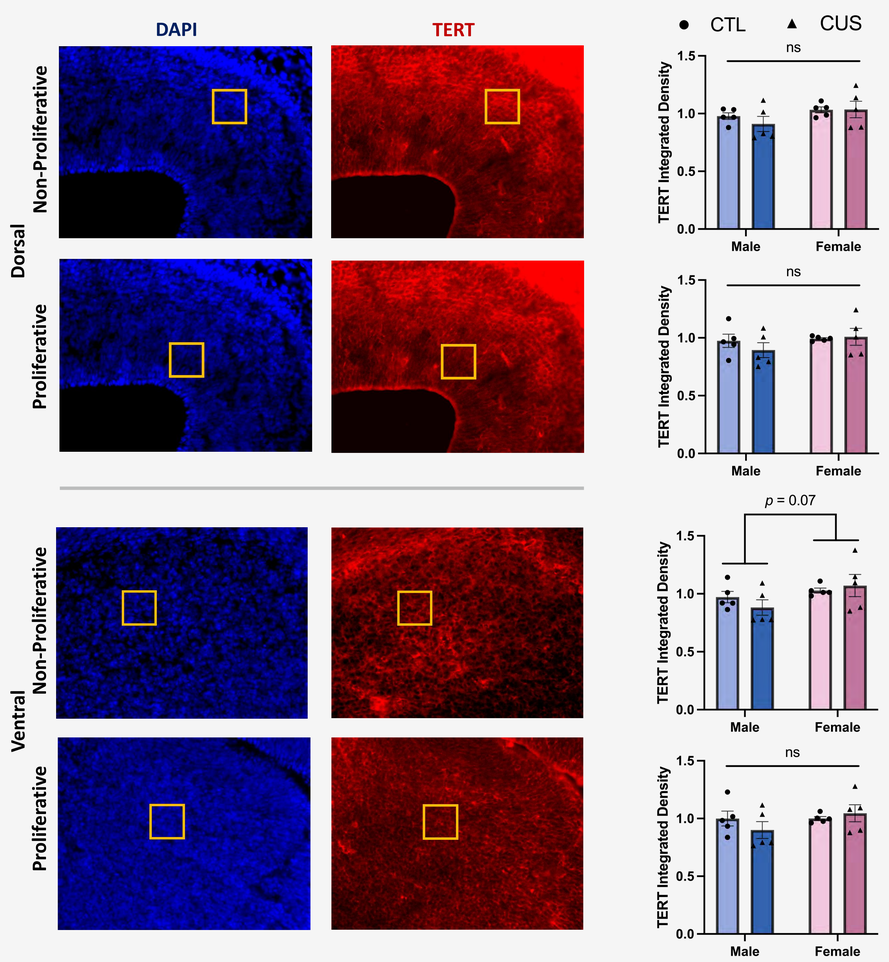

Results

- CUS had no effect on TERT levels in any brain regions tested.
- Females trended toward higher levels of TERT in the ventral non-proliferative zone compared to males (two-way ANOVA main effect of sex, $F_{(1, 16)} = 3.6$, $p = 0.074$).

Conclusions

- The data did not support our original hypothesis that CUS would increase TERT levels in the male but not female embryonic brains.
- CUS had no effects on TERT levels like restraint stress did for E14 mouse brains.
- Differing results from the restraint stress experiment may be due to:
  - Differences in stress modality (restraint vs. cage shaking, wet bedding, and colder temperatures)
  - Different cohorts of mice used in experiments, e.g., bedding differences
- Trending higher levels of TERT in the ventral non-proliferative zone in females may result from different hormone environments *in utero* due to placental sex differences.

Future Directions

- Investigate a later embryonic age, allowing a longer prenatal exposure to stress
- Explore additional stress models and their impacts
- Measure telomere length using qPCR after prenatal CUS stress exposure
- Observe effects on different brain regions such as cerebellum or brain stem

Acknowledgements

Project Funding: R01 MH122485-01 to H.E.S.; F31 MH131259 to M.M.E.

Figures created with **BioRender.com**

Special thanks to the invaluable support from Maya Evans, Dr. Stevens, and other Stevens Lab members and SSTP.

1. Giardini, M. A., Segatto, M., da Silva, M. S., Nunes, V. S., & Cano, M. I. (2014). Telomere and telomerase biology. Progress in molecular biology and translational science, 125, 1–40. https://doi.org/10.1016/B978-0-12-397898-1.00001-3
2. Zvereva, M. I., Shcherbakova, D. M., & Dontsova, O. A. (2010). Telomerase: structure, functions, and activity regulation. Biochemistry. Biokhimiia, 75(13), 1563–1583. https://doi.org/10.1134/s0006297910130055
3. Dratwa, M., Wysoczańska, B., Łacina, P., Kubik, T., & Bogunia-Kubik, K. (2020). TERT-Regulation and Roles in Cancer Formation. Frontiers in immunology, 11, 589929. https://doi.org/10.3389/fimmu.2020.589929
4. Marchetto, N. M., Glynn, R. A., Ferry, M. L., Ostojic, M., Wolff, S. M., Yao, R., & Haussmann, M. F. (2016). Prenatal stress and newborn telomere length. American journal of obstetrics and gynecology, 215(1), 94.e1–94.e948. https://doi.org/10.1016/j.ajog.2016.01.177

DNA damage accumulates in direct pathway medium spiny neurons of male 16p11.2 deletion model mice

Manvitha Chinnam[3], Benjamin A. Kelvington[1,2], Regan Fair[1,2], Junko Kasuya[1,2], Jaekyoon Kim[1,2], Ted Abel[1,2]

[1]Department of Neuroscience and Pharmacology, Carver College of Medicine, University of Iowa
[2]Iowa Neuroscience Institute, University of Iowa
[3]Secondary Student Training Program, Belin-Blank Center, University of Iowa

Introduction

- 16p11.2 microdeletion is associated with neurodevelopmental disorders (NDDs) including ASD and ADHD (Chung et. al, 2021).
- Both humans with NDDs and mouse models exhibit striatal dysfunction affecting reward processing (Fuccillo, 2016).
- In mice modeling 16p11.2 microdeletion (16p), male-specific reward learning deficits are linked to striatal dysfunction, which is consistent with the male bias of NDDs in humans (Grissom et. al, 2017).

Research Objectives

- Investigate the molecular mechanisms in the striatum of 16p mice underlying male-specific reward learning deficits.
- Understanding these mechanisms will inform potential therapeutic interventions for NDDs.

Methods

- Operant reward-learning was conducted, where mice were placed in operant chambers and trained to nose poke for a sweetened liquid reward, and the number of trials perform in 30 minutes was used as an assessment of reward learning.
- Translating ribosome affinity purification with sequencing (TRAP-seq) was used to isolate and analyze ribosome-bound mRNA from D1 expressing medium spiny neurons (D1+ MSNs) in bacTRAP transgenic mice, allowing for the precise assessment of the impact of 16p11.2 deletion on the translatome of D1 MSNs.
- Immunohistochemistry (IHC) was used to analyze markers of DNA damage and repair specifically in D1+ MSNs. yH2AX was used as a marker of DNA damage, and 53BP1 was used as a marker of DNA repair via the non-homologous end joining mechanism. Colocalization between these markers, labeled with red fluorescence, and D1+ MSNs, marked with green, was quantified using confocal microscopy and ImageJ software.

Male-specific reward-learning deficits in 16p11.2 deletion animals are mediated by D1+ MSNs.

Figure 1. 16p male mice exhibit reward-learning deficits mediated by D1 MSNs. Behavioral data comparing reward learning performance between male and female mice with the 16p11.2 deletion. Conditional deletion of the 16p region in D1 MSNs produces reward-learning deficits in males (A), but not females (B).

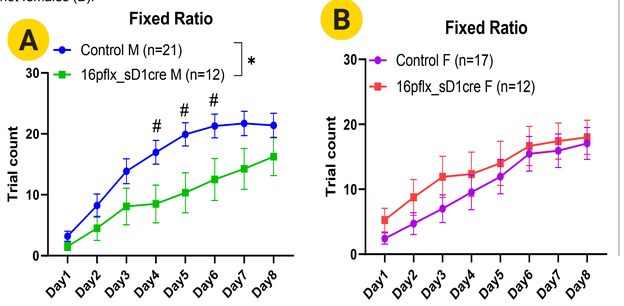

TRAP-sequencing of D1 MSNs reveals sex-specific impact of 16p11.2 deletion on DNA damage and repair.

Figure 2. DNA damage and repair, transcriptional regulation, and chromatin organization pathways are impacted in D1 MSNs of 16p11.2 deletion mice. Drd1a promoter was used to drive expression of EGFP-L10a ribosomal fusion transgene in the bacTRAP transgenic mouse model (A). Pathway analysis of differential gene expression in the translatome of male 16p compared to male wild-type (WT) animals in naive conditions (B). Pathways of differential gene expression between female 16p and female WT animals in naive conditions (C). Mice were provided with 50% Ensure (0.2mL/g BW) for 7 days (D). Pathway analysis of differential gene expression in male WT animals between reward and naive conditions (E). Differential gene expression pathway analysis comparing female 16p animals between reward and naive conditions (F).

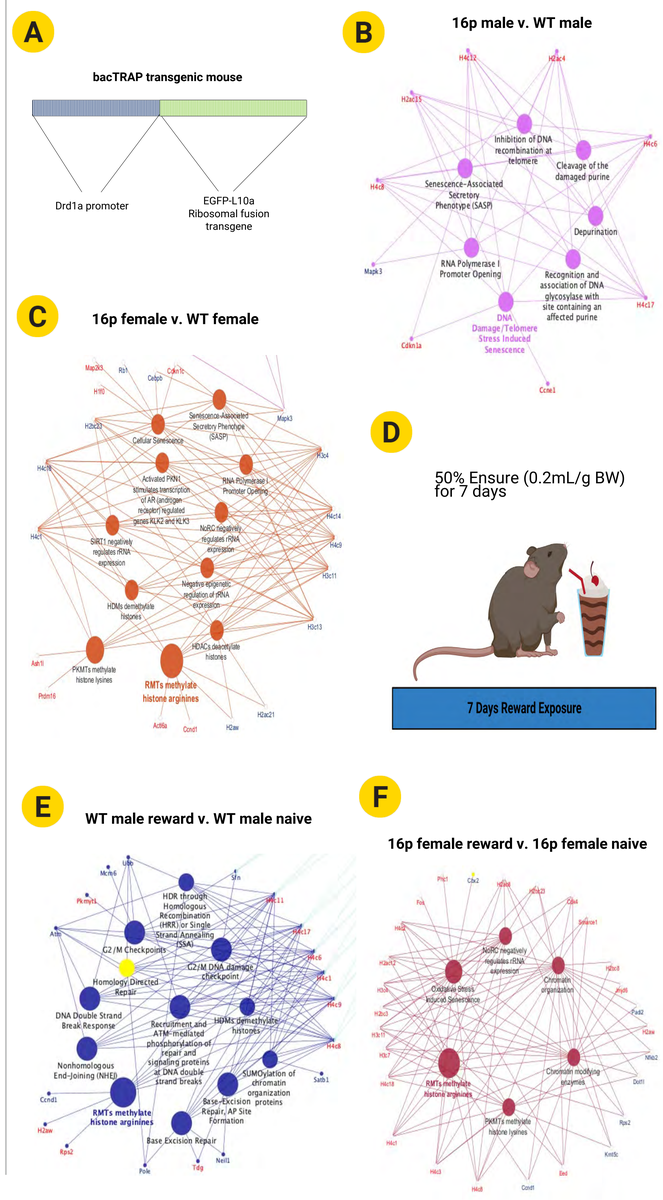

DNA damage is exacerbated in the D1+ MSNs of 16p males.

Figure 3. DNA damage in D1+ MSNs of male 16p11.2 deletion mice is increased. Immunofluorescent staining showing yH2AX (red), EGFP-L10a (green), and DAPI (blue) (A). yH2AX is a marker for DNA damage. EGFP-L10a marks D1+ MSNs. DAPI is a nuclear stain. DNA damage is significantly increased in D1+ MSNs of male 16p mice (B). There is no change in the amount of DNA damage in cells that are not D1+ MSNs (C). Data was analyzed using a Two-Way ANOVA. "#" indicates a significant interaction between sex and genotype ($p < 0.05$).

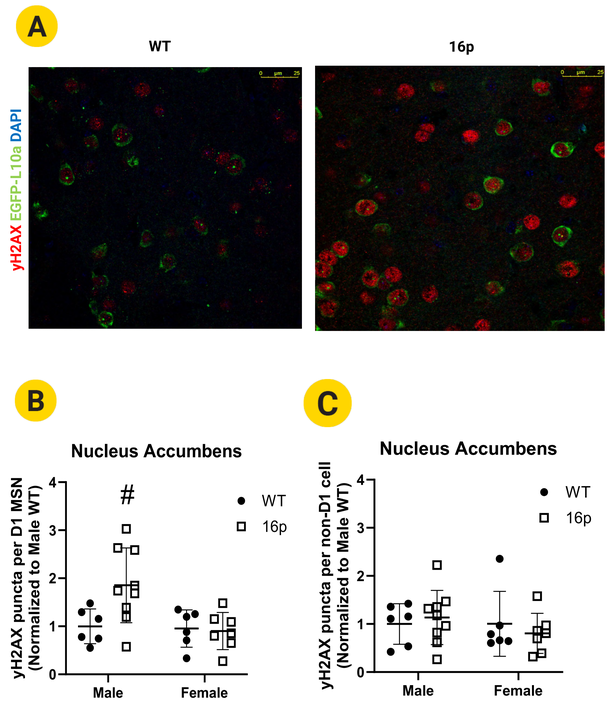

Conclusions

- **16p male mice exhibit reward-learning deficits mediated by D1+ MSNs.**
- **DNA damage and repair pathways are dysregulated in the translatome of D1+ MSNs in 16p mice.**
- **D1+ MSNs of male 16p mice exhibit increased DNA damage likely due to disruption of DNA repair capacity.**

Acknowledgments

Support for this work has been provided by the Secondary Student Training Program (SSTP).

16p male D1+ MSNs are deficient in DNA repair.

Figure 4: Reduced 53BP1 expression indicates DNA repair deficiency in 16p Male D1+ MSNs. Representative images of 53BP1 and EGFP-L10a (D1+ MSNs) expression in WT and 16p mice are shown with nuclei counterstained by DAPI (A). Quantification of 53BP1 puncta per D1+ MSN in the nucleus accumbens, normalized to male WT, is presented for both male and female mice (B). A comparison of 53BP1 puncta per D1+ MSN in males only shows a trend toward a reduction in 53BP1 puncta in 16p males (Student's t-test, $p = 0.0777$) (C).

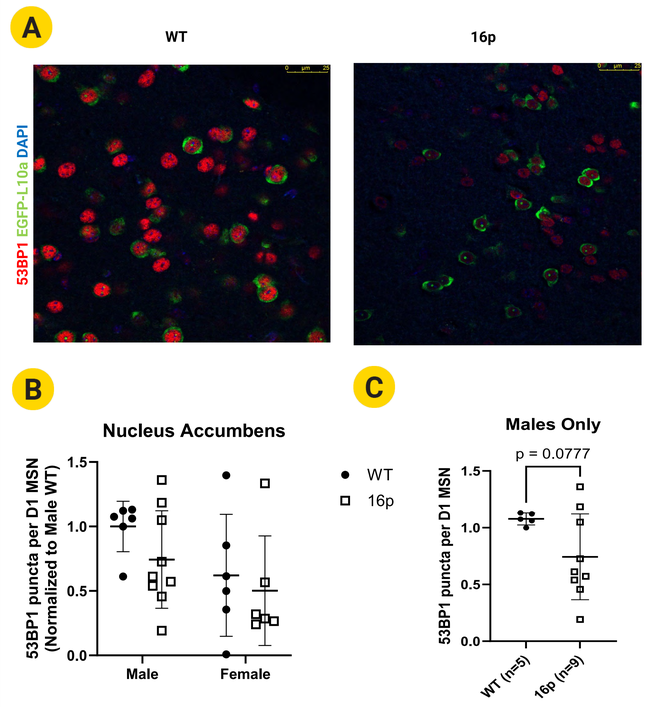

Future Directions

- Track the progression of reward-learning deficits over time and across different developmental stages in 16p mice.
- Compare the mechanisms observed in 16p with other genetic models of NDDs to identify common pathways.
- Determine the causal impact of DNA damage on sex-specific reward learning deficits in 16p mice.

References

Chung, W. K., Roberts, T. P., Sherr, E. H., Snyder, L. G., & Spiro, J. E. (2021). 16p11.2 deletion syndrome. *Current Opinion in Genetics & Development*, 68.

Fuccillo, M. V. (2016). Striatal circuits as a common node for autism pathophysiology. *Frontiers in Neuroscience*, 10.

Grissom, N. M., McKee, S. E., Schoch, H., Bowman, N., Havekes, R., O'Brien, W. T., Mahrt, E., Siegel, S., Commons, K., Portfors, C., Nickl-Jockschat, T., Reyes, T. M., & Abel, T. (2017). Male-specific deficits in natural reward learning in a mouse model of neurodevelopmental disorders. *Molecular Psychiatry*, 23(3), 544–555.

Identifying MRI Biomarkers of Physical Exercise Adherence in Older Adults

A. Garg[1,2], B. Madero[2], M. Pipoly[2], Z. Gilliam[2], C. Oehler[2], G. Pierce[3], M. Voss[2]

[1]Dublin High School, Dublin, CA, [2]Department of Psychological and Brain Sciences, University of Iowa,
[3]Department of Health and Human Physiology, University of Iowa

Introduction

- Physical exercise can mitigate natural age-related cognitive decline [1] and recent studies show **brain biomarkers** (structural/functional) are **associated with adherence** to exercise [2, 3]
- Previous research has only included group-based interventions and didn't include brain connectivity measures [4]
- Based on their relationship between aging [5], **we hypothesize** that **brain biomarkers vulnerable to aging predict adherence to exercise**

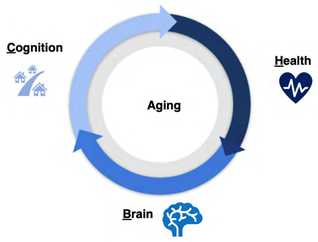

Methods: *Dataset and Preprocessing*

- Bike EXTEND data was used (see below)
- Adherence to each session was measured using a heart rate monitor, turned into percentage completed, and binned to Low/Mid/High
- Age + Sex were regressed out of all features to reduce correlations

Bike EXTEND Study Design

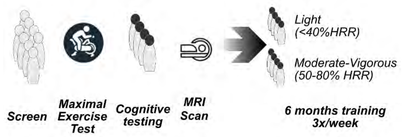

Adherence Distribution Plot

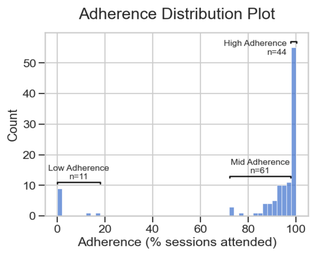

Modalities Used

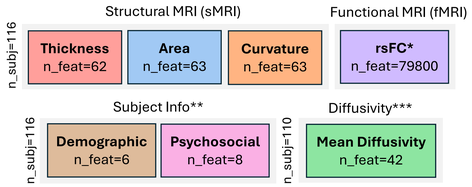

Resting-state functional connectivity, with a 400x400 matrix of connections

***These modalities did not go through a PCA. Demographic data was not regressed with Age + Sex residuals.*

****6 subjects did not have Diffusivity data. For other modalities, PCA was performed on all 116 subjects, then the 6 extra subjects were dropped for model training*

Methods: *Training and Feature Extraction*

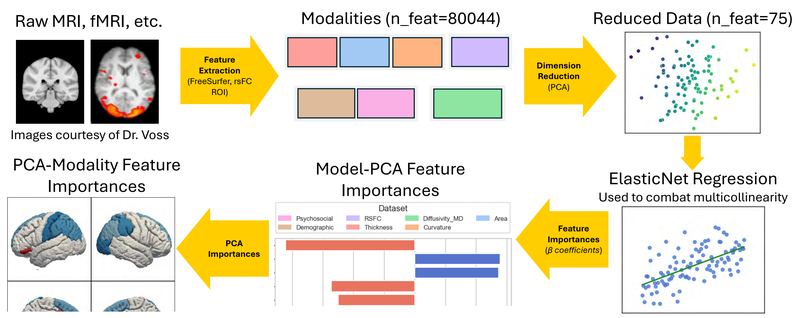

Results: *ElasticNet Evaluation*

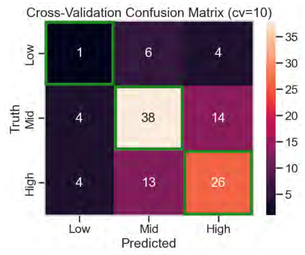

- K-fold cross validation (cv=10) was performed to determine the performance of ElasticNet
- Achieved 59.09% accuracy and 28.44% Cohen's Kappa score (which accounts for imbalances in classifications), cumulative confusion matrix on left
- Other tests were run where low subjects were dropped and models were weighted 5x for the Low class with no significant change

Results: *Model-PCA Feature Importance*

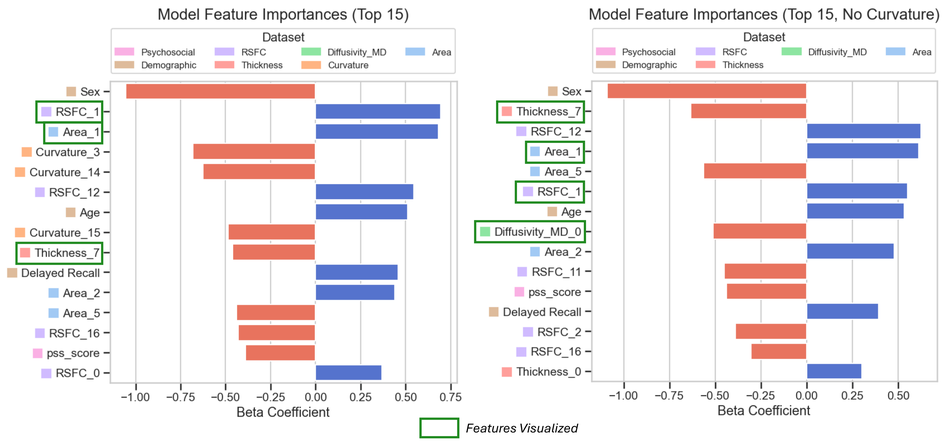

- β coefficients were extracted from ElasticNet and ranked by absolute magnitude
- Tested with both Curvature and No Curvature as Curvature might contain noise

Results: *PCA-Modality Feature Importance*

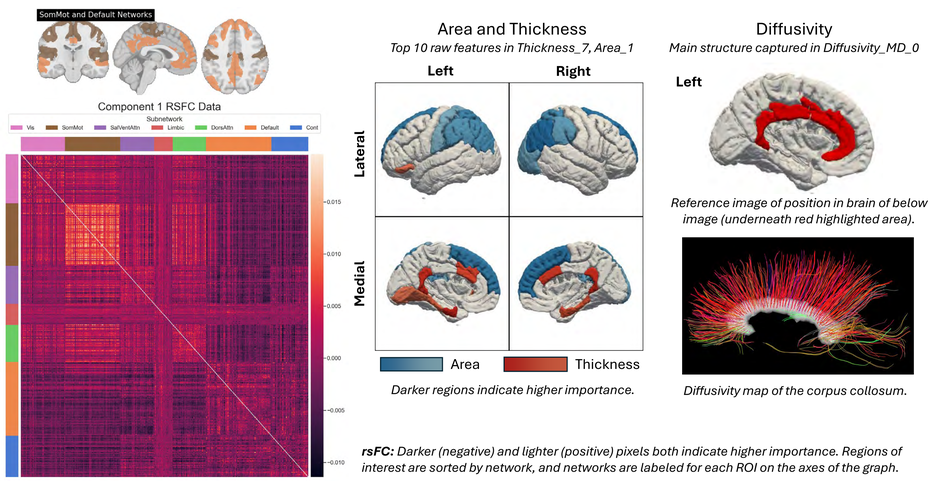

rsFC: *Darker (negative) and lighter (positive) pixels both indicate higher importance. Regions of interest are sorted by network, and networks are labeled for each ROI on the axes of the graph.*

Results: *PCA Component Selection*

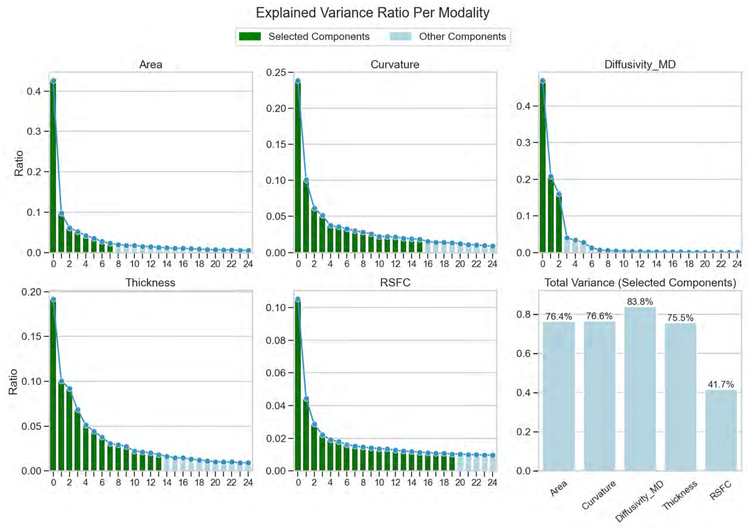

Conclusions

- Important regions for prediction **correlated with age-related structural decline** [5] – future research needs to investigate the **specific effects** between age, biomarkers, and adherence (is higher or lower thickness related to adherence?)
- Convergence between Area and rsFC (DMN and SMN networks), Diffusivity and Thickness (Corpus Collosum and Caudal Cingulate) suggest **highly important regions for adherence**
- Results corroborate and expand on existing research [2, 3, 4] while using only a data driven approach
- **Future directions** include testing statistical significance of results, using non-linear models to find nuanced relationships

Acknowledgements

Special thanks to Bryan Madero, Dr. Marco Pipoly, Zak Gilliam, and Dr. Michelle Voss for providing valuable guidance throughout my research process, and to Chris Oehler for helping with data collection. Thanks also to the Belin-Blank Center and the amazing organizers at the SSTP program for this incredible research opportunity.

References

[1] Xu et al. *Int. j. of environmental and public health*. **2023**, *20*(2), 1088.
[2] Gujral et al. *Psychosomatic medicine*. **2018**, *80*(1), 69-77.
[3] Best et al. *J. of gerontology, Biomed. and med. sciences* **2017**, *72*(6), 804-810.
[4] Morris et al. *Medicine and science in sports and exercise*. **2022**, *54*(9), 1483-1492.
[5] Vinke et al. *Neurobiology of aging*. **2018**, *71*, 32-40.

Correspondence: ayushgargemail@gmail.com

Void generation in energetic materials via pressure-assisted binder jetting additive manufacturing

Michael Gearing, Steve Zhang, Arnold Bangel MS, Nazanin Tabatabaei BS, Jackson Berlage BS, Xuan Song PhD
Department of Industrial and Systems Engineering, University of Iowa

Contact Info:
xuan-song@uiowa.edu
mgearing@uiowa.edu

Introduction

- **Goal of research:**
  - This study aims to develop a system of generating voids within energetic materials through smart additive manufacturing
  - Determine whether the pattern of these voids affects the dynamic properties of the composite when high-impact stress is induced
  - We hope to utilize these results to improve the performance of energetic materials, including explosives and other protective composites such as that on an airplane wing

- **Polymer bonded explosive (PBX) composites:** are a group of composite materials composed of explosive crystals held together by a polymer binder (Xiao et. al, 2024)
- **Polymer bonded sugar (PBS) composites:** are used in this study to emulate PBX materials without the hazardous chemical properties associated with these composites

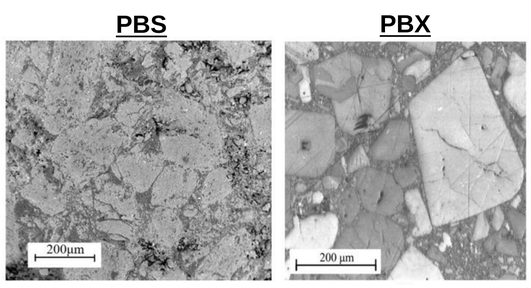

(Xiao et. al, 2024)

- **Pressure-assisted binder jetting additive manufacturing (PBJAM) System**
  - Uses layer-by-layer powder deposition in combination with a binder-jetting nozzle to build up layers of composite material (Kirby et. al, 2023)
  - This system will be used to create precise PBS samples of varying sugar-to-binder ratios and tailored void-generating additives

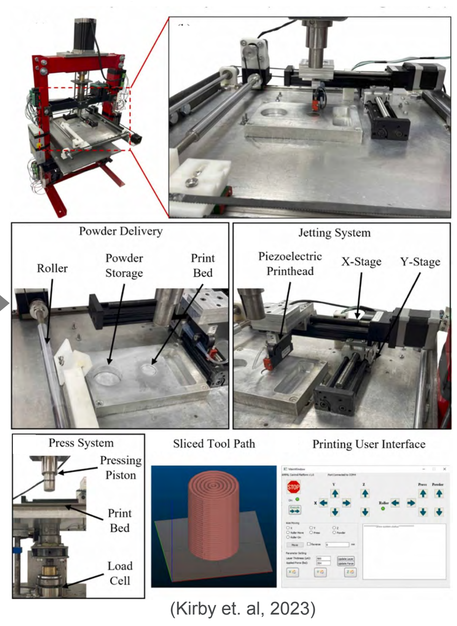

(Kirby et. al, 2023)

- **Split Hopkinson pressure bar (SHPB)**
  - This testing configuration is used to test the mechanical properties of materials at high-impact stresses
  - In the study, the SHPB will be useful in comparing these properties between different PBS compositions and void patterns in a manner similar to that undergone during detonation

Methods

- **Creating samples**
  - Specimens were formulated using the PBJAM system to selectively add hydrogen peroxide: a chemical that generates voids within the PBS composite when heated
  - The binder used for the final demonstration was hydroxyl-terminated polybutadiene, or HTPB
  - Samples were composed of 60% sugar, 40% binder, and varying amounts of additive
  - They were then cured in a furnace at 100 degrees Celsius for 24 hours

Press on the PBJAM compressing a layer of composite

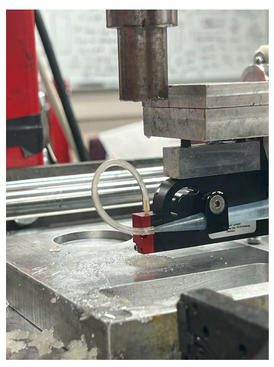

Nozzle on the PBJAM depositing hydrogen peroxide into the composite

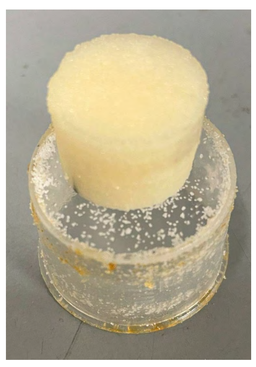

Sample composed of 60% sugar, 40% binder, and 0% hydrogen peroxide

Second sample composed of 60% sugar, 40% binder, and 0% hydrogen peroxide

- **Testing the split Hopkinson pressure bar**
  - Determining velocity vs. pressure relationship
  - To find this correlation, we created a system utilizing two IR LED and phototransistor setups in combination with a microcontroller

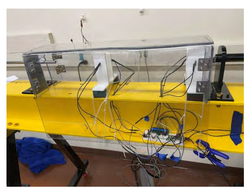

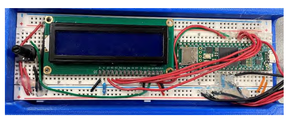

Speed sensor setup using Teensy 4.1

```
if(analogRead(A0) < 5 && trigger1 == true) {
  firstRod = ms;
  trigger1 = false;
  Serial.print("Rod1: ");
  Serial.println(firstRod);
}

if(analogRead(A1) < 5 && trigger2 == true && trigger1 == false) {
  secondRod = ms;
  trigger2 = false;
  Serial.print("Rod2: ");
  Serial.println(secondRod);
  calculate();
  Serial.print("Speed: ");
  Serial.println(speed);
  lcd.clear();
  lcd.print("Speed:");
  lcd.setCursor(0,1);
  lcd.print(speed);
}
```

Code utilizing sensors to calculate striker bar speed

- **High-speed camera**
  - To identify a deformation field of the samples, a high-speed camera is used, capturing 150,000 fps
  - By using the fps of the camera we can also verify the speed calculated by our speed sensor system, as shown in the graph below (right)

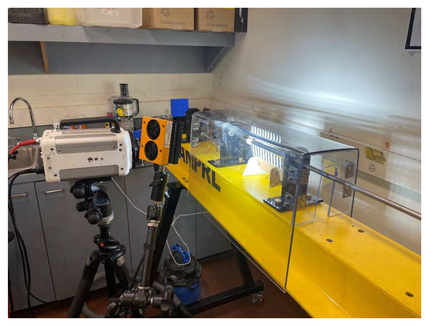

Camera setup viewing the specimen chamber

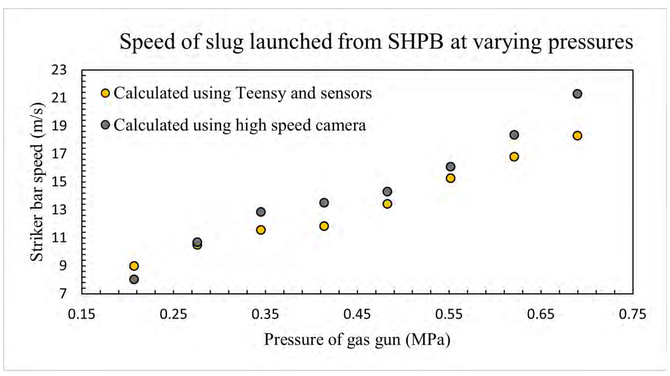

Results

Samples without voids present (microscope)

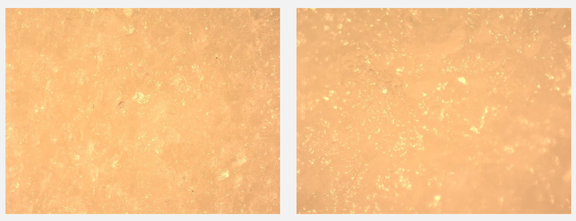

Samples with voids present (microscope)

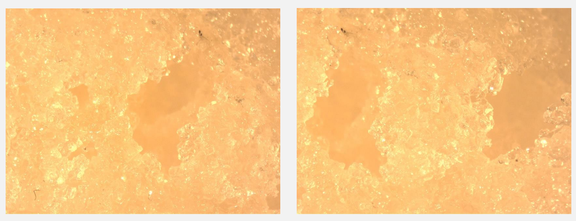

- **Sample 1 (80% sugar, 20% binder, no voids, cut to size) hit at 0.138 MPa in the SHPB**

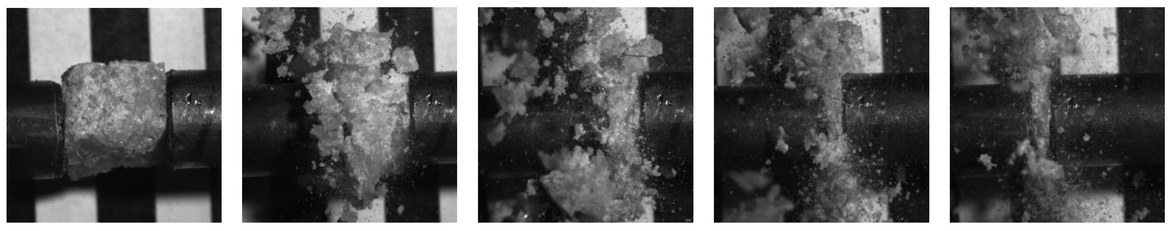

time = 0.0000 sec | time = 0.0025 sec | time = 0.0050 sec | time = 0.0075 sec | time = 0.0100 sec

- **Sample 2 (60% sugar, 40% binder, no voids) hit at 0.138 MPa in the SHPB, strain rate = 60.9756 s^{-1}**

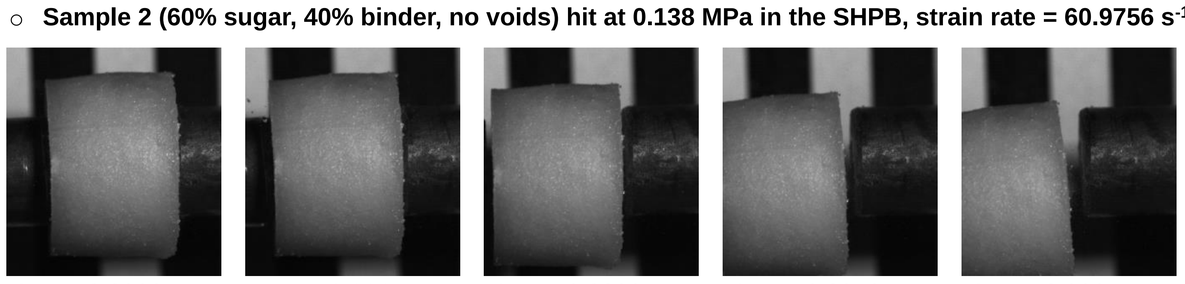

time = 0.0000 sec | time = 0.0017 sec | time = 0.0033 sec | time = 0.0050 sec | time = 0.0067 sec

- **Sample 3 (60% sugar, 40% binder, no voids) hit at 0.345 MPa in the SHPB**

time = 0.0000 sec | time = 0.0033 sec | time = 0.0067 sec | time = 0.0100 sec | time = 0.0133 sec

- **Sample 4 (60% sugar, 40% binder, voids present, cut to size) hit at 0.207 MPa in the SHPB, strain rate = 83.6172 s^{-1}**

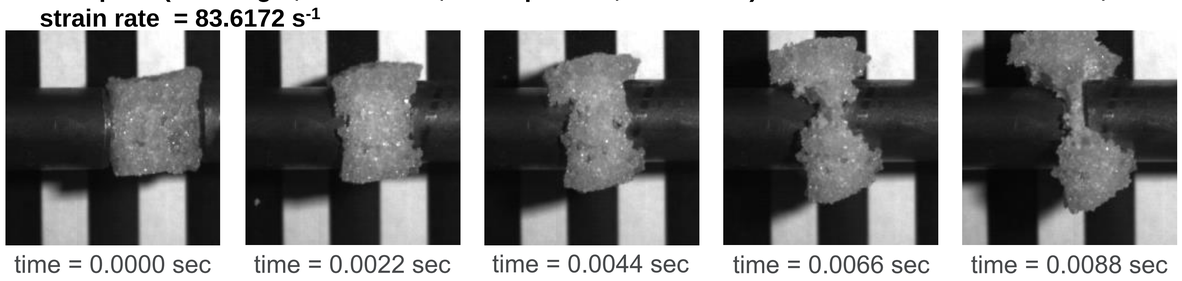

time = 0.0000 sec | time = 0.0022 sec | time = 0.0044 sec | time = 0.0066 sec | time = 0.0088 sec

Conclusion

Able to generate voids within the PBS composite using the binder-jetting 3D printer. We can see from the strain rate of the samples that having voids in the sample increased dynamic sensitivity. To this end we also successfully created a testing rig for finding speed and the optimal camera setup on the SHPB, verifying our sensor speed with that from the camera.

- **Future Directions:**
  - Create samples with varying void patterns and test them using the SHPB or an alternate experimental setup
- **Acknowledgment:**
  - We thank the support from National Science Foundation (Grant No. 2236905) and Air Force Office of Scientific Research (Grant No. FA9550-24-1-0147)

References

Kirby, L., Lawrence, A., Udaykumar, H., Sippel, T., & Song, X. (2023). Pressure-assisted binder jet additive manufacturing of solid propellants. *Additive Manufacturing*, 77, 103808. https://doi.org/10.1016/j.addma.2023.103808

Xiao, Y., Fu, Q., Yu, W., Fan, C., Zou, Y., & Sun, Y. (2024). Experimental and numerical investigation of dynamic damage and load transfer of PBX substitute material under low velocity impact. *Polymers*, 16(9), 1235. https://doi.org/10.3390/polym16091235

Comparison of Renewal Subtypes of Challenging Behavior at an Intensive Outpatient Clinic

Yueyi (Ella) Guan[1], Matthew J. O'Brien[2], PhD, Alex Pauls[2], MA

[1]Amador Valley High School, CA, [2]University of Iowa, IA

IOWA HEALTH CARE
Stead Family Children's Hospital

Introduction

- Severe challenging behaviors (CB; e.g., self-injurious behavior (SIB), aggression, destruction, and severe generalized refusal) are observed in 10 to 20% of children in the U.S.[1,2] Children with intellectual and developmental disabilities (IDDs) are even more likely to engage in challenging behavior.[3,4]
- Treatments based on the principles of applied behavior analysis (ABA), such as functional communication training (FCT), are highly effective at reducing CB and increasing adaptive behaviors in children with IDDs and autism.[5]
- However, context changes (e.g. change in the treatment setting or implementer) encountered during treatment commonly produce recurrence of previously reduced CB.[6,7] This phenomenon is called renewal.
- In basic laboratory research, ABA renewal (relapse following a familiar context change) is considerably stronger than ABC renewal (relapse following a novel context change).[8]
- Previous applied research has not evaluated ABA and ABC renewal data separately.

The purpose of this study was to retrospectively examine instances of renewal in an intensive outpatient clinic and determine if there are differences in prevalence and persistence of behavioral relapse following a novel (i.e., ABC renewal) or familiar (i.e., ABA renewal) context change.

Methods

Participants and Setting

The study sample included 98 individuals (74 male, 24 female) who exhibited CB and received 30-45 hours of behavioral therapy in an intensive outpatient clinic within an academic medical center. Ages ranged from 2 to 27 years (M = 8.3, SD = 4.6). The study sample was 83% White, 8% Black, 3% Asian, and 6% multiple races. Fifty-two percent of patients had IDD, and 61% had autism spectrum disorder.

Data Analysis

Data were collected on rates of CB in 5 min treatment sessions for all patients. Setting and therapist changes were coded as ABA or ABC renewal opportunities based on whether the context change was a familiar (e.g., home, school, parent, teacher) or novel (e.g., new therapy room, new clinician) context. Renewal was determined using Muething et al. (2020) criteria and the point of renewal (i.e., 1st, 2nd or 3rd post-change session) was recorded. Persistence of renewal effects for each instance of renewal was calculated as the number of consecutive post-change sessions where the rate of CB was above pre-change sessions. Comparison of the persistence of renewal effects between ABA and ABC incidents was done using an independent samples *t*-test. To compare the prevalence of ABA and ABC renewal, chi squared tests, with a Yate's Continuity Correction, were utilized. All analyses were performed in R version 4.3.3.

Results

A total of 540 context changes were observed, and renewal occurred in 136 (25.2%) of those changes.

A **Table 1.** Prevalence of Renewal by Subgroups

	Prevalence of ABA Renewal (# of Subgroup Context Changes)	Prevalence of ABC Renewal (# of Subgroup Context Changes)
All Context Changes	26.1% (333)	23.7% (207)
Person Context Changes Only	26.3% (251)	23.8% (172)
Setting Context Changes Only	25.6% (82)	22.9% (35)

There was not a statistically significant difference between ABA and ABC renewal sequences across settings, X^2 (1, N = 117; p = .93) or therapists X^2 (1, N = 423; p = .74).

B **Figure 1.** Persistence of Renewal

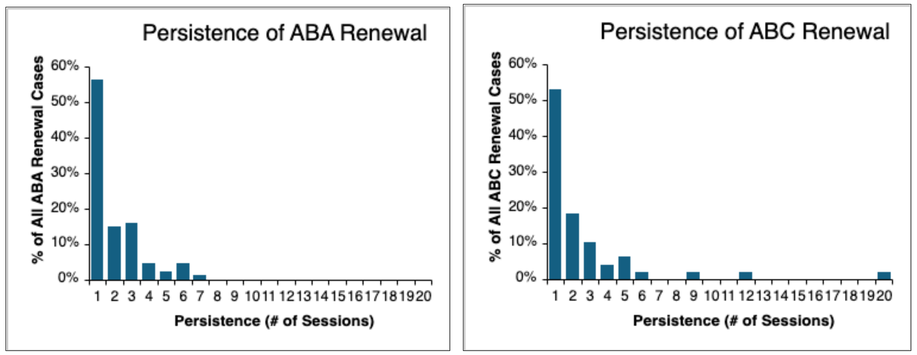

Persistence for ABA renewal (M = 2.87, SD = 2.67) was not statistically different than persistence for ABC renewal (M = 3.39 SD = 3.74), t(134) = 0.927, p = .3.

C **Figure 2.** Point of Occurrence of Renewal

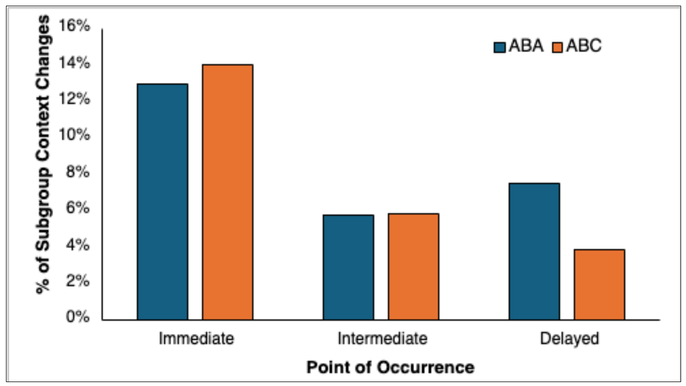

A greater proportion of ABA renewal occurred after the first post-change session than was observed for ABC renewal.

Discussion

- Across our sample, 1 in 4 context changes resulted in relapse; renewal is relatively common. Even with high fidelity, clinicians should be prepared for relapse when context changes occur.
- Persistence of renewal effects was transient (just over 2 sessions in duration, on average), but there were instances of renewal that lasted as long as 20 sessions.
- Nearly half of all instances of renewal did not occur until the second or third session. Clinicians should be prepared for relapse, even without an initial onset.
  - In our sample, delayed renewal was higher within ABA context changes, but this may not generalize across other clinics.
- Prevalence and persistence of renewal **did not differ** between ABA and ABC renewal types. Contrary to findings in basic research, ABA context changes did not bring on increased prevalence of relapse in this applied study.
  - Thus, in practice, clinicians should feel comfortable returning patients to familiar contexts (e.g., parents, home) early in treatment so long as procedures are conducted with high fidelity.

Acknowledgments

I am grateful for the invaluable guidance and support of Matt O'Brien and Alex Pauls. I also want to thank the SSTP program for this great opportunity.

References

1. Bitsko RH. Mental health surveillance among children—United States, 2013–2019. MMWR supplements. 2022;71.
2. Merikangas KR, He JP, Burstein M, Swanson SA, Avenevoli S, Cui L, Benjet C, Georgiades K, Swendsen J. Lifetime prevalence of mental disorders in US adolescents: results from the National Comorbidity Survey Replication–Adolescent Supplement (NCS-A). Journal of the American Academy of Child & Adolescent Psychiatry. 2010 Oct 1;49(10):980-9.
3. Alimovic S. Emotional and behavioural problems in children with visual impairment, intellectual and multiple disabilities. Journal of Intellectual Disability Research. 2013 Feb;57(2):153-60.
4. Poppes P, Van der Putten AJ, Vlaskamp C. Frequency and severity of challenging behaviour in people with profound intellectual and multiple disabilities. Research in developmental disabilities. 2010 Nov 1;31(6):1269-75.
5. Lindgren S, Wacker D, Schieltz K, Suess A, Pelzel K, Kopelman T, Lee J, Romani P, O'Brien M. A randomized controlled trial of functional communication training via telehealth for young children with autism spectrum disorder. Journal of autism and developmental disorders. 2020 Dec;50:4449-62.
6. Falligant JM, Kranak MP, McNulty MK, Schmidt JD, Hausman NL, Rooker GW. Prevalence of renewal of problem behavior: Replication and extension to an inpatient setting. Journal of Applied Behavior Analysis. 2021 Jan;54(1):367-73.
7. Muething C, Call N, Pavlov A, Ringdahl J, Gillespie S, Clark S, Mevers JL. Prevalence of renewal of problem behavior during context changes. Journal of Applied Behavior Analysis. 2020 Jul;53(3):1485-93.
8. Bouton ME, Todd TP, Vurbic D, Winterbauer NE. Renewal after the extinction of free operant behavior. Learning & behavior. 2011 Mar;39(1):57-67.

IOWA HEALTH CARE

Exploring the Association between Anterior Left Temporal Lesions and Psychiatric Symptoms

Alexandra Ally Hatakeyama[1, 2], Brianna McNichol[2], Joel Bruss[3], Daniel Tranel, PhD[2, 5] & Aaron Boes, MD, PhD[2, 3, 4]

[1]Los Alamitos High School, CA; Departments of [2]Neurology [3]Pediatrics, and [4]Psychiatry, University of Iowa Carver College of Medicine, University of Iowa, Iowa City, IA | [5]Department of Psychological and Brain Sciences, University of Iowa, Iowa City, IA

Introduction

Temporal lobe epilepsy (TLE) is the most common focal seizure disorder and affects 50 million individuals globally.

- 30% of TLE are intractable, for which anterior temporal lobectomies (ATL) are the most common treatment.
- Studies show mixed results on ATL's impacts on Psychosis Spectrum Symptoms (PSS) and dysphoric disorders, with some patients improving and others worsening or experiencing de novo developments post-operation.
- Glosser et al. (2000) found that 31% of the patients experienced an exacerbation or new onset of a psychiatric diagnosis after surgery, and specifically, 83% of these patients developed a mood disorder with features exhibiting depression, anxiety, and irritability.

Further research has sought to understand the biological basis of these psychiatric outcomes.

- Lopez et al. (2023) performed multivariate lesion-symptom mapping to understand the biological basis of PSS and found significant associations between the left anterotemporal cortex and right frontal pole lesions.
- Wong et al. (2019) found that significant cortical thinning, a common epilepsy structural abnormality, is strongly associated with positive symptom severity in the left inferior and middle temporal gyrus. This highlights the link between PSS and structural brain abnormalities in the anterior temporal lobe.

Aims

Aim 1: Determine if there are significantly higher number of psychiatric symptoms for individuals after surgical resection when compared to normative data.
Aim 2: Examine the relationship between Minnesota Multiphasic Personality Inventory (MMPI) scales and anterior temporal lobe lesions.

Methods

- 46 individuals who had undergone right or left temporal lobectomies were identified from the Iowa Neurological Patient Registry, and their MMPI-2 data was collected and analyzed.
- Focused on running and analyzing all MMPI-2 scales for preliminary testing.
- Multivariate lesion-symptom mapping was performed using LESYMAP (Pustina et al., 2018) and Sparse Canonical Correlation Analyses to identify associations between anterior left temporal lesions, personality functioning, and PSS as defined by the MMPI-2 scales.

Demographics		Iowa Registry (n=46)
Gender	Women | Men	28 | 18
Years of Education	Mean | SD	13.8 | 2.19
Age at Lesion Onset	Mean | SD	37.2 | 11.8
Race	White | Unknown	45 | 1
Diagnosis	LTL | LIL | RTL | RFL	32 | 1 | 11 | 2
Handedness	L | R | M	5 | 33 | 8

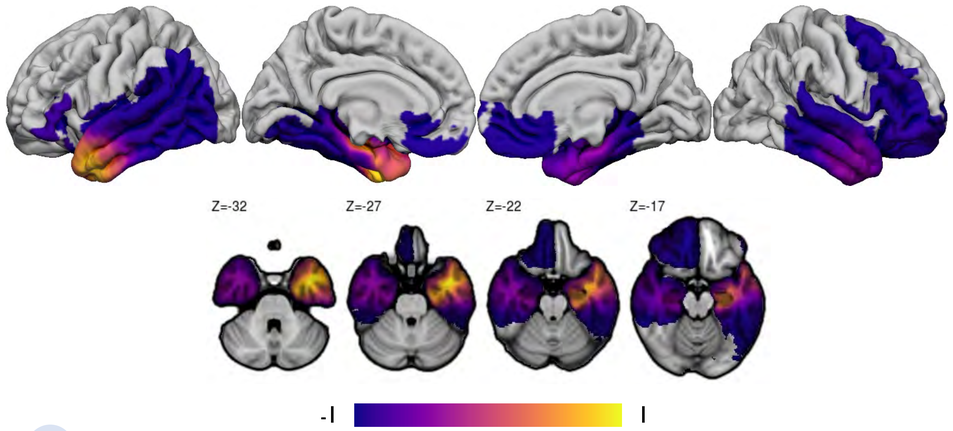

1 **Figure 1. A meta-analysis derived brain network overlap**

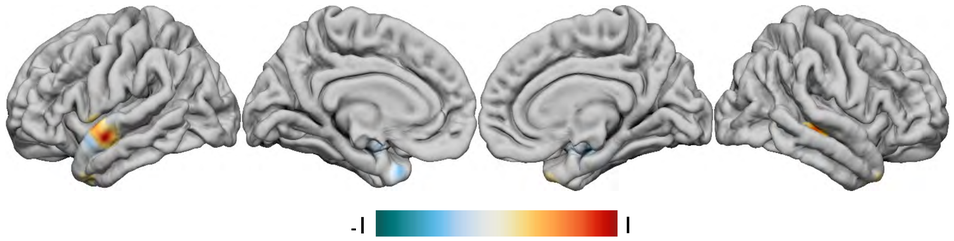

2 **Figure 2. Brain locations associated with MMPI-2 Dep, Depression Scale**

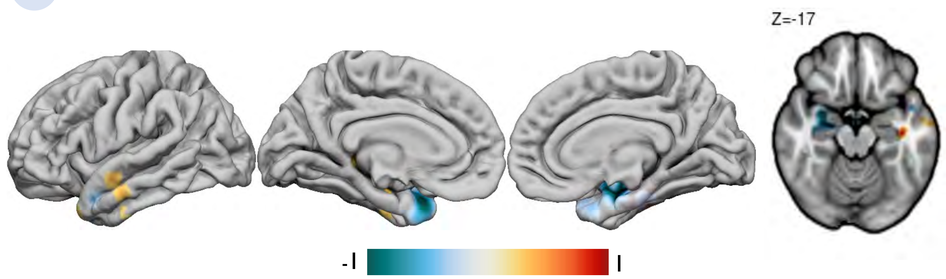

3 **Figure 3. Brain locations associated with MMPI-2 RC4, Psychopathic Deviate Scale**

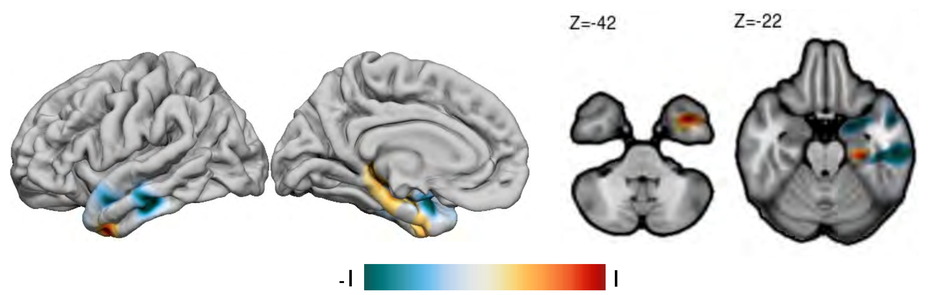

4 **Figure 4. Brain locations associated with MMPI-2 RC9, Hypomania Scale**

Results

We found significant results for the following scales:

- RC1/Hs (Hypochondriasis) scale: $r = .37$, $p < .01$ with higher scores associated with the far inferior insula and temporal operculum.
- RC4 (Psychopathic deviate) scale: $r = .33$, $p < .04$ with higher scores associated with the right basolateral amygdala.
- RC9 (Hypomania) scale: $r = .33$, $p < .03$ with higher scores associated with the left parahippocampal gyrus.
- Dep (Depression) scale: $r = .35$, $p < .02$ with higher scores associated with the superior temporal gyrus on the left side.
- Do (Dominance) scale: $r = .41$, $p < .01$ with higher scores associated with the medial wall and parahippocampal gyrus.
- Pk (PTSD) scale: $r = .40$, $p < .001$ with higher scores associated with the superior temporal gyrus on the right side.

One-tailed direction due to the nature of MMPI scales and scoring.

Discussion

Based on our preliminary findings from LESYMAP, our data shows significant results of elevated scores on several MMPI scales, including (RC4, RC9, DEP, DO, PK), and a strong negative correlation for (AAS). These findings may suggest future areas of interest and psychopathology targets or measures necessary to investigate further in patients after temporal lobe resections. With psychopathology and personality functioning after operations yielding mixed results in past literature, it is important to pursue further efforts to ensure validity. Future research to completely capture pre- and post-op information, differing from our study's focus on chronic patients, regarding personality, psychopathology, and MMPI-2 scores would be of great interest for researchers and healthcare professionals, adding to the literature to further investigate the typical post-operative symptoms and severity for patients with TLE and resections. Additionally, designing longitudinal studies and working with patient families to understand pre- and post-operation differences may be beneficial.

Acknowledgements

I would like to express my gratitude for Brianna McNichol, Dr. Tranel, and the Tranel Lab for their guidance and support on this project. I would also like to thank the University of Iowa and SSTP for this enriching opportunity.

References

1. Glosser, G. (2000). Psychiatric aspects of temporal lobe epilepsy before and after anterior temporal lobectomy. *Journal of Neurology, Neurosurgery & Psychiatry*, *68*(1), 53–58. https://doi.org/10.1136/jnnp.68.1.53
2. Lopez, J. W., Bruss, J., Tranel, D., McCleery, A., & Boes, A. D. (2023). Lesion network localization of psychosis spectrum symptoms. *SOBP Conference*.
3. Pustina, D., Avants, B., Faseyitan, O. K., Medaglia, J. D., & Coslett, H. B. (2018). Improved accuracy of lesion to symptom mapping with multivariate sparse canonical correlations. *Neuropsychologia*, *115*, 154–166. https://doi.org/10.1016/j.neuropsychologia.2017.08.027
4. Wong, T. Y., Radua, J., Pomarol-Clotet, E., Salvador, R., Albajes-Eizagirre, A., Solanes, A., Canales-Rodriguez, E. J., Guerrero-Pedraza, A., Sarro, S., Kircher, T., Nenadic, I., Krug, A., Grotegerd, D., Dannlowski, U., Borgwardt, S., Riecher-Rössler, A., Schmidt, A., Andreou, C., Huber, C. G., & Turner, J. (2019). An overlapping pattern of cerebral cortical thinning is associated with both positive symptoms and aggression in schizophrenia via the ENIGMA consortium. *Psychological Medicine*, *50*(12), 2034–2045. https://doi.org/10.1017/s0033291719002149

Establishment of the First Paired Normal and Tumor Endometrial Cell Lines Using Conditional Reprogramming

William Cheung Ho[1]; Tianyue Li[2]; Shujie Yang, PhD[2]
[1]Phillips Exeter Academy, NH; [2]Department of Pathology, University of Iowa

Introduction

Endometrial cancer is the only cancer for which the survival rate has decreased over the past 40 years and is the fourth most diagnosed cancer among women (Siegel et al., 2024).

Current landscape:

❖ The currently available endometrial normal and tumor cell lines often do not accurately represent cells *in vivo*, resulting in disparities between *in vitro* and clinical drug testing results (Rush et al., 2022).

❖ There are no paired normal and tumor endometrial cell lines available at the moment, making it difficult to screen for drug toxicity *in vitro*.

❖ Cell lines are incredibly difficult to establish using standard methods due to cells undergoing senescence and a lack of proliferation, making next-generation techniques a necessity.

Research Question:

Can the conditional reprogramming technique facilitate the generation of paired (normal and tumor) endometrial cell lines?

Conditional Reprogramming:

Conditional Reprogramming (CR) is a next generation cell culturing technique that involves co-culturing normal or tumor cells with J2 mice fibroblast feeder cells a ROCK inhibitor, allowing cells to achieve a stem-cell-like state and proliferate rapidly (Liu et al., 2017).

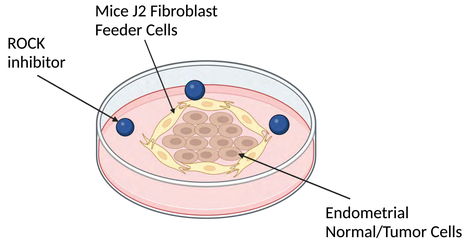

Figure 1: Co-culture of normal/tumor cells in the presence of the ROCKi

Objective

Use the Conditional Reprogramming technique to establish paired normal and tumor endometrial cell lines from the same patient, facilitating *in vitro* drug toxicity testing.

Theory and Mechanism

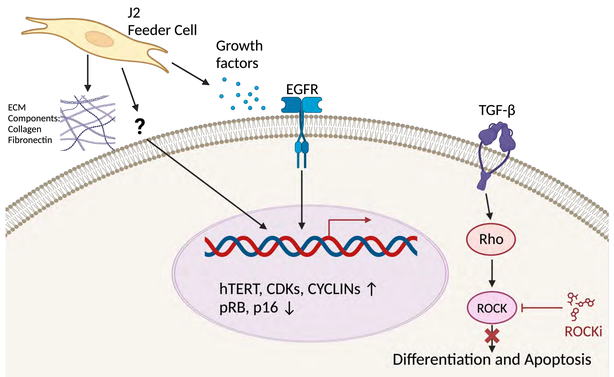

Figure 2: Function of J2 feeder cells and ROCKi

Underlying Mechanism:

❖J2 cells: hTERT activation, cell cycle acceleration, enhanced growth, ECM components (Wu et al., 2020).

❖ROCK inhibitor: Inhibition of apoptosis and Rho/ROCK mediated differentiation, cell cycle acceleration (Wu et al., 2020).

The stem-cell-like state of cells that undergo CR results in a significantly faster proliferation rate, allowing for the establishment of cell lines.

Upon changing to standard cell culture media, the cells revert to their original cell type and phenotype (Wu et al., 2020).

Methodology

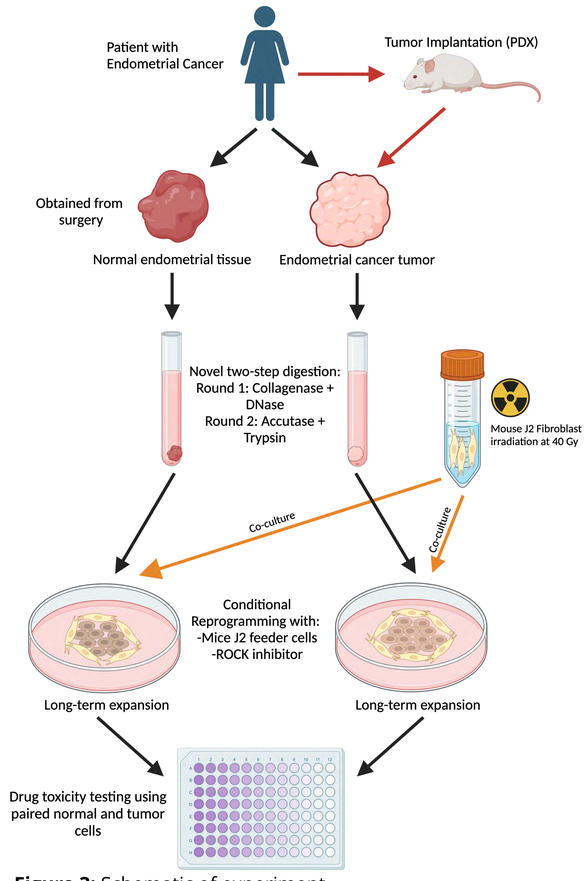

Figure 3: Schematic of experiment

Results

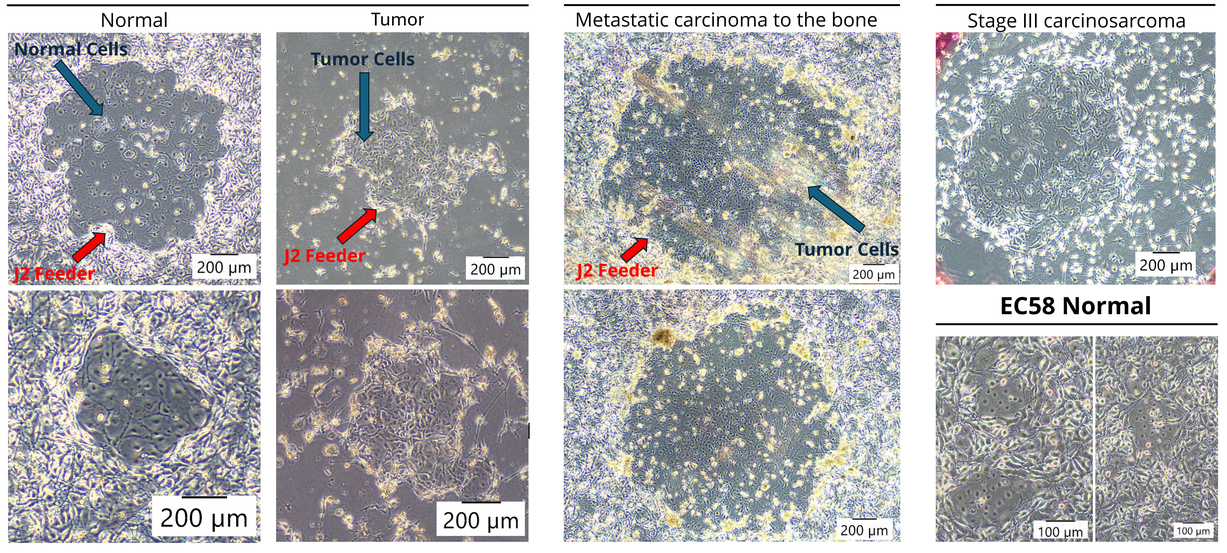

Conclusion

This study established the first paired normal and tumor endometrial cell lines, which can serve as an essential tool for drug toxicity screening and the creation of targeted chemotherapeutics with reduced side effects.

Future Directions

❖Continue to grow cell lines to full confluency and multiple passages.

❖Establish additional paired cell lines from patient samples.

❖Verify cells using immunofluorescence staining for endometrial epithelial markers such as claudin-11 and mucin-1.

❖Use a 96-well plate to screen for drug toxicity, facilitating the examination of the effects that chemotherapies have on normal cells while simultaneously testing for drug effectiveness.

References

Liu, X., Krawczyk, E., Suprynowicz, F. A., Palechor-Ceron, N., Yuan, H., Dakic, A., Simic, V., Zheng, Y.-L., Sripadhan, P., Chen, C., Lu, J., Hou, T.-W., Choudhury, S., Kallakury, B., Tang, D. G., Darling, T., Thangapazham, R., Timofeeva, O., Dritschilo, A., … Schlegel, R. (2017). Conditional reprogramming and long-term expansion of normal and tumor cells from human biospecimens. *Nature Protocols*, *12*(2), 439–451. https://doi.org/10.1038/nprot.2016.174

Rush, C. M., Blanchard, Z., Polaski, J. T., Osborne, K. S., Osby, K., Vahrenkamp, J. M., Yang, C.-H., Lum, D. H., Hagan, C. R., Leslie, K. K., Pufall, M. A., Thiel, K. W., & Gertz, J. (2022). Characterization of HCI-EC-23 a novel estrogen- and progesterone-responsive endometrial cancer cell line. *Scientific Reports*, *12*(1). https://doi.org/10.1038/s41598-022-24211-8

Siegel, R. L., Giaquinto, A. N., & Jemal, A. (2024). Cancer statistics, 2024. *CA: A Cancer Journal for Clinicians*, *74*(1), 12–49. https://doi.org/10.3322/caac.21820

Wu, X., Wang, S., Li, M., Li, J., Shen, J., Zhao, Y., Pang, J., Wen, Q., Chen, M., Wei, B., Kaboli, P. J., Du, F., Zhao, Q., Cho, C. H., Wang, Y., Xiao, Z., & Wu, X. (2020). Conditional reprogramming: Next Generation Cell Culture. *Acta Pharmaceutica Sinica B*, *10*(8), 1360–1381. https://doi.org/10.1016/j.apsb.2020.01.011

Acknowledgements

A huge thank you to Dr. Yang and Tianyue Li for all your invaluable mentorship and support.

This project was supported by NIH R37-CA238274 (SY) and the Department of Pathology Start-Up Fund (SY).

Polymerization of Hydrazides to Yield Colorful Polymers with Conjugated -NS- and -NSS- Backbones

Zikun Hu[1], Shanari Wickremasinghage, Graduate[2], Ned Bowden, PhD[2]

[1]Shanghai World Foreign Language Academy, [2]Department of Chemistry, University of Iowa

Introduction

Biodegradable and Electrically Conductive Polymers (BECPs)

- Biomaterial compatible with & degradable in the biological environment
- Have great engineering properties, e.g. chemical stability & electrical conductivity
- Application in medical materials, pharmaceuticals, diagnostics *(Jadoun et al., 2020)*

Polymeric metal -- Polythiazyl $(SN)_x$

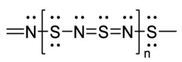

Fig. 1. Polythiazyl Structure (Goehring et al., 1953)

- Conjugated alternating S-N bond
- Great electrical properties & conductivity
- Propose a new structure motif for polymer chemistry

Synthesis of S-N containing polymers

- Polymers with NSSN backbones has excellent power density, e.g. poly[bis(phenylamino)disulfide]
- S-N bond containing polymer also found to be biodegradable, e.g. polydiaminosulfides

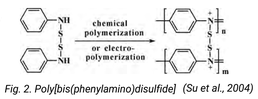

Fig. 2. Poly[bis(phenylamino)disulfide] (Su et al., 2004)

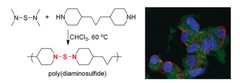

Fig. 3. Polydiaminosulfides *(Yoo et al., 2012)*

Poly[(*N*,*N*-phenylamino)disulfides]

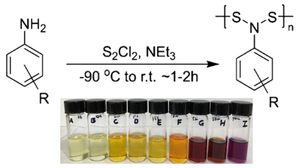

Fig. 4. Synthesis of Poly-NADs *(Grace et al., 2021)*

Poly[(*N*,*N*-amino)sulfide]

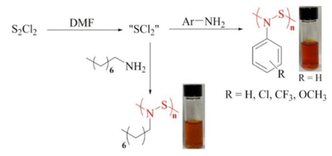

Fig. 5. Synthesis of Poly-NAS *(Paudel et al., 2023)*

Research Question

What is the result of reacting hydrazides with sulfur monochloride and sulfur dichloride?

Methodology

Synthesis and Isolation of Polymers

N_2 Purge → Cool to -90℃ (NSS) / Cool to -61℃ (NS) → Hydrazide addition → Warm at r.t.

NSS Polymers
S_2Cl_2 + THF, N_2

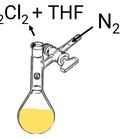

Liquid N_2 + Acetone cooling bath

Hydrazides THF, NEt_3

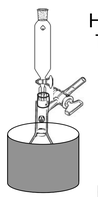

NS Polymers
S_2Cl_2 + DMF

$CHCl_3$ + dry ice cooling bath

Hydrazides DMF, NEt_3

Isolation of Polymers

NSS Polymers

Vacuum Filtration → Rotary Evaporator → Precipitation in water → High Vacuum

Spectroscopy & Characterization Techniques

^{1}H NMR	UV-Vis	SEC-MALS

Results & Discussion

NSS Polymerization

General NSS Hydrazide Polymerization Scheme

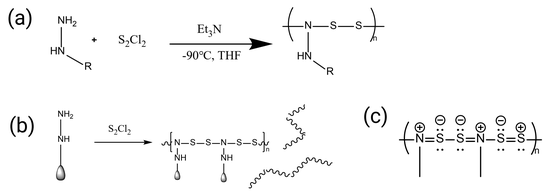

Fig. 6. a) Basic polymerization of hydrazides derivatives b) Schematic of polymerization process and result c) –NSS- conjugated backbone

Monomers Used:

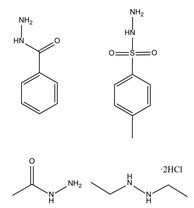

Fig. 7. Monomers used

Characterizations

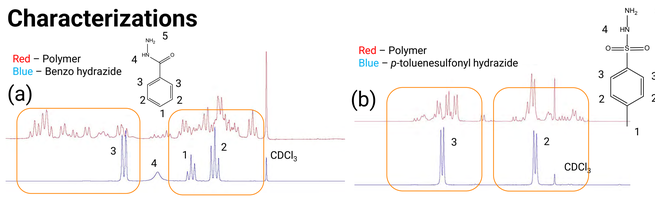

Fig. 8. ^{1}H NMR for a) polymer of benzohydrazide b) polymer of p-toluenesulfonyl hydrazide. From the elimination of sharp peaks from monomers and occurrence of broad peaks both polymerization has occurred successfully

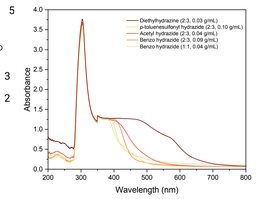

Fig. 9. UV-vis spectrum for NSS polymers

Molar mass of polymers

Monomer	Ratio	Color	Molar mass (g/mol)
Benzo hydrazide	1:1	Yellow	---
	1:1.5	Orange-red	4280
p-toluenesulfonyl hydrazide	1:1.5	Yellow	8214

Table 1. Benzo hydrazine and p-toluenesulfonyl hydrazine polymers' molar mass

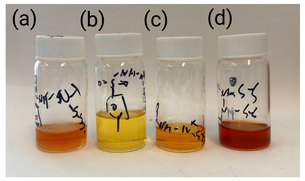

Fig. 10. (a-d) NSS Polymers of benzo hydrazide, p-toluenesulfonyl hydrazide, acetyl hydrazide, diethylhydrazine

Further Hypothesis

For 2:3 ratio, the proposed schematic diagram of polymer is highly crosslinked.

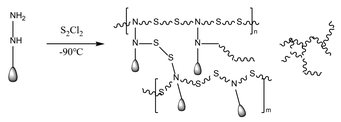

However, the crosslinked polymer is not shown by the low molecular weight.

According to new molecular weight, we proposed a new hypothesis of cyclization.

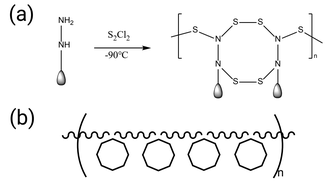

Fig. 11. a) Cyclization hypothesis b) Schematic of new polymerization and cyclization hypothesis

NS Polymerization

General NS Hydrazide Polymerization Scheme

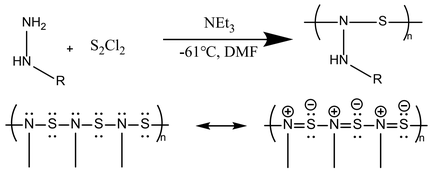

Fig. 12. Schematic of polymerization of diamine derivatives to yield -NS- conjugated backbone polymers

Characterizations

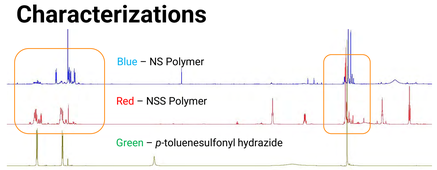

Fig. 13. ^{1}H NMR comparison of NS and NSS polymers of p-toluenesulfonyl hydrazide

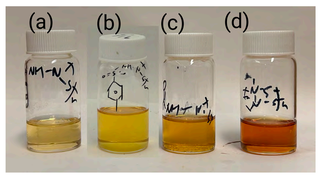

Fig. 14. (a-d) NS Polymers of benzo hydrazide, p-toluenesulfonyl hydrazide, acetyl hydrazide, diethylhydrazine

New hypothesis

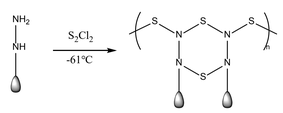

Similar to above, the synthesis of NS backbone with 2:3 ratio is suggested to have cyclization, but needs further prove from characterizations.

Colorful polymers such as these with conjugated -NS- and -NSS- backbone are stable in organic solvents and potentially poses no toxicity to cells. They are ideal materials for applications including drug delivery, medicine and fertilizer as well as biocompatible devices.

Conclusion & Future Works

Conclusions

- **Polymers with conjugated –NS– and –NSS– backbones** were produced, and their synthesis was confirmed using ^{1}H NMR and GPC.
- The colors of these polymers arise from their **conjugated backbone** that has an **energy band gap in the visible light range**, confirmed using UV-vis.
- **Different ratio** & **reaction time** affected polymer characteristics and molar mass.
- A hypothesis for formation **of 8-membered ring** during polymerization is proposed.

Future Works

- Use elemental analysis to confirm the cyclization during polymerization.
- Methods for improving electrical conductivity and biocompatibility of polymers.

Acknowledgements

Thanks Prof. Bowden and Shanari Wickremasinghage for mentoring and supporting me on this project. Thanks to all members in Bowden's Group for extra help.

References

Arjun Paudel, Campbell, E. J., Van, W. Z., Otting, G. W., Shepherd, J. J., & Bowden, N. B. (2023). Polymerization of Primary Amines with Sulfur Monochloride to Yield Red Polymers with a Conjugated SN Backbone. Macromolecules, 56(10), 3721–3730. https://doi.org/10.1021/acs.macromol.2c02507

Goehring, M., & Voigt, D. (1953). Über die Schwefelnitride (SN)2 und (SN)x. Naturwissenschaften, 40(18), 482–482. https://doi.org/10.1007/bf0062899

Grace, J. P., Flitz, E. S., Dae Sun Hwang, & Bowden, N. B. (2021). Polymerization of Aniline Derivatives to Yield Poly[N,N-(phenylamino)disulfides] as Polymeric Auxochromes. Macromolecules, 54(22), 10405–10414. https://doi.org/10.1021/acs.macromol.1c01548

Jadoun, S., Riaz, U., & Budhiraja, V. (2020). Biodegradable conducting polymeric materials for biomedical applications: a review. MEDICAL DEVICES & SENSORS. https://doi.org/10.1002/mds3.10141

Su, Y., Niu, Y., Xiao, Y.-Z., Xiao, M., Liang, Z., & Gong, K. (2004). Novel conducting polymer poly[bis(phenylamino)disulfide]: Synthesis, characterization, and properties. Journal of Polymer Science Part A, 42(10), 2329–2339. https://doi.org/10.1002/pola.2007

Yoo, J., D'Mello, S. R., Graf, T. A., Salem, A. K., & Bowden, N. B. (2012). Synthesis of the First Poly(diaminosulfide)s and an Investigation of Their Applications as Drug Delivery Vehicles. Macromolecules, 45(2), 688–697. https://doi.org/10.1021/ma2023167

IOWA

Integrating Obstruction Removal into a Raspberry Pi-based Camera to Improve Stream Stage Monitoring

[1]Colin Hu, [2]Omer Mermer, [2]Yusuf Sermet, [2,3]Ibrahim Demir

[2]University of Iowa, Department of Hydroinformatics, [2]IIHR-Hydroscience and Engineering, University of Iowa, Iowa City, Iowa, USA, [3]Electrical and Computer Engineering, University of Iowa, Iowa City, Iowa, USA

Introduction

- Water-related natural disaster have caused over 300,000 fatalities and over $1. Trillion USD in economic damages worldwide from 2001 to 2018 (Lee et al., 2020)
- Reliable, real -time monitoring of water sources is essential to reduce property damages and casualties but is often hindered by the high cost of sensors and rain gauges (Sermet & Demir, 2023; Wagner et al., 2023)
- Federal and state agencies in the US currently use sensors costing $3,000 $15,000 with anural maintenance costs ranging from $1,000 to $15,000 (Sermet & Demir, 2023)

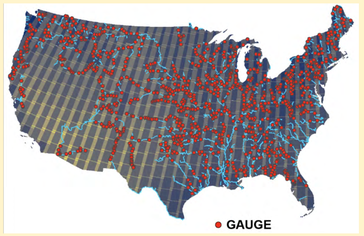

Figure 1. Diagram of all United States Geological Survey streamgages within the US (Allen et al., 2020)

- A Raspberry Pi-based camera system, including necessary components, could operate at a few hundred dollars (Sermet & Dermir, 2023)
- Machine learning techniques can remove obstructions from camera images, mahjong them more reliable (Liu et al., 2020)
- Using machine learning models like U-Nets, cameras can focus on water levels by identifying bodies of water (Fathi & Moradkhani, 2022)

Research Goals

By utilizing a **Raspberry Pi-based camera sensor**, coupled with a machine learning technique to **remove obstructions** (reflections, raindrops, etc.), it is possible to create a **much cheaper** stream stage sensor that will be able to **cover more** water bodies and support environmental monitoring and decision-making. The camera would be integrated into the Iowa Flood Information System (IFIS) where experts would be able to set up their own sensors by implementing the coordinates of their sensor and setting time intervals (e.g every 5 minutes) for the camera to **analyze** the river stream stage.

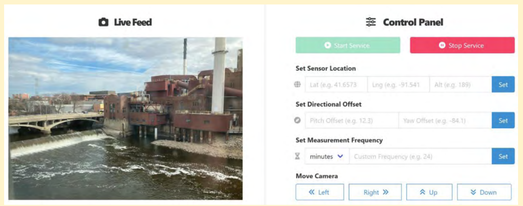

Figure 2. Demonstration of the flask web application **(Sermet & Demir, 2023)**

Methods

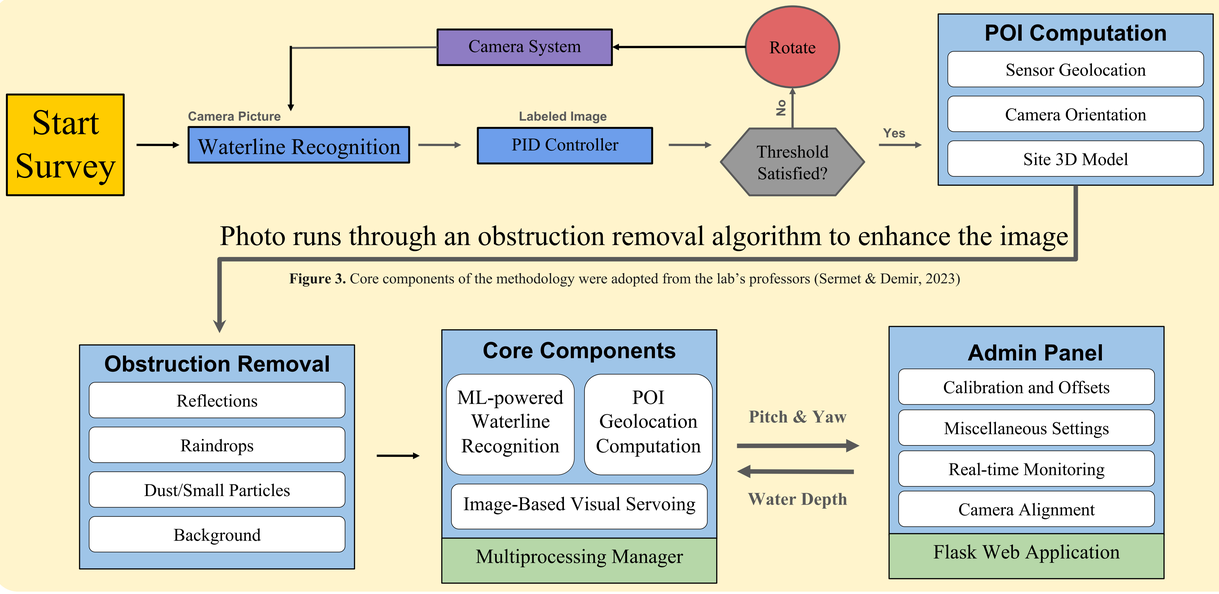

Figure 3. Core components of the methodology were adopted from the lab's professors (Sermet & Demir, 2023)

Preliminary Results

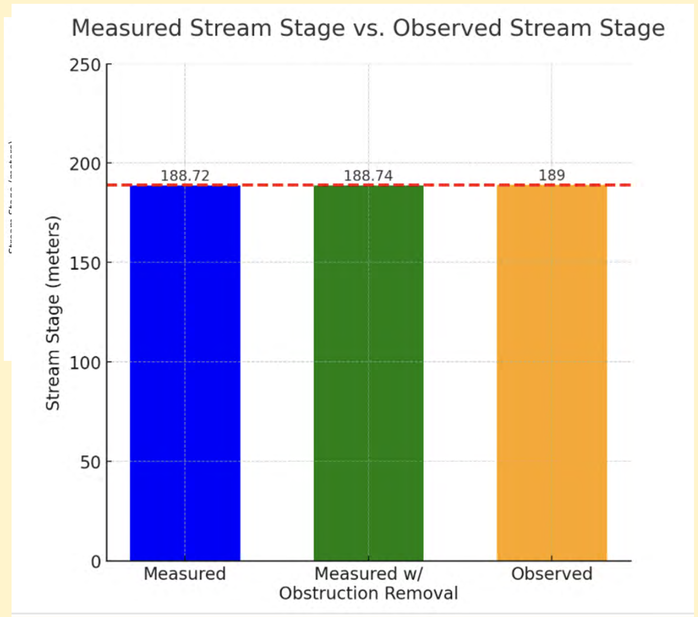

Figure 4. Bar graph demonstrating the measured heights between each model and the ground truth

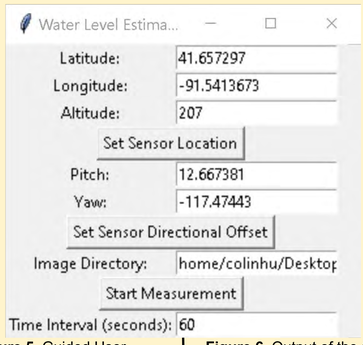

Figure 5. Guided User Interface (GUI) for experts to input their own sensors

Figure 6. Output of the GUI with a full display of the Estimated POI's coordinates

```
 * Serving Flask app 'stage-sensor-web-panel'
 * Debug mode: off
WARNING: This is a development server. Do not use it in a production d
eployment. Use a production WSGI server instead.
 * Running on http://127.0.0.1:8000
Press CTRL+C to quit
2024-07-23 20:55:26.727285: I tensorflow/core/platform/cpu_feature_gua
rd.cc:193] This TensorFlow binary is optimized with oneAPI Deep Neura
 Network Library (oneDNN) to use the following CPU instructions in per
formance-critical operations:  AVX AVX2
To enable them in other operations, rebuild TensorFlow with the approp
riate compiler flags.
1/1 [==============================] - 1s 571ms/step
Estimated POI: (41.657666244, -91.5404815, 188.719804635763)
Water level: 188.719804635763
```

Discussion

- The measured water level height had a percent error of 0.1487% without the obstruction removal algorithm; on the other hand the measured water level height had a percent error of 0.1376%.
- This very small difference can be attributed to the fact that only one image was used as a test case rather than an entire live video feed (time restraint).
- Nonetheless, the algorithm was able to outperform previous models that did not remove obstructions from photos, demonstrating the effectiveness and suitability for a cheap but also accurate stream stage sensor; more tests will be done in the future to ensure that the obstruction removal algorithm is successful.

Future Research

- Although the obstruction removal algorithm is able to account for smaller things like dust particles or rain droplets, it should also be adjusted to account for boats or large floating objects (such as a log).
- Instead of using a Proportional-Integral-Derivative (PID) controller a Convolutional Neural Network (CNN) can be used to adjust the camera's movement with one single motion with each model being tuned to the camera's location (POI distance and environmental factors).
- Add more case studies to determine effectiveness in different areas

Acknowledgements

I would like to extend my gratitude to the UIHI Lab and Dr. Demir for the opportunity to participate and contribute to this project. I am profoundly grateful to the SSTP program for offering this invaluable experience. My heartfelt thanks go to the Belin-Blank Center and the University of Iowa for organizing this year's summer research program. Lastly, I would like to thank Dr. Sermet and Dr. Mermer for their constant communications and their everlasting support. The success of this project would not have been possible without their expertise and guidance.

References

Allen, G. H., Yang, X., Gardner, J., Holliman, J., David, C. H., & Ross, M. (2020). Timing of landsat overpasses effectively captures flow conditions of large rivers. *Remote Sensing*, *12*(9), 1510. https://doi.org/10.3390/rs12091510

Lee, J., Perera, D., Glickman, T., & Taing, L. (2020). Water-related disasters and their health impacts: A global review. *Elsevier*, *8*. https://doi.org/10.1016/j.pdisas.2020.100123

Liu, Y. L., Lai, W. S., Yang, M. H., Chuang, Y. Y., & Huang, J. B. (2020). Learning to see through obstructions. *CVPR*, 14215-14224. https://www.cmlab.csie.ntu.edu.tw/yulunliu/ObstructionRemoval

Moradkhani, K., & Fathi, A. (2022). Segmentation of waterbodies in remote sensing images using deep stacked ensemble model. *Applied Soft Computing*, *124*, 109038. https://doi.org/10.1016/j.asoc.2022

Sermet, Y., & Demir, I. (2023). Camera-based intelligent stream stage sensing for decentralized environmental monitoring. *Journal of Hydroinformatics*, *25*(2), 163-173. https://doi.org/10.2166/hydro.2023.032

Wagner, F., Eltner, A., & Maas, H.-G. (2023). River water segmentation in surveillance camera images: A comparative study of offline and online augmentation using 32 cnns. *International Journal of Applied Earth Observation and Geoinformation*, *119*, 103305. https://doi.org/10.1016/j.jag.2023

Xue, T., Rubinstein, M., Liu, C., & Freeman, W. T. (2015). A computational approach for obstruction-free photography. *ACM Transactions on Graphics*, *34*(4), 1-11. https://doi.org/10.1145/2766940

Measuring Graft Tunnel Diameters and Placement after ACL Reconstruction from Weight Bearing CT Scans

Kaylee Hwang,[1,2] Tyce C. Marquez,[2] Donald D. Anderson[2]
[1]College of Education, [2]Department of Orthopedics & Rehabilitation, University of Iowa

IOWA College of Education
Belin-Blank Center

Introduction

- The anterior cruciate ligament (ACL) connects the femur to the tibia and helps to stabilize the knee joint (Figure 1). [1]
- ACL tears are common in sports that put significant stress on the knee. [2]
- ACL injuries account for approximately 50% of all knee injuries and often require ACL reconstruction (ACLR) [3], which is typically done arthroscopically.
- Around 50% of those who suffer an ACL injury later develop post-traumatic osteoarthritis. [4]
- During ACLR, remnants of the damaged ACL are removed and replaced with a tissue graft (taken from another part of the patient's body or a donor).
  - This involves drilling tunnels in the femur and tibia to secure the graft. [5]
- Tunnel placement can influence outcomes, and the way in which tunnels are placed varies among surgeons and across cases.
- Weight-bearing CT (WBCT) captures images of a joint while the patient is standing (Figure 2), allowing for 3D assessment of the knee under natural weight-bearing conditions [6] and visualization of tunnel placement.

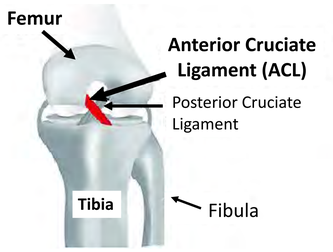

Figure 1. Diagram of an intact knee [Wahid et al., 2020]

Figure 2. Weight bearing knee pose were obtained using weight bearing CT scans.

Objective

Develop a process to analyze WBCT scan data from ACL reconstruction patients to measure tunnel diameter and orientation.

Methods

- WBCT scans of the knee acquired from 4 patients
  - Positions: semi-flexed (~20°) and fully extended
  - Time points: 3 months and 1 year
- Bone tunnels for all tibia and femur ACLR models were segmented using Materialise Mimics software.
- Cylinders were fit to bone tunnels using the MATLAB pcfitcylinder function.
- Each of the models for the tibia and femur were aligned to a template intact knee model using a non-rigid iterative closest point algorithm.
- Fitted cylinders were then transformed to match the aligned ACLR model.
- A coordinate system was established on the intact tibia and femur models (Figures 3 and 4).
- Tunnel orientation angles were measured from the cylinder axis to the XYZ axes using MATLAB.

Methods (cont'd)

Figure 3. Tibia coordinate system

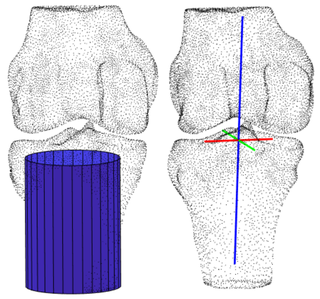

1. X-axis: Line connecting midpoints of the two compartments of the tibial plateau
2. Z-axis: The central axis of cylinder fit to the tibial shaft
3. Y-axis: Cross product of x and z axes

Figure 4. Femur coordinate system

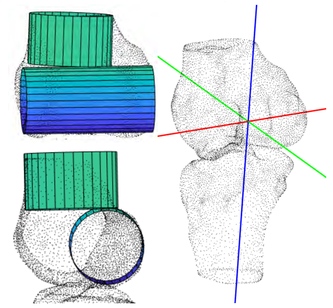

1. X-axis: Central axis of cylinder fit to the two femoral condyles
2. Y-axis: Cross product of x-axis and central axis of cylinder fit of femoral shaft
3. Z-axis: Cross product of x and y axes

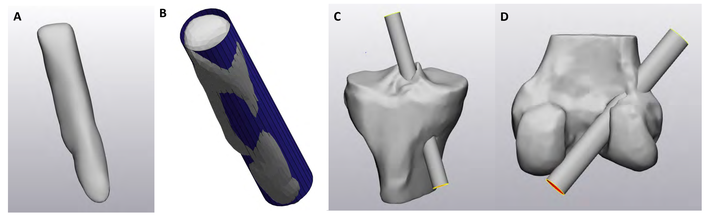

Figure 5. A: ACLR tunnel from tibia model. **B:** Cylinder fit to the tunnel. **C:** Fitted cylinder placed into the tibia model. **D:** Fitted cylinder placed into the femur model.

Results

Figure 6. A, B: Tunnel diameters measured with MATLAB for each model at 3 months and 1 year.

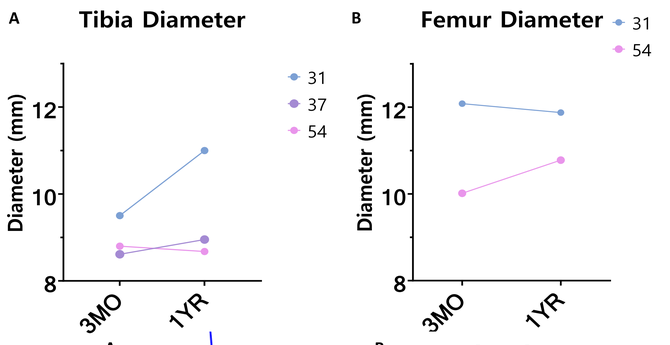

Figure 7. A: Central axes of cylinder fits plotted in cyan on the tibia and femur coordinate systems

B: X-axis angles measured to the closest x-axis; angles to y and z axes measured relative to their positive directions.

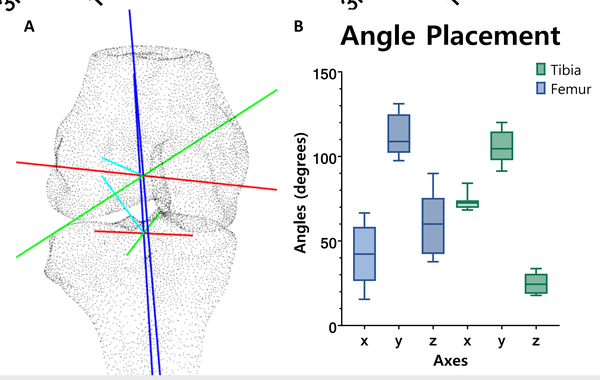

Discussion

- Mimics and MATLAB were effective in analyzing ACLR tunnel diameter and placement.
- Tunnel diameters changed over time. Notably, for patient 31 the tibia tunnel was enlarged by 1.5mm at 1 year compared to at 3 months.
- We observed greater variability in femur angle placements compared to tibia placements.
- The femur tunnel diameters are greater than the tibia tunnel diameters.
- Tibia tunnel X-angle values clustered closely, with one outlier.
- Limitations of this study:
  - The cylinder fitting process requires manual user input, which could introduce variability.
  - The tunnel segmentation may have had an impact on the diameters, depending on how much was taken off the surface when smoothing it.
  - Our small sample size limits our ability to draw conclusive findings.
  - The non-rigid ICP function failed for one model.
- Future directions:
  - Work towards automating the process to reduce manual input.
  - Using a larger dataset would allow us to better analyze tunnel diameter changes over time and compare differences between flexed and extended states.
  - Explore correlations between tunnel placement and diameter with future complications, such as osteoarthritis and re-operation rates.

Acknowledgements

This research was supported by a grant from the Arthritis Foundation (Award #851789).

Arthritis Foundation®

- Research conducted in the Orthopedic Biomechanics Laboratory

References

1. Yoo H & Marappa-Ganeshan R. (2024). In *StatPearls*. StatPearls Publishing. https://www.ncbi.nlm.nih.gov/books/NBK559233/
2. Mayo Clinic. (n.d.). ACL injury. https://www.mayoclinic.org/diseases-conditions/acl-injury/symptoms-causes/syc-20350738
3. Joseph AM, et al. (2013). *J Athletic Training*, 48(6), 810–817. https://doi.org/10.4085/1062-6050-48.6.03
4. Lohmander LS, Englund PM, Dahl LL, Roos EM. (2007). *Am J Sports Med*, 35(10), 1756-1769. https://doi.org/10.1177/0363546507307396
5. Hospital for Special Surgery. (2024, July 18). https://www.hss.edu/condition-list_acl-surgery.asp
6. Lôbo CFT, Bordalo-Rodrigues M, WBCT International Study Group. (2021). *Acta Ortopedica Brasileira*, 29(2), 105–110. https://doi.org/10.1590/1413-785220212902236939

Love in a Spiral: Sex Ratios and Their Impact on Mating Behavior

Aman Jajodia[1], Clare Mulcahy BS[2], Maurine Neiman, PhD[2]

[1]Piedmont High School, Piedmont, CA
[2]University of Iowa, Department of Biology

Why do we care?

- Sex ratio is an important population-level trait that often varies in nature
- Skewed sex ratio can influence behavior
- Open question: how does sex ratio influence mating behavior when males coexist with both sexual and asexual females?

Why snails?

- *Potamopyrgus antipodarum*
- New Zealand snail that can be sexual (male & females) or asexual (female)
- Populations vary widely in sex ratio
- Males do not appear to discriminate

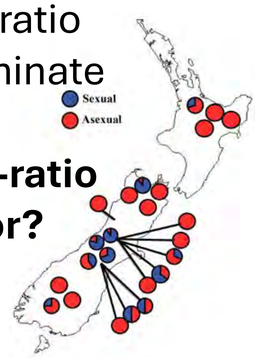

What is the influence of sex-ratio variation on mating behavior?

Main Goals

Measure <u>frequency</u> and <u>duration</u> of mating in environments with different male-to-female ratios

Experimental Design

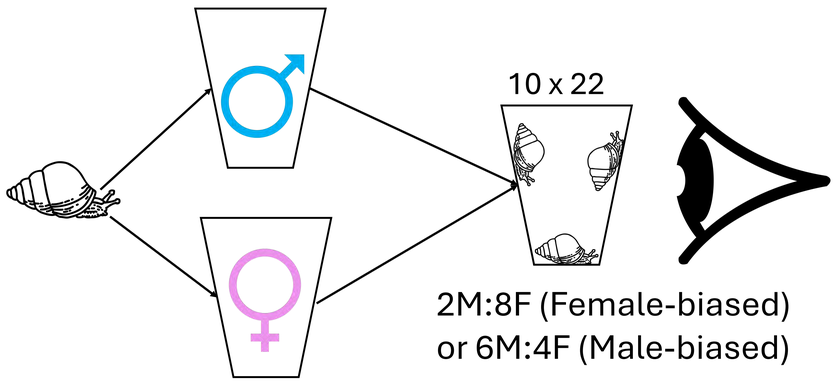

Acknowledgements:
The Neiman lab for assistance in painting and sexing snails.
References: Dybdahl, M. F., & Lively, C. M. Lively. (1995). Diverse, endemic and polyphyletic clones in mixed populations of a freshwater snail. *Journal of Evolutionary Biology 8* (3) 385-398, Neiman, M & Lively, C(2005) Male New Zealand Mud Snails (Potamopyrgus antipodarum) Persist in Copulating with Asexual and Parasitically Castrated Females. *BioOne.*
Weir, L. K., Grant, J. W. A., & Hutchings, T.A. (2011). The influence of operational sex ratio on the intensity of competition for mates. *The American Naturalist, 177* (2) 167-176,

Mating Frequency Distribution

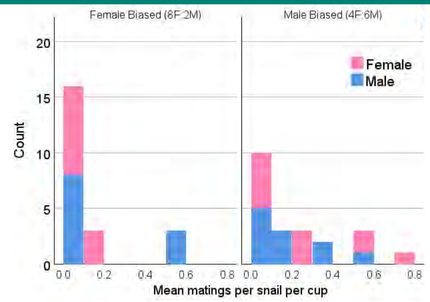

Figure 1. Per-snail mating of cups across different sexes and sex ratios

Mean Mating Frequency

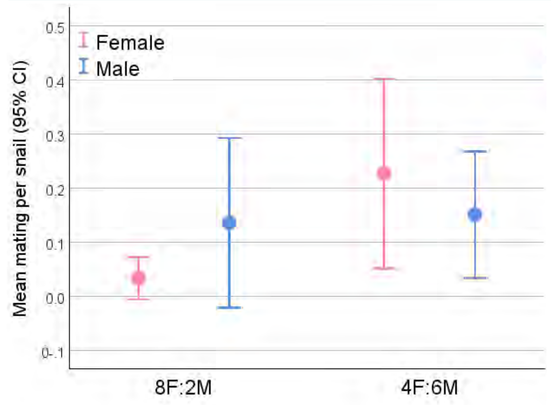

Figure 2. Per-snail mating of different sexes in populations with different sex ratios.

Mating Frequency Variation

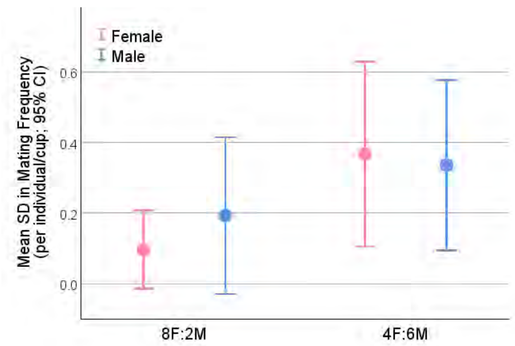

Figure 3. Variation in mating frequency per snail as a function of sex and sex ratio, expressed as mean standard deviation (SD).

Summary & Conclusions

- Total and mean mating frequency and variation is higher in male-biased treatment.
- Low variation across females in female-biased treatment hints at benefit of diversity
- Females mate less when males are rare
- Females could be sperm limited when asexuals are common
- Consistent with scenario where female-biased sex ratio could increase cost of sex

IOWA College of Education Belin-Blank Center

The relationship between gifted programming and self-concept for Twice-Exceptional Students

Exploring the correlation between gifted program participation and the self-concepts of 2e students with ADHD

Steffi Kim, Brandon LeBeau Ph.D.

Introduction

- Twice-Exceptional (2e) youth have high cognitive ability along with a co-occurring disability [1]
- 2e students with ADHD have similar cognitive characteristics to gifted children without a diagnosis [2]
- Symptoms of ADHD appear similar to the excitabilities that gifted children typically exhibit [3]
- Thus, 2e students with ADHD may feel socially and academically comfortable in a gifted program
- 2e Students with ADHD tend to have lower self-concepts or perceptions of themselves [4]
- However, there are conflicting results on whether gifted programming increases or decreases self-concept [5]
- Self-concept is central to wellbeing, yet many 2e students don't get the support and gifted services they need [1]

Research Questions

1. How does gifted program participation relate to self-concept among twice-exceptional students with ADHD?

2. How do comorbidities, in addition to ADHD, correlate with the self-concepts of twice-exceptional students?

3. What variances in self-concept exist between gifted program students with and without an ADHD diagnosis?

Methods

- R software was used for a descriptive statistical analysis
- Clinical sample of 210 high ability, school-aged children (avg. 10.12 years)
- All data had an IQ ≥ 115 (avg. 126.36, SD = 8.68)
- About 72% were in a gifted program
- The Piers-Harris Self-Concept Scale (PH-2) was used to test self-concept across six domains
- Scores were reported as T-scores (mean = 50, SD = 10) and percentiles
- Data was divided into groups based on gifted program/typical classroom participation and diagnosis/comorbidities. Self-concept for each group was analyzed

Diagnoses

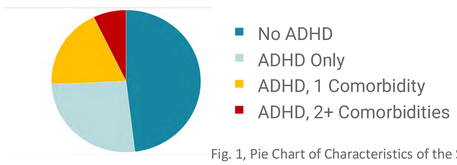

Fig. 1, Pie Chart of Characteristics of the Sample

Results

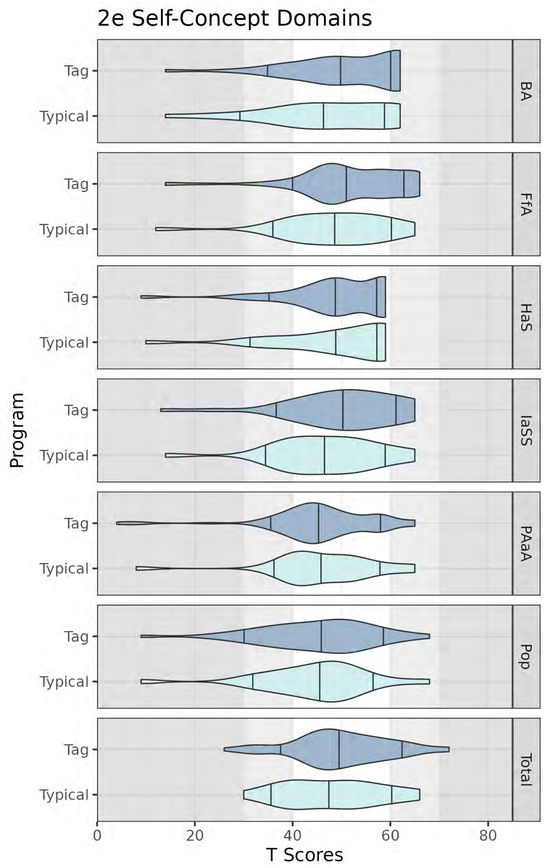

Fig. 2, Violin Plots of T-scores across six self-concept domains. The 10th, 50th, and 90th quantiles are marked

Light gray shading is 1+ SD from the mean, dark gray is 2+ SD

BA = Behavioral Adjustment
FfA = Freedom from Anxiety
HaS = Happiness & Satisfaction
IaSS = Intellectual & School Status
PAaA = Physical Appearance & Attributes
Pop = Popularity
Total = Total Self-Concept

2e Mean Percentiles

	Tag	Typical	Difference
Total	50.06	44.31	5.75
BA	56.69	47.17	9.53
Ffa	57.91	47.79	10.11
HaS	51.24	53.21	-1.97
IaSS	52.99	41.96	11.03
PAaA	38.58	40.17	-1.59
Pop	39.12	36.08	3.04

Fig. 3, Table comparing the mean self-concept percentiles of 2e students in Gifted Programs (Tag) vs. Typical Classrooms across PH-2 domains

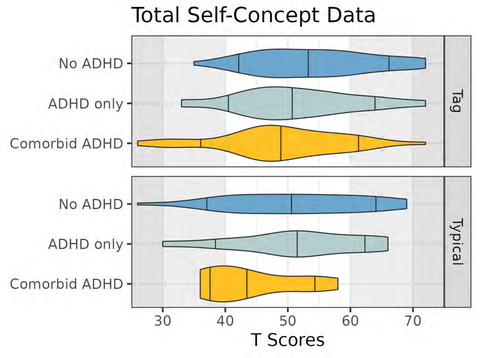

Fig. 4, Violin Plot of T-Scores for analyzing relationships with comorbidities. *Tag = Gifted Program, Typical = Typical Classroom*

- Within gifted programs, more diagnoses resulted in lower self-concept across all six domains
- The decline in self-concept was more pronounced for typical classrooms than gifted programs

Discussion

- Participation in a gifted program correlated to higher total self-concept, which replicates some literature but contradicts others [5]
- The 2e Gifted Program group had noticeably higher scores for total self-concept, behavioral adjustment (BA), freedom from anxiety (FfA), and intellectual & school status (IaSS) than 2e in a typical classroom *(Fig. 2,3)*
    - Gifted program criteria may favor students with higher behavioral and emotional moderation, or this may be a result of the environment
    - Being labeled as "gifted" most likely boosted IaSS scores
- 2e Tag and Typical Classroom students scored similarly for Happiness & Satisfaction, Physical Appearance & Attributes, and Popularity
- Additional comorbidities were consistently associated with lower self-concept *(Fig. 4)*
- Future research should focus on the extent and effects of comorbidities, and whether gifted programming helps minimize self-concept drops
- Self-concept varies greatly within gifted programs and typical classrooms and should not be overly generalized

Acknowledgements

- All data used was collected by licensed psychologists at the Belin-Blank Center Clinic through extensive assessments
- This research relied heavily on previous studies at the Belin-Blank Center, including research by Megan Foley-Nicpon and others
- A special thanks to Brandon LeBeau for mentorship and guidance during every step of the research process, and to Katie Schabilion

References

[1] Reis, S. M., Baum, S. M., & Burke, E. (2014). An operational definition of Twice-Exceptional learners: Implications and applications. *Gifted Child Quarterly, 58*(3), 217-230. https://doi.org/10.1177/0016986214534976

[2] Cornoldi, C., Giofrè, D., & Toffalini, E. (2023). Cognitive characteristics of intellectually gifted children with a diagnosis of ADHD. *Intelligence, 97*. https://doi.org/10.1016/j.intell.2023.101736

[3] Rinn, A. N., & Reynolds, M. J. (2012). Overexcitabilities and ADHD in the gifted: An examination. *Roeper Review, 34*(1), 38–45. https://doi.org/10.1080/02783193.2012.627551

[4] Foley-Nicpon, M., Rickels, H., Assouline, S. G., & Richards, A. (2012). Self-esteem and self-concept examination among gifted students with ADHD. *Journal for the Education of the Gifted, 35*(3), 220-240. https://doi.org/10.1177/0162353212451735

[5] Vogl, K., & Preckel, F. (2014). Full-time ability grouping of gifted students: Impacts on social self-concept and school-related attitudes. *Gifted Child Quarterly, 58*(1), 51-68. https://doi.org/10.1177/0016986213513795

Effects of N-acetylcysteine on a *Drosophila* model of epilepsy and autism

Henry Li[1]; Jessie Newbanks[2]; Siera Rossi[2]; Brady Williquett[2]; J. Robert Manak, PhD[2,3]

[1]Millburn High School, [2]Department of Biology, University of Iowa, [3]Department of Pediatrics, Carver College of Medicine, University of Iowa

Introduction

Epilepsy & Autism Spectrum Disorders

- Epilepsy and autism spectrum disorders (ASD) are two disorders characterized by an ongoing predisposition to developing seizures and difficulties in social communication, repetitive behaviors, and restricted interests, respectively.[1,2]
- Epilepsy and ASD have been linked to one another, with high rates of comorbidity suggesting common causes.[1,2]
- Approximately 30% of epilepsy patients do not respond to currently available antiseizure drug therapies.[3]

PRICKLE

- Mutations in the *PRICKLE1* gene have been associated with cases of epilepsy and ASD.[4,5]
- Mutations in *prickle* (*pk*), an ortholog of *PRICKLE1* found in *Drosophila*, have been shown to cause spontaneous myoclonic seizures similar to those observed in human patients.[4]

Oxidative Stress & Innate Immune Response

- Evidence of oxidative stress and activation of the innate immune response (IIR) have been reported in cases of epilepsy and ASD.[6,7]
- Recent work by the Manak laboratory has shown that a *Drosophila* model of *prickle*-mediated epilepsy shows brain oxidative stress leading to IIR activation, which in turn causes neuronal cell death and seizure exacerbation.[8]
- N-acetylcysteine (NAC) is a strong antioxidant that has been shown to reduce oxidative stress and improve disease prognosis among epilepsy patients and mouse models.[3,9,10]
- In *Drosophila*, NAC has been shown to increase lifespan, rescue locomotor defects, and modulate apoptosis.[11,12]

Research Objectives

- We aim to investigate the effects of NAC antioxidant treatment on the oxidative stress, IIR, and seizure progression in *prickle* mutant flies. Additionally, we seek to ascertain whether *prickle* mutant flies experience learning deficits similar to those frequently observed in cases of ASD, and whether NAC treatment will rescue such learning deficits.

Methods

Drosophila Stocks

- The pk^{sple} mutation was outcrossed into Canton-S (*CS*) flies for a minimum of 5 generations and used for all current experiments.

NAC Feeding

- Standard cornmeal molasses medium was mixed with NAC to yield a final concentration of 1mM. Adult flies were transferred to fresh control or drug food every several days.

Spontaneous Seizure Assay

- Flies were aged to 14-16 days post-eclosion (dpe) at 25°C.
- Flies were individually mouth pipetted into circular enclosed chambers and their behavior was recorded using high-resolution videography.
- Videos were manually analyzed for spontaneous seizure events.

Learning Assay

- Flies were aged to 7-10 days post-eclosion (dpe) at 25°C.
- Learning was assessed with a T-maze apparatus using an aversive Pavlovian olfactory conditioning procedure.[13]

Results

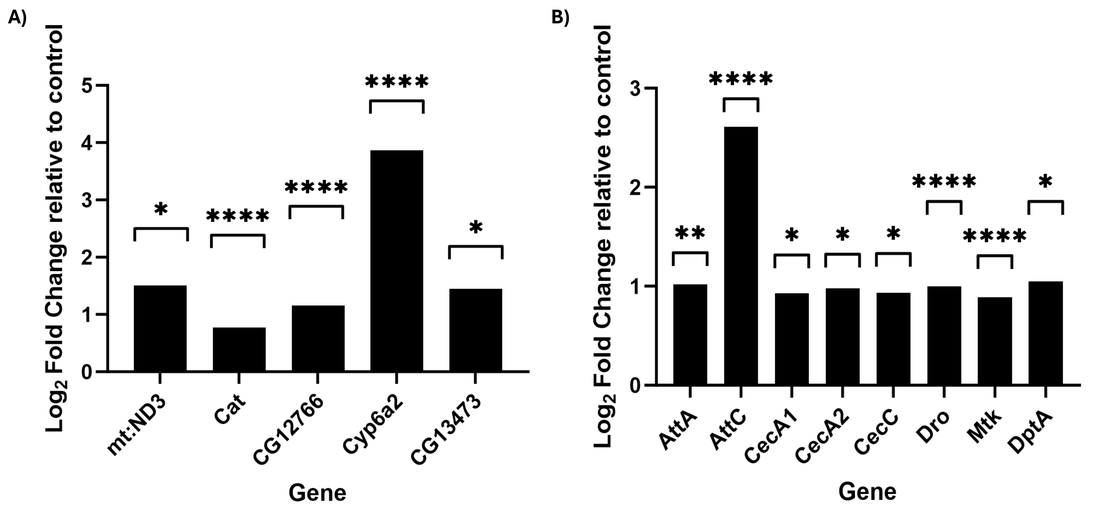

Figure 1: Brain microarray analysis shows upregulation of both oxidative stress mitigators and innate immune response genes. Bars show the mean fold-change of gene expression in pk^{sple} mutants relative to controls for A) key oxidative stress mitigator genes and B) innate immune response genes. n =2 biological replicates with 4 technical replicates each. P-values calculated using the GEO2R program from the GEO database. *p ≤ 0.05, **p ≤ 0.01, ***p ≤ 0.001, ****p ≤ 0.0001

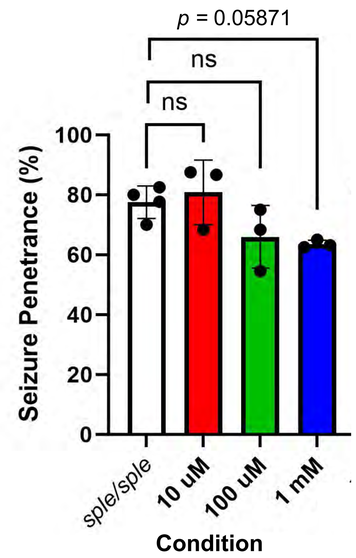

Figure 2: NAC treatment of pk^{sple} mutant flies leads to a reduction in seizure penetrance trending towards significance. Previous spontaneous seizure assays performed with 14-16 dpe w^{1118} males treated with no NAC, 10µm, 100µm, and 1mM. Data are shown as mean ± SEM; Mann-Whitney U test. n = 2-4 flies/treatment; ns = no significance

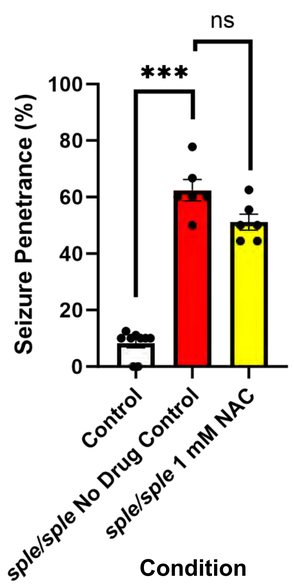

Figure 3: Treatment with 1 mM NAC shows slight suppression of seizures in pk^{sple} mutant flies. Spontaneous seizure assays performed with 14-16 dpe males. Data are shown as mean ± SEM; Mann-Whitney U test. n ≥ 6 biological replicates, 8-10 flies/replicate; ***p ≤ 0.001, ns = no significance

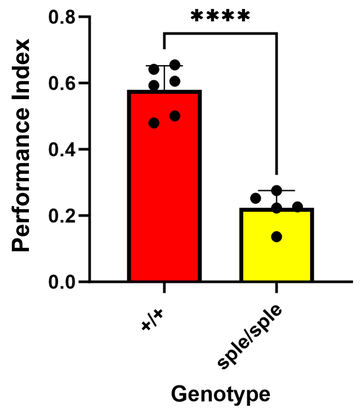

Figure 4: Homozygous pk^{sple} mutants show significantly lower learning ability relative to controls at 7-10 dpe. Analysis of performance index indicates significant deficits in short-term olfactory learning ability among *sple/sple* mutants compared to controls. Data are shown as mean ± SEM; unpaired T-test. n ≥ 5 biological replicates, 100 flies/replicate; ****p ≤ 0.0001

Conclusions

- Preliminary data generated in our laboratory showed that NAC suppresses seizures to near significance in male pk^{sple} mutant flies.
- We find with an additional trial, significance is once again not reached, although the data shows some decrease in seizure penetrance after NAC treatment.
- Learning assay data demonstrate pk^{sple} mutants have a significantly lower learning capability, supporting the comorbidity of ASD and epilepsy in our model.

Future Directions

- Increase the number of biological replicates to increase statistical power and demonstrate NAC treatment suppresses seizure penetrance to a significant level.
- Run qRT-PCR on NAC-treated *prickle* mutant brains to determine whether NAC treatment reduces oxidative stress & IIR at the level of gene expression.
- Conduct learning assay on NAC-treated *prickle* mutants to evaluate whether NAC improves learning.

References

1. Kwon, C.-S., Wirrell, E. C., & Jetté, N. (2022). Autism spectrum disorder and epilepsy. *Neurologic Clinics, 40*(4), 831–847. https://doi.org/10.1016/j.ncl.2022.03.011
2. Keller, R., Basta, R., Salerno, L., & Elia, M. (2017). Autism, epilepsy, and synaptopathies: a not rare association. *Neurological Sciences, 38*(8), 1353–1361. https://doi.org/10.1007/s10072-017-2974-x
3. Pauletti, A., Terrone, G., Shekh-Ahmad, T., Salamone, A., Ravizza, T., Rizzi, M., Pastore, A., Pascente, R., Liang, L.-P., Villa, B. R., Balosso, S., Abramov, A. Y., van Vliet, E. A., Del Giudice, E., Aronica, E., Antoine, D. J., Patel, M., Walker, M. C., & Vezzani, A. (2017). Targeting oxidative stress improves disease outcomes in a rat model of acquired epilepsy. *Brain: A Journal of Neurology, 140*(7), 1885–1899. https://doi.org/10.1093/brain/awx117
4. Ehaideb, S. N., Wignall, E. A., Kasuya, J., Evans, W. H., Iyengar, A., Koerselman, H. L., Lilienthal, A. J., Bassuk, A. G., Kitamoto, T., & Manak, J. R. (2016). Mutation of orthologous prickle genes causes a similar epilepsy syndrome in flies and humans. *Annals of Clinical and Translational Neurology, 3*(9), 695–707. https://doi.org/10.1002/acn3.334
5. Paemka, L., Mahajan, V. B., Skeie, J. M., Sowers, L. P., Ehaideb, S. N., Gonzalez-Alegre, P., Sasaoka, T., Tao, H., Miyagi, A., Ueno, N., Takao, K., Miyakawa, T., Wu, S., Darbro, B. W., Ferguson, P. J., Pieper, A. A., Britt, J. K., Wemmie, J. A., Rudd, D. S., … Bassuk, A. G. (2013). PRICKLE1 interaction with SYNAPSIN I reveals a role in autism spectrum disorders. *Plos One, 8*(12), e80737. https://doi.org/10.1371/journal.pone.0080737
6. Rossignol, D. A., & Frye, R. E. (2014). Evidence linking oxidative stress, mitochondrial dysfunction, and inflammation in the brain of individuals with autism. *Frontiers in Physiology, 5*, 150. https://doi.org/10.3389/fphys.2014.00150
7. Xu, D., Miller, S. D., & Koh, S. (2013). Immune mechanisms in epileptogenesis. *Frontiers in Cellular Neuroscience, 7*, 195. https://doi.org/10.3389/fncel.2013.00195
8. Nukala, K. M., Lilienthal, A. J., Lye, S. H., Bassuk, A. G., Chtarbanova, S., & Manak, J. R. (2023). Downregulation of oxidative stress-mediated glial innate immune response suppresses seizures in a fly epilepsy model. *Cell Reports, 42*(1), 112004. https://doi.org/10.1016/j.celrep.2023.112004
9. Ben-Menachem, E., Kyllerman, M., & Marklund, S. (2000). Superoxide dismutase and glutathione peroxidase function in progressive myoclonus epilepsies. *Epilepsy Research, 40*(1), 33–39. https://doi.org/10.1016/s0920-1211(00)00096-6
10. Ghanizadeh, A., & Derakhshan, N. (2012). N-acetylcysteine for treatment of autism, a case report. *Journal of Research in Medical Sciences : The Official Journal of Isfahan University of Medical Sciences, 17*(10), 985–987.
11. Niraula, P., & Kim, M. S. (2019). N-Acetylcysteine extends lifespan of Drosophila via modulating ROS scavenger gene expression. *Biogerontology, 20*(4), 533–543. https://doi.org/10.1007/s10522-019-09815-4
12. Shaposhnikov, M. V., Zemskaya, N. V., Koval, L. A., Schegoleva, E. V., Zhavoronkov, A., & Moskalev, A. A. (2018). Effects of N-acetyl-L-cysteine on lifespan, locomotor activity and stress-resistance of 3 Drosophila species with different lifespans. *Aging, 10*(9), 2428–2458. https://doi.org/10.18632/aging.101561
13. Tully, T., & Quinn, W. G. (1985). Classical conditioning and retention in normal and mutant Drosophila melanogaster. *Journal of Comparative Physiology. A, Sensory, Neural, and Behavioral Physiology, 157*(2), 263–277. https://doi.org/10.1007/BF01350033

Acknowledgments

I would like to thank Jessie Newbanks, Brady Williquett, and Dr. Manak for their continued guidance, support, and mentorship throughout this project and Siera Rossi for help with data collection. Special thanks to the University of Iowa and the Belin-Blank Center for this amazing opportunity. This research was supported by a University of Iowa Investment in Strategic Priorities Grant, the Office of Executive Vice President and Provost, and the University of Iowa Stead Family Children's Hospital and Stead Family Department of Pediatrics Research Grant Programs (to JRM).

How Does Reinforcement Affect the Variability of Pigeons' Response Sequences?

Sophia Li[1], Odysseus Orr[2], Edward Wasserman[2]
[1]Great Neck North High School, [2]Department of Psychological and Brain Sciences, The University of Iowa

Introduction

- Performing response sequences is a common aspect of human behavior.
- Studying variability in animals may provide a better understanding of the basic mechanisms underlying these complex behaviors.
- The Law of Effect holds that reinforcement increases prior responses' frequency, but how reinforcement affects the variability of prior responses is still unclear.
- Past research involving one stimulus shows that variability decreases as reinforcement is continuously given.
- This study will explore how pigeons' response variability changes over time when the task requires any sequence of five nonrepeating responses to be made.

Research Questions

How will the pigeons' response sequences vary over training sessions? Will they become more stable or more variable?

Will the pigeons' response sequences trend toward more efficient routes (i.e., only responding to the nearest neighbor) over time?

How will the pigeons differ from one another in their patterns of responding?

Methods

Three pigeons had daily training sessions of 120 trials each. A simulation was also conducted to represent a pigeon behaving randomly.

Task

For each trial, pigeons pecked a start stimulus and then pecked five visually distinct stimuli, with each peck removing the corresponding stimulus from the screen. Reinforcement was provided after pecking all five stimuli.

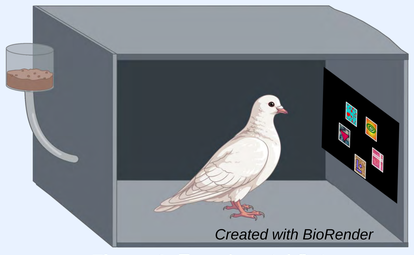

Figure 1. Experimental Setup

Pretraining

Before the full task, pigeons were first introduced to the task by seeing each stimulus in its respective position. Each stimulus was presented an equal number of times (24 times each) per pretraining session.

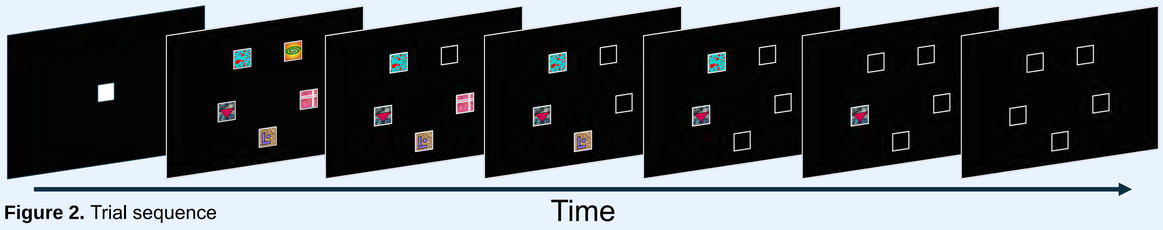

Figure 2. Trial sequence

Results

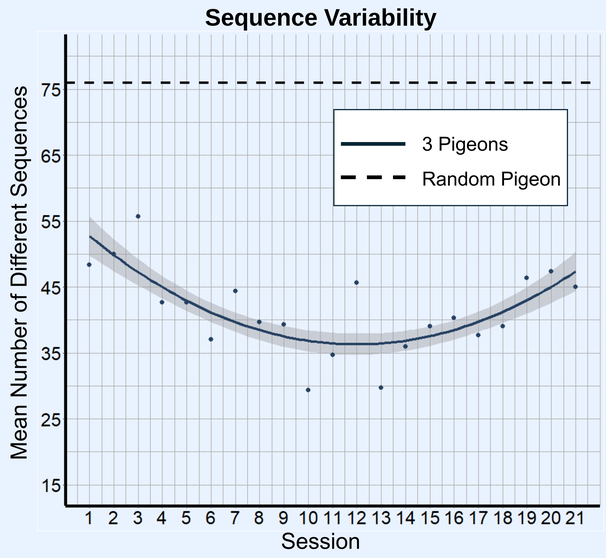

Figure 3. Responses get decrease in variability then increase.

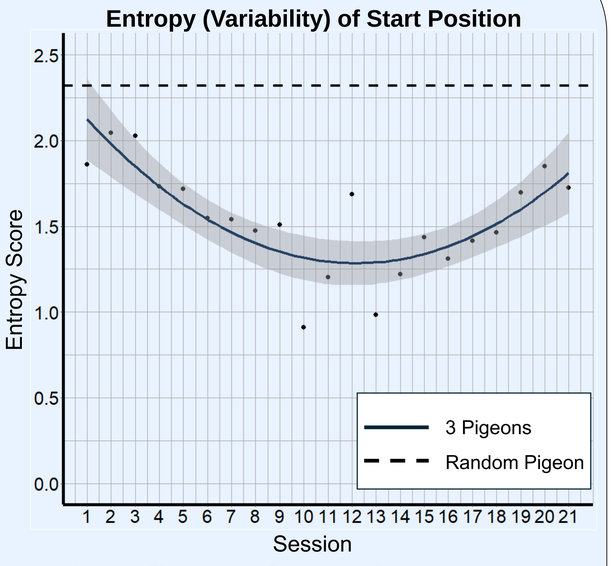

Figure 4. The entropy of responses fluctuates.

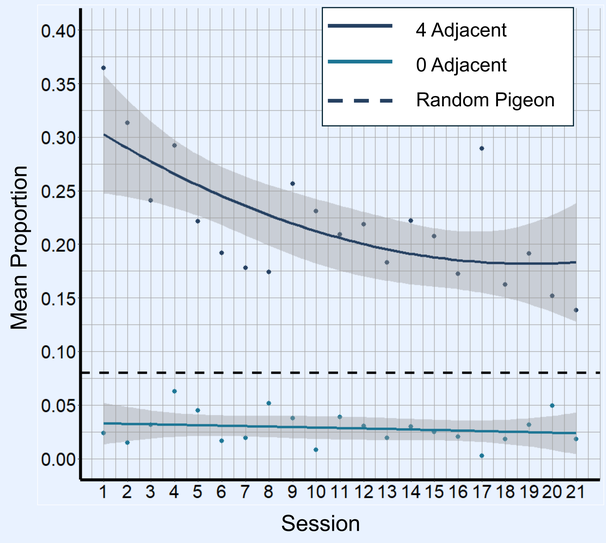

Figure 5. Pigeons are biased toward the most efficient sequences, although with decreasing frequency.

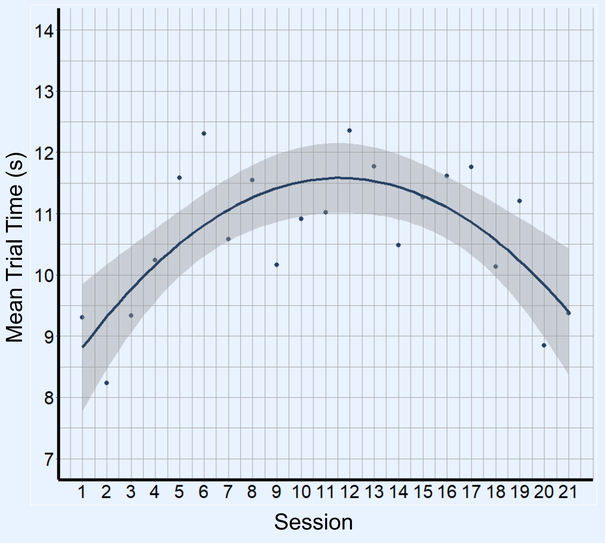

Figure 6. Pigeons initially take more time to complete trials before decreasing the time again.

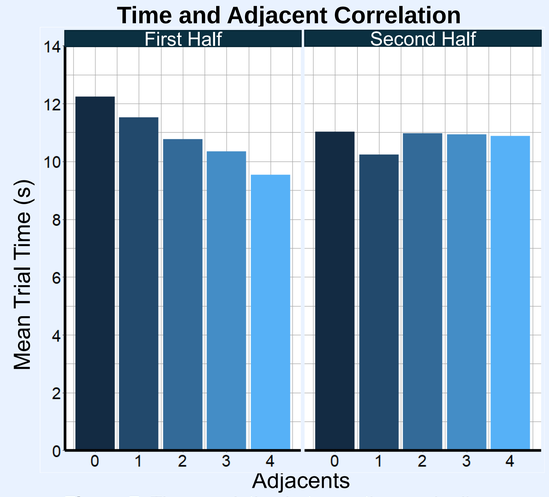

Figure 7. The correlation between time and adjacency in the first and second half of training.

Conclusions

- At no point in time were pigeons behaving randomly.
- Pigeons' response variability decreased during the first half of training, and then increased.
- Interestingly, the initial narrowing of sequences was NOT due to the pigeons utilizing the most efficient sequence.
- Although pigeons preferred the most efficient sequence, this bias decreased over the course of training.
- More inefficient sequences initially came at a cost, but this cost disappeared by the end of the training.
- Future research should attempt to increase the cost of making inefficient responses.
  - Increase distance between stimuli
  - Increase peck requirement
- Contributes knowledge into how organisms alter behavior even when not explicitly told to do so

Acknowledgements

I would like to give special thanks to Professor Wasserman and Odysseus Orr for mentoring me. I would also like to thank the Belin Blank Center and Secondary Student Training Program for providing me with the resources and guidance to perform research in a professional setting.

References

Antonitis, J. J. (1951). Response variability in the white rat during conditioning, extinction, and reconditioning. *Journal of Experimental Psychology*, *42*(4). https://doi.org/10.1037/h0060407

Eckerman, D. A., & Lanson, R. N. (1969). Variability of response location for pigeons responding under continuous reinforcement, intermittent reinforcement, and extinction. *Journal of the Experimental Analysis of Behavior, 12*(1), 73–80. https://doi.org/10.1901/jeab.1969.12-73

Stahlman, W. D., Young, M. E., & Blaisdell, A. P. (2010). Response variability in pigeons in a Pavlovian task. *Learning & Behavior*, *38*(2), 111–118. https://doi.org/10.3758/LB.38.2.111

Investigating the genomic binding profile of methyltransferase in SETDB1 targets from patient-derived endometrial cancer cells

Vera Lin[1]; Kiarash Salari[2]; Shujie Yang, PhD[2]

[1]BASIS Independent Fremont, CA; [2]Department of Pathology, University of Iowa

Introduction

- The incidence of **endometrial cancer (EC)** has increased by approximately 50% over the past decade (American Cancer Society)
  - EC is the most common cancer of the female reproductive organs
  - EC is the most common gynecological malignancy equating to around 13,250 deaths every year

Figure 1. the female reproductive organ. EC commonly begins in the lining of the uterus.

- **SETDB1**, or SET domain bifurcated histone lysine methyltransferase, is a histone methyltransferase that catalyzes H3K9 trimethylation and represses transcription
- The SETDB1 gene is located on **chromosome 1q21.3**
- SETDB1 is a key player in epigenetic mechanisms with significant implications on various cancers

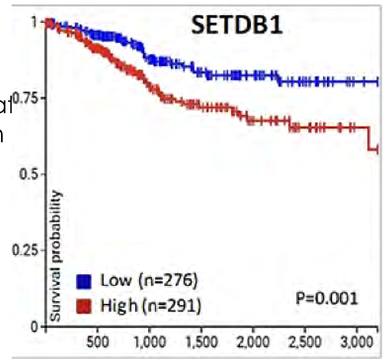

- Previous experiments have shown that SETDB1 **promotes** H3K9me3 on regions such as ZNF genes and SAR sequences

Figure 2. EC-TCGA Kaplan Meyer survival curve for SETDB1 high and low expressing patients

Objective

1. Use chromatin immunoprecipitation (ChIP) to capture specific DNA-protein interactions in patient-derived cells
2. Explore differential H3K9 and H3K4 methylation on previously observed gene promotors in wildtype and SETDB1 knockout patient-derived cells

Significance

Endometrial cancer is one of the few cancers with an actively increasing mortality rate. A rise in other diseases that are associated with increased risk in EC, such as obesity, emphasizes the need for improved therapy and earlier detection of diagnosis.

Methodology

Experiment 1: ChIP Procedure

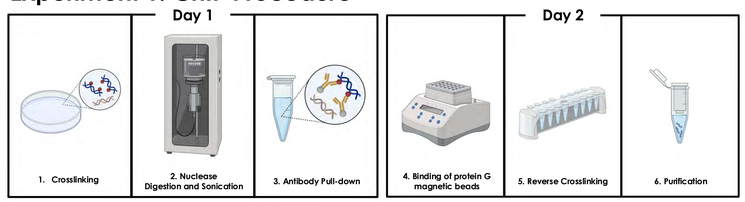

Experiment 2: RNA Extraction

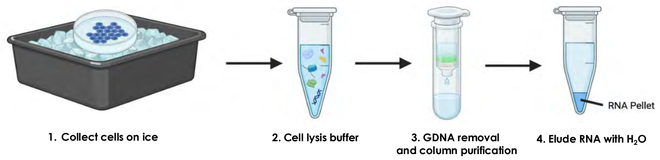

Results

Trimethylation on the H3K9 at that promoter site is being regulated by SETDB1.

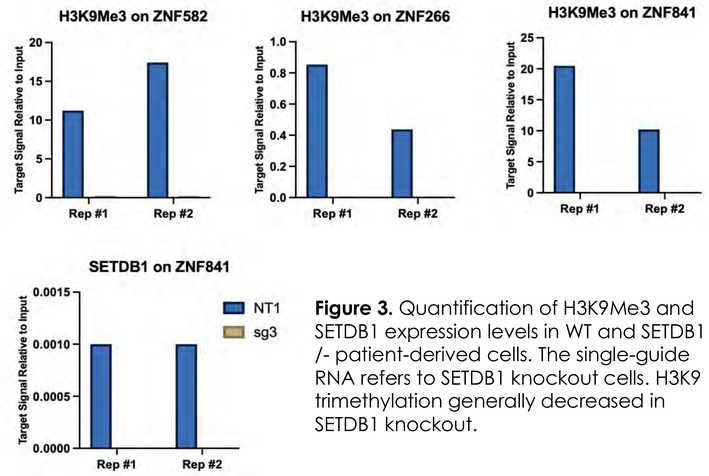

Figure 3. Quantification of H3K9Me3 and SETDB1 expression levels in WT and SETDB1 -/- patient-derived cells. The single-guide RNA refers to SETDB1 knockout cells. H3K9 trimethylation generally decreased in SETDB1 knockout.

Depletion of SETDB1 causes the upregulation of ZNF582.

Figure 4. Bar graph detailing the quantification of regulation of ZNF582 and SETDB1 in the presence and absence of SETDB1. Overall, ZNF582 expression increased in sg2-1 and sg3 samples and SETDB1 expression was greatest in WT SETDB1 cells.

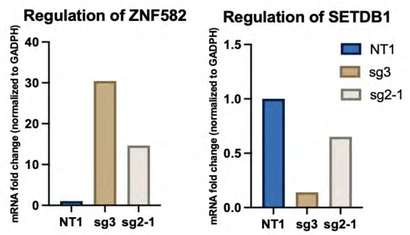

Conclusions

1. Confirmed H3K9 trimethylation in ZNF582, ZNF266, and ZNF841 decreased in SETDB1 knockout patient-derived cells
2. SETDB1 binding to ZNF582, ZNF266, and ZNF841 did not have a major change in wildtype and SETDB1 knockout cells as previously seen in the human Ishikawa cell line

Future Directions

Our data confirms that SETDB1 regulates H3K9 trimethylation expression levels at specific tested promotor sites of ZNF gene

- Further monitor the biochemical mechanisms of SETDB1 to provide insight into how resistance towards SETDB1 knockout may develop
- Evaluate quantitative data gained from ChIP-sequencing and qPCRs to analyze change in H3K9Me3 expression levels and potentially the loss of function of selective genes
- The application of qPCR will give us a better understanding of SETDB1 regulation differences with quantifiable data

Acknowledgements

I would like to thank Dr. Yang, Kiarash, and the Yang Lab for their invaluable guidance over these past five weeks, as well as the Belin Blank Center for providing this amazing opportunity to conduct research. Funding for this poster was supported by NIH R37-CA238274 (SY) and the Department of Pathology Start-Up Fund (SY).

References

Delaney, C. E., Methot, S. P., Kalck, V., Seebacher, M., & Padeken, J. (2022a). Setdb1-like MET-2 promotes transcriptional silencing and development independently of its h3k9me-associated catalytic activity. *Nature Structural & Molecular Biology*, *29*(2), 85–96. https://doi.org/10.1038/s41594-021-00712-4

Griffin, G. K., Wu, J., Iracheta-Vellve, A., Patti, J. C., Hsu, J., Davis, T., Dele-Oni, D., Du, P. P., Halawi, A. G., Ishizuka, J. J., Kim, S. Y., Klaeger, S., Knudsen, N. H., Miller, B. C., Nguyen, T. H., … Bernstein, B. E. (2021). Epigenetic silencing by setdb1 suppresses tumour intrinsic immunogenicity. *Nature*, *595*(7866), 309–314. https://doi.org/10.1038/s41586-021-03520-4

Lazaro-Camp, V. J., Salari, K., Meng, X., & Yang, S. (2021). SETDB1 in cancer: overexpression and its therapeutic implications. *American journal of cancer research*, *11*(5), 1803–1827

Strepkos, D., Markouli, M., Klonou, A., Papavassiliou, A. G., & Piperi, C. (2021). Histone methyltransferase setdb1: A common denominator of tumorigenesis with therapeutic potential. *Cancer Research*, *81*(3), 525–534. https://doi.org/10.1158/0008-5472.can-20-2906

Sun, L., & Fang, J. (2016). E3-independent constitutive monoubiquitination complements histone methyltransferase activity of SETDB1. *Molecular Cell*, *62*(6), 958–966. http://doi.org/10.1016/j.mocel 2016.04.022

Assessing motor control advantages in unimanual and bimanual task processing

Cindy Lin[1]; Eliot Hazeltine, Ph.D.[2]

[1]The Loomis Chaffee School, Windsor, CT; [2]University of Iowa, Dept. of Psychological and Brain Sciences, Iowa City, IA

Introduction & Background

Reflex Theory of Motor Control: movement is controlled by stimulus → response

Bimanual coordination: simultaneous use of the two hands to perform actions

Bimanual interference occurs when simultaneously performing asymmetric movements with each hand

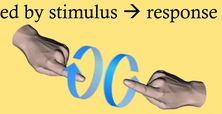

Figure 1. Rotating one index finger forward while simultaneously rotating the other index finger backwards causes bimanual interference.

Previous research observed a bimanual advantage (i.e. faster two-finger responses) when responses are made to *a combination of* two stimuli (e.g. mouse + fish = left index + right thumb) (Schumacher et al., 2018). When the two stimuli don't correlate with each other, (e.g. mouse = left index finger, crab = right thumb), there exists a unimanual advantage.

- ❖ Previous conclusions: 1. Interference between task representations contributes to dual-task costs, so making one response is faster when the stimuli aren't related. 2. Participants interpret two relational stimuli as a single task, so making a double-hand response is faster in the relational condition.

The present study aims to explore the underlying causes of conditional advantages by varying the quantity of stimuli.

Objectives

Research Questions

(1) Under what circumstances of stimulus-response mappings do bimanual tasks incur reactional advantages over unimanual tasks, and vice versa? (2) What conditional differences in stimulus perception and/or task planning contribute to these advantages?

Hypotheses & Alternatives

- Two movements require more activation in the motor cortex and contribute to feature-binding interference (Hommel, 2004), leading to slower bimanual responses
- Unimanual responses require single-side inhibition (Kürten et al., 2022), which demands additional motor cortex activation and leads to slower unimanual responses
- Number of stimuli and stimulus-response mappings do not affect conditional advantages

Methods

Participants make responses as quickly & accurately as possible to a single stimulus (Experiment 1) or two adjacent stimuli (Experiment 2) presented on a screen.

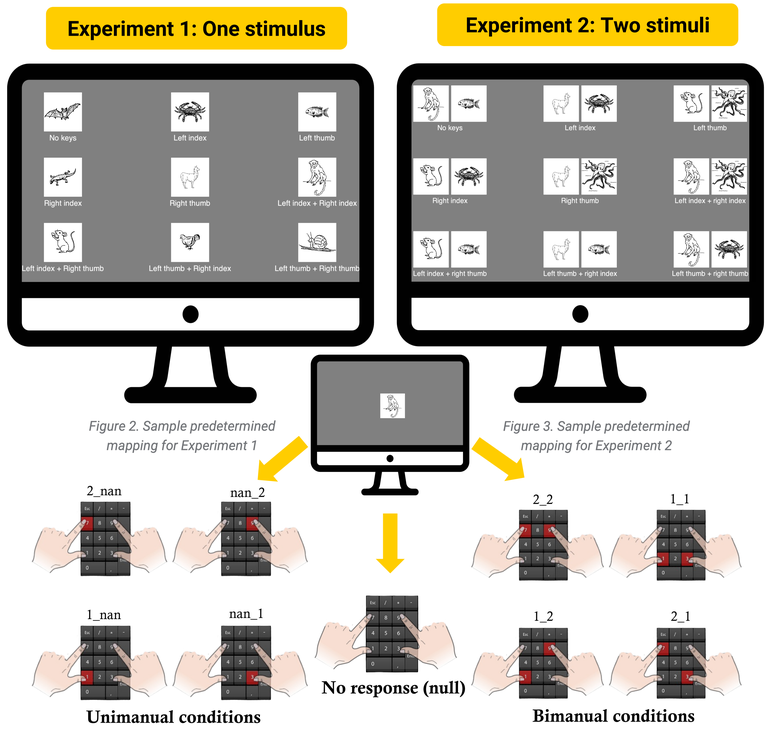

Figure 2. Sample predetermined mapping for Experiment 1

Figure 3. Sample predetermined mapping for Experiment 2

Figure 4. All possible responses (tasks). Note that label numbers denote fingers (e.g. 2_2 = left index + right index)

Discussion/Analysis

Hypothesis Testing

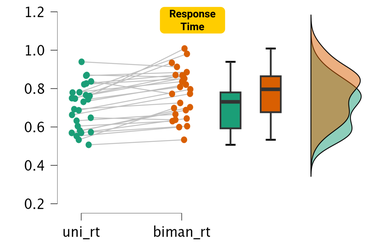

Figure 10. Raincloud plot of paired samples t-test using average unimanual response time (uni_rt) and bimanual response time (biman_rt) for each subject

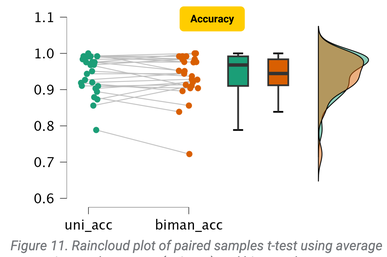

Figure 11. Raincloud plot of paired samples t-test using average unimanual accuracy (uni_acc) and bimanual accuracy (biman_acc) for each subject

Table 2. Paired sample t-test for response time and accuracy by condition (unimanual vs. bimanual)

	Measure 1		Measure 2	t	df	p	Cohen's d	SE Cohen's d
Response Time	uni_rt	–	biman_rt	−5.120	26	< .001	−0.985	0.139
Accuracy	uni_acc	–	biman_acc	1.051	26	0.303	0.202	0.097

Note. Student's t–test.

Experiment 1 (Refer to Experiment 1 Results)

- Bimanual responses with two distinct fingers result in longer RT regardless of previous response (Table 1, 2nd and 3rd rows). Anatomically parallel responses (1_1 or 2_2) result in relatively shorter RTs (1st and 4th rows) due to compatibility of conceptualization (Hazeltine, 2005).
- Same consecutive responses results in decreased RT (less cognitive processing) → navy diagonal

Experiment 2 (Refer to Experiment 2)

- Participants significantly more likely to respond on wrong side than with wrong finger (Figure 8) → evidence of side-stimulus association
- Bimanual responses in the hierarchy (see Figure 6) do not require recollection of side → side-stimulus association still applies, but side-response association no longer necessary → shorter RT

T-test Observations

- Statistically, unimanual and bimanual response times are significantly different, indicating that condition likely affects response time [$t(26) = 5.120$, $p < .001$, $d = 0.202$]
- Effect size for response time is significant
- Accuracy is **NOT** significantly affected by condition [$t(26) = 1.051$, $p = 0.303$, $d = 0.202$]

Experiment 1 Results

Table 1. Transitional response time (in seconds) by current trial and previous trial response fingers (Refer to Methods for finger combination key)

Current finger combination	Previous finger combination: biman 1_1	biman 1_2	biman 2_1	biman 2_2	uniman 1_nan	uniman 2_nan	uniman nan_1	uniman nan_2
biman 1_1	0.692358	0.731115	0.800341	0.733048	0.685699	0.737918	0.764552	0.755891
biman 1_2	0.969743	0.702621	0.843316	0.936384	0.935992	0.917814	0.884639	0.924224
biman 2_1	0.950720	0.829171	0.715569	0.870823	0.898318	0.904049	0.919551	0.916242
biman 2_2	0.713524	0.710714	0.705304	0.603056	0.718187	0.719678	0.708685	0.743537
uniman 1_nan	0.769897	0.771971	0.749554	0.801683	0.623545	0.781515	0.737427	0.795748
uniman 2_nan	0.743965	0.677650	0.705451	0.666058	0.677543	0.617384	0.665268	0.656280
uniman nan_1	0.806511	0.757145	0.740178	0.717060	0.699614	0.751377	0.641205	0.730125
uniman nan_2	0.784848	0.751707	0.759853	0.799715	0.766735	0.787038	0.722666	0.602253

Color Scale: 0.95, 0.90, 0.85, 0.80, 0.75, 0.70, 0.65

Response Error Analysis

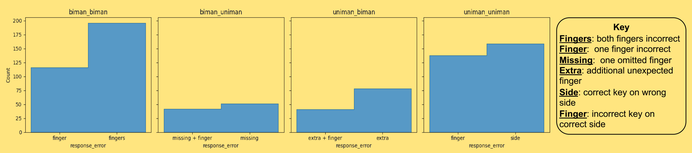

Key
Fingers: both fingers incorrect
Finger: one finger incorrect
Missing: one omitted finger
Extra: additional unexpected finger
Side: correct key on wrong side
Finger: incorrect key on correct side

Figure 5. Count of response error by side (left or right) vs. finger (thumb or index) for each expected-actual condition combination. (e.g. biman_biman = expected bimanual response, actual bimanual response)

Experiment 2*

Hypothetical Model

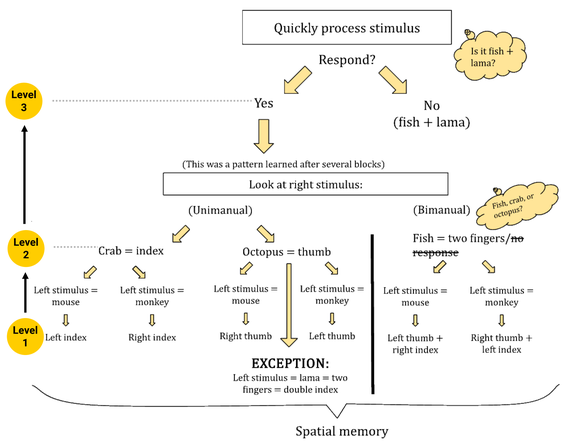

Figure 6. Hypothetical model for response processing hierarchy

Model Testing

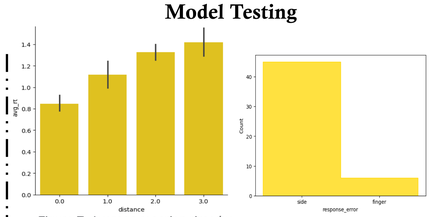

Figure 7. Average reaction time by "distance" measured in levels of hierarchy (see left). Note that 0.0 denotes same stimuli combination.

Figure 8. Count of response error by side (left or right) vs. finger (thumb or index)

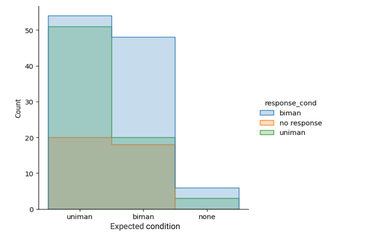

Figure 9. Count of actual response condition by expected condition

**NOTE: Experiment 2 consisted of model-based hypothesis testing with the creator of this poster as sole participant*

Conclusion & Future Extension

Combined Outcomes

- When one stimulus is consistently mapped to one action, we observe a unimanual advantage; when individual stimuli aren't consistently mapped to one action, we observe a bimanual advantage.
- Bimanual advantage arises from inherent bias in experimental design and, as such, can be manipulated (see Table 3 on right)

Table 3. Revised stimuli-response mapping structure for mitigating inherent hierarchical bias† ("LS" and "RS" denote left stimulus and right stimulus, respectively)

	Left thumb	Left index	Right thumb	Right index
LS1-RS1	–	–	–	★
LS1-RS2	–	★	★	–
LS1-RS3	★	–	★	–
LS2-RS1	–	–	–	–
LS2-RS2	–	★	–	–
LS2-RS3	–	–	★	–
LS3-RS1	★	–	–	–
LS3-RS2	★	–	–	★
LS3-RS3	–	★	–	★

†Design proposed by Dr. Eliot Hazeltine and Dr. Tim Raettig

Acknowledgements

I would like to thank Dr. Hazeltine, Marco, and Kalyani for their guidance and inspiration throughout my research process; Dr. Eric Schumacher, Jens Kürten, and Dr. Tim Raettig for their collaboration on the project; and the Belin-Blank center for arranging the SSTP program and providing me this opportunity.

References

Expression of GILT in Macrophages of Lean and Obese Mice Pancreas

Ethan Liu[1,2], Tate Neff[1], Qingwen Qian MD, PhD[1], Ling Yang PhD[1]

[1]Department of Anatomy and Cell Biology, Fraternal Order of Eagles Diabetes Research Center, Pappajohn Biomedical Institute, University of Iowa Carver College of Medicine, Iowa City, IA 52242
[2]Troy Athens High School, Troy, MI 48085

Abstract

Immune cell infiltration is a critical feature of chronic human diseases, including obesity and diabetes. In innate immunity, macrophage lysosomes play a key role in regulating phagocytic properties and inflammatory signature. Previous studies have found the inflammatory status of lysosomes to be linked with the onset of chronic metabolic diseases. An enzyme located in lysosomes, Gamma-interferon-inducible lysosomal thiol reductase (GILT), plays both an immunological and metabolic role, although its metabolic role is relatively unknown. Numerous studies have proven GILT to be a substantial enhancer of antigen processing and presentation in macrophages by direct reduction of antigen disulfides. Although aberrant macrophage infiltration and activation has been demonstrated contributes to pathogenesis of diabetes, the precise localization and expression of GILT alongside macrophages in pancreatic islets are unknown. Here we found that GILT is expressed in islet macrophages by immunofluorescence histochemistry assay. There is elevated GILT expression in pancreas/islet from mice with diet-induced obesity when compared to wild-type, regular diet mice. Furthermore, GILT gene (*Ifi30*) expression is increased upon glucose stimulation after 24 hours, demonstrating its potential metabolic role in insulin secretion and glucose metabolism.

Hypothesis

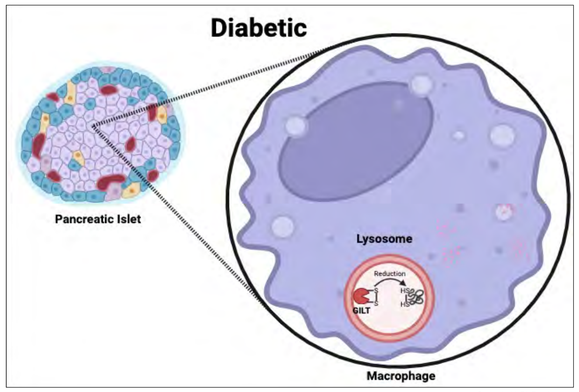

Materials and Methods

Mice: Animal care and experimental procedures were performed with approval from the University of Iowa Institutional Animal Care and Use Committee. All tissues were harvested, frozen in liquid nitrogen, and kept at −80℃ until processed for experimentation.

Imaging and Microscopy: Tissue was fixed in frozen sections, sectioned using Leica CM1850 cryostat microtome and stained for IHC analysis. Images were observed under a Zeiss 700 microscope.

Protein Expression: RT-qPCR was used to assess mRNA expression levels in the treated vs. nontreated groups. Followed the standard TRIzol protocol to extract RNA from mice.

Results

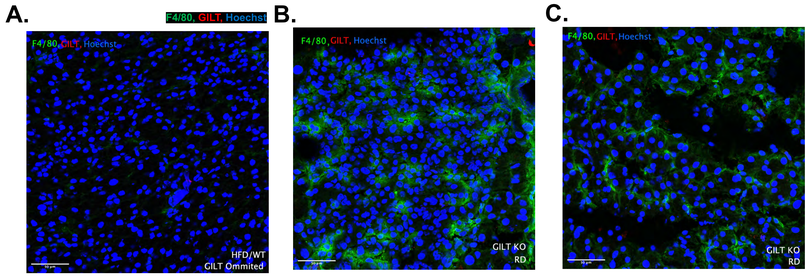

Figure 1. Macrophages are expressed in pancreatic tissue. (A-C) Immunohistochemistry staining of frozen fixed mice pancreatic tissue taken with a Zeiss 700 scope at 20x magnification. All images are representative samples. Macrophages marked using the F4/80 biomarker, NOVUS rabbit antibody in a 1:300 dilution. The protein GILT marked using NOVUS mouse antibody in a 1:300 dilution. (A) Islet from a GILT knockout mouse age 16 weeks, with primary omitted GILT as a negative control. (B-C) Different islets from a GILT knockout mouse age 16 weeks.

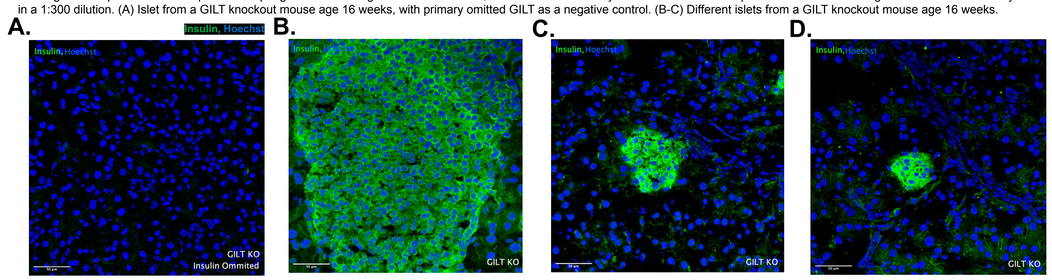

Figure 2. Insulin expression and islets in pancreatic tissue of GILT knockout mice. (A-D) Immunohistochemistry staining of frozen fixed mice pancreatic tissue taken with a Zeiss 700 scope at 20x magnification. All images are representative samples. Insulin marked using Fitzgerald guinea pig antibody in a 1:300 dilution. (A) Islet from a GILT knockout mouse age 16 weeks, with primary omitted insulin as a negative control. (B-D) Different islets from a GILT knockout mouse age 16 weeks.

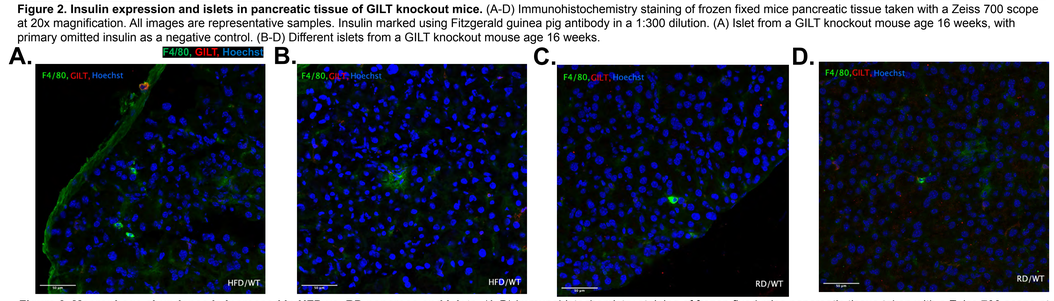

Figure 3. Macrophage abundance is increased in HFD vs. RD pancreas and islets. (A-D) Immunohistochemistry staining of frozen fixed mice pancreatic tissue taken with a Zeiss 700 scope at 20x magnification. All images are representative samples. Macrophages marked using the F4/80 biomarker, NOVUS rabbit antibody in a 1:300 dilution. The protein GILT marked using NOVUS mouse antibody in a 1:300 dilution. (A-B) Different islets from a high-fat wild type mouse age 16 weeks. (C-D) Different islets from a regular diet wild type mouse age 16 weeks.

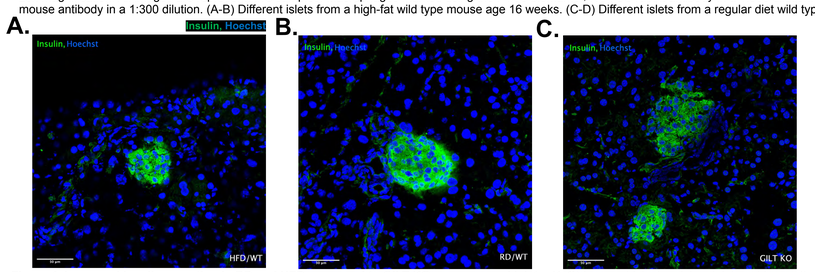

Figure 4. Increased insulin secretion in RD and HFD compared to GILT KO pancreas and islets. (A-C) Immunohistochemistry staining of frozen fixed mice pancreatic tissue taken with a Zeiss 700 scope all at 20x magnification. All images are representative samples. Insulin marked using Fitzgerald guinea pig antibody in a 1:300 dilution. (A) Islet from a high-fat diet wild type mouse age 16 weeks. (B) Islet from a regular diet wild type mouse age 16 weeks. (C) Islet from a GILT knockout mouse age 16 weeks.

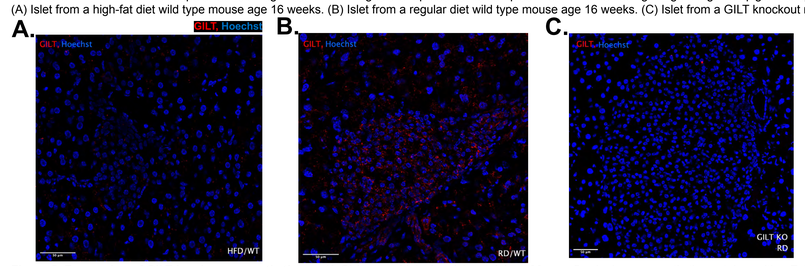

Figure 5. Expression of GILT in mice pancreatic tissue. (A-C) Immunohistochemistry staining of frozen fixed mice pancreatic tissue taken with a Zeiss 700 scope at 20x magnification. All images are representative samples. The protein GILT marked using NOVUS rabbit antibody in a 1:300 dilution. (A) Islet from a high-fat wild type mouse age 16 weeks. (B) Islet from a regular diet wild type mouse age 16 weeks. (C) Islet from a GILT knockout mouse age 16 weeks.

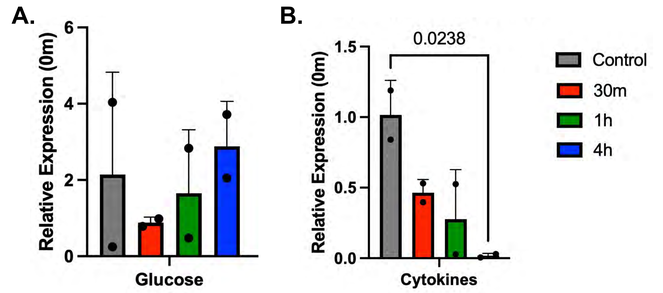

Figure 6. Expression of *Ifi30* is suppressed in INS-1 cells by administered cytokines. (A) Relative expression of *Ifi30* following glucose administration at 0 m, 30 m, 1h, and 4h. (B) Relative expression of *Ifi30* following glucose administration at 0 m, 30 m, 1h, and 4h.

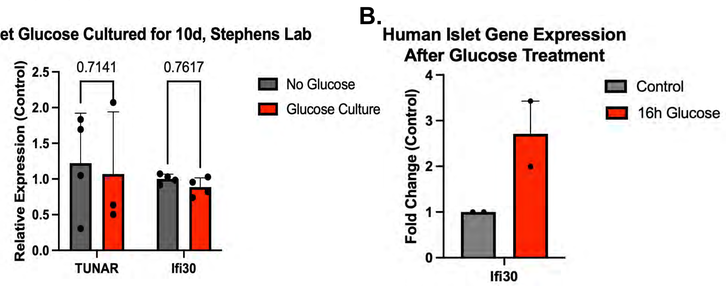

Figure 7. Islet *Ifi30* expression has increasing trends after 16h glucose treatment. (A) Relative expression of *TUNAR* and *Ifi30*, comparing mouse islet cell lines cultured with 10d, treated with no glucose and glucose. (B) Gene expression of human islet, comparing the no treatment group and treatment after 16h of glucose.

Summary and Future Directions

- A set of tools is now available for the study of *Ifi30* and GILT in vitro and in vivo, across several different species
- Obesity alters pancreatic beta-islet GILT transcription levels
- F4/80 is more strongly expressed in HFD compared to RD
- GILT is possibly expressed in macrophages and present in pancreatic tissue of mice models
- Expression of GILT affects insulin secretion (although not yet quantified)
- Generating GILT-knockout mice for systemic and tissue-related metabolic studies
- Future studies of insulin secretion in GILT KO mice using ELISA test and/or Western blot; qPCR and/or Western blot for expression of GILT

Acknowledgements

This work has been generously supported by Prof. Ling Yang- without whose constant guidance this wouldn't have been possible! I am so grateful to Tate Neff for being patient with me and teaching me the techniques I needed to know to do experimentations on pancreatic tissue. We thank to Dr. Longsheng Song and the Song Lab for allowing us to use their cryostat machine, and Dr. Stephens for assistance in data collection.

References

Arunachalam, B., Phan, U. T., Geuze, H. J., & Cresswell, P. (2000). Enzymatic reduction of disulfide bonds in lysosomes: characterization of a gamma-interferon-inducible lysosomal thiol reductase (GILT). *Proceedings of the National Academy of Sciences of the United States of America*, *97*(2), 745–750. https://doi.org/10.1073/pnas.97.2.745

Balce, D. R., Allan, E. R. O., McKenna, N., & Yates, R. M. (2014). γ-Interferon-inducible lysosomal thiol reductase (GILT) maintains phagosomal proteolysis in alternatively activated macrophages. *The Journal of Biological Chemistry*, *289*(46), 31891–31904. https://doi.org/10.1074/jbc.M114.584391

Lackman, R. L., Jamieson, A. M., Griffith, J. M., Geuze, H., & Cresswell, P. (2007). Innate immune recognition triggers secretion of lysosomal enzymes by macrophages. *Traffic (Copenhagen, Denmark)*, *8*(9), 1179–1189. https://doi.org/10.1111/j.1600-0854.2007.00600.x

Prentice, K. J., Saksi, J., Robertson, L. T., Lee, G. Y., Inouye, K. E., Eguchi, K., Lee, A., Cakici, O., Otterbeck, E., Cedillo, P., Achenbach, P., Ziegler, A. G., Calay, E. S., Engin, F., & Hotamisligil, G. S. (2021). A hormone complex of FABP4 and nucleoside kinases regulates islet function. *Nature*, *600*(7890), 720–726. https://doi.org/10.1038/s41586-021-04137-3

Rausch, M. P., & Hastings, K. T. (2015). Diverse cellular and organismal functions of the lysosomal thiol reductase GILT. *Molecular Immunology*, *68*(2 Pt A), 124–128. https://doi.org/10.1016/j.molimm.2015.06.008

Investigating Seizure Susceptibility and Sleep-Wake Cycle in APP/PS1 Mouse Models of Alzheimer's Disease

Luyi Liu[1,2,5,6], Benjamin L Kreitlow[3-6], Peyton D Alder [3,5,6], Allysa Jones[5,6], and Gordon F Buchanan MD, PhD[3-6]

[1]St. George's School, Middletown, RI, USA; [2]Secondary Student Training Program, [3]Medical Scientist Training Program, [4]Interdisciplinary Graduate Program in Neuroscience, [5]Iowa Neuroscience Institute, [6]Department of Neurology, The University of Iowa Carver College of Medicine, Iowa City, IA, USA

Introduction

Background

- Alzheimer's disease (AD) is a progressive disorder causing memory loss, cognitive decline, and amyloid beta (Aβ) plaques in the brain.
- Genetically modified APP/PS1 mice have mutations causing amyloid beta buildup similar to human Alzheimer's.[1]
  - The amyloid precursor protein (APP) is a membrane protein that, when cleaved, produces Aβ peptides, which aggregate to form plaques in AD.
  - Presenilin-1 (PS1) is part of the γ-secretase complex; mutations in PS1 promote Aβ42 aggregation and plaque formation.

Research Focus

- The earliest seizure onset in APP/PS1 mice.
- Why APP/PS1 mice have a higher incidence of epileptiform-like discharges.
- Differences in sleep-wake cycles between APP/PS1 and wild-type (WT) mice.

Hypothesis: APP/PS1 mutation in the mice causes changes in their brain excitability and altered sleep-wake cycles compared to WT mice.

Materials and Methods

Experiment #1: Genotyping

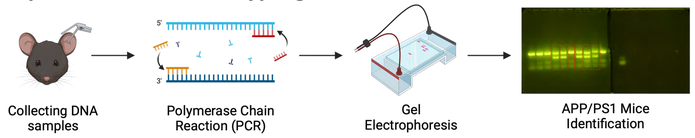

Experiment #2: Neuroanatomy

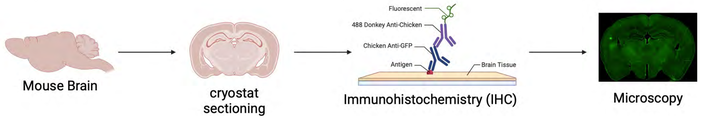

Experiment #3: Maximal Electroshock Thresholding (MEST)

*experimental animals are 3-month-old APP/PS1 mice

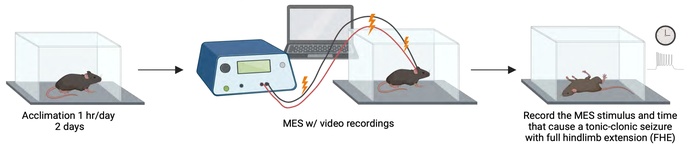

Experiment #4: EEG/EMG Analysis

*experimental animals are 3-month-old APP/PS1 mice

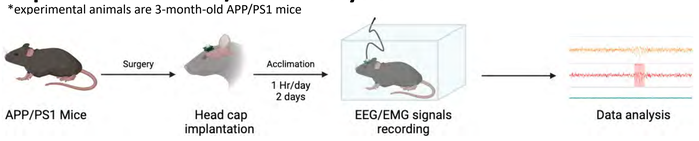

Results

Experiment #1: Genotyping

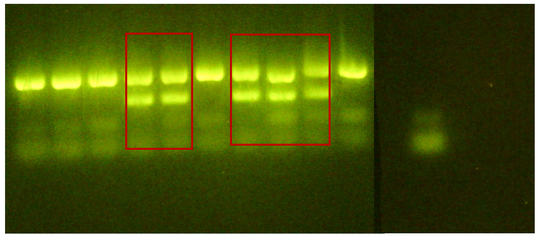

Figure 1. Gel electrophoresis image identifying APP/PS1 mice, highlighted in red squares.

Experiment #2: Neuroanatomy

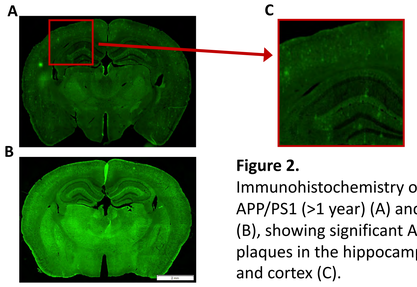

Figure 2. Immunohistochemistry of APP/PS1 (>1 year) (A) and WT (B), showing significant Aβ plaques in the hippocampus and cortex (C).

Experiment #3: MEST Analysis

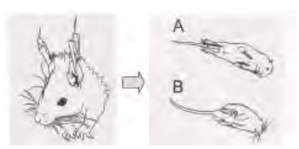

Figure 3. Generalized tonic-clonic seizure with hindlimb extension used as an endpoint in MES (A), typically followed by clonic seizures (B).[3]

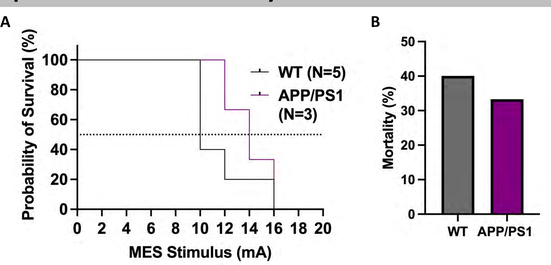

Figure 4. Survival curves (A) and mortality rate (B) of WT and APP/PS1 mice. Mortality occurs during MEST.

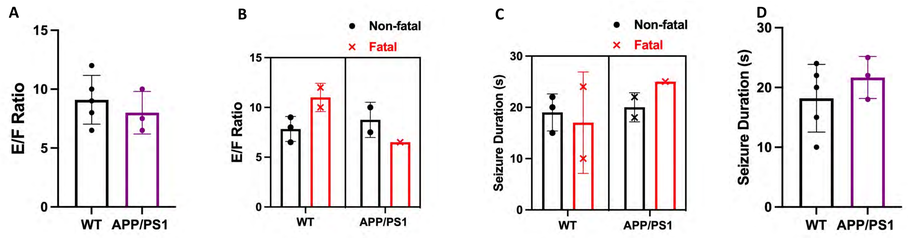

Figure 5. Severity of MES-induced seizures. Extension-to-Flexion (E/F) ratio (A,B) and seizure duration (C,D) in WT (N=5) and APP/PS1 (N=3) mice were calculated from the recordings. E/F ratio (B) and seizure duration (D) between these WT (N=3/5) and APP/PS1 (N=2/3) that are non-fatal vs. fatal.

Experiment #4: EEG/EMG Analysis

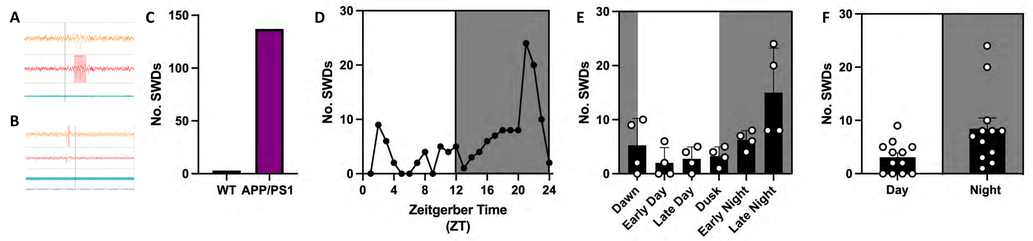

Figure 6. Spike-and-Wave Discharges (SWDs) in APP/PS1 (A) and a single spike epileptiform-like discharge (B). Number of SWDs in APP/PS1 (N=137) compared to WT (N=3) (C). SWDs in APP/PS1 Relative to Zeitgeber Time (ZT) with an increase during the dark phase (ZT 12–24) (D). SWD distribution across times of day: Dawn (ZT 0±2h), Early Day (ZT 4±2h), Late Day (ZT 8±2h), Dusk (ZT 12±2h), Early Night (ZT 16±2h), Late Night (ZT 20±2h) (E). SWDs during Day (ZT 0–12) and Night (ZT 12–24) (F).

Conclusion

Genotyping & Neuroanatomy:

- Confirmed APP/PS1 mutations and significant Aβ deposition in the hippocampus and cortex.

MEST showed increased epileptiform activity:

- APP/PS1 mice show more frequent SWDs and SSs compared to WT mice.

EEG/EMG analysis reflected sleep-wake cycle alternations:

- Increased SWDs and SSs during night-time in APP/PS1 mice.
- Indicates disrupted sleep architecture, mirroring sleep disturbances in AD.

Future Directions

- Complete current experiments to investigate potential covert pathology in the brains of young APP/PS1 mice.
- Explore early seizure phenotypes in other AD-related mouse models, such as PS19 mice, which exhibit tau protein deposition[2], and 5X FAD mice[4], which exhibit both tau and Aβ protein, for comparative studies.
- Administer anti-seizure drugs to APP/PS1 mice upon the first occurrence of seizures to observe the indirect impact on AD histopathology in later years.
- Evaluate sleep stages in APP/PS1 mice to determine sleep fragmentation, using EEG cluster scoring demonstrated in Figure 7.

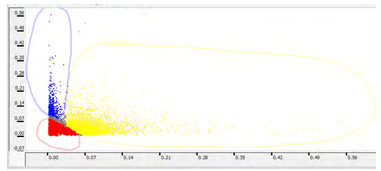

Figure 7. EEG cluster scoring for APP/PS1 mice. The plot shows EEG theta/delta power over time: blue for Non-REM, red for REM, and yellow for wakefulness.

Acknowledgments

This work was supported by the ADRD Supplement R01NS095872-05S1 (to GFB), University of Iowa 2024 Kwak-Ferguson Fellowship (to BLK), NIH/NIGMS T32 CM007337 (to Iowa MSTP), NIH/NINDS R01 NS095842 (to GFB), NIH/NINDS R01 NSNS129722 (to GFB), Cure Epilepsy Award - The Joanna Sophia Foundation (to GFB), and the Beth L. Tross Epilepsy Professorship (to GFB).

References

1. Jankowsky, J. L., Fadale, D. J., Anderson, J., Xu, G. M., Gonzales, V., Jenkins, N. A., Copeland, N. G., Lee, M. K., Younkin, L. H., Wagner, S. L., Younkin, S. G., & Borchelt, D. R. (2003). Mutant presenilins specifically elevate the levels of the 42 residue β-amyloid peptide in vivo: Evidence for augmentation of a 42-specific γ secretase. *Human Molecular Genetics*, *13*(2), 159-170. https://doi.org/10.1093/hmg/ddh019
2. Oakley, H., Cole, S. L., Logan, S., Maus, E., Shao, P., Craft, J., Guillozet-Bongaarts, A., Ohno, M., Disterhoft, J., Van Eldik, L., Berry, R., & Vassar, R. (2006). Intraneuronal β-Amyloid aggregates, neurodegeneration, and neuron loss in transgenic mice with five familial alzheimer's disease mutations: Potential factors in amyloid plaque formation. *The Journal of Neuroscience*, *26*(40), 10129-10140. https://doi.org/10.1523/jneurosci.1202-06.2006
3. Peterson, M. (1998). Electroshock. In *Neuropharmacology methods in epilepsy research* (pp. 1-26). CRC Press. https://doi.org/10.1201/9780429186851
4. Yoshiyama, Y., Higuchi, M., Zhang, B., Huang, S.-M., Iwata, N., Saido, T., Maeda, J., Suhara, T., Trojanowski, J. Q., & Lee, V. M.-Y. (2007). Synapse loss and microglial activation precede tangles in a p301s tauopathy mouse model. *Neuron*, *53*(3), 337-351. https://doi.org/10.1016/j.neuron.2007.01.010

Geocoding Birthplaces in Temporally Continuous Crowd-Sourced Family Tree Data

Ariana Luan[1], Maryam Torkashvand[2], Chun Hang Chan[2] , Caglar Koylu, PhD[2],

[1]Amador Valley High School, [2]Department of Geographical and Sustainability Sciences, University of Iowa

Background

- Previous work by Koylu et al., 2021, generated, to date, the largest population-scale family tree, which connects 40 million relatives to their common ancestors using crowdsourced genealogical data (Koylu et al., 2020).
- Tree data contains information on names, birth and death dates and places, and kinship ties such as parent-child and spouse, which can be used to measure long term migration patterns and social processes in United States at state level (Koylu et al., 2022)

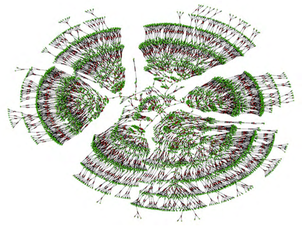

Figure 1 Example tree displaying around 6000 individuals (shown in green) and marriages (shown in red) over 7 generations. (Kaplanis et al., 2018)

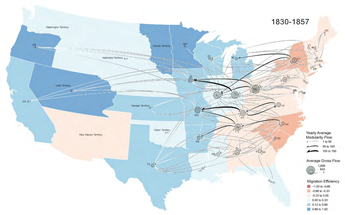

Figure 2 Example of a migration flow map derived from family tree data set. The choropleth map represents migration efficiency, flow lines represent the state-to-state migration flows (Koylu et al., 2022).

- Unlike census data, that only provide snapshots of population dynamics, tree data enables the study of a continuous evolution of population, movement, and social dynamics. However, this requires fine–scale geographic locations.
- In this research, we enrich the tree dataset by geocoding birthplaces within this data set from 1789 to 1940 on an even finer scale, down to **county or city level.**

Geocoding is the process of converting place names into geographic coordinates. However, geocoding historical places is challenging, especially for crowdsourced datasets. This works aims to address the challenges of historical geocoding:

- **Temporal factor** – constantly changing county and city names and boundaries
- **Crowdsourced data** – misspellings, inaccurate locations, inconsistent formatting

Methods

- We introduce an AI-based historical geocoding workflow to address the uncertainties in geocoding of historical crowdsourced data.
- Genealogical data stored in GEDCOM file format: name, birth date, birthplace, mother's name, father's name, etc.
- The closest possible census to birth date is found to match birth location within the correct administrative boundaries
- Hierarchical matching performed to identify first the state, then county, then city/township.

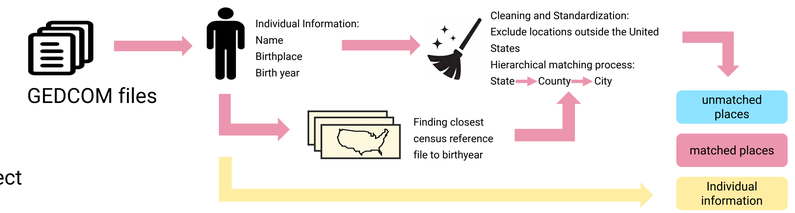

Figure 3 Overall process of geocoding. Individual information is extracted from the GEDCOM files, matched to the closest census reference (census taken in decennial intervals), and the location is matched hierarchically, from state to county to city level. Unmatched places, matched places, and individual information are then stored for further use and analysis.

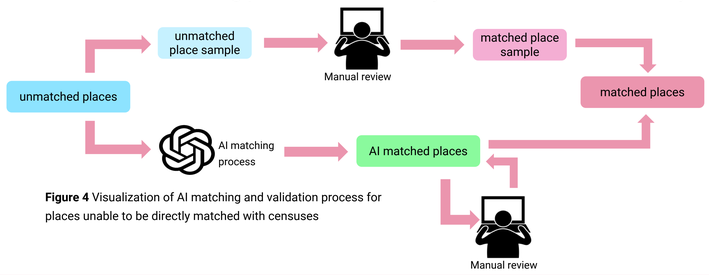

Figure 4 Visualization of AI matching and validation process for places unable to be directly matched with censuses

- Locations unable to be located directly within census references are attempted to be matched by AI

AI Validation Component

- Two main processes conducted: manual matching of unmatched places and validation and cleaning of large language model matches
- Recognize recurring problems and issues from matches with and without AI assistance
- Write scripts to pull them into separate CSVs and correct them into the proper format for further use

Results

We manually matched over 10,000 birthplaces. We found many recurring errors made for locations from both the AI-based and the code-based matching. Some of the most common errors were misrecognition of abbreviations, unnecessary phrases in the input flagged as city or county names, foreign locations marked as locations in the U.S., and confusion over administrative boundaries.

Examples of Common Errors in AI Matching:

- "stdbirthplace" contained the word probably: the "state" column would be filled out incorrectly, the city and county would be random places within the incorrect state, and the "exist" column would be "no" even if the state was within the United States.
  - Python script was written that first scanned for any state abbreviations, then string fuzzy-matched using the partial token set ratio for any shortened state names, and finally checked for the full state name to identify the correct state. Ninety-nine rows out of a sample of around forty thousand AI matches were flagged as having this issue.

task-637	probably in virginia	virginia	yes		task1_StateNocoNoc
task-738	probably nc	north carolina	yes		task1_StateNocoNoc
task-749	probably in kentucky	kentucky	yes		task1_StateNocoNoc
task-757	probably maryland	maryland	yes		task1_StateNocoNoc
task-361	probably in wales great britton		no		task2_StateNocoNoc
task-617	probably nj	new jersey	yes		task2_StateNocoNoc
task-35	probably md	maryland	yes		task3_StateNocoNoc
task-47	connecticut probably	connecticut	yes		task3_StateNocoNoc
task-455	probably tenn	tennessee	yes		task3_StateNocoNoc

- "stdbirthplace" contained a place name that identified the location specifically as a county (ex: included abbreviation "co" or word "county), the AI would also put a record in the "city" column if there was one present with the same name as the county

task-1	culpepper county virginia		virginia	culpeper	culpeper	yes
task-187	breckenridge co ky	kentucky	breckinridge		breckinridge	yes
task-592	orangeburgh co sc	south carolina	orangeburg	orangeburg		yes

Examples of Common Errors in Code-Based Matching:

- Five locations in the table below are all located in France, but have the phrase "la", which the code flagged as belonging to the state "Louisiana." This error was then manually corrected.

;la chapelle montlinard	la chapelle montlinard	la		1790	no
lac ;la biche	lac la biche	la		1880	no
;la cluse	la cluse	la		1790	no
;la durantaye	la durantaye	la		1790	no
;la durantaye bellechasse	la durantaye bellechasse	la		1790	no

- "stdbirthplace" input would contain the state "south dakota," the AI would mark the state as just "dakota." because of right-to-left string processing

aberdeen ;south dakota	aberdeen south dakota	dakota	1930
arlington kingsbury ;south dakota	arlington kingsbury south dakota	dakota	1910
badger kingsbury county ;south dakota	badger kingsbury county south dakota	dakota	1900
britton marshall county ;south dakota	britton marshall county south dakota	dakota	
brookings ;south dakota	brookings south dakota	dakota	

Conclusion and Future Directions

- We were able to identify over fifteen common issues within the AI matches and resolve five of them, so far. These issues were mostly due to the challenges of crowdsourced and unstructured data: inconsistent formatting, inaccurate and inconsistent place names, and other parsing problems.
- This work will allow for previously unmatched places to be accurately geocoded at the finest geographic scale as possible. Without the AI validation process, 48.09% of exact places were able to be matched. In the future, the hope is that 70 or even 80% of locations will be accurately geocoded.
- Fine-scale geocoded locations opens doors to tracking families through space and time and analyzing broader population dynamics, such as migration patterns and kinship networks.

Acknowledgements

I want to thank all of my mentors in the GeoSocial lab: Dr. Koylu, Maryam, Loretta, and Henry. Thank you all for being so supportive and helpful throughout this process! I also want to recognize my lab mates Devesh and Sumin for being so encouraging, our collaboration was invaluable. Thank you to the Belin Blank Center for granting me this research opportunity. Finally, I want to thank of my friends here, the people I've met are just as important as the research I've done!

Full List of References

Selected References

1. Kaplanis, J., GordoSheikh, M., Gymrek, M., Bhatia, G., MacArthur, D. G., Price, A. L., & Erlich, Y. (2018). Quantitative analysis of population-scale family trees with millions of relatives. *Science*, *360*(6385), 171–175. https://doi.org/10.1126/science.aam9309
2. Koylu, C., & Bee Kasakoff, A. (2024). Population-Scale kinship networks. *International Encyclopedia of Geography*, 1–12. https://doi.org/10.1002/9781118786352.wbieg2193
3. Koylu, C., & Kasakoff, A. (2022). Measuring and mapping long-term changes in migration flows using population-scale family tree data. *Cartography and Geographic Information Science*, *49*(2), 154–170. https://doi.org/10.1080/15230406.2021.2011419
4. Koylu, C., Guo, D., Huang, Y., Kasakoff, A., & Grieve, J. (2020). Connecting family trees to construct a population-scale and longitudinal geo-social network for the U.S. *International Journal of Geographical Information Science*, *35*(12), 2380–2423. https://doi.org/10.1080/13658816.2020.1821885
5. Torkashvand, M. (2024). A Hierarchical Approach for Geocoding Birthplaces in Temporally Continuous Crowd-Sourced Family Tree Data. CAGIS+ UCGIS Symposium 2024

Testing Combinations of WEE1 inhibitor ZN-c3 with Paclitaxel, Romidepsin, or Olaparib to Inhibit Proliferation of Endometrial Cancer Cells

Brandon Ma[1]; Xiangbing Meng, PhD[2]; Shujie Yang, PhD[2]

[1]Crystal Springs Uplands School, CA; [2]Department of Pathology, University of Iowa

Introduction

- Endometrial Cancer (EC) is the fourth **most common** cancer in women
- Estimated **67,880 new cases** and **13,250 deaths** in the US in 2024
- Incidence rates have **risen** 1% annually
- **Increasing mortality** over past 4 decades

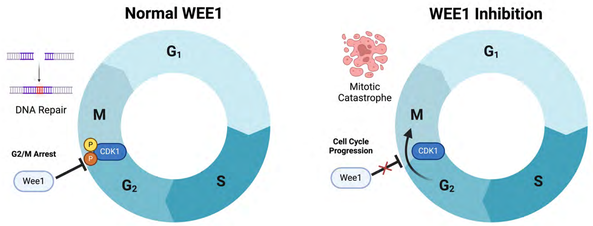

- **WEE1 upregulation** has **pro-tumorigenic** functions by maintaining tolerable level of genomic instability

Paclitaxel: a common chemotherapy drug

- Causes microtubules to stabilize by binding to tubulin
- Cell cycle arrest in mitosis

Romidepsin: a HDAC inhibitor approved for treatment of cutaneous T-cell lymphoma

Methods

Cell Viability

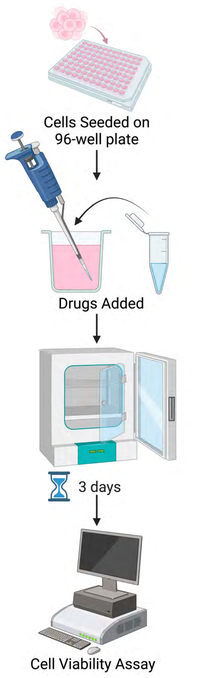

Western Blotting

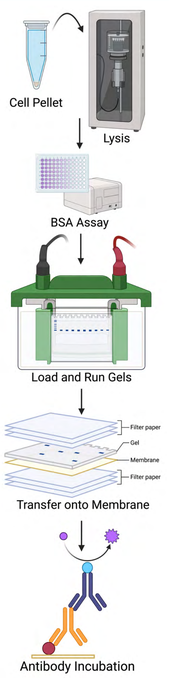

Flow Cytometry

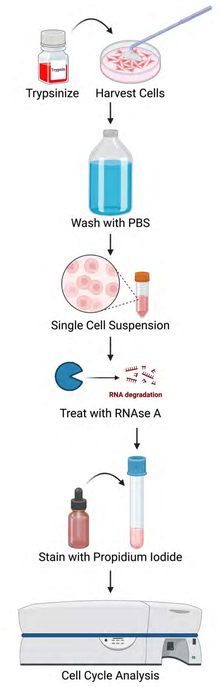

Results

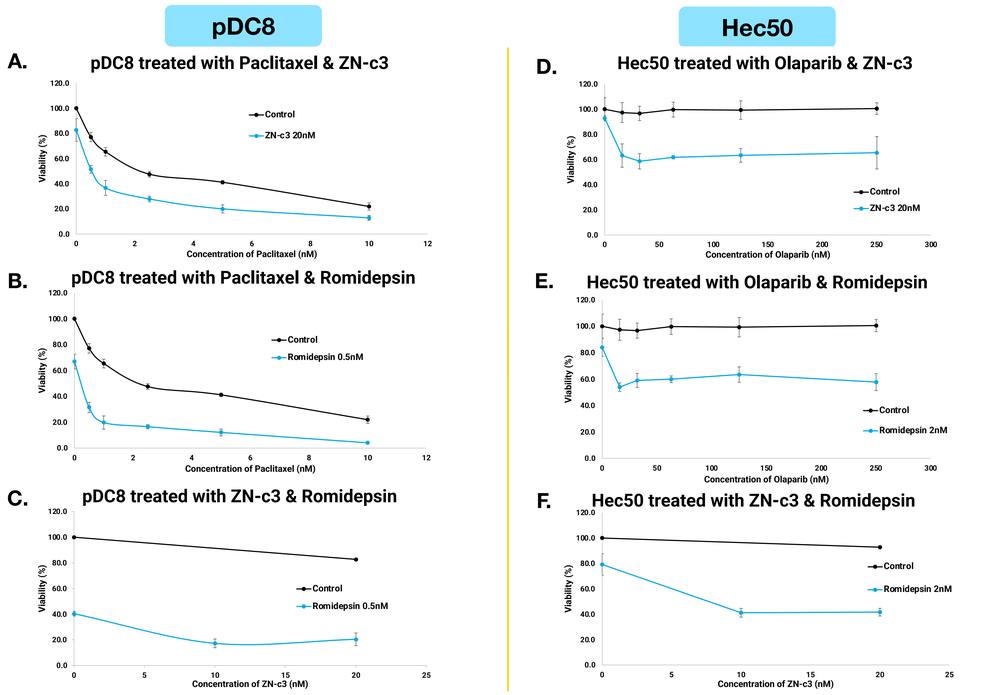

Figure 1. Synergistic Cell Death Induction in pDC8 and Hec50

(A) Paclitaxel and ZN-c3 in pDC8. **(B)** Paclitaxel and Romidepsin in pDC8. **(C)** ZN-c3 and Romidepsin in pDC8. **(D)** Olaparib and ZN-c3 in Hec50. **(E)** Olaparib and Romidepsin in Hec50. **(F)** ZN-c3 and Romidepsin in Hec50.

In both pDC8 and Hec50, ZN-c3 and Romidepsin lowered cell viability significantly compared to ZN-c3 alone. Comparing **(A)** and **(B)** cell viability, 0.5nM Romidepsin and 20nM ZN-c3 had similar effects when paired with Paclitaxel. Olaparib alone had little effect on Hec50 cells no matter the concentration. However, in combination with ZN-c3 or Romidepsin, even a low concentration of Olaparib resulted in an increased effect.

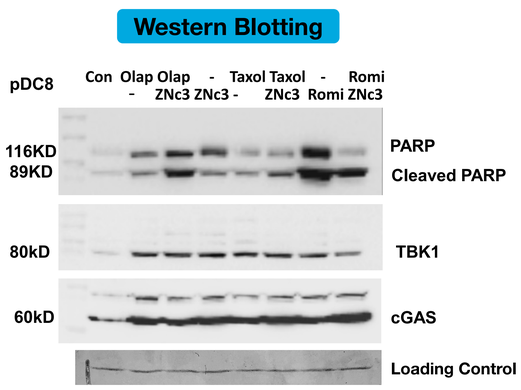

Figure 2. Effect of Drug Combination on PARP Cleavage and Immune Response Pathway in pDC8

Specific antibodies against PARP (cell signaling), TBK1 and cGAS (Santa Cruz Biotech) were used. Increase from PARP to Cleaved PARP indicates apoptosis. TBK1 and cGAS have role in innate immune response and triggering interferons.

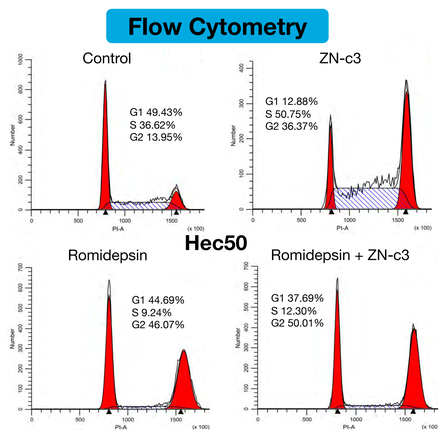

Figure 3. Representative Flow Cytometry for Cell Cycle Analysis

Individual ZN-c3 and Romidepsin showed increase G2 cells compared to the control. Combination Romidepsin and ZN-c3 showed slight G2 cell increase compared to single drugs.

Results

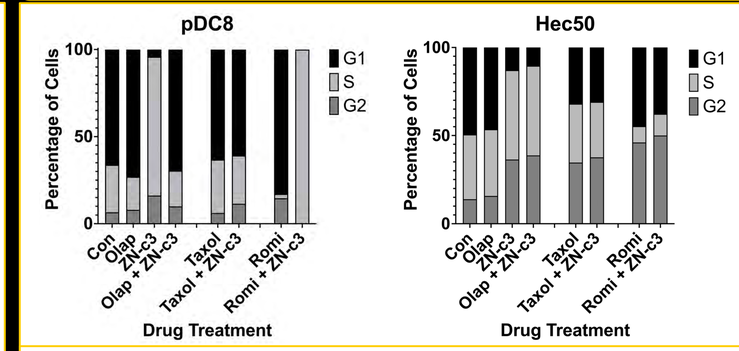

Figure 4. Cell Cycle Analysis Across Drug Combinations

*pDC8 Romi + ZN-c3: majority of cells in G1 and S phase. For pDC8 treatment, ZN-c3 alone and Romidepsin alone caused the greatest G2 cells.

For Hec50 treatment, ZN-c3 + Romidepsin had the highest percentage of G2 cells, while ZN-c3 + Taxol, and ZN-c3 + Olaparib had similar G2 cell percentages.

Conclusion and Future Directions

ZN-c3 and Romidepsin are novel drugs. To enhance and find more treatment options, various combinations were tested. Our findings were:

1. The combination of ZN-c3 and Romidepsin led to G2 arrest, effectively induced apoptosis, and proved to be synergistic in effect in pDC8 and Hec50
2. TBK1 and cGAS upregulation indicated activation of innate immune response by all drug combinations
3. ZN-c3 toxicity not dose-dependent in concentrations above 10nM

Further studies should include lowering the concentrations used in combinations for flow cytometry. Ex: 5nM Romi and 50nM Zn-c3 instead of 20nM and 100nM respectively. This should hopefully produce a greater synergistic or additive effect. Conducting *in vivo* testing and eventual clinical trials are the next steps.

Acknowledgments

Thank you to Dr. Meng and Dr. Yang for welcoming me in the lab and their invaluable mentorship. Thank you to SSTP and the Belin-Blank Center for this amazing opportunity. This project was supported by NIH R37-CA238274(SY) and the Department of Pathology Start-Up Fund (SY). Images created with BioRender.com.

References

1. Li, Y., et al, (2022). Enhancing progestin therapy via HDAC inhibitors in endometrial cancer. *American journal of cancer research*, *12*(11), 5029–5048.

2. Meng, X., et al, (2013). Induction of mitotic cell death by overriding G2/M checkpoint in endometrial cancer cells with non-functional p53. *Gynecologic Oncology*, *128*(3), 461–469. https://doi.org/10.1016/j.ygyno.2012.11.004

3. Meng, X., et al, (2021). Recent advances of WEE1 inhibitors and statins in cancers with p53 mutations. *Frontiers in Medicine*, *8*. https://doi.org/10.3389/fmed.2021.737951

Implications of Developmental Onset Brain Lesions on Emotional Regulatory Abilities and Overall Function-A Comparative Study:

Noah J. Martenson[1, 2]; Emma Brandt[2]; Daniel T. Tranel[2, 4], PhD; Carolina Deifelt Streese[2, 3], PhD; Joel Bruss[2]

[1]Bettendorf High School, Bettendorf, IA; [2]Department of Neurology, University of Iowa, Iowa City, IA; [3]Department of Neurosurgery, University of Iowa, Iowa City, IA; [4]Department of Psychological and Brain Sciences, University of Iowa, Iowa City, IA

Introduction:

Background:

- While there have been several studies on the academic, behavioral, and psychiatric effects of developmental onset brain lesions, (abnormal areas of brain tissue caused by injury, infection, or disease occurring in individuals whose brains are still in stages of increased development) there is extremely limited research and literature when it comes to the long-term implications of developmental onset lesions on emotional regulatory ability.

Objectives/Goals:

- This study aims to determine if lesion onset occurring during critical periods of brain development leads to worse emotional regulation when compared to adults whose lesions developed during adulthood. Poor emotional regulatory ability, which can present as persistent negative emotions and can be measured through neuropsychological evaluations, may be disproportionately high among developmental onset patients due to the increased vulnerability of the developing brain.

Methods:

Evaluations:

- The two neuropsychological evaluations utilized here to measure emotional regulation and overall function are the BDI (Beck Depression Inventory: Scored from 0, indicating no depression, to 63, indicating severe depression) and the MMPI (Minnesota Multiphasic Personality Inventory). The four subscales of the MMPI (EID, RCd, RC2, and RC7) utilized in this study are used to measure emotional/internalizing dysfunction, demoralization, low positive emotion, and dysfunctional negative emotion, respectively.

Matching/Comparison:

- Through matching and comparing developmental onset patients to adult-onset patients by their lesions and demographics, we can minimize the differences between the two subject groups to critical variables such as age at lesion onset, ultimately removing many outside, confounding variables.

Factors taken into consideration:

- Sex, race, epilepsy diagnosis, lesion laterality, lesion volume, age at lesion onset, years of education, and handedness
- Presence or past substance abuse, history of serious mental illness (schizophrenia, bipolar, etc.), and/or other neurological disorders not associated with an individual's lesion were all considered exclusion criteria for this study.
- Availability of MMPI/BDI data was also taken into consideration when considering potential matches

(Highlights and underlines for representing factors treated with more importance when searching for matches due to being more significant in potentially affecting results)

Results:

Significance:

- The data show a significant relationship between lesion onset occurring during important periods of development and higher levels of depression later in life.
- All other data are approaching significance but have not yet passed the threshold for statistical significance (indicated by a p value of ≤.05).

Conclusions:

- From the data (p values, mean difference in scores, t scores, etc.) we can gather that there seems to be a strong correlation between sustaining a brain lesion at a young age and presenting with higher levels of depression as an adult when compared to patients who match demographically and sustained their lesions as adults. However, the data do not yet provide support for claims of significance for any of the MMPI subscales associated with emotional regulation

Independent Samples Test **Figure A**: Combined results of statistical analyses

#	t	df	Two Sided p	Mean Difference	std. Error Difference	Lower	Higher
BDI Total	2.791	35.162	.008	5.680	2.035	1.588	9.772
EID	1.809	25.359	.082	5.944	3.285	-.817	12.706
RC2	1.898	23.596	.070	7.513	3.958	-.662	15.689
RC7	1.326	26.572	.196	4.026	3.037	-2.209	10.561
RCd	2.039	27.687	.051	7.069	3.467	-.036	14.174

Participant/Sample Info:

CATEGORIES	PARTICIPANT DATA
N	50 (25 developmental onset patients and their matches)
Sex	54% male/46% Female
Mean years of education at scan date	13.36 years
Lesion laterality	12% bilateral, 20% left lateral, 68% right lateral
Mean age at onset (developmental)	7.9052
Mean age at onset (adult)	53.94
Race	100% of participants were white

Conclusion

Future Directions:

- While many of the MMPI subscales showed that they were approaching significance, the resulting data show that there is a strong relationship between having an early age of lesion onset and subsequently higher scores/increased severity of depression as measured by the BDI. A possible future project could delve more in depth into this result and explore the possible links between developmental brain lesions and increased presence and severity of depression
- If someone were to looking into this further, I would recommend working with a larger sample size. A larger sample size would not only allow for closer to perfect matches, but also would allow some of the outliers that can skew data to be rounded out by the number of other people in the study.

Limitations:

- One issue with the data which limited the study was the small sample size. Due to a lack of data for patients affected by developmental onset lesions, we were unable to find a large enough sample size to round out some of the outliers and paint a more complete picture of the effects.
- Another major limitation was time. Because of a lack of time, we were unable to match lesion location and specificity beyond the lesion's laterality and volume. The inconsistency in lesion location between the two groups is a variable which we cannot rule out for effecting the results of the study.

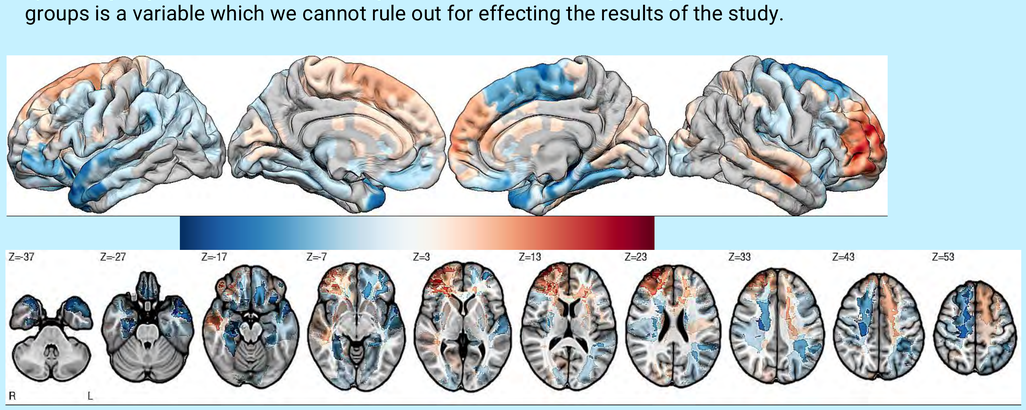

Figure B: Overlay of lesion onset location of both groups. Warmer colors denoting the developmental-onset group and cooler colors denoting the adult-onset group.

Implications:

- The findings of this study could better help physicians anticipate the potential long-term support that patients with developmental onset lesions could need, and so therefore those patients will be able to receive the resources and support they need.

Acknowledgments:

I would like to thank the whole Tranel Cognitive Neuroscience Lab for being incredibly supportive and helpful throughout the program. Additionally, I would also like to specifically thank my mentor, Emma Brandt, for all her time and energy spent guiding me through my project. Finally, I would like to thank Dr. Tranel, Dr. Deifelt Streese, and Joel Bruss for their tremendous help and support.

References: Sullivan, Alyssa, et al. 2022. Academic Skills after Brain Injury: A Lifespan Perspective, American Psychological Association

Sullivan, Alyssa, et al. 2023. Implications of age at lesion onset for neuropsychological outcomes: A systematic review focusing on focal brain lesions

Lidzba, Karen, et al. 2009. Early Plasticity versus early vulnerability: the problem of heterogeneous lesion type

IOWA
Carver College of Medicine

Hot Dog Water and Cooking Snails: Temperature Regime Influences Snail Memory

Joseph Nangle[1,2], Morgan Anderson[3], & Maurine Neiman[3]
[1]Inglemoor High School, Kenmore, WA
[2]Cascadia Community College, Bothell, WA
[3]Department of Biology, University of Iowa

The Significance of Memory in Snails

- Memory is critical in key behaviors like foraging, predator avoidance, migration, and territoriality (Soravia et al. 2021)
- Thermal stress (TS) can negatively impact the ability to retain these memory functions

What is our main goal?

- **Part 1:** Find a stimulus that a) influences snail behavior and b) the snail can learn to associate with ("carrot") or avoid ("stick")
- **Part 2:** Place snails under TS to determine how it impacts their ability to remember the presence of a stimulus

Entrainment & Assessing Memory as a Function of Temperature

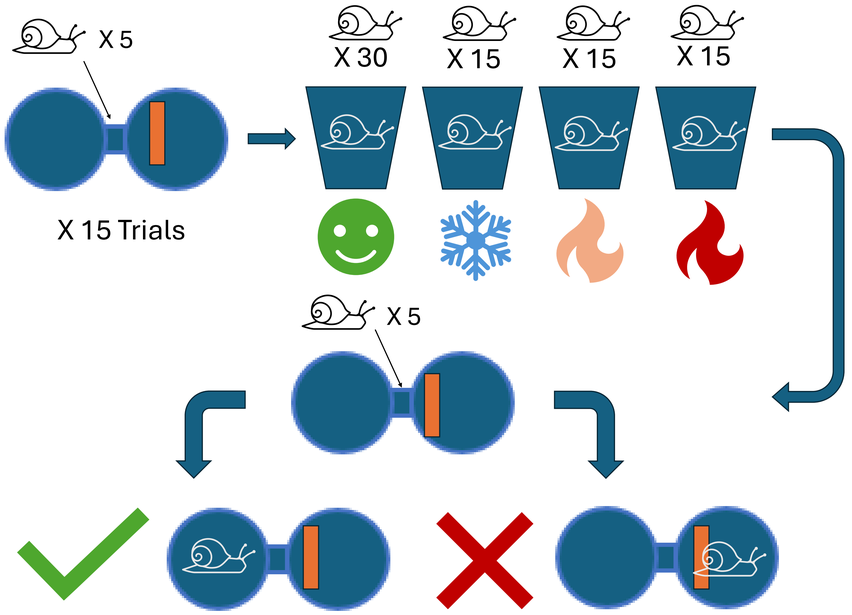

How do snails give us insight into climate change?`

- *P. antipodarum* are invasive around the world and growing in importance as an aquatic sentinel species and ecotoxicology model
- Knowing how TS impacts *P. antipodarum* can give insight into how TS effects might affect organisms and ecosystems on a global scale

Cold Temperature Seems to Facilitate Memory Retention

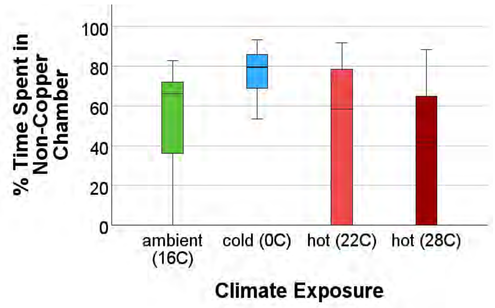

Fig. 1. Memory retention as a function of TS. Temperature treatment significantly affected memory retention (Fisher's Exact Test (p = 0.023).

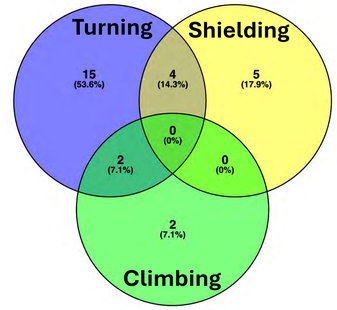

Fig. 2. Snails displayed multiple different avoidant behaviors in the presence of copper.

Conclusions & Future Applications

- *P. antipodarum* can be trained to avoid copper
- Snail avoidance of copper is facilitated by cold and hindered by heat
- Testing cold temperatures in relation to memory in other organisms could help us develop treatments for memory loss
- We could test TS effects on memory and further implications of TS for key behaviors

References & Acknowledgments

Soravia et al. 2021, WIREs Climate Change.
Barnes et al., 2022, Marine Ecology Progress Series.
Nowogrodzki et al. 2024, Nature.

Thank you to the Neiman Lab for feedback and assistance.
We also appreciate helpful discussions with Dr. Mark Blumberg and Bennett Brown.

IOWA College of Education Belin-Blank Center

Comparative Analysis of Sleeve Gastrectomy and Gastroplasty Efficacy in Diet-Induced Obesity Mouse Models

Suhani Pahuja[1], Mohammad Jarrah[2], Mohamad Mokadem[2]

[1]Monta Vista High School, [2]Department of Internal Medicine, Division of Gastroenterology and Hepatology, University of Iowa, Iowa City, IA

Introduction

Sleeve gastrectomy and sleeve gastroplasty are weight loss procedures that restrict food intake by altering the stomach's anatomy. Sleeve gastrectomy involves removing about 80% of the stomach, significantly reducing its capacity (Mokadem Lab, n.d.). Sleeve gastroplasty, often performed endoscopically, sutures the stomach into a tube-like shape without removal (Mokadem Lab, n.d.). While both limit stomach size, sleeve gastrectomy is more invasive with a longer recovery and higher risks, whereas sleeve gastroplasty is less invasive with quicker recovery and fewer complications.

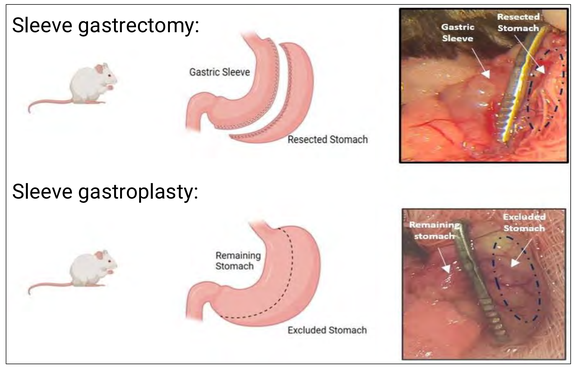

Figure 1. Sleeve gastrectomy vs. Sleeve gastroplasty: Sleeve gastrectomy (top) involves incision of the stomach whereas sleeve gastroplasty (bottom) makes the stomach smaller through a suturing device.

Objectives

The objective of this study was to compare the efficacies of sleeve gastrectomy and gastroplasty in mitigating diet-induced obesity (DIO) in mice. Specifically, we aimed to evaluate and contrast the effects of these two surgical interventions on weight changes, lipid profile, and feeding behavior over a 6-week period, using a sham-operated group as a control.

Methods

Diet Induced obesity (DIO) mice were divided into three intervention groups: Sham, Sleeve Gastrectomy, and Gastroplasty, and observed for 6 weeks.

Results

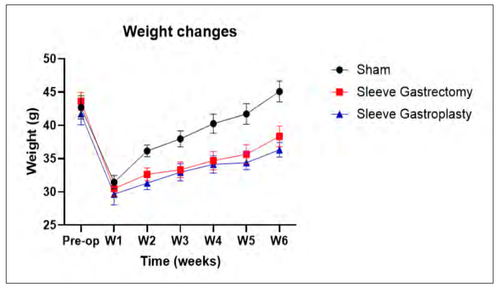

Figure 2. Weight changes: Mice under all conditions experienced rapid weight loss during the first week after initiation, and then slowly regained weight over a period of 5 weeks. Mice treated with sleeve and gastroplasty experienced a regain in weight at almost identical rates which were significantly less than that of the sham or control mice.

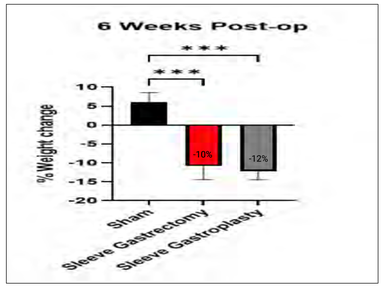

Figure 3. 6 Weeks Post-Op Weight Change: Sham mice experienced minor weight gain, in contrast to sleeve and gastroplasty mice, which experienced weight loss. However, the magnitude of weight loss for sleeve and gastroplasty mice is roughly equal.

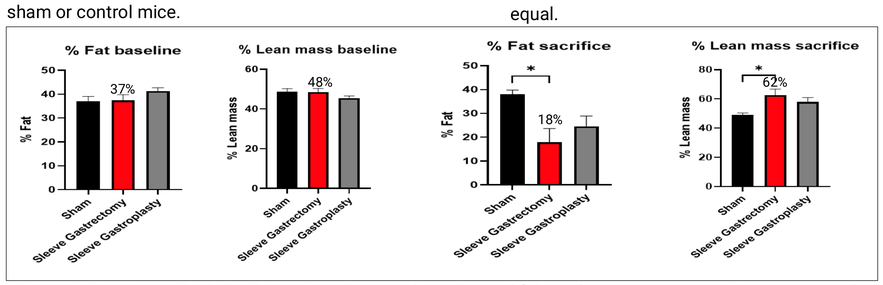

Figure 4. Pre-Op vs. Post-Op Body Mass Composition: Original fat and lean mass composition was roughly the same amongst all mice models, but after surgery the sleeve gastrectomy mice had a much higher lean-to-fat mass ratio than the sham mice.

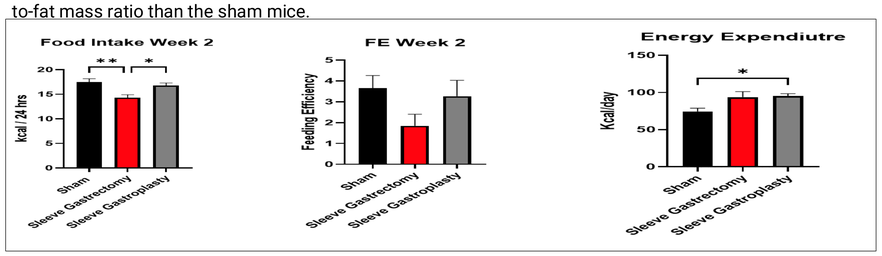

Figure 5. Mechanisms Causing Weight Loss: Food intake for Sham and gastroplasty mice are comparable whereas that for gastrectomy treated mice is considerably less. Feeding efficiency* is roughly the same amongst all mice, and energy expenditure is comparable between the sham and gastrectomy mice but significantly higher for the gastroplasty mice.

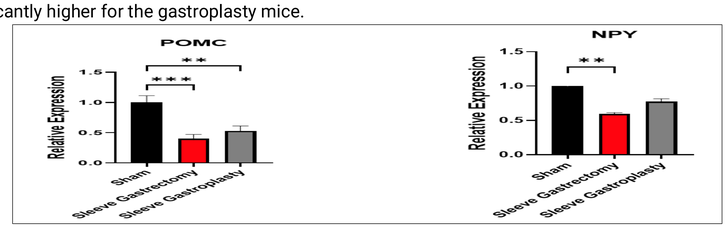

Figure 6. POMC and NPY Expression: Decreased POMC expression in both gastrectomy and gastroplasty mice as well as decreased NPY expression in gastrectomy mice.

Conclusions & Implications

- Weight loss efficacy for sleeve gastrectomy and sleeve gastroplasty are comparable
- Both procedures result in a net weight loss after a period of 6 weeks. Sleeve gastrectomy resulted in around 10% weight loss, and sleeve gastroplasty, 12%.
- Sleeve gastrectomy results in a higher lean-to-fat mass ratio post-operation as opposed to sleeve gastroplasty, which has little effect on body mass composition
- Sleeve gastrectomy induces weight loss via regulation of food intake
- Sleeve gastroplasty induces weight loss via regulation of energy expenditure
- Reduced POMC and NPY expression suggests that both surgical interventions not only physically restrict the stomach but also induce neurochemical changes that modulate appetite and energy expenditure

Acknowledgments

I would like to thank Dr. Yi Chu for demonstrating several experiments in the lab to me and helping me interpret data from basic experiments. I would also like to thank Dr. Mohamad Mokadem for his oversight in the lab. Finally, I would like to thank Dr. Mohammad Jarrah for his help collecting data and overseeing the creation of this poster.

References

Ballsmider, L. A., Vaughn, A. C., David, M., Hajnal, A., Di Lorenzo, P. M., & Czaja, K. (2015). Sleeve gastrectomy and Roux-en-Y gastric bypass alter the gut-brain communication. *Neural Plasticity*, 2015. https://doi.org/10.1155/2015/601985

Fayad, L., Adam, A., Schweitzer, M., Cheskin, L. J., Ajayi, T., Dunlap, M., Badurdeen, D. S., Hill, C., Paranji, N., Lalezari, S., Kalloo, A. N., Khashab, M. A., & Kumbhari, V. (2019). Endoscopic sleeve gastroplasty versus laparoscopic sleeve gastrectomy: A case-matched study. *Gastrointestinal Endoscopy, 89*(4), 782–788. https://doi.org/10.1016/j.gie.2018.08.030

Lutz, T. A., & Bueter, M. (2016). The use of rat and mouse models in bariatric surgery experiments. *Frontiers in Nutrition, 3*, 25. https://doi.org/10.3389/fnut.2016.00025

Stefater, M. A., Wilson-Pérez, H. E., Chambers, A. P., Sandoval, D. A., & Seeley, R. J. (2012). All bariatric surgeries are not created equal: Insights from mechanistic comparisons. *Endocrine Reviews, 33*(4), 595–622. https://doi.org/10.1210/er.2011-1044

Sullivan, S., Edmundowicz, S. A., & Thompson, C. C. (2017). Endoscopic bariatric and metabolic therapies: New and emerging technologies. *Gastroenterology, 152*(7), 1791–1801. https://doi.org/10.1053/j.gastro.2017.01.044

Utilizing RAG and CoT Frameworks for Augmenting and Improving LLM Capabilities in Prediction of Patient ICD-10 Diagnosis

Rudransh Pathak[1], Gabriel Vald[2], M.S., Yusuf Sermet[2], PhD., Ibrahim Demir[2], PhD.

[1]William P. Clements High School, Sugar Land, TX, [2]University of Iowa, College of Engineering

IIHR—Hydroscience and Engineering

UIHI Lab

Introduction

- Currently, ICD-10 Prediction using Large Language Models(LLMs) is a very underexplored topic in the current literature and has not provided high accuracy rates in prediction[1,2].
- In the increasing usage of AI in the modern world today, using LLMs for this task can be extremely helpful for doctors and hospital patients alike[2,3].

LLMs

AI deep learning models that are pre-trained on vast amounts of data for language generation tasks

GPT-4o

ICD-10 DX

The modern code used to classify and diagnose healthcare patients, used universally.

- Thus, we explore:

"Which LLM frameworks can be optimized to enhance the predictive accuracy of LLMs in medical diagnosis?"

Objectives

- To **challenge and explore** existing assumptions about the limitations and capabilities of AI in interpreting complex medical data; facilitating new research and applications in AI and healthcare integration, improving on previous application attempts.
- Aim to make the medical diagnostic process less complex and **easy-to-use** for doctors and patients, leading to more accurate and **cost-effective healthcare** delivery.

Methodology

- Utilized the **HCUP Dataset**: Largest publicly available pediatric database in the US, providing data on hospitalizations for children under 21. Comprises **3000000+** patient records with **1000+** relevant parameters to predict ICD-10 diagnoses.

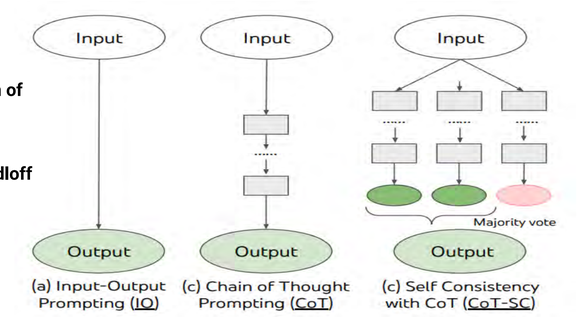

Figure 1: Chain of Thought(CoT) Prompting visualized(Heidloff 2023)[4]

Test Bed Flow

Employed key Python libraries of **Pandas, OpenAI, and LangChain** in order to create test bed to analyze four different LLM frameworks and methodologies using GPT-4o.

Figure 2: Test Bed Flowchart

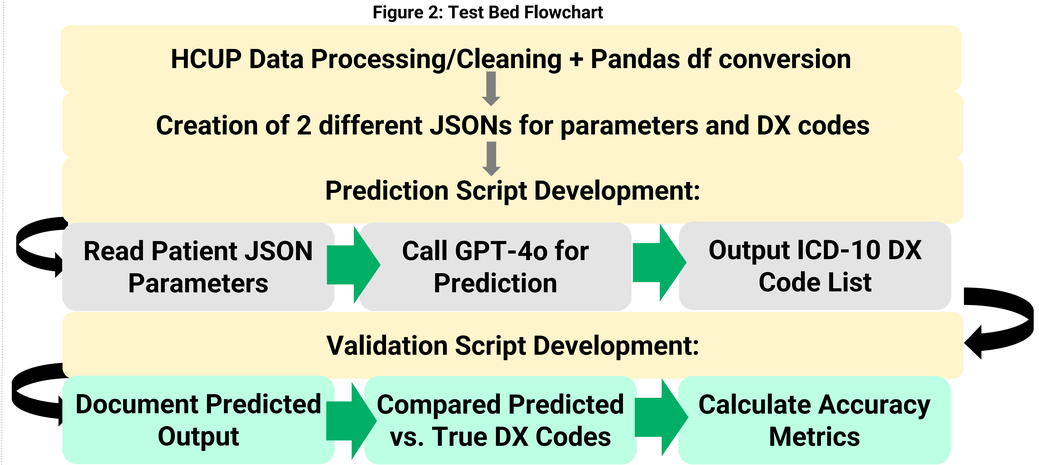

Figure 3: Retrieval Augmented Generation(RAG) Process (Hazem et. al 2023)[5]

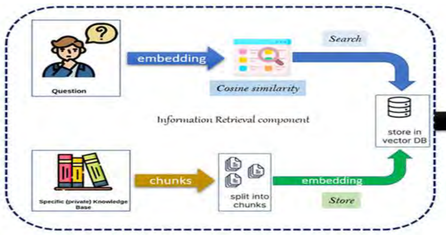

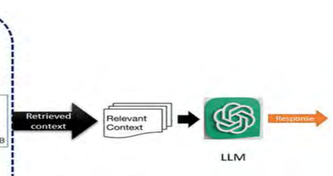

Figure 4: Table of key accuracy prediction metrics comparing all 4 frameworks/methods

Results

Our most important metric!

Cumulative Accuracy Table	Base GPT-4o	GPT-4o + CoT	GPT-4o + RAG	GPT-4o+ CoT + RAG
Patient Acc	8.01%	27.33%	31.80%	**47.27%**
Diagnosis Acc	5.83%	20.87%	21.84%	**34.47%**
Output Length Acc	90.78%	**100%**	93.69%	97.09%
Distinctness Acc	84.67%	96.79%	96.93%	**97.44%**
Real Acc	79.68%	**100%**	88.26%	95.15%

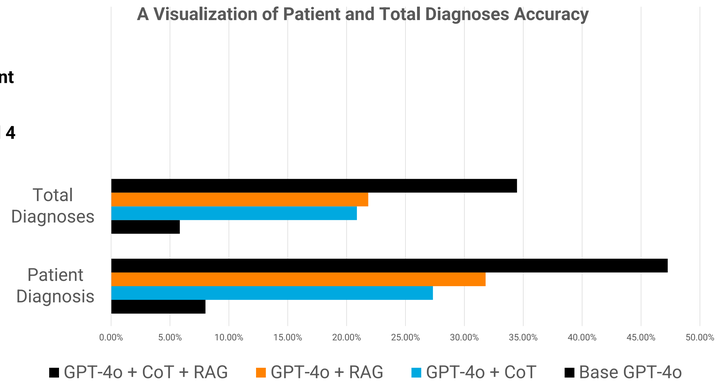

Figure 5: Chart of Patient and Total Diagnosis Accuracy comparing all 4 frameworks/methods

Discussion

- RAG coupled with CoT showcased the greatest improvement in performance from the base model, having the highest patient diagnosis accuracy and improving on the base model by **>39%.**
- CoT had impressive results in the diagnosis length and real accuracies, having **100% accuracy** for both metrics.
- Overall, the implementation and success of the combination of RAG and CoT with GPT-4o shows that adding another complexity layer of finetuning can potentially increase accuracy further.

Limitations:

- The intense use of resources required by the RAG framework may not be applicable to all healthcare scenarios, especially in less economically privileged areas.
- Because AI fully relies on the data it is trained on, proper care must be taken in order to not introduce bias and not overfit the AI model.
- A wide variety of different data variables and features are required for proper ICD-10 diagnosis, some of which may not be available in all settings.

Future Direction

- Finetuning model to add another layer of complexity and **learn patterns** of ICD-10 DX codes better to enhance performance.
- Implement further data cleaning and processing techniques for **detecting and correcting biases** in data.
- Utilize more records within the dataset and experiment with different RAG retrievers for the optimal RAG setup.

Acknowledgments

Thank you so much to Gabriel Vald for his exceptional mentorship throughout this project, as well as to Dr. Sermet and Professor Demir for their expertise and project guidance. Thank you to the SSTP program and the Belin-Blank Center for this research opportunity, which I plan to continue even after the program finishes.

References

1. Li, R., Wang, X., & Yu, H. (2024). Exploring LLM multi-agents for ICD coding. *arXiv preprint*. https://arxiv.org/abs/2406.15363
2. Lee, S. (2024). Can large language models abstract medical coded language?. *arXiv preprint.* https://arxiv.org/html/2403.10822v3
3. Pedersen, B., Islam, M., Kristoffersen, D. T., Bongo, L. A., Garrett, E., Reid, A., & Sommerseth, H. (2024). Coding historical causes of death data with large language models. *arXiv preprint.* https://arxiv.org/abs/2405.07560
4. Heidloff, N. (2023). *Understanding Chain of Thought Prompting.*
5. Abdelazim, Hazem & Waheed, Mohamed & Mohamed, Ammar. (2023). Semantic Embeddings for Arabic Retrieval Augmented Generation (ARAG). *International Journal of Advanced Computer Science and Applications.* 14.10.14569/IJACSA.2023.01411135.

EFFECTS OF ACADEMIC ACCELERATION ON THE SELF-CONCEPT OF TWICE-EXCEPTIONAL STUDENTS

Alicia Ran[1], Brandon LeBeau Ph.D.[2]

[1]Harker Upper School, [2]University of Iowa Belin-Blank Center

Introduction

- All students need challenges in their **zone of proximal development**, but proper academic challenge often not provided to high-ability or twice-exceptional students by grade-level classes (Lubinski & Vanderbilt University, 2004)
- The heterogeneous nature of disabilities also leaves many disabled and twice-exceptional students feeling **unsupported** in a traditional learning environment (Dell'Anna et al., 2020)
- Support for twice-exceptional students, specifically, needs to be **highly individualized** and administered by qualified professionals (Dell'Anna et al., 2020).
- Furthermore, high-ability and twice-exceptional students may feel **socially isolated** because of their greater intellectual capabilities (Gross & Smith, 2019; Chapman, 2009)
- This lack of academic challenge and support combined with social isolation may cause high-ability and twice-exceptional students to **have less positive self-concepts** than the general population (Chapman, 2009)
- Academic acceleration helps many high-ability students increase their self-concept & engagement with school (Gross & Smith, 2019)

How does academic acceleration relate to the self-concept twice-exceptional students?

Methods

TERMINOLOGY

- *High-ability*: IQ ≥ 120
- *Twice-exceptional*: high-ability with one or more disabilities

DATA OVERVIEW

- 376 students aged 5-18 (M=10.7, SD=2.76)
- 286 males, 86 females
- Patients at the Belin-Blank Clinic

KEY MEASURES

- IQ
- Piers-Harris Self-Concept Scale

Results

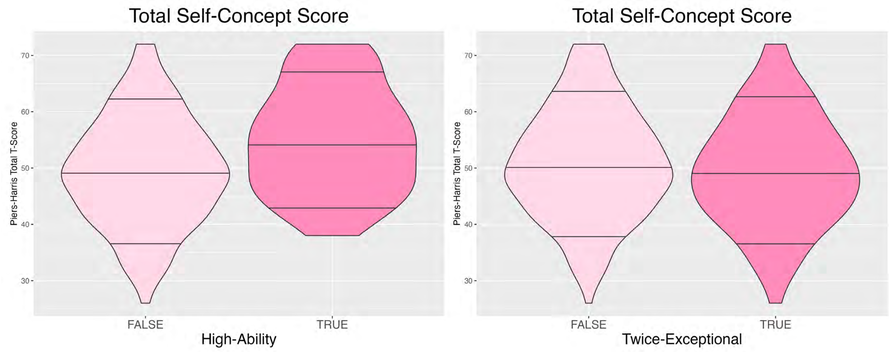

Figure 1: Distribution of total Piers-Harris assessment scores across diagnoses

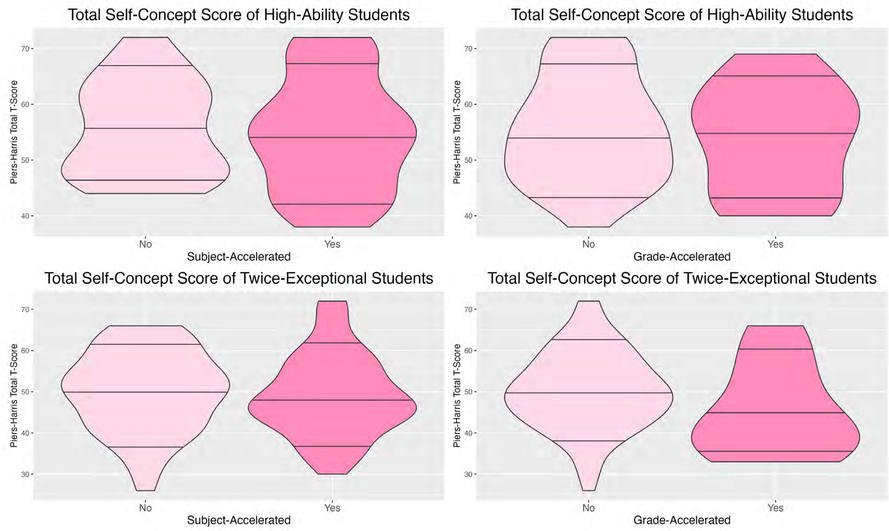

Figure 2: Distribution of total Piers-Harris assessment scores across ability groups and acceleration statuses.

References

Chapman, C. (2009). A smoother acceleration: Addressing transition issues that arise for accelerated gifted students. *The Science Teacher*, *76*(3), 42-45.

Dare, L., Nowicki, E. A., & Smith, S. (2019). On deciding to accelerate: High-Ability students identify key considerations. *Gifted Child Quarterly*, *63*(3), 159-171. https://doi.org/10.1177/0016986219828073

Dell'Anna, S., Pellegrini, M., Lanes, D., & Vivanet, G. (2020). Learning, social, and psychological outcomes of students with moderate, severe, and complex disabilities in inclusive education: A systematic review. *International Journal of Disability, Development and Education, 69*(6), 2025–2041. https://doi.org/10.1080/1034912X.2020.1843143

Gross, M. U. M., & Smith, S. R. (2019). Put them together and see how they learn! Ability grouping and acceleration effects on the self-esteem of academically gifted high school students. In *Handbook of Giftedness and Talent Development in the Asia-Pacific edited by Susen R. Smith* (pp. 1-26). Springer, Singapore. https://doi.org/10.1007/978-981-13-3021-6_17-1

Discussion

While acceleration can benefit students, our study showed that acceleration can also have **neutral or negative effects** on the self-concept of high-ability and twice-exceptional students. Some **key factors** which may have caused our results are listed below:

- Many students are **not supported** during and after their acceleration by their school and community (Dare et al., 2016)
- Students may experience **additional stigma** from their new and grade-level peers because they are accelerated
- Many teachers receiving high-ability and twice-exceptional accelerated students need **more special education training** (Dare et al., 2016)

The level of support required to aid disabled students is often not available for accelerated twice-exceptional students, explaining their **negative experiences** with acceleration.

- Additionally, twice-exceptional students may continue to exhibit symptoms other students perceive as different even after acceleration, causing the continuation of their **social isolation.**
- As a result, twice-exceptional students may be more impacted by the **decrease in self-efficacy** correlated with acceleration (Chapman, 2009).

Limitations

Our sample is a male-dominated, predominantly white clinical sample of students from Midwestern families with high socioeconomic statuses. Because of these demographic limitations, this study cannot be generalized to the greater twice-exceptional and high-ability accelerated population.

Acknowledgements

Special thanks to Professor Brandon LeBeau and Dr. Katie Schabilion for their guidance on this study. Thank you to the University of Iowa, Belin-Blank Center, and SSTP for providing us with the incredible opportunity to conduct research in a professional setting.

Evaluating Neurocognitive Differences in Hemophilia A Through Comparison of Behavioral Tests and Brain Presence of Factor VIII

Julia Ran[1], Kevin Gubner[2], Danielle York[2], Janice Staber, MD[2]

[1]Unionville High School; [2]Department of Pediatrics, University of Iowa Stead Family Children's Hospital

Background

Hemophilia A (HA):

- X-linked genetic bleeding disorder affecting 400,000 individuals
- Caused by deficiencies in coagulation factor VIII (FVIII)
  - FVIII is a large glycoprotein responsible for thrombin generation to form a fibrin clot (Shen et al., 2008)
  - Left untreated, hemorrhagic bleeding events may lead to early death (Staber & Pollpeter, 2016)

Coagulation Cascade

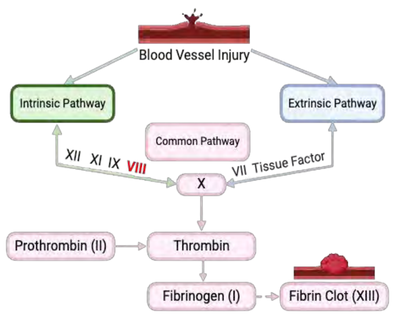

Neurocognition:

- People with HA have an increased prevalence of anxiety (16%), depression (14.5%), and ADHD (15.3%) compared to the general population (Al-Huniti et al., 2020)

Objectives

1. Examine anxiety and depression-like behavior in hemophilia mice
2. Investigate factor VIII levels in brains of wild-type (WT) mice

To determine if there is a correlation between the behavior phenotype and level of FVIII protein in the brain.

Methodology

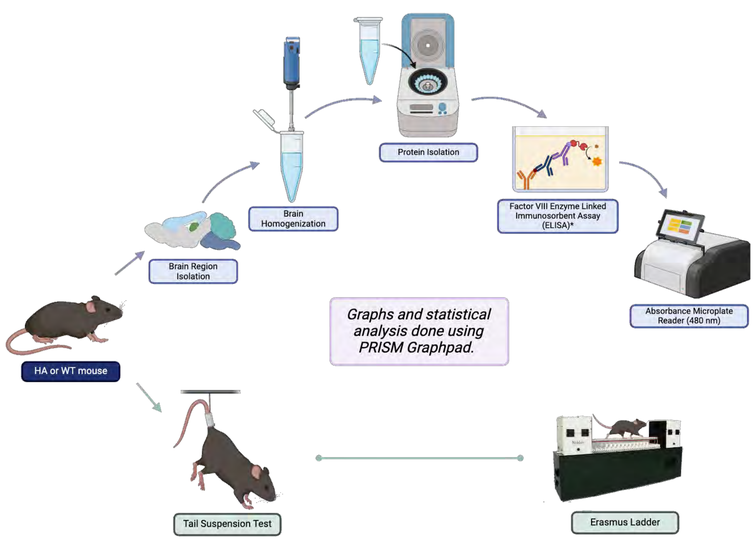

*ELISA test run with the VisuLize™ Factor VIII Antigen Kit by Affinity Biologicals™ INC. REF FVIII-AG

Methodology

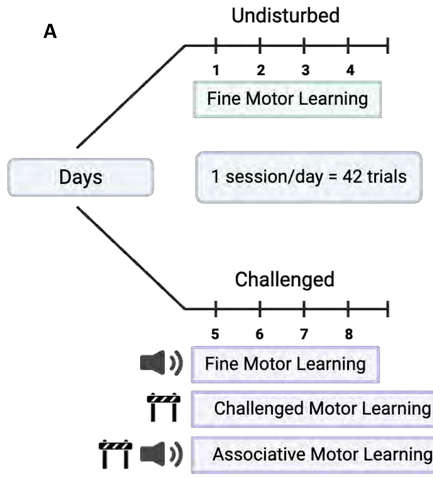

B

Parameters Assessed	
Missteps	Defined as a step down from a high rung to a low rung or remaining on the low rungs. Measures motor performance, learning/cognition, and fear response. Calculated out of total steps.
Latency Leaving After Cue	Defined as the time it takes for a mouse to move out of the start box after being presented with a primary cue (light) and a secondary cue (pressurized air stream). Measures motor learning, coordination, and fear response.

Figure 1. Description of Erasmus Ladder protocol and assessments
(A) Sessions: Days 1-4 intended for mice to learn how to use the ladder without stimulus. Tones and obstacles introduced on days 5-8 to test locomotion and learning.
(B) Parameters: Missteps (%) and latency leaving after cue (%) test motor skills and cognition.

Results

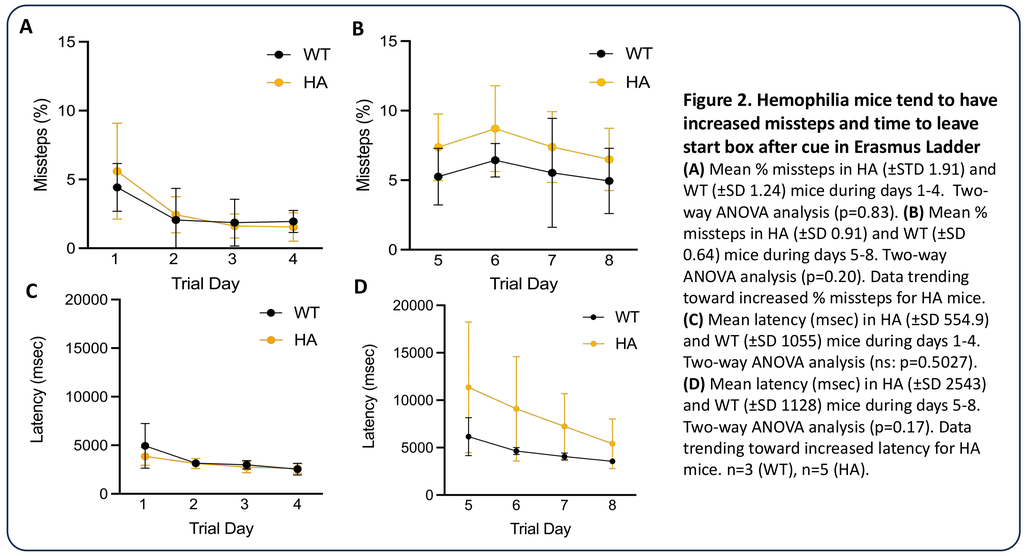

Figure 2. Hemophilia mice tend to have increased missteps and time to leave start box after cue in Erasmus Ladder
(A) Mean % missteps in HA (±STD 1.91) and WT (±SD 1.24) mice during days 1-4. Two-way ANOVA analysis (p=0.83). **(B)** Mean % missteps in HA (±SD 0.91) and WT (±SD 0.64) mice during days 5-8. Two-way ANOVA analysis (p=0.20). Data trending toward increased % missteps for HA mice. **(C)** Mean latency (msec) in HA (±SD 554.9) and WT (±SD 1055) mice during days 1-4. Two-way ANOVA analysis (ns: p=0.5027). **(D)** Mean latency (msec) in HA (±SD 2543) and WT (±SD 1128) mice during days 5-8. Two-way ANOVA analysis (p=0.17). Data trending toward increased latency for HA mice. n=3 (WT), n=5 (HA).

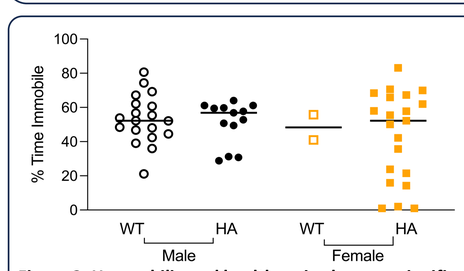

Figure 3. Hemophilia and healthy mice have no significant differences in time immobile for tail suspension test
Percent time immobile in male WT (±SD 14.17), male HA (±SD 12.59), female WT (±SD 10.44), and female HA (±SD 26.09). Two-tailed unpaired t-test analysis for male (p=0.67) and female (p=0.81). n=19 (WT M), n=13 (HA M), n=2 (WT F), n=21 (HA F)

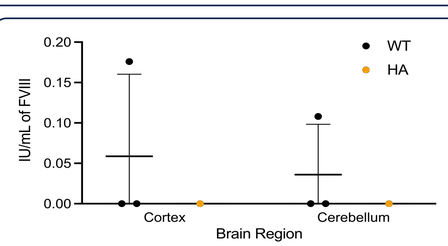

Figure 4. FVIII Protein Present in Discrete Mouse Brain Subregions
Protein was collected from the cortex and cerebellum. For each the cortex and the cerebellum, factor VIII measured as 0.176 IU/mL and 0.108 IU/mL, respectively in two different mice. HA mice displaced no detectable FVIII detected in brain samples. Mean and SD bars included on graph. n=3 (WT), n=1(HA)

Conclusions

1. To our surprise, we detected factor VIII in the cortex and cerebellum of WT mice.
   - Presence of FVIII in WT mice indicates a potential role for FVIII in normal brain function.
2. Hemophilia A mice demonstrated trends toward decreased neurocognition and motor abilities.
   - Erasmus Ladder is heavily connected to cerebellar functioning: trends indicate decreased cerebellar functioning in hemophilia mice.
3. Tail suspension test revealed no significant differences between WT and HA mice. Therefore, a depressive phenotype may not accurately reflect the behavior differences in hemophilia A.

Due to FVIII being detected at higher levels in WT mice, this research challenges the dogma of FVIII roles. The results indicates a potential positive correlation between brain FVIII levels and neurocognition/brain function, opening a new avenue of treatment for mental health in people with hemophilia A.

Future Directions

1. Erasmus Ladder pilot data were used in a power analysis to calculate the number of samples needed. Plan to increase the sample size to n=6 each for HA and WT mice.
2. Examine paw-clasping behavior in hemophilia A mice compared to wild-type mice in tail suspension tests as a marker of behavioral despair.
3. Measure FVIII levels with newly adjusted ELISA parameters including standard protein concentration loaded onto plate.

Acknowledgements

I would like to thank the Belin-Blank Center for curating this opportunity, and Dr. Staber for welcoming me into her lab. Special thanks to Kevin Gubner for his help on protein isolation and ELISAs, as well as to Danielle York for her help on behavior test analyses. *All graphics created on Biorender. All behavior tests performed at the Neural Circuits and Behavior Core, part of the Iowa Neuroscience Institute.*

References

Al-Huniti, A., Hernandez, M. R., Eyck, P. T., & Staber, J. M. (2020). Mental health disorders in haemophilia: Systematic literature review and meta-analysis. *Haemophilia*, *26*(3), 431-442. https://doi.org/10.1111/hae.13960

Shen, B. W., Spiegel, P. C., Chang, C.-H., Huh, J.-W., Lee, J.-S., Kim, J., Kim, Y.-H., & Stoddard, B. L. (2008). The tertiary structure and domain organization of coagulation factor VIII. *Blood*, *111*(3), 1240-1247. https://doi.org/10.1182/blood-2007-08-109918

Staber, J. M., & Pollpeter, M. J. (2016). Shortened lifespan and lethal hemorrhage in a hemophilia A mouse model. *PLoS One*, *11*(5). https://doi.org/10.1371/journal.pone.0154857

Comparing Gastric Sleeve and Gastroplasty's Effectiveness as Obesity Treatments Using Mice Models

Using Comparative Analysis to Understand Weight Loss Interventions

Jacklyn Saddler, Dr. Mohammed Mokadem, Mohammed Jarrah

INTRODUCTION

Obesity is a global health crisis on the rise, with over a third of Americans affected. Traditional weight loss methods such as diet and exercise often fall short for individuals with severe obesity, making surgical interventions necessary. Sleeve gastrectomy surgery is the most common procedure: the stomach is removed, leaving a narrow tube of the stomach remaining (Johns Hopkins Medicine, n.d.). Sleeve gastroplasty, a newer and minimally invasive approach, involves inserting a suturing device endoscopically to reduce the size of the stomach (Mayo Clinic, n.d.). Both interventions induce weight loss by reducing stomach size and caloric intake, but more studies are needed to observe the mechanisms of action for these procedures. This project used *in vivo* mice models to comparatively analyze gastrectomy and gastroplasty to understand their effects on weight loss, food intake, and energy expenditure. By elucidating the physiological mechanisms underlying both interventions, this study seeks to have more insights on weight loss procedures.

METHODS

Diet Induced obesity (DIO) mice were divided into three intervention groups: Sham, Sleeve Gastrectomy, and Gastroplasty, and observed for six weeks.

SLEEVE GASTRECTOMY

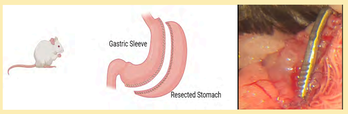

SLEEVE GASTROPLASTY

Figure 1A (sleeve gastrectomy) and **Figure 1B (sleeve gastroplasty**). Visualization of sleeve gastrectomy and sleeve gastroplasty procedures.

WEIGHT MANAGEMENT

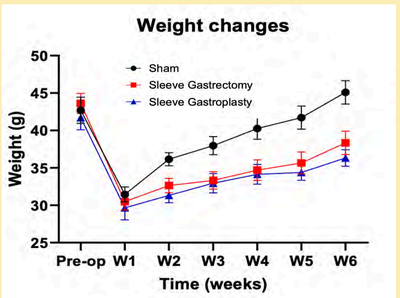

Figure 2 Weight changes in DIO mice over six weeks: Gastrectomy and Gastroplasty groups show significant weight reduction compared to the Sham group.

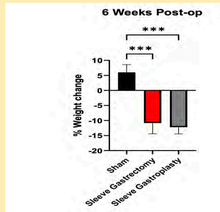

Figure 1 % Weight Change 6 Weeks Post-Op: Sham group increased in weight while both gastrectomy and gastroplasty groups experienced a significant weight reduction (~10%).

GLUCOSE METABOLISM

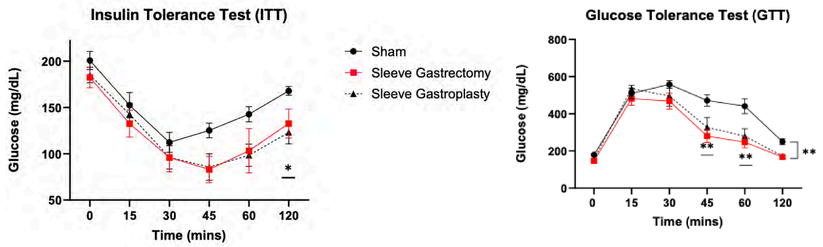

Figure 4: ITT results showing glucose levels over 120 minutes post-insulin injection. Gastrectomy and Gastroplasty groups maintain lower glucose levels, indicating improved insulin sensitivity.

Figure 5: GTT results showing glucose levels over 120 minutes post-glucose administration. Both Gastrectomy and Gastroplasty groups demonstrate significantly lower glucose levels compared to the Sham group, indicating better glucose tolerance.

LIPID AND HORMONE LEVELS

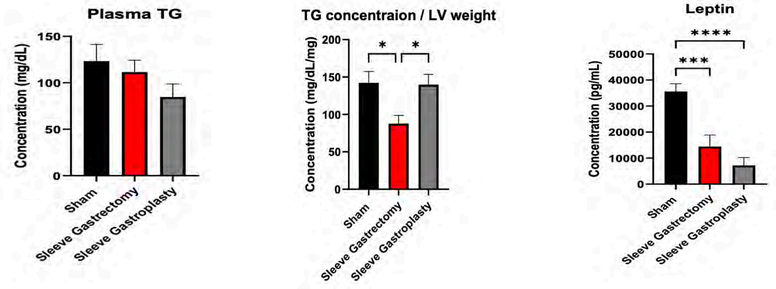

Figure 6: There are no statistical differences across all three groups in plasma triglyceride levels.

Figure 7: Only the gastrectomy group had significantly lower triglyceride concentrations per liver weight.

Figure 8: There are significantly lower leptin hormone levels in both gastrectomy and gastroplasty groups compared to the sham group.

STOMACH TISSUE IMAGING

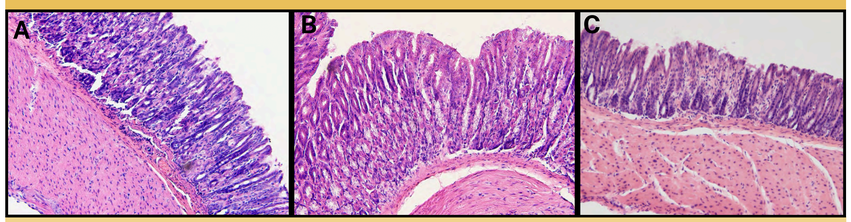

Hematoxylin and eosin staining were used for all images, taken with brightfield microscopy. A scale of 50µm used.

- **Figure 9A**: Mouse stomach morphology of sham
- **Figure 9B**: Mouse stomach morphology of sleeve gastrectomy
- **Figure 9C**: Mouse stomach morphology of sleeve gastroplasty

ILEUM IMAGING

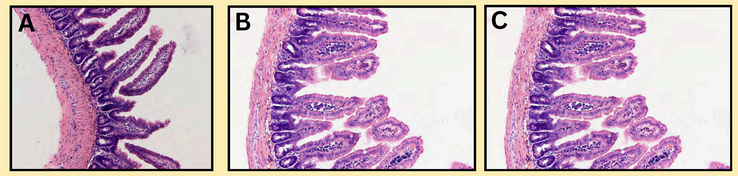

Hematoxylin and eosin staining were used for all images, taken with brightfield microscopy. Magnification of 20x.

- **Figure 10A:** Mouse ileum morphology of sham.
- **Figure 10B:** Mouse ileum morphology of sleeve gastroplasty.
- **Figure 10C:** Mouse ileum morphology of morphology of sleeve gastrectomy. Insignificant differences are detected.

DISCUSSION

The comparative analysis of sleeve gastrectomy and gastroplasty in DIO mice demonstrates that both are effective weight loss interventions.

- **Weight Management:** Both procedures led to significant weight loss compared to the sham.
- **Glucose Metabolism:** Both interventions showed improved insulin sensitivity and glucose tolerance compared to the sham.
- **Lipid Profiles:** Both interventions significantly lowered the liver triglyceride levels.
- **Hormonal Changes:** Both groups showed significant reductions in leptin levels, with Gastroplasty showing a notable decrease. This suggests effective fat mass reduction and improved hormonal balance.

CONCLUSION

- Both sleeve gastrectomy and gastroplasty are effective weight loss interventions.
- They have been observed to have different mechanisms for achieving effective weight loss results.
- Sleeve gastrectomy and sleeve gastroplasty both improve glucose and insulin levels
- Only sleeve gastrectomy improves lipid profiles along with histological changes at the stomach level.
- Further studies are needed to explore the full mechanism of action for each intervention.

ACKNOWLEDGEMENTS

Thank you to my mentors, Dr. Mohammed Mokadem, Mohammed Jarrah, Dr. Yi Chu, and Sanaz Saleh for their support and guidance. Also thank you to the Belin-Blank Center for this program and my friends and family for always encouraging my passion for STEM.

REFERENCES

Bariatrics, R. (2024, March 20). Bariatric Surgery Statistics & Facts [Updated 2024]. Renew Bariatrics. https://renewbariatrics.com/bariatric-surgery-statistics/

Endoscopic Sleeve Gastroplasty. (2022, October 13). Johns Hopkins Medicine. https://www.hopkinsmedicine.org/health/treatment-tests-and-therapies/endoscopic-sleeve-gastroplasty

Coblijn, U. K., Karres, I., De Raaff, C. a. L., De Castro, S. M. M., Lagarde, S. M., Van Tets, W. F., Bonjer, H. J., & Van Wagensveld, B. A. (2017). Predicting postoperative complications after bariatric surgery: the Bariatric Surgery Index for Complications, BASIC. Surgical Endoscopy/Surgical Endoscopy and Other Interventional Techniques, 31(11), 4438–4445. https://doi.org/10.1007/s00464-017-5494-0

Endoscopic sleeve gastroplasty - Mayo Clinic. (2023, September 29). https://www.mayoclinic.org/tests-procedures/endoscopic-sleeve-gastroplasty/about/pac-20393958

Gala, K., Brunaldi, V., McGowan, C., Sharaiha, R. Z., Maselli, D., Vanderwel, B., Kedia, P., Ujiki, M., Wilson, E., Vargas, E. J., Storm, A. C., & Dayyeh, B. K. A. (2023). Performance of Endoscopic Sleeve Gastroplasty by Obesity Class in the Clinical United States Setting. Clinical and Translational Gastroenterology, 15(1), e00647. https://doi.org/10.14309/ctg.0000000000000647

Department of Internal Medicine, University of Iowa, Carver College of Medicine, Iowa City, IA

Investigating the Synergistic Effect and Mechanisms of PHB2 Inhibitors in Combination with HDAC Inhibitor Romidepsin in Endometrial Cancer Cells

Summer Tang[1]; Xiangbing Meng, PhD[2]; Shujie Yang, PhD[2]

[1]Del Norte High School, CA; [2]Department of Pathology, University of Iowa

1. Introduction

- Endometrial cancer (EC) cells form in the inner lining of the uterus.[5]
- EC is one of the few cancers with both increasing incidence and mortality rates.[1]
- Prohibitin (PHB) proteins have two isoforms: PHB1 and PHB2.[7]
- PHB2 has varying oncogenic and tumor suppressor function in different types of cancer.[7]
- In EC, PHB2 has an oncogenic function: higher expression is associated with poorer prognosis and worse survival.[2]
- PHB2 inhibitors (PHB2i) include FL3 and JI130.[7]
- PHB2 downregulates p21, a tumor suppressor that helps cell cycle arrest at G1.[3]
- PHB2 is associated with low progesterone receptor (PR), and low PR correlates with worse EC patient survival.[4]
- PHB2 interacts with histone deacetylases (HDACs) interact in the nucleus to repress transcription.[7]
- HDACi Romidepsin induces cell cycle arrest and apoptosis.[6]
- Romidepsin has shown high effectiveness when combined with other anticancer drugs for treatment.[6]

Fig 1. In the uterus, tumors for endometrial cancer forms in the inner lining.

2. Problem and Question

- PHB2 and its inhibitors lack thorough studies in the context of endometrial cancer cell lines.
- PHB2i FL3 and JI130 alone or in combination with Romidepsin have not been tested in endometrial cancer cell lines.

Which combination of PHB2i and HDACi exhibits optimal, synergistic repression of cancer cell proliferation? How do PHB2 inhibitors function in relation to the various biological pathways in endometrial cancer?

3. Objectives

1. Test different combinations of PHB2i and HDACi to determine optimal synergistic effect.
2. Verify the mechanisms in which PHB2i affect signaling pathways and the cell cycle.

4. Methodology

I. Testing for Synergism

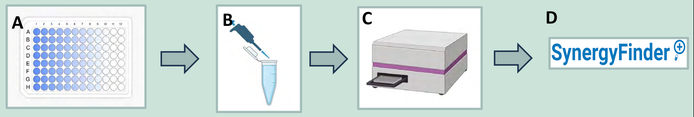

Fig 2. (A) Prepare two 96 well plates of cells (Hec50 and pDC8). **(B) A**dd desired drug combinations to each well. **(C) A**fter 72 hours, use a plate reader to determine number of viable cells. **(D)** Feed data in SynergyFinder to determine if combinations had synergistic effects.

4. Methodology (Continued)

II. Western Blot for Protein Expression

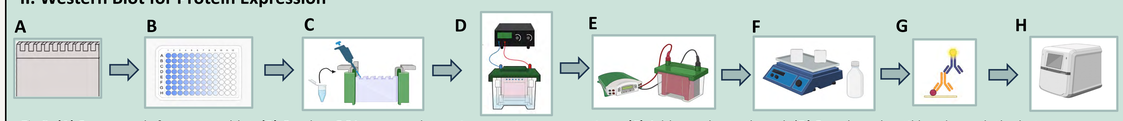

Fig 3. (A) Prepare gels for western blot. **(B)** Conduct BCA assay to determine protein concentrations. **(C)** Add samples to the gel. **(D)** Run the gel until bands reach the bottom. **(E)** Transfer gel onto a membrane in cold room. **(F)** Block membrane with 5% milk. **(G)** Add primary and secondary antibodies. **(H)** Obtain results with an imaging system.

III. Flow Cytometry with PI for Cell Cycle Analysis

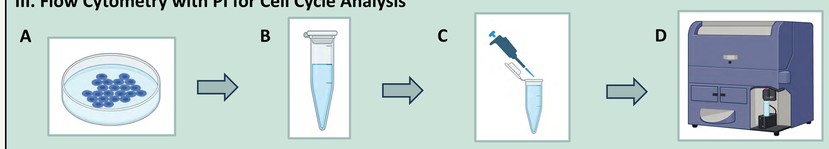

Fig 4. (A) Harvest treated cells and wash with PBS. **(B)** Fix in 70% ethanol and wash with PBS. **(C)** Add RNase to ensure binding of Propidium Iodide (PI) to DNA only, and then add PI. **(D)** Analyze results using a flow cytometer.

Images created in BioRender.com

5. Results and Data

Testing for Synergism

Hec50 cell line

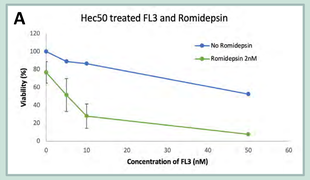

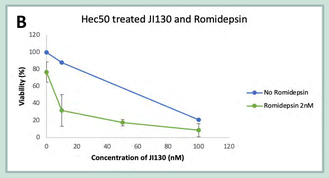

- In Hec50 cells, 2nM of Romidepsin and 10nM of FL3 had high toxicity.
- Also, 2nM of Romidepsin and 50nM of JI130 were effective treatments.
- Both FL3 and JI130 showed synergistic effect when combined with Romidepsin.

Fig 5. (A) Hec50 cells treated with FL3 (PHB2i) and Romidepsin (HDACi) combination. **(B)** Hec50 cells treated with JI130 (PHB2i) and Romidepsin (HDACi) combination.

pDC8 cell line

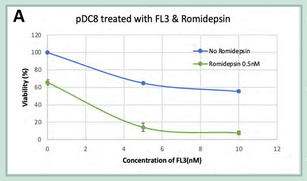

- In pDC8 cells, the following combinations had high toxicity: 0.5nM of Romidepsin + 5nM of FL3 and 0.5nM of Romidepsin + 10nM of JI130.
- As concentration increases past 10nM for JI130 or 5nM for FL3, changes in cell viability plateau, as toxicity has been optimized.
- Both trials showed a preliminary synergistic effect.

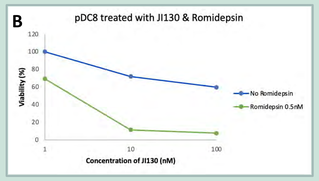

Fig 6. (A) pDC8 cells treated with FL3 (PHB2i) and Romidepsin (HDACi) combination. **(B)** pDC8 cells treated with JI130 (PHB2i) and Romidepsin (HDACi) combination.

ISH cell line

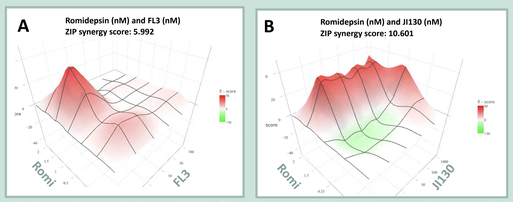

- Since Romidepsin and FL3 combination had a synergy score between -10 to 10, their effect is additive.
- Synergy is maximized at 2nM Romi and 10 nM FL3.
- Romidepsin and JI130 have a synergistic interaction, as their synergy score is slightly above 10.
- Synergy is maximized at 2nM Romi with varying concentrations of JI130.

Fig 7. (A) SynergyFinder analysis of Romidepsin and FL3. **(B)** SynergyFinder analysis of Romidepsin and JI130.

Western Blot

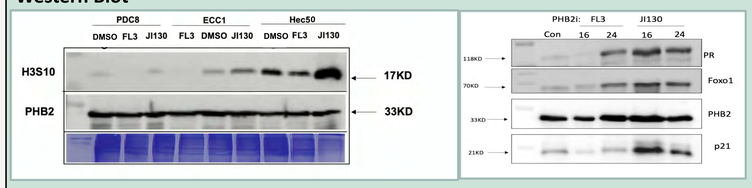

- H3S10 is upregulated in Hec50 cells with JI130 treatment.
- PR and tumor suppressor Foxo1 concentration increases as JI130 concentration increases.
- PHB2 concentration shows no significant changes in varying treatments.
- p21 is upregulated by JI130.

Fig 8. Western blot results of concentration of different proteins based on treatments with DMSO (control), FL3, and JI130.

5. Results and Data (Continued)

Flow Cytometry

pDC8 cell line

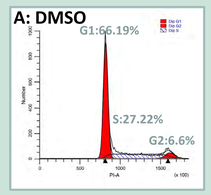

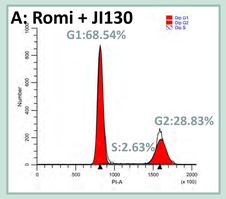

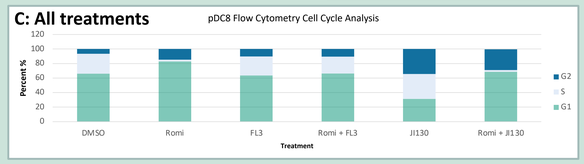

Fig 9. (A) pDC8 cells treated with DMSO (control). **(B)** pDC8 cells treated with 10nM Romidepsin and 1nM of JI130. There is more cell cycle arrest at G2 for the combination (Romidepsin and JI130) treatment. **(C)** Segmented bar graph illustrating percentage of cells in each phase of the cell cycle among different treatment groups: DMSO (control), individual treatments (Romidepsin, FL3, JI130), and combination treatments (Romidepsin + FL3 and Romidepsin + JI130).

6. Conclusion and Future Directions

- In Hec50 and pDC8 cell lines, synergism was shown from varying Romidepsin and FL3/JI130 concentrations.
- Further analysis could test more concentrations for mapping on Synergyfinder for Hec50 and pDC8 cell lines.
- ISH cells had synergistic effects for the JI130 and Romidepsin combination.
- Inhibition of PHB2 upregulated tumor suppressors (p21 and Foxo1) and induced cell cycle arrest.
- Romidepsin and JI130 combinations are highly effective in inducing cell cycle arrest at G2 in pDC8 cells.
- HDACi with FL3 and JI130 show promising efficacy for the three EC cancer cell lines.
- By understanding which treatments have optimal inhibition of PHB2 and cell proliferation in EC, novel and improved treatment options could be implemented.
- Future experiments could test the efficiency of other PHB2 inhibitors such as RocA and FLZ combinations with HDACi.

7. Acknowledgements

I would like to express my gratitude toward Dr. Meng and Dr. Yang for guiding me and providing the opportunity to gain a wonderful lab experience. Also, I would like to thank the Belin Blank Center for the opportunity to conduct research in a wet lab. Funding for this project was supported by NIH R37-CA238274 (SY) and the Department of Pathology Start-Up Fund (SY).

8. References

[1] American Cancer Society. (2024). *Key Statistics for Endometrial Cancer*. American Cancer Society. https://www.cancer.org/cancer/types/endometrial-cancer/about/key-statistics.html
[2] Human Protein Atlas. (n.d.). *Expression of PHB2 in Endometrial Cancer*. The Human Protein Atlas. https://www.proteinatlas.org/ENSG00000215021-PHB2/pathology/endometrial+cancer
[3]Chouha, N., Hussein Abou-Hamdan, Hajime Yurugi, Yoshii, R., Ito, H., Najem, A., Ghanem, G. E., Nakata, S., Krishnaraj Rajalingam, Yu, P., Wang, D., Nebigil, C. G., & Laurent Désaubry. (2022). Development of fluorizoline analogues as prohibitin ligands that modulate C-RAF signaling, p21 expression and melanogenesis. *European Journal of Medicinal Chemistry*, *242*, 114635–114635. https://doi.org/10.1016/j.ejmech.2022.114635
[4]Li, Y., Huang, C., Kavlashvili, T., Fronk, A., Zhang, Y., Wei, Y., Dai, D., Devor, E. J., Meng, X., Thiel, K. W., Leslie, K. K., & Yang, S. (2020). Loss of progesterone receptor through epigenetic regulation is associated with poor prognosis in solid tumors. *American journal of cancer research*, *10*(6), 1827–1843.
[5] Mayo Foundation for Medical Education and Research. (2023). *Endometrial cancer*. Mayo Clinic. https://www.mayoclinic.org/diseases-conditions/endometrial-cancer/symptoms-causes/syc-20352461
[6]Petrich, A., & Nabhan, C. (2016). Use of class I histone deacetylase inhibitor romidepsin in combination regimens. *Leukemia & lymphoma*, 57(8), 1755–1765. https://doi.org/10.3109/10428194.2016.1160082
[7] Qi, A., Lamont, L., Liu, E., Murray, S. D., Meng, X., & Yang, S. (2023). Essential Protein PHB2 and Its Regulatory Mechanisms in Cancer. *Cells*, *12*(8), 1211. https://doi.org/10.3390/cells12081211

Specific Tunable 3D-Printed Silk Fibroin Structures:

Ion Effects on Silk Fibroin

Hailey Van[1], Reza Amouzandeh[2], Nyvaeh Bowen[2], Derek Hua[3], Xuan Mu[2]*

[1]Portola High School, CA; [2] Roy J. Carver Department of Biomedical Engineering, University of Iowa; [3]West High School, IA; Email: xuan-mu@uiowa.edu

Introduction

Silk Proteins

- Protein-based biomaterials are **sustainable** alternatives to current synthetic polymers
- **Silk fibroin** (SF) conformation dominated by β-sheet structures or amorphous random coils [1]
- Protein folding is influenced by pH, salt ions, and shear [2, 3]
- SF scaffolds support cell differentiation, and tissue regeneration[3]

Figure 1. Silkworms grown in lab.

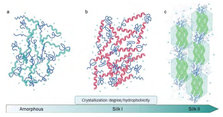

Figure 2. Conformational change in silk protein from aqueous to dense β-sheets[4].

Fabrication Techniques

	Kurland et al., 2013	Valente et al., 2022	Sun et al., 2015	Mu et al., 2020
Method	Photolithography	Two photon lithography	Femtosecond Lasers	3D Printing
Young's modulus	~15.6 GPa	~.0096–.047 MPa	~2.2 GPa (dry)	~2 GPa (dry)
Biocompatibility	Murine fibroblasts	Human dermal fibroblasts	Bone cell culturing	Adipose-derived stem cells
Dimension	2D	2D, 3D	2D, 3D	2D, 3D
Resolution	1.5 μm	100 nm	20 nm	100 μm
External inputs	UV light	Infrared lasers	Femtosecond laser beams	Solvent cues

Table 1. Comparison table summarizing silk technologies based on required resources, morphological quality, and mechanical properties [1, 5, 6, 7].

Figure 3. Schematic of INKREDIBLE 3D printer used to fabricate circular and dog bone SF films.

Methods

Production of Regenerated Silk Solution	Fabrication of Silk Fibroin Films	Solvent Cue Testing
Process and purify silk from silkworm cocoons	3D printing of circular, dog bone, and trapezoidal solid films with SF monolithic ink	Apply salt ion treatment and conduct transparency, morphological, and mechanical testing

- **Salts:** NaCl, KCl, K_2HPO_4, Na_2HPO_4
- **Concentrations:** 0.5, 1, 2, 3, 4 M
- **Circular samples** (D = 6mm) absorbance spectrum was collected using SpectraMax iD3 microplate reader (Molecular Devices)
- **Dog bone samples** (W = 2mm) printed for uniaxial tensile testing using HR-30 rheometer (TA Instruments)

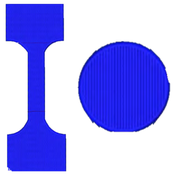

Figure 4. Printing path of circular and dog bone films written with G-code and printed using Repetier-Host (Version 2.2.2).

Results and Discussion

Optical Transmittance

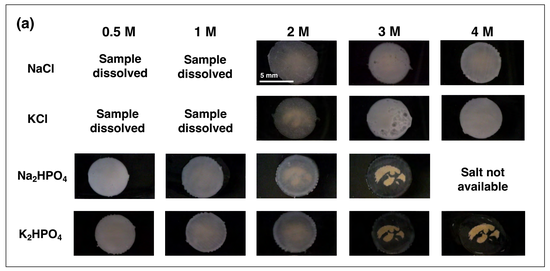

Figure 5. Optical images of circular films after 2-day salt treatment with different concentrations in wet (a) and dry (b) conditions. Transparency decreases with increasing concentration of NaCl and KCl and increases with concentration of Na_2HPO_4 and K_2HPO_4. Transparency characterization follows qualitative images and transmittance varies with concentration depending on the salt anion (c). Transmittance spectrum spikes at a critical wavelength (d) across all salts. Significant variations are evident with the change of anion at the same concentration (d). (****, P<0.0001).

Mechanical Properties

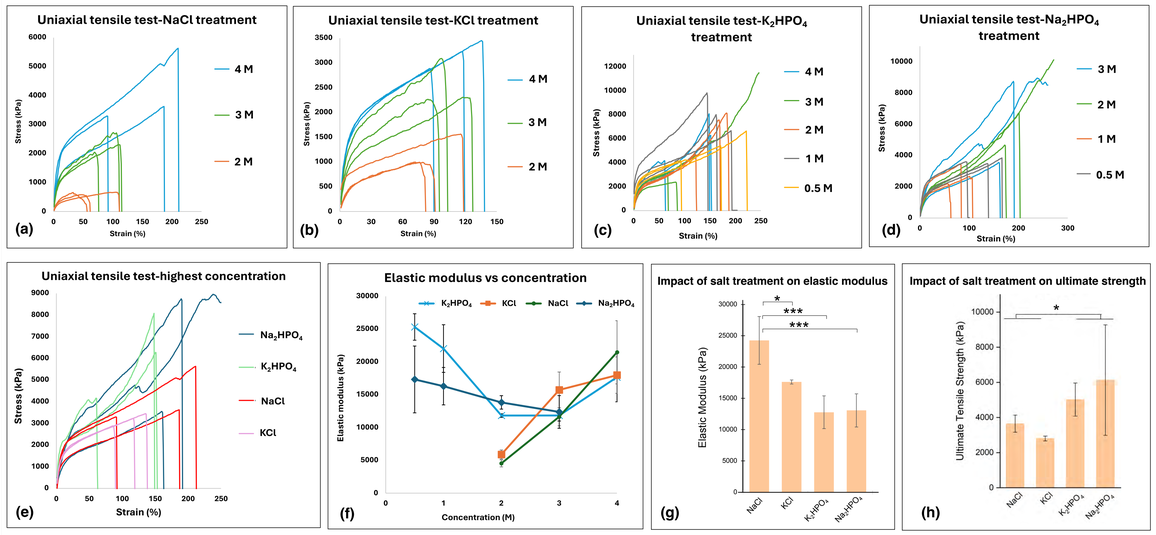

Figure 6. Stress-strain curves of each salt treatment were obtained from tensile tests. Each sample was treated with NaCl (a), KCl (b), K_2HPO_4 (c), and Na_2HPO_4 (d) and stretched until broken. Strain-stress curve for the highest concentration tested for all salts (e). Non-linear dependence between concentration and Young's modulus in the elastic region (f) in which modulus increases with concentration (K_2HPO_4, Na_2HPO_4) whereas the inverse is observed (NaCl, KCl). Significant differences in elastic modulus arise when the anion differs or both anion and cation (g). (*, P<0.05, ***, P<0.001, and ns, no significance). Significant correlation is observed between anions and maximum stress (h).

SEM Imaging

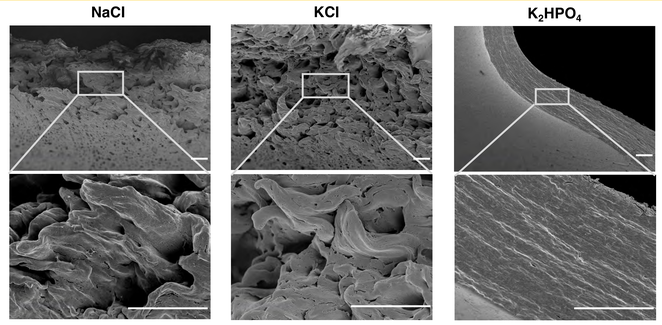

Figure 7. Cross-sectional scanning electron microscope (SEM) images of dog bone silk films after tensile tests. The compact cross-section of transparent films compared to the porous cross-section of opaque films can be attributed to the rank of anions in the Hofmeister series (scale bars: 10 μm).

Effect of Salt Ions

- Ions influence surface charges and chain-chain interactions
- **Hofmeister series:** salts induce protein aggregation at different levels [8]

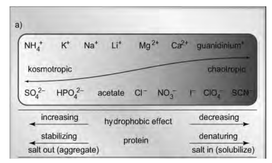

Figure 8. Hofmeister series and salt effects on proteins [8].

- In **Fig 5a**, transparency trends with concentration (Na_2HPO_4, K_2HPO_4) indicate a shift from aggregation to a more compact structure
- Greater elastic modulus when the material can withstand more stress may be attributed to fibrous structures as shown in **Fig 7** [9]
- **Anions**, **elastic modulus, strength, and transparency** are correlated to each other from a broad perspective

Conclusions and Implications

Bioinspiration	Analysis	Application
Inspired by natural silk spinning process	Different anions and cations induce distinct protein configurations	Fabrication of 3D prints can be tuned for precision medicine

- The combination of straightforward, aqueous, and ambient fabrication process makes **salt bath-assisted 3D printing** a unique method worthy of further exploration for SF-enabled biomedical tools

Acknowledgements: The authors would like to thank Ashlee Donithan from the Belin-Blank Center and all members of the Mu Lab at the University of Iowa for supporting this research.

References:

[1] Mu, X., Wang, Y., Guo, C., Li, Y., Ling, S., Huang, W., Cebe, P., Hsu, H., De Ferrari, F., Jiang, X., Xu, Q., Balduini, A., Omenetto, F. G., & Kaplan, D. L. (2020). 3D printing of silk protein structures by aqueous solvent-directed molecular assembly. *Macromolecular Bioscience*, 20(1), 1900191. https://doi.org/10.1002/mabi.201900191
[2] Heinrich, M. A., Liu, W., Jimenez, A., Yang, (2019). 3D bioprinting: from benches to translational applications. *Small*, 15(23), 1805510. https://doi.org/10.1002/smll.201805510
[3] Guo, C., Li, C., Mu, X., & Kaplan, D. L. (2020). Engineering silk materials: From natural spinning to artificial processing. *Applied Physics Reviews*, 7(1), 011313. https://doi.org/10.1063/1.5091442
[4] De Giorgio, G., Matera, B., Vurro, D., Manfredi, E., Galeyan, V., Tarabella, G., Ghezzi, B., & D'Angelo, P. (2024). Silk fibroin materials: biomedical applications and perspectives. *Bioengineering*, 11(2), 167. https://doi.org/10.3390/bioengineering 11020167
[5] Kurland, N. E., Dey, T., Kundu, S. C., & Yadavalli, V. K. (2013). Precise patterning of silk microstructures using photolithography. *Advanced Materials*, 25(43), 6207–6212. https://doi.org/10.1002/adma.201302823
[6] Valente, F., Hepburn, M. S., Chen, J., Aldana, A. A., Allardyce, B. J., Shafei, S., Doyle, B. J., Kennedy, B. F., & Dilley, R. J. (2022). Bioprinting silk fibroin using two-photon lithography enables control over the physico-chemical material properties and cellular response. *Bioprinting*, 25, e00183. https://doi.org/10.1016/j.bprint.2021.e00183
[7] Sun, Y.-L., Li, Q., Sun, S.-M., Huang, J.-C., Zheng, B.-Y., Chen, Q.-D., Shao, Z.-Z., & Sun, H.- B. (2015). Aqueous multiphoton lithography with multifunctional silk-centred bio-resists. *Nature Communications*, 6(1), 8612. https://doi.org/10.1038/ncomms9612
[8] Heim, M., Keerl, D., & Scheibel, T. (2009). Spider silk: from soluble protein to extraordinary fiber. *Angewandte Chemie (International ed. in English)*, *48*(20), 3584–3596. https://doi.org/10.1002/anie.200803341
[9] Mu, X., Yuen, J. S. K., Choi, J., Zhang, Y., Cebe, P., Jiang, X., Zhang, Y. S., & Kaplan, D. L. (2022). Conformation-driven strategy for resilient and functional protein materials. *Proceedings of the National Academy of Sciences*, *119*(4).

Psychiatric Conditions associated with Gender Diversity

Vern Van Asdale[a]; Ashton J. Tener, BA[b]; Jacob J. Michaelson, PhD[b,c,d]
[a]The Davidson Academy of Nevada
[b]Department of Psychiatry
[c]Department of Communication Sciences and Disorders
[d]Iowa Neuroscience Institute University of Iowa

BACKGROUND: In current studies, transgender people have higher prevalence of mental illness, however these studies are often not inclusive of non-binary people. This study aims to clarify the prevalence of mental illnesses among transgender and nonbinary (TGNB) people.

METHODS

1. Simon's Powering Autism Research (SPARK) participants take the gender self-report (GSR) and or answer a categorical gender survey. They also self-report mental illness diagnoses.
   - ⚧ The GSR has two scores: a binary trans score and a nonbinary score.
2. For comparing GSR scores and psychiatric diagnoses, we used a generalized linear model to calculate correlation and p-value.
   - ⚧ 22.0% Male, 58.0% Autistic, 29.6% Gender Diverse
3. For comparing categorical gender and psychiatric diagnoses, we used fisher's exact test. Only genders and diagnoses with n >50 were used.
   - ⚧ 22.4% Male, 60.0% Autistic, 30.8% Gender Diverse
4. For the boxplots, participants were sorted into never diagnosed, diagnosed in the past, and currently diagnosed.

RESULTS.

- ⚧ Gender-diverse people tend to have higher odds of having mental illnesses like anxiety, and depression.
- ⚧ PTSD and anorexia correlate with gender diversity in the boxplots, linear model, and heatmap.

Gender diversity correlated with PTSD and anxiety disorders.

GSR Scores vs Diagnosis

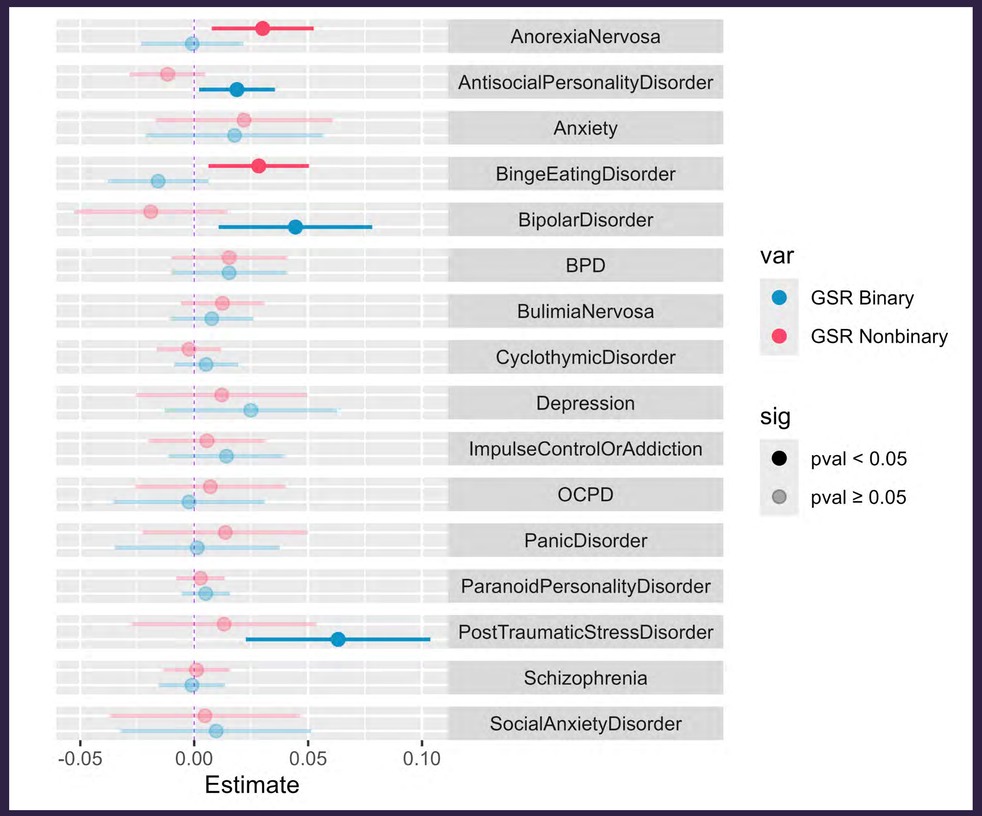

APD: Antisocial Personality Disorder
BPD: Borderline Personality Disorder
IC/A : Impulse Control or Addiction Disorder
OCPD: Obsessive Compulsive Personality Disorder
PPD: Paranoid Personality Disorder
PTSD: Post-Traumatic Stress Disorder

Generalized Linear Model estimates for correlation between gender self report (GSR) scores and mental illnesses.

GSR Nonbinary vs Anxiety

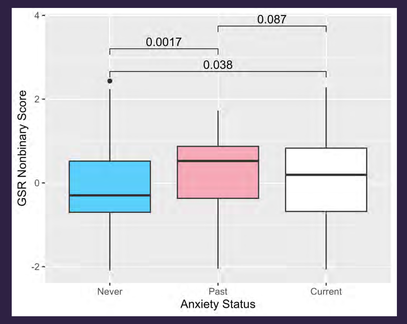

GSR Nonbinary vs PTSD

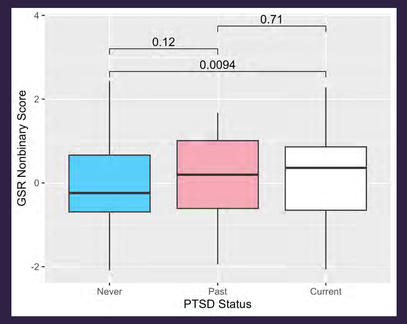

GSR Nonbinary vs Anorexia

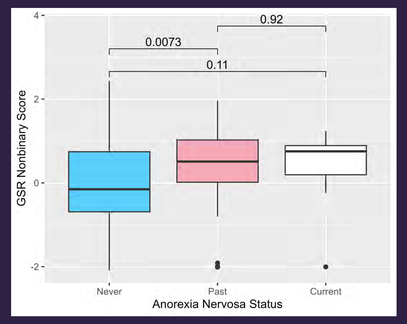

Boxplots of the GSR Nonbinary scores with p-values for differences shown.

Categorical Gender vs Ever Diagnosis

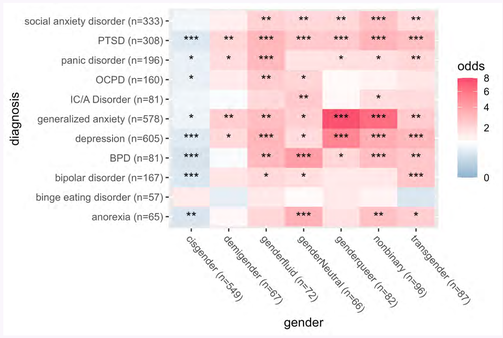

(* = p < 0.05, ** = p < 0.01, *** = p < 0.001)

DISCUSSION

- ⚧ More research needs to be done on why transgender and gender diverse people have higher rates of mental illness.
- ⚧ Transgender people do not seem to have higher genetic risk for these mental illnesses. (Thomas et al., 2024)
- ⚧ Minority stress theory suggests that stressors lead to health outcomes.
- ⚧ Work should be done on developing unique treatment plans for gender diverse individuals.

REFERENCES

Budge, S. L., Adelson, J. L., & Howard, K. A. S. (2013). Anxiety and depression in transgender individuals: The roles of transition status, loss, social support, and coping. *Journal of Consulting and Clinical Psychology*, *81*(3), 545–557. https://doi.org/10.1037/a0031774

Hanna, B., Desai, R., Parekh, T., Guirguis, E., Kumar, G., & Sachdeva, R. (2019). Psychiatric disorders in the U.S. transgender population. *Annals of Epidemiology*, *39*, 1-7.e1. https://doi.org/10.1016/j.annepidem.2019.09.009

Thomas, T. R., Tener, A. J., Pearlman, A. M., Imborek, K. L., Yang, J. S., Strang, J. F., & Michaelson, J. J. (2024). Polygenic Scores Clarify the Relationship Between Mental Health and Gender Diversity. *Biological Psychiatry Global Open Science*, *4(2)*, 100291. https://doi.org/10.1016/j.bpsgos.2024.100291

ACKNOWLEDGEMENTS
Special thanks to Dr. Jacob Michaelson, Ashton Tener, and the rest of the Michaelson Lab for mentoring me. Thanks as well to SSTP and the Belin Blank Center for this opportunity.

CONTACT
michaelson.lab.uiowa.edu
jacob-Michaelson@uiowa.edu

SPARK
Simons Powering Autism Research

IOWA

Leptin regulates aldosterone-sensitive neurons in the hindbrain

Harini Venkatesh[1], Madelin R Schwager[2], Miriam McDonough[3], and Jon M Resch[2,3]

Phillips Exeter Academy[1], Department of Neuroscience and Pharmacology[2],
Interdisciplinary Graduate Program in Molecular Medicine[3], University of Iowa Carver College of Medicine

Introduction

Sodium facilitates vital processes in the body including growth, development, and extracellular fluid volume regulation, making it critical for survival. Sodium intake is highly regulated by the renin-angiotensin-aldosterone system (RAAS), particularly by the mineralocorticoid hormone, aldosterone. Aldosterone, released from the adrenal gland, acts to increase sodium retention in the kidneys and to influence the brain by increasing sodium appetite. Aldosterone activates a specific population of neurons in the hindbrain that are uniquely aldosterone-sensitive. This sensitivity is due to their expression of the mineralocorticoid receptor (MR), to which aldosterone binds, and 11ß-hydroxysteroid dehydrogenase 2 (HSD2), which prevents stimulation of MR by glucocorticoids (**Fig. 1**). Notably, hindbrain HSD2 neurons have been shown to be necessary and sufficient for sodium appetite.

Using single-nucleus RNA sequencing, we recently discovered that HSD2 neurons also express the leptin receptor (*Lepr*). Leptin, released from adipocytes, acts to reduce hunger and mediates the motivation and reward for eating as well as satiety. HSD2 neuron expression of *Lepr* is of interest because leptin stimulates aldosterone-synthesizing cells in the adrenal gland, and obesity causes increased leptin and aldosterone levels.

Thus, we hypothesize that obesity and leptin may activate HSD2 neurons in two ways: 1) through the control of aldosterone release by leptin and 2) leptin activation of HSD2 neurons directly. To investigate whether leptin regulates HSD2 neurons, we injected mice with leptin and performed immunofluorescence on brain sections from mice injected with leptin and vehicle and stain for pSTAT3, a leptin signal transduction pathway molecule. Our cell counts show that HSD2 neurons are sensitive to leptin. (**Fig. 3**). Further, we performed aldosterone and leptin ELISAs on mice fed for twelve weeks on a normal chow diet versus a high fat diet and found that leptin and aldosterone levels were positively correlated in female mice (**Fig. 4**).

Aldosterone-sensitive neurons in the hindbrain

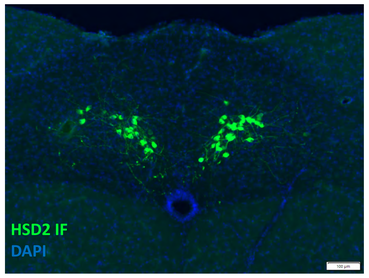

Fig. 1 HSD2 expression in the NTS (nucleus of the solitary tract) labels a unique population of neurons.

Arcuate neurons of brains injected with leptin express pSTAT3

Fasting: Fast mice overnight to minimize endogenous leptin.
Intraperitoneal injection: Inject mice with leptin or vehicle.
Perfusion: Perfuse mice with PBS and formalin to preserve brain.
Preparation: Extract brain and store in sucrose at -4° C to prevent cell lysis when cutting.

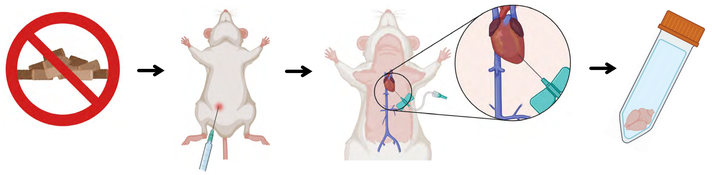

Slicing: Cut brain into 40µm slices and block non-specific antibody binding.
Primary antibody binding: Incubate overnight to allow antibodies to bind target.
Secondary antibody binding: Incubate for two hours to allow secondary antibodies to bind to primary antibodies.
Mounting: Mount slices with antibodies on slide, stain with DAPI, and visualize with slide scanner microscope.

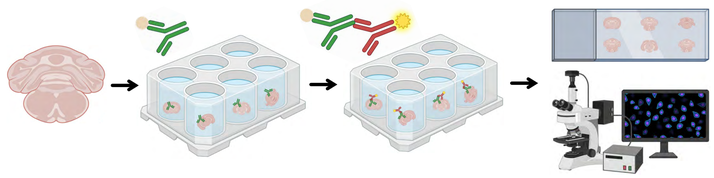

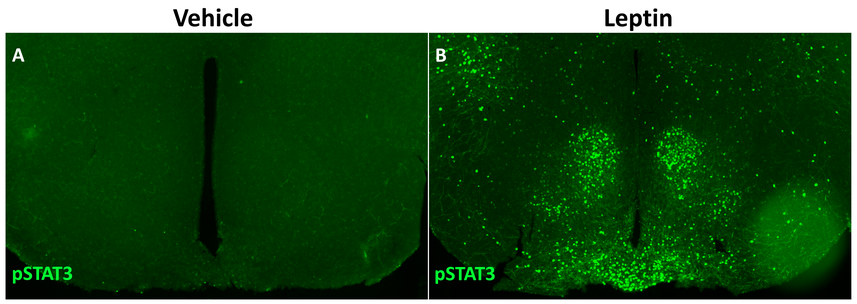

Fig. 2 Phosphorylated STAT3 expression (as part of the leptin signal transduction pathway) in the arcuate nucleus of the hypothalamus in mice injected with leptin (**B**) is higher than in mice injected with vehicle (**A**).

HSD2 neurons in the NTS are sensitive to leptin

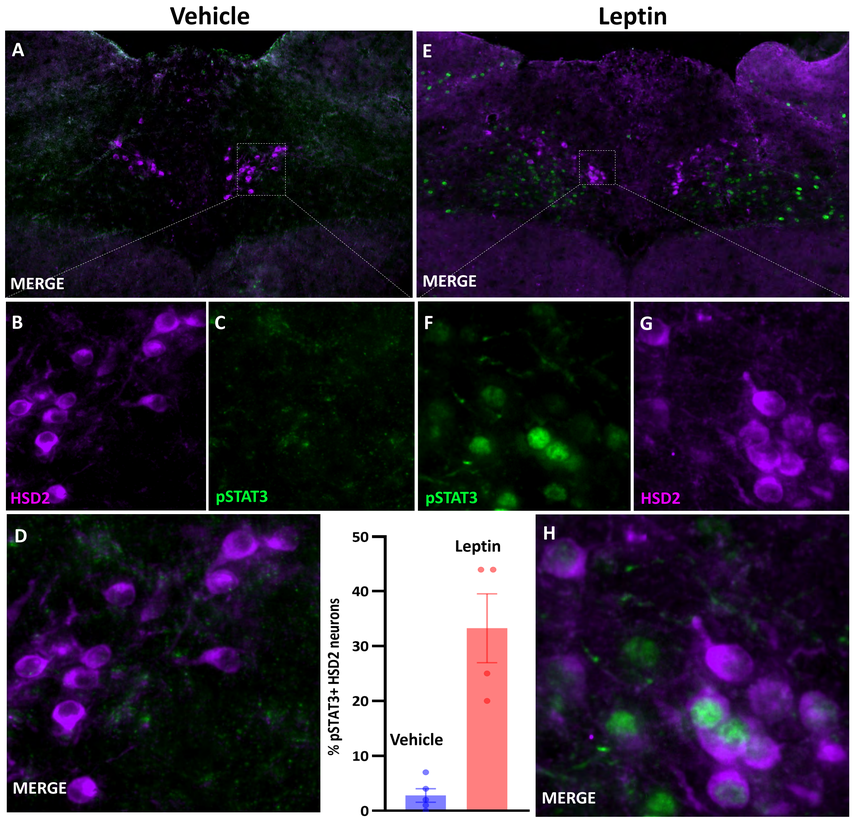

Fig. 3 pSTAT3 expression is significantly higher in HSD2 neurons in the NTS of mice injected with leptin (**E-H**) than mice injected with vehicle (**A-D**) ($p<0.05$).

Leptin and aldosterone levels are positively correlated in female mice

First reaction: Antigen binds antibody bound to plate and an added antibody.
Second reaction: HRP-conjugated antibody binds this complex.
Enzyme reaction: HRP oxidizes the TMB added to solution, causing a color change.
Absorbance measurement: Spectro-photometer reads absorbance values.

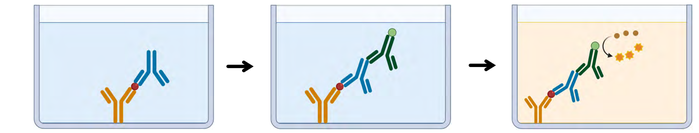

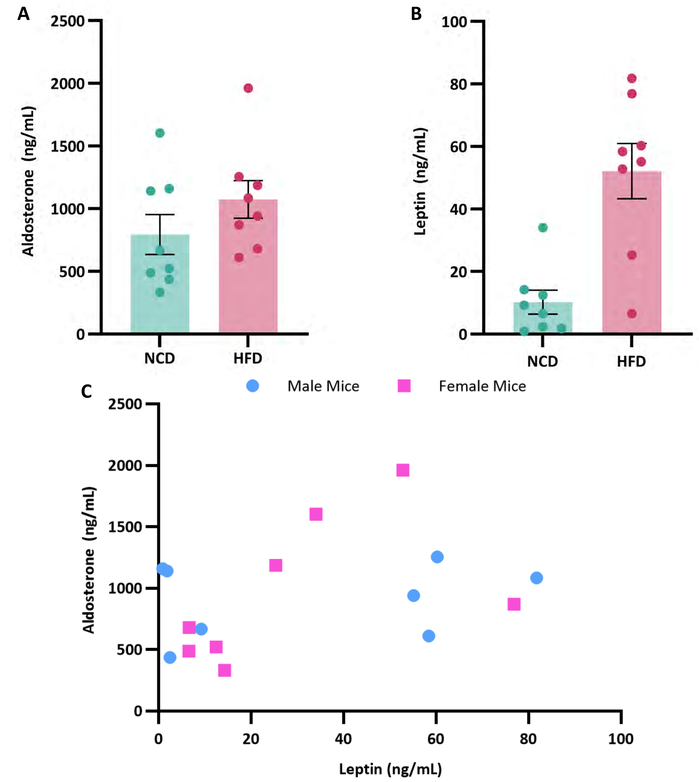

Fig. 4 Blood aldosterone (**A**) and leptin (**B**) levels are higher in mice fed on high-fat diet than on normal chow. Leptin and aldosterone levels are correlated in female mice ($R^2 = 0.295$) (**C**).

Conclusions and Future Directions

- HSD2 neurons in the NTS are sensitive to leptin.
- Leptin and aldosterone levels in the blood are correlated strongly in female mice, but a similar correlation is not demonstrated by this experiment in male mice.
- We will increase the number of mice treated with normal chow or high fat diet due to the variability in leptin and aldosterone levels in these mice.
- To determine whether leptin is activating HSD2 neurons, we will measure cFos, a neuronal activity marker, in pSTAT3+ HSD2 neurons.

References

- Graphics sourced from BioRender.
- Kuralay, A., McDonough, M. C., & Resch, J. M. (2024). Control of sodium appetite by hindbrain aldosterone-sensitive neurons. *Molecular and Cellular Endocrinology*, 592, 112323. Advance online publication. https://doi.org/10.1016/j.mce.2024.112323

Acknowledgments

Special thanks to Madelin Schwager and Miriam McDonough for their mentorship, and to Dr. Resch for the opportunity to work in this lab. Thanks also to the SSTP program and the Belin-Blank Center for this opportunity.

Funding for this project was provided to J.M.R. by US National Institutes of Health grants (K99/R00 HL144923) and the American Heart Association (935362). Funding was provided to M.C.M through the US National Institute of Health funded Pharmacological Sciences T32GM144636 Training Grant and F31 HL170784 fellowship.

Optimizing TEMPO Concentrations For Non-Aqueous Redox Flow Batteries

IOWA
Department of Chemistry

Joshua Wang[1], Darby H. Duffy[2], Chamini Perera[2], Scott K. Shaw, PhD.[2]

[1]Maumee Valley Country Day School, [2]Department of Chemistry, University of Iowa

The University of Iowa

Introduction

Motivation

While alternative energy sources continue to improve, there remains the problem of storing the excess energy[1]

Redox Flow Batteries

Redox Flow batteries could be the answer to this problem:

- Power decoupling[2]
  - Scalability
  - Flexibility
- Organic non-aqueous redox flow batteries[2]
  - Abundant
  - High tunability
  - Safety

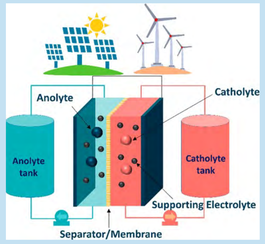

Fig 1. Diagram of a typical RFB[3]

- Electrolyte: Tetrabutylammonium Hexafluorophosphate ($TBAPF_6$)
- Analyte: 2,2,6,6-tetramethyl-1-piperidinyloxy (TEMPO)
- Viscosity

Rotating Disk Electrode (RDE)

- Cyclic Voltammetry (CV)
- At higher concentrations, higher viscosity creates too much resistance for standard CV to provide useful data
- RDE solves this with convection-based mass transport[4]

Objective

- Optimize concentration for Redox Flow Batteries
  - Test different concentrations of TEMPO and $TBAPF_6$
  - Calculate Diffusion coefficient and electron transfer constant

Methodology

Solution Preparation

1. Desired amount of TEMPO and $TBAPF_6$ were massed into a volumetric flask and acetonitrile was poured to the 50mL mark
2. Density was calculated by massing the flask before and after and the solution was transferred to a 3-neck round bottom flask

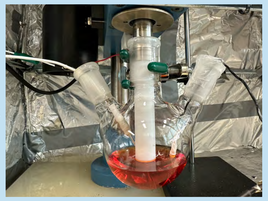

Fig 2. Solution in round bottom flask with electrodes

Fig 3. Mechanically polishing working electrode

Polishing Electrodes

3. The 5 mm platinum disk working electrode was mechanically polished in aqueous slurries of 3.0μm, 1μm, and 0.5μm alumina powder, rinsing between each grit
4. A hydrogen flame was used to flame polish the platinum coil counter electrode
5. For reference electrode, a non-aqueous Ag/Ag+ reference electrode was used

Setup

7. Working electrode was attached to Pine AFASR Analytical Rotator inside Faraday cage
8. The round bottom was clamped under working electrode and the three electrodes were placed in the solution while being connected to the CHI1100B potentiostat

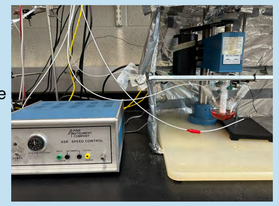

Fig 4. Full Apparatus

Measurements

9. Cyclic Voltammetry scans were run at six different rotation speed at a scan rate of 10 mV/s
10. Viscosity of solution was taken using a plate DV2T-LV viscometer with CPA-40Z and Brookfield cone equipped with a TC-550 temperature control at 25°C

Results

TEMPO:$TBAPF_6$ (mM)	ρ (g/mL)	μ (cP)	ν (cm^2/s)
10:100	0.780	0.390	0.00500
10:200	0.810	0.440	0.00543
100:500	0.843	0.575	0.00682
200:500	0.847	0.567	0.00669
250:1250	0.941	0.917	0.00974

Table 1. The density (ρ) and dynamic viscosity (μ) was recorded for each of the five concentrations. The kinematic viscosity (ν) was then calculated by dividing μ by ρ

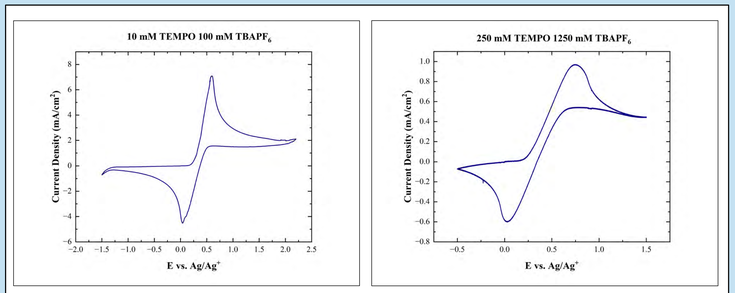

Fig 5. Cyclic voltammograms ran at 0 RPM for the lowest (left) and highest (right) concentrations

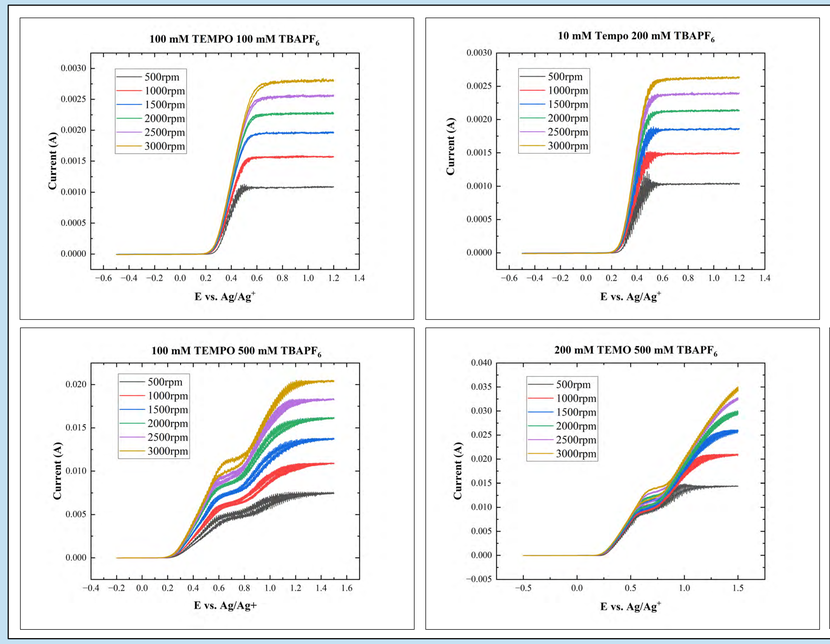

Fig 6. Voltammograms were taken at rotation speeds of 500, 1000, 1500, 2000, 2500, and 3000 RPM for each of the five concentrations. The potential applied on the top two ranged from -0.5V to 1.2V while it ranged from -0.5V to 1.5V for the three on the bottom. Note that the bottom three have two plateau each but the ones of interest take place around 0.6-0.8V.

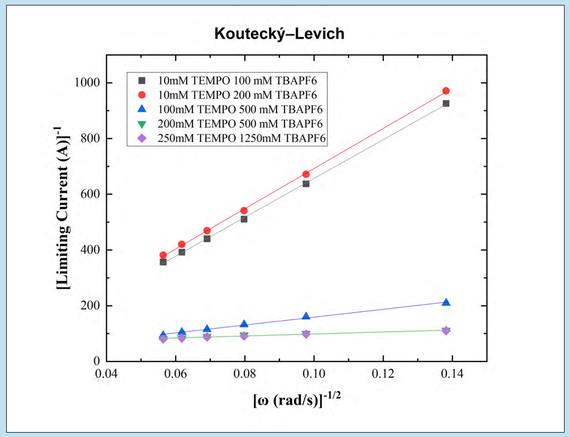

Fig 7. The Koutecký-Levich graph was created by plotting the inverse square root of the rotation speed by the inverse of the limiting current, which can be found from the peaks in Fig 5. Note that the purple and green lines overlap each other due to having very similar equations.

TEMPO:$TBAPF_6$ (mM)	D (cm^2/s)	K^0 (cm/s)
10:100	0.00001870	0.1310
10:200	0.00001910	0.1880
100:500	0.00000330	0.0300
200:500	0.00000041	0.0042
250:1250	0.00000033	0.0034

Table 2. The diffusion coefficient (D) was calculated using the Levich equation and the heterogenous electron transfer rate constant was calculated from the Butler-Volmer equation.

Discussion

- Take average of all values in the plateau to get limiting current
- Plug all known values into the Levich equation to calculate diffusion coefficient (D)[4]

$$I_L = 0.62nFAD^{2/3}\omega^{1/2}\nu^{-1/6}C$$

- Where I_L is the limiting current, n is the number of electrons transferred, F is Faraday's constant, A is the area of the working electrode surface, ω is the rotation rate, ν is the kinematic viscosity, and C is the concentration of analyte
- Simplification of Butler-Volmer's equation can be derived to calculate heterogenous electron transfer rate constant[5]

$$I_k = nFAk^0C$$

- Where I_k is the kinetic current, which is found by taking the inverse of the intercept from the Koutecký-Levich graph

Conclusion

- Lower concentration of TEMPO produced expected sigmoidal curve
- Higher concentrations had two plateaus instead of one
- 10 mM TEMPO and 200 mM $TBAPF_6$ appears to be the most effective
- No definitive trend between viscosity and D or K^0
- Higher ratio of $TBAPF_6$ to TEMPO tended to yield a greater D and K^0

Next Steps

- Investigate higher concentrations
  - Smaller electrode surface area
  - Higher RPM
  - Determine the cause of the 2nd plateau on higher concentrations

References

1. Stumme, N., Perera, A. S., Horvath, A., Ruhunage, S., Duffy, D. H., Koltonowski, E. M., Tupper, J., Dzierba, C., McEndaffer, A. D., Teague, C. M., Risko, C., & Shaw, S. K. (2023). Probing redox properties of extreme concentrations relevant for nonaqueous redox-flow batteries. *ACS Applied Energy Materials*, 6(5), 2819–2831. https://doi.org/10.1021/acsaem.2c03712
2. Liu, B., Tang, C. W., Jiang, H., Jia, G., & Zhao, T. (2021). Carboxyl-functionalized tempo Catholyte enabling high-cycling-stability and high-energy-density aqueous organic redox flow batteries. *ACS Sustainable Chemistry & Engineering*, 9(18), 6258–6265. https://doi.org/10.1021/acssuschemeng.0c08946
3. Li, M., Odom, S. A., Pancoast, A. R., Robertson, L. A., Vaid, T. P., Agarwal, G., Doan, H. A., Wang, Y., Suduwella, T. M., Bheemireddy, S. R., Ewoldt, R. H., Assary, R. S., Zhang, L., Sigman, M. S., & Minteer, S. D. (2021). Experimental protocols for studying organic non-aqueous redox flow batteries. *ACS Energy Letters*, 6(11), 3932–3943. https://doi.org/10.1021/acsenergylett.1c01675
4. Nikolic, J., Expósito, E., Iniesta, J., González-Garcia, J., & Montiel, V. (2000). Theoretical concepts and applications of a rotating disk electrode. *Journal of Chemical Education*, 77(9), 1191. https://doi.org/10.1021/ed077p1191
5. Reedijk, J., & Poeppelmeier, K. R. (2023). *Comprehensive inorganic chemistry III*. Elsevier.

Acknowledgements

I would like to give a huge thanks to Professor Shaw and the Shaw Research Group, the Belin-Blank Center, and everyone involved with SSTP for this amazing opportunity.

Investigating the Effects of Mixed Ligands on the Flexibility of Metal-Organic Frameworks

Junhao Wang[1], Akalanka Ekanayake, B.Sc.[2], Thumini Dias, B.Sc.[2], Alexei Tivanski, PhD[2]

[1]Los Gatos High School, [2]University of Iowa, Department of Chemistry

Introduction

- **Metal-organic frameworks** (MOFs) are porous polymers made of metal ions and organic linkers
- **Zeolitic imidazolate frameworks** (ZIFs) are a subclass of switchable MOFs known for its thermal stability, tunability, and flexibility
- **Atomic force microscopy** (AFM) uses probes with sharp tips (~15nm) to generate high resolution images at the atomic scale, as well as collect force vs. Indentation data

Figure 1. Relation of mixed ligands to gate opening effect

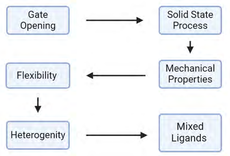

Figure 2. Gate opening effect of ZIF-8 (Tiba et al., 2022)

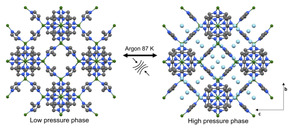

Figure 3. Synthesis of ZIF-90, ZIF-8, and ZIF-8-90

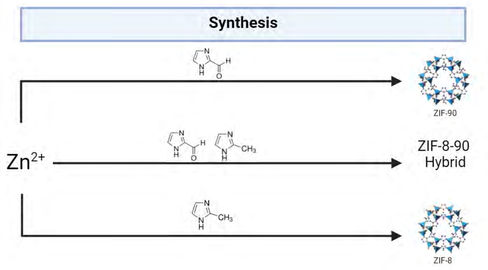

Hypothesis: hybrid ZIFs will have different flexibilities than their parent MOFs

Research Questions

- How does the introduction of defects through a mixed ligand approach affect the flexibility of zeolitic imidazolate frameworks?
- How does the fraction of different ligands in a MOF affect its flexibility?

Methodology

1. **Nonsolvent induced crystallization** synthesis of ZIF-8-90
   - Sodium formate as modulator
2. **Powdered x-ray diffraction** confirmed that synthesized ZIF-8-90 is crystalline
3. **Nuclear magnetic resonance** quantified composition of mixed ligands
4. **AFM** is used to collect images of individual crystals
   - ZIF crystals were drop casted onto a mica substrate
5. **AFM** nanoindentation is then used to collect force vs. indentation plots
   - Size range of nanocrystals studied: 500 nm – 1500 nm
6. **Johnson-Kendall-Roberts** (JKR) contact model is used to analyze data to yield Young's modulus

Figure 4. Laser beam deflection for atomic force microscopes (*Atomic Force Microscopy | Nanoscience Instruments*, n.d.)

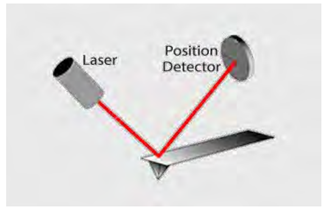

$$F_{JKR} = F + 3\pi W R^* + \sqrt{6\pi W R^* + 9\pi^2 W^2 R^{*2}}$$

- F – loading force
- W – work of adhesion
- R* - relative radius of curvature

Figure 5. JKR fit of force vs. indentation data

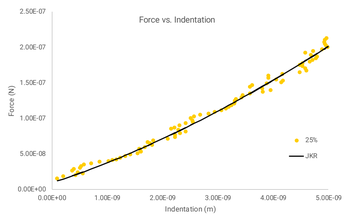

Results

Figure 6. PXRD graphs of synthesized ZIF-8-90

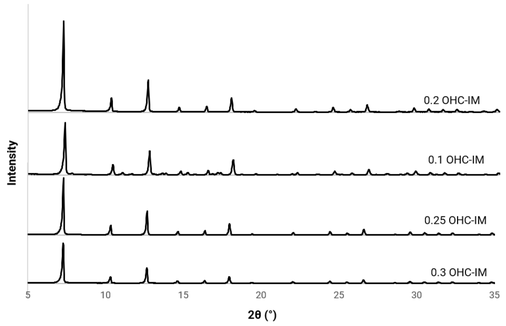

Note: the peaks confirmed the crystallinity of synthesized ZIF-8-90

Figure 7. NMR graph of ZIF-8-90

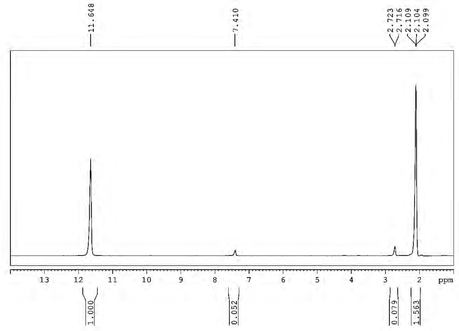

Note: NMR analysis of ZIF-8-90 is used to determine the exact fraction of ligands

Figure 8. AFM 3D Height Image for a representative ZIF-8-90 crystal

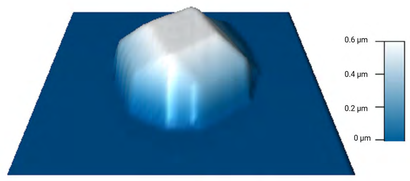

Note: The above crystal exhibits a typical cubic morphology

Figure 9. Plot of Young's Modulus vs. %ZIF-90

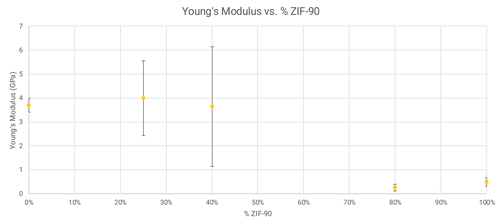

Note: Young's Modulus decreases as composition of ZIF-90 increases

Error bars: ±SD

Data of 0% was taken from Tiba et al. 2019

Conclusions

- The molar fraction of each ligand incorporated into the ZIF-8-90 metal-organic frameworks is different than that used in synthesis
- Linker substitution affects the flexibility of metal-organic frameworks
- An increase of a fraction of the imidazole-2-carboxaldehyde ligand increase the flexibility of metal-organic frameworks

Future Studies

- Force data may be collected on other ZIF compositions (40%, 50%, 60%)
- Gas adsorptions isotherms may be collected to gain a deeper understanding on structural changes
- Examining the flexibility of other hybrid MOFs through AFM (such as ZIF-7-8)
- Using more than two linkers to further increase entropy of MOFs

References

1. *Atomic Force Microscopy | Nanoscience Instruments*. (n.d.). Retrieved July 22, 2024, from https://www.nanoscience.com/techniques/atomic-force-microscopy/
2. Thompson, J. A., Blad, C. R., Brunelli, N. A., Lydon, M. E., Lively, R. P., Jones, C. W., & Nair, S. (2012). Hybrid Zeolitic Imidazolate Frameworks: Controlling Framework Porosity and Functionality by Mixed-Linker Synthesis. *Chemistry of Materials*, *24*(10), 1930–1936.
3. Tiba, A. A., Tivanski, A. V., & MacGillivray, L. R. (2019). Size-Dependent Mechanical Properties of a Metal–Organic Framework: Increase in Flexibility of ZIF-8 by Crystal Downsizing. *Nano Letters*, *19*(9), 6140–6143.
4. Tiba, A. A., Perman, J. A., MacGillivray, L. R., & Tivanski, A. V. (2022). Supramolecular modification of a metal–organic framework increases sorption switching: Insights into reversible structural deformation of ZIF-8. *Journal of Materials Chemistry A*, *10*(39), 21053–21060.

Acknowledgments

I would like to thank the Tivanski group for their help and guidance, as well as Akalanka for his invaluable mentorship.

Hemophilia A and Mental Health Disorders: Exploring Aberrant Purkinje Cells in the Cerebellum

Lucy Wei[1] , Danielle York[2] , Kevin Gubner[2], Janice Staber, MD[2]

[1]Lexington High School, [2]Department of Pediatrics, University of Iowa Stead Family Children's Hospital

INTRODUCTION

- Hemophilia A (HA) is an X-linked bleeding disorder caused by factor VIII deficiency, a vital clotting factor in the coagulation cascade. (Mehta et al., 2023)
- Mental health disorders are overrepresented in people with Hemophilia (Al-Huniti et al., 2020). Comparisons of brain region volumes between mice with HA and wild-type mice (WT) in the Staber lab highlighted the cerebellum as a significant region of interest.
- Purkinje cells are specific to the cerebellar cortex and play an important role in the cerebellar circuits that affect emotion and cognition (Paul et al., 2022). Morphologically aberrant Purkinje cells are associated with neurological disorders such as autism (Tsai et al., 2012).

OBJECTIVES

1. Use statistical analysis to investigate possible subregions of interest in the cerebellum by comparing WT and HA subregion volumes.
2. Examine aberrant Purkinje cells in cerebellar subregions of interest through immunofluorescent staining.

METHODOLOGY

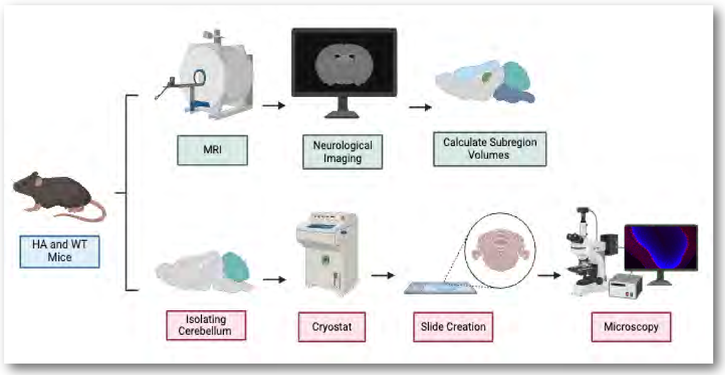

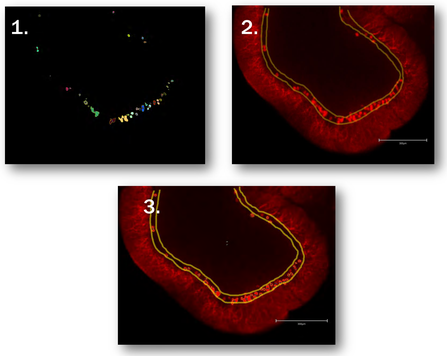

1. Image J was used to count Purkinje cells. Outlines were stored to ROI manager.
2. Arbitrary lines were blindly drawn to encompass the top and bottom of the Purkinje cell layer.
3. Outlines were then imported and those that did not touch the lines were counted as aberrant.

RESULTS

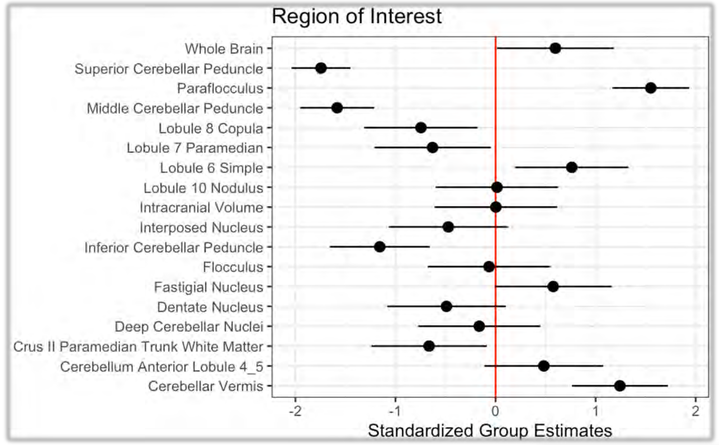

Figure 1. Forest Plot of Cerebellar Subregion Volumes of HA Mice Compared to WT Mice

18 out of the 132 comparisons of cerebellar subregion volumes between WT and HA mice in units of standard deviation. The peduncles, paraflocculus, lobule 8 copula, lobule 7 paramedian, lobule 6 simple, crus II paramedian trunk white matter, and cerebellar vermis in HA mice show significant differences compared to WT mice. The paraflocculus, lobule 6, and cerebellar vermis stand out as subregions to examine due to their size and observable morphology under a microscope.

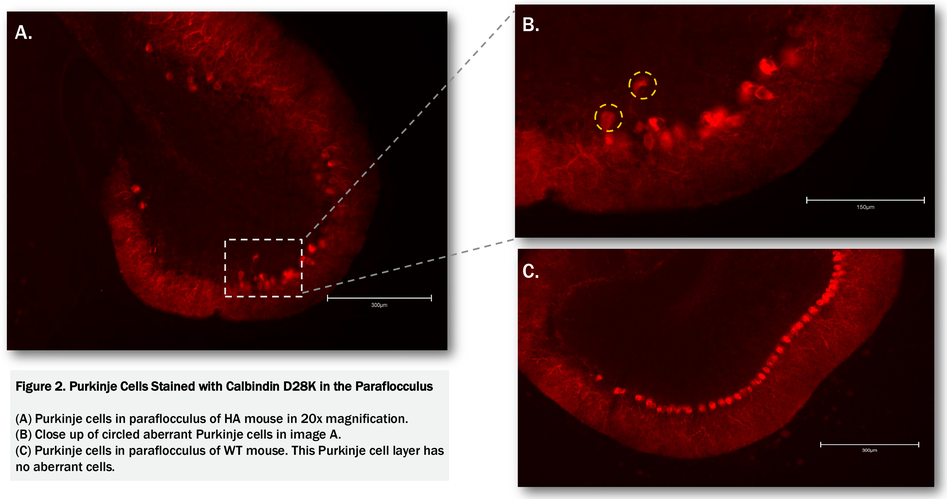

Figure 2. Purkinje Cells Stained with Calbindin D28K in the Paraflocculus

(A) Purkinje cells in paraflocculus of HA mouse in 20x magnification.
(B) Close up of circled aberrant Purkinje cells in image A.
(C) Purkinje cells in paraflocculus of WT mouse. This Purkinje cell layer has no aberrant cells.

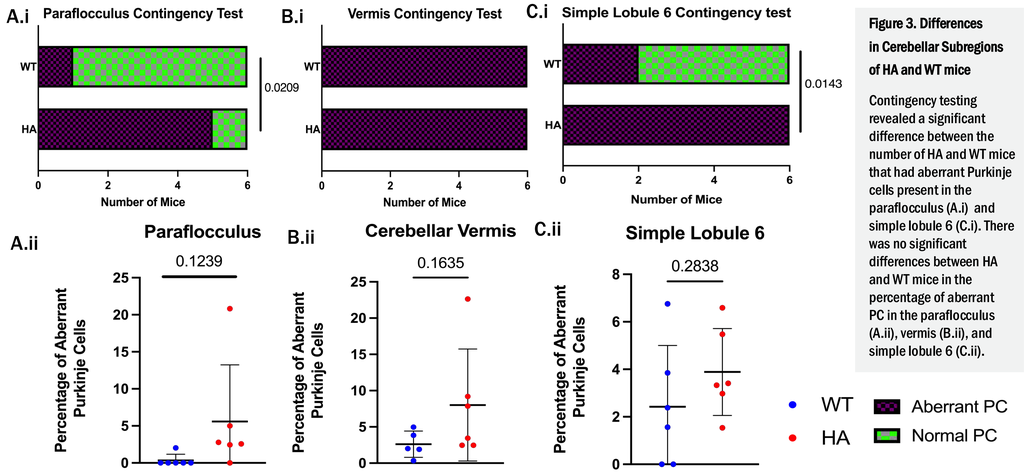

Figure 3. Differences in Cerebellar Subregions of HA and WT mice

Contingency testing revealed a significant difference between the number of HA and WT mice that had aberrant Purkinje cells present in the paraflocculus (A.i) and simple lobule 6 (C.i). There was no significant differences between HA and WT mice in the percentage of aberrant PC in the paraflocculus (A.ii), vermis (B.ii), and simple lobule 6 (C.ii).

CONCLUSION

- The peduncles, paraflocculus, lobule 8 copula, lobule 7 paramedian, lobule 6 simple, crus II paramedian trunk white matter, and vermis are subregions of interest due to their significant volumetric differences in HA mice, along with subregions not shown in Fig. 1 such as the fastigial nucleus and non- cerebellum subregions such as ventricle 4 and the olivary complex.
- Contingency testing shows a significant increase in the number of mice with aberrant Purkinje cells in the paraflocculus and simple lobule 6 of HA mice compared to WT mice.
- No statistically significant relationship between aberrant Purkinje cell percentage and genotype could be determined. However, a trend towards increased percentage of aberrant Purkinje cells in HA mice can be observed.

It should be noted that as the statistical significance increased for subregion volumes of HA mice compared to WT mice the statistical significance of an increased percentage of aberrant Purkinje cells in HA mice increased as well.

FUTURE DIRECTIONS

- A power analysis should be conducted to determine the correct sample size to draw a statistically significant conclusion.
- Due to microscope quality parvalbumin did not show in imaging. Therefore, CD28K marked cells should be validated with another Purkinje cell marker.
- The activity of astrocytes in the cerebellum of HA and WT mice should be compared. Work was done in the staining for astrocytes, however, Bergmann glia, astrocytes specific to the Purkinje cell layer, were not stained, so no data was acquired.

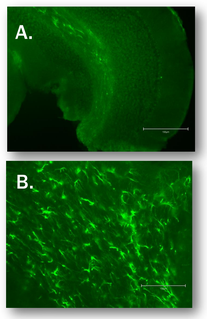

Figure 4. Astrocytes Stained with GFAP

(A) Astrocytes in the paraflocculus of HA mouse in 20x magnification.
(B) Astrocytes in a non-paraflocculus subregion in 20x magnification. The astrocyte stained for is much more abundant in this location.

ACKNOWLEDGEMENTS

Thank you Dr. Staber for giving me the privilege to learn in the Staber lab and truly participate in ongoing, hands-on research. Special thanks to Danielle for her meaningful guidance during the slide creation and microscopy portion of my project, as well as Kevin for not only providing the R studio script for the volume comparisons but also constant encouragement.

Non-microscopy images were created on BioRender whereas graphs were created on R Studio and Prism 10.

REFERENCES

1. Al-Huniti, A., Reyes Hernandez, M., Ten Eyck, P., & Staber, J. M. (2020). Mental health disorders in haemophilia: Systematic literature review and meta-analysis. Haemophilia : the official journal of the World Federation of Hemophilia, 26(3), 431–442. https://doi.org/10.1111/hae.13960
2. Mehta, P., & Reddivari, A. (n.d.). (2023). Hemophilia. StatPearls. https://www.ncbi.nlm.nih.gov/books/NBK551607/
3. Paul, M. S. (2022). *Histology, purkinje cells.* StatPearls. https://www.ncbi.nlm.nih.gov/books/NBK545154/#:~:text=As%20an%20important%20part%20of,such%20as%20cognition%20and%20emotion.
4. Tsai, P. T., Hull, C., Chu, Y., Greene-Colozzi, E., Sadowski, A. R., Leech, J. M., Steinberg, J., Crawley, J. N., Regehr, W. G., & Sahin, M. (2012, August 30). *Autistic-like behaviour and cerebellar dysfunction in Purkinje cell TSC1 mutant mice.* Nature. https://www.ncbi.nlm.nih.gov/pmc/articles/PMC3615424/

The role of Protein Phosphatase 2A (PP2A) in neurological diseases

Looking at the effect of PPP2R5D knock out on activity level and cognition function in mouse model to investigate if E198K mutation is a loss of function mutation

Yuhan Wu, Chunling Chen, Chian Ju Jong, Stefan Strack

Carver College of Medicine

Introduction

PP2A is a Ser/Thr phosphotase that dephosphorylates proteins and controls cell growth. It is made up by 3 subunits - a scaffolding subunit A, a regulatory subunit B, and a catalytic subunit C, forming a heterotrimeric holoenzyme as shown in Figure 1.

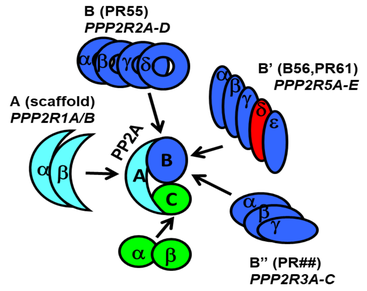

Figure 1. PP2A enzyme structure

There are three gene families encoding the B subunit - *PPP2R2, PPP2R5, PPP2R3*. There are more isoforms within each gene family. The substrate-specificity of the holoenzyme depends on the diverse structures formed by various combinations of subunits (Sandal, 2021). They play significant roles in the process of neuronal development. More specifically, *de novo* mutations of *PPP2R5D* gene encoding B'δ subunit can result in a disruption in PP2A's function of substrate recognition and dephosphorylation (Biswas, 2020).

E198K is a highly pathogenic mutation. Hypophosphorylation of PKA substrates, hyperactivity and cognitive deficits are observed in E198K knock-in mice models. Clinically, it is found to cause neurodevelopmental diseases (Jordan's syndrome) with clinical signs like global neurodevelopmental delay, intellectual disability, autism spectrum disorder, hypotonia, Parkinsonism, etc.

Next, to find out whether E198K mutation is a loss of function mutation, we created PPP2R5D KO (loss of function) mouse models to investigate if the activity level or cognitive function are different than E198K knock-in mice.

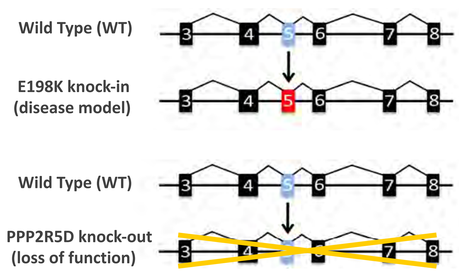

Methods

There is normal amount of PPP2R5D protein expression in E198K mice compared to WT.

E198K mice

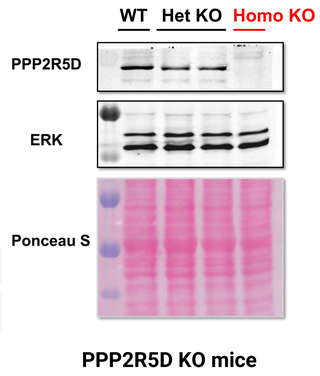

PPP2R5D KO mice

Figure 2. Western Blots show no PPP2R5D in homozygous KO mice.

Results

RotaRod

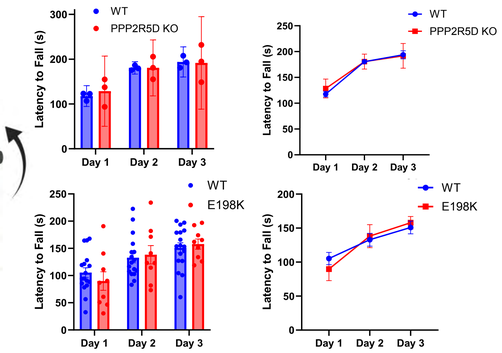

Figure 3. In RotaRod, neither PPP2R5D KO mice or E198K mice showed a significant difference in motor abilities. This might be due to a difficulty of displaying Parkinsonism in mice models.

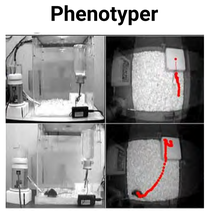

Phenotyper

Figure 4. In Phenotyper, distance traveled (DT) and mobility are recorded. No significant difference is found between total distance traveled and total mobility between wild type mice and PPP2R5D KO mice, but there is a significant difference between wild type and E198K mice.

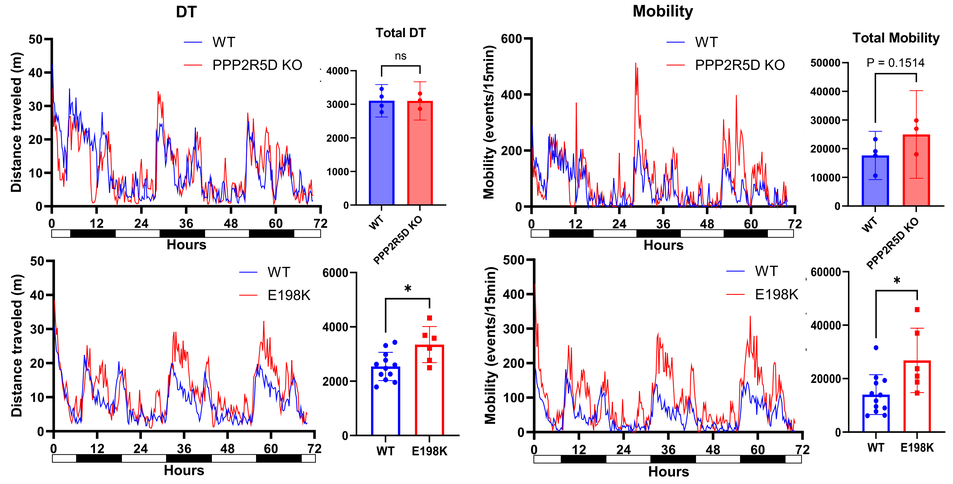

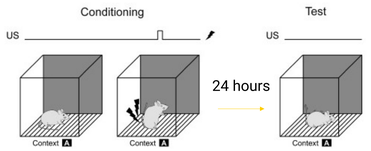

Contextual Fear Conditioning

Figure 5. In contextual fear conditioning, no significant difference is observed between the PPP2R5D KO mice and the WT, but E198K mutation mice show significant cognitive deficit, reflecting on their decreased ability of recognizing the environment where they received an electric shock 24 hours ago.

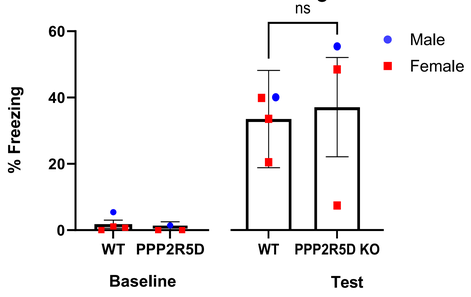

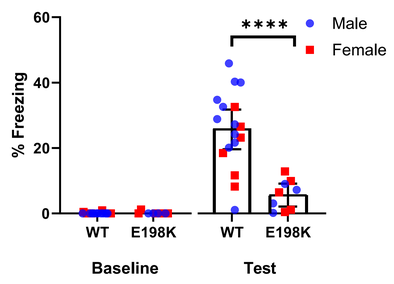

Conclusions & Discussion

1. E198K demonstrates an expression of PPP2R5D similar to WT mice in Western Blot, but the fact that homozygous E198K mutation is embryonic lethal while homozygous KO is not suggests that E198K might not simply be a loss of function mutation.

2. Further behavioral experiments support this hypothesis. E198K mice show alternative phenotypes compared to loss of function model (PPP2R5D KO). E198K mice show hyperactivity and cognitive deficits compared to WT mice, while PPP2R5D KO mice remain normal. Thus, **E198K might be a toxic change of function mutation.**

With the same heterozygous missense mutation as Jordan's Syndrome patients, E198K is a faithful mouse model for studying the disease.

It mirrors clinical symptoms in terms of dysmorphism and cognitive functions, but it still has shortcomings on its reflection of motor disabilities like Parkinsonism.

Further research may focus on **understanding motor deficits displayed by Jordan's Syndrome animal models or patients**. Wire hang test is useful in measuring hypotonia in mice.

Since E198K is likely not a loss of function mutation, future research may aim to **find out the mechanism and pathology of E198K mutation in B' δ subunit of PP2A**.

However, as a phosphatase, it has a large variety of substrates and is involved in many critical cellular pathways. It can be challenging to identify the specific substrates that this mutation affects.

Hypophosphorylation of PKA substrates (some overlaps with PP2A substrates) are found in mice brain with E198K mutation, further suggesting a toxic change of function. Accordingly, **drug development may focus on enhancing phosphorylation of these substrates**.

Acknowledgments

We would like to thank the many people and the core facilities for their help investigating Jordan's Syndrome: Marisol Lauffer and Shane Heiney of Neural Circuit and Behavioral Core, William Paradee of Genome Editing Core.

Fundings

1. PPP2R5D support by State of California/JGA (#A19-3376-S004)
2. PPP2R5D support by State of California/JGA
3. PPP2R5D support by Simons Foundation Autism Research Initiative (#877875)

References

Biswas, D., Cary, W., & Nolta, J. A. (2020). PPP2R5D-related intellectual disability and neurodevelopmental delay: a review of the current understanding of the genetics and biochemical basis of the disorder. *International Journal of Molecular Sciences*, *21*(4), 1286. https://doi.org/10.3390/ijms21041286

Panicker, N., Coutman, M., Lawlor-O'Neill, C., Kahl, R. G. S., Roselli, S., & Verrills, N. M. (2020). *Ppp2r2a* knockout mice reveal that protein phosphatase 2A regulatory subunit, PP2A-B55α, Is an essential regulator of neuronal and epidermal embryonic development. *Frontiers In Cell and Developmental Biology*, *8*, 358. https://doi.org/10.3389/fcell.2020.00358

Sandal, P., Jong, C. J., Merrill, R. A., Song, J., & Strack, S. (2021). Protein phosphatase 2A - structure, function and role in neurodevelopmental disorders. *Journal of Cell Science*, *134*(13), jcs248187. https://doi.org/10.1242/jcs.248187

Wlodarchak, N., & Xing, Y. (2016). PP2A as a master regulator of the cell cycle. *Critical Reviews in Biochemistry and Molecular Biology*, *51*(3), 162–184. https://doi.org/10.3109/10409238.2016.1143913

Department of Neuroscience& Pharmacology, University of Iowa, Carver College of Medicine, Iowa City, IA

A Comprehensive Review of Large Language Models in Hydrology and Environmental Science

Shirley Xiong[1], Omer Mermer[2], PhD, Yusuf Sermet[2], PhD, Ibrahim Demir[2,3,4], PhD

[1]Ward Melville High School, [2]University of Iowa, Department of Hydroinformatics, IIHR—Hydroscience and Engineering, University of Iowa, Iowa City, Iowa, USA, [3]Civil and Environmental Engineering, University of Iowa, Iowa City, Iowa, USA, [4]Electrical and Computer Engineering, University of Iowa, Iowa City, Iowa, USA

Belin-Blank Center, College of Education, The University of Iowa

UIHILAB

Introduction

- Since the early 2000s, the technological era has impacted nearly every field of research.
- Hydrology, the study of the water cycle and its related processes, has been impacted greatly as well (Yeşilköy et al., 2024).
- Large Language Models (LLMs) are artificial intelligence that utilize deep learning techniques to perform tasks such as text recognition and generation (Erazo et al., 2024).
- ChatGPT is one example of a well-known LLM.
- In the domain of Hydrology, LLMs are used in rainfall-runoff modeling (Wu et al., 2022), data augmentation, and climate forecasting (Kadiyala et al., 2024).
- **This research focuses on the application of LLMs in the fields of Hydrology and Environmental Science, as well as the potential of LLMs to aid research in these fields.**

Gemini ChatGPT

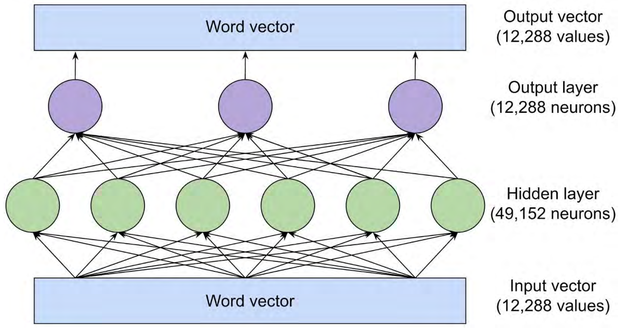

Methods

- The analysis of the usage of LLMs was conducted through a literature review.
- Articles related to LLMs published between 2018 and 2024 were selected by use of a Google Scholar API.
- After a manual review, 144 articles related to LLMs were selected to analyze. Selected articles both involved LLMs and belonged to the spheres of Environmental Sciences or Hydrology.
- Metadata relating to publication date, author affiliation, and publication type were collected through SerpAPI.
- All code was written in Python and the data mining utilized Python Requests and Pandas.
- Graphs of publication year, country affiliation, and publication type analyses were produced through Matplotlib and HoloViews.

IOWA IIHR—Hydroscience and Engineering

Results

Figure 1: Top 10 Publishing Countries

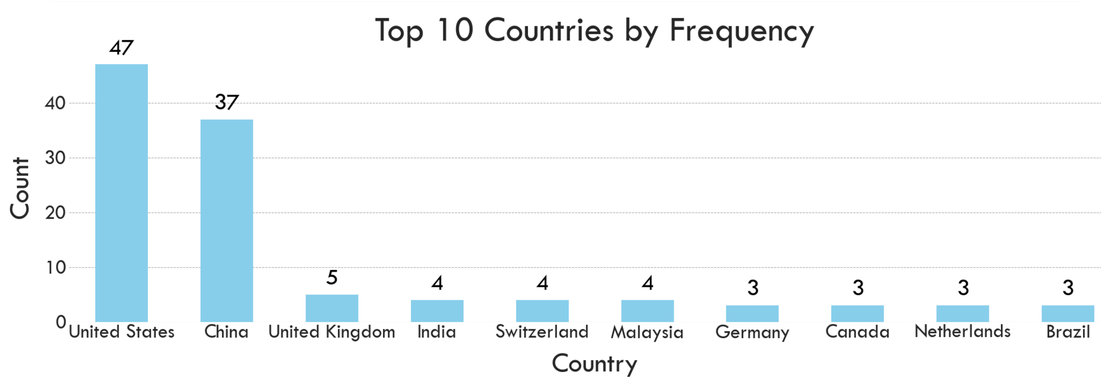

Figure 2: Publications by Year

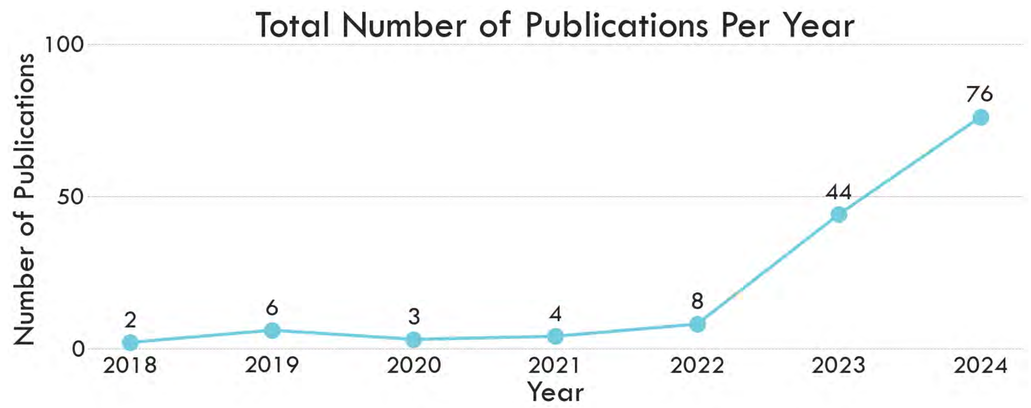

Figure 3: Publications by Type

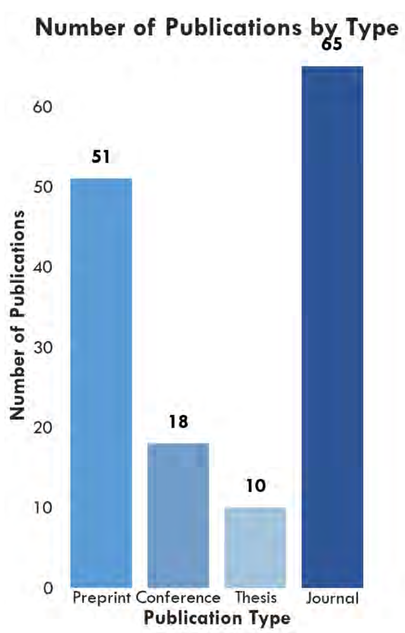

Figure 4: Chord Diagram of Country Affiliations

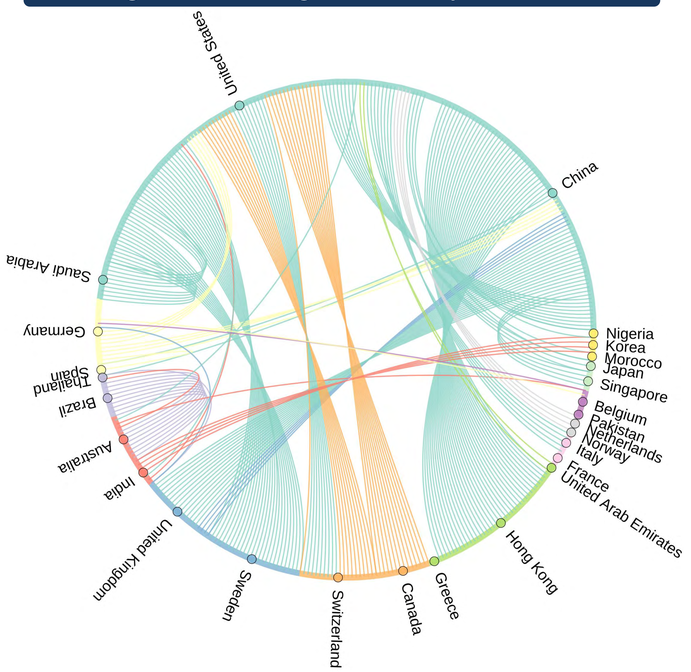

Discussion

- Fig. 1 shows the country affiliations of the first authors of the papers. The top country affiliated is the United States with 47 papers, and the second is China with 37 papers.
- Depicted in Fig. 2 is a large increase in the number of papers related to LLMs published between 2018 and 2024. The slight decrease in papers published between 2019 and 2020 is due to the impact of Covid.
- This demonstrates the rising popularity of LLM as a tool for research in Hydrology and Environmental Science, particularly recently.
- Additionally, in Fig. 3, of all papers found, 65 were published in journals, 51 were preprints, and 18 were from conferences.
- Most of these preprints were received in 2024, further confirming the increasing trend in usage of LLMs.
- Fig. 4 shows the crossovers between countries. A large majority of papers were published in collaboration between China and Hong Kong or China and the UK.
- These results provide future direction and context for researchers hoping to apply LLMs to Hydrology.

Future Studies

- Currently, we are in the process of conducting further analysis on the ethics, scalability, and costs of the LLMs used in the research articles.
- We will analyze the impact factor and citation scores of the articles, as well as the publishing journals.
- Additionally, all of the articles analyzed have been in English. In the future, adding articles from all around the world may create a more holistic review of the trends of LLMs.

Acknowledgements

I would like to thank the UIHI Lab and Dr. Demir for allowing me to participate and work on this project. Additionally, I would like to thank SSTP for this valuable experience, and the Belin-Blank Center and the University of Iowa for organizing this summer research program. Finally, I would like to thank Dr. Sermet and Dr. Mermer for their help and guidance throughout the project.

References

Erazo Ramirez, C., Song, K., & Demir, I. (2024). Technological trends in the field of hydrology and environmental sciences: A bibliometric analysis. *EarthArXiv*. https://doi.org/10.31223/x5dh56

Kadiyala, L., & Mermer, O., & Samuel, D., & Sermet, Y., & Demir, I. (2024). A comprehensive evaluation of Multimodal Large Language Models in hydrological applications. *EarthArXiv*. https://doi.org/10.31223/X5TQ37

Wu, X., Zhang, Q., Wen, F., & Qi, Y. (2022). A water quality prediction model based on Multi-Task Deep Learning: A case study of the Yellow River, China. *Water*, 14(21), 3408. https://doi.org/10.3390/w14213408

Yeşilköy, S., Baydaroğlu, Ö., Singh, N., Sermet, Y., & Demir, I. (2024). A contemporary systematic review of Cyberinfrastructure Systems and applications for flood and drought data analytics and communication. *EarthArXiv*. https://doi.org/10.31223/x5937w

Detecting and segmenting excess metal on sand casted parts using deep learning

Katherine Yoseloff [1], Martell Bell [2], Rachel Vitali [3]
[1-3]Department of Mechanical Engineering University of Iowa

Introduction

- Sand casting is a metal casting technique in which liquid metal is poured into molds made of sand to produce parts

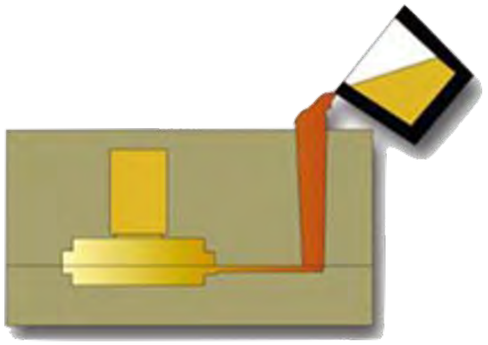

Figure 1 Liquid metal being poured into sand casting mold

Figure 2 Diagram of sand casted part

- Currently, sand casted parts are made manually, which is:
  - Time consuming, leading to short production runs (Peres et al., 2020) (Bosman et al., 2019)
  - Costly for companies (Peres et al., 2020) (Bosman et al., 2019)
  - Dangerous and low paying for employees

  52.5% of jobs in manufacturing will be unfilled by 2030 (Wellener et al., 2023)
- The purpose of this study is to use deep learning to detect the sprues and risers on sand casted parts, in the hopes of one day being able to automate their removal

Methods

1. Take pictures of sand casted pieces, rotating the piece 20 degrees between each picture. Repeat this process twice – once with the part facing up and once with the part facing down
2. Scan sand casted pieces and make digital models of them on Blender, take pictures of Blender models in same positions as before
3. Augment 3D scans with CAD models of the original part
4. Label images for sprues, risers, and the actual part
5. Conduct image quality analysis (Entropy, Structural Similarity (SSIM))
6. Assess model performance (Mean Average Precision (mAP), Precision, Recall)

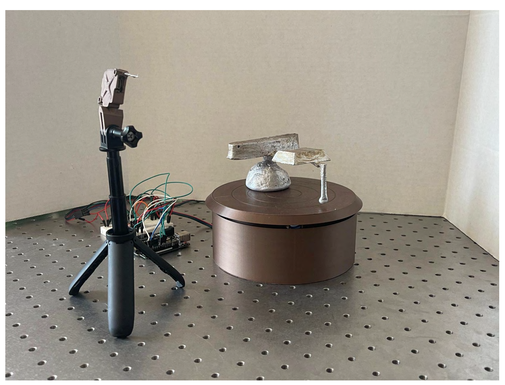

Figure 3 Set up for taking pictures of sand casted parts

Figure 4 3D scan of sand casted part imported on Blender

Results

Dataset	mAP	Precision	Recall	Split	Entropy	SSIM
Augmented -> Augmented	91.20%	94.20%	87.30%	70-20-10	5.926	90.96%
Real -> Real	97.60%	97.10%	94.10%	70-20-10	6.754	76.34%
Synthetic -> Synthetic	TBA	TBA	TBA	70-20-10	5.770	91.63%

Table 1: Deep learning model performance + image quality metrics.

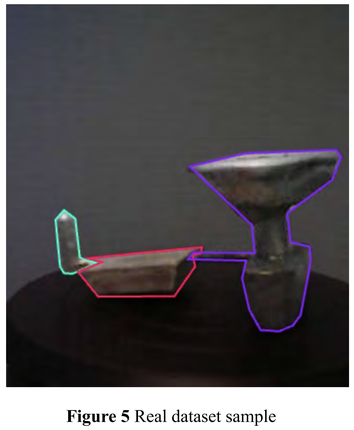

Figure 5 Real dataset sample

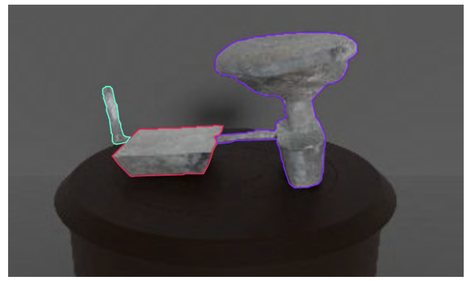

Figure 6 Augmented dataset sample

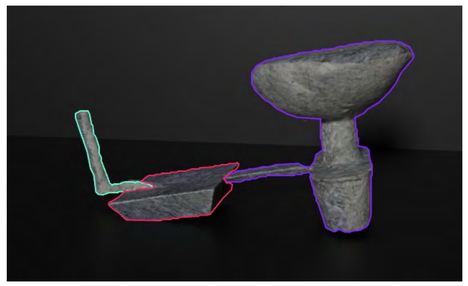

Figure 7 Synthetic dataset sample

Discussion

Conclusions:

- The Real dataset had the highest Precision and Recall at 97.10% and 94.10% respectively.
- The Real dataset had the highest entropy at 6.754.
- The Synthetic dataset had the highest structural similarity (SSIM) at 91.63%, and the Real dataset had the lowest SSIM at 76.34%.
- These findings are consistent with the literature, since Real data contains the most information and hence yields the highest training performance. Additional results are required to confirm.

Future Research:

- In the future, full results for the Synthetic dataset should be found
- A long term goal would be to test out these trained models on real time video footage of the sand casted parts in order to get closer to the ultimate goal of adding this technology into foundries.

Significance

By automating the process of creating sand casted parts, we can:

- Save companies money
- Improve working conditions in foundries

References

Acknowledgements

Thank you to Sam Murphy and others in the Human Instrumentation and Robotics lab for their help and support with my research and learning.

Thank you to the Belin-Blank Center for providing me the opportunity to be here and organizing this program.

Using Language Patterns as “Vital Signs” in Detecting Mental Disorders

[a]Canyon Crest Academy, CA
[b]Department of Psychiatry
[c]Department of Communication Sciences and Disorders
[d]Iowa Neuroscience Institute
University of Iowa

Haeeun (Mina) Yun[a]; Lucas Casten, BA[b]; Jacob J. Michaelson, PhD[b,c,d]

SCAN ME

Introduction

One of the greater setbacks in the field of Psychiatry is the lack of **“vital signals”** (e.g., heart rate, blood draws, oxygen saturation) that allow for quick, efficient diagnosis in **mental disorders** (Stein et al., 2022).

- **Language** is easy to collect & analyze; time and cost efficient
- **Machine learning** easily detects differences in **verbal and phonemic fluency**

We hypothesized that individuals diagnosed with psychiatric disorders will show **distinctions in language patterns** compared to those who are cognitively healthy.

Methods

Participants from SPARK (n>1000) were asked to take the **Controlled Oral Word Association Test (COWAT)** which assessed them on verbal fluency and nonverbal reasoning skills (e.g. sentence repetition, picture narration, vocal rhythm entertainment, rapid automized naming). Participants were also asked to take the **Adult Self-Report (ASR)** which assessed them on their mental well-being. We conducted correlation analyses to understand pairwise associations between COWAT-based language features and ASR scores; features were adjusted for sex, age, educational attainment, and batch.

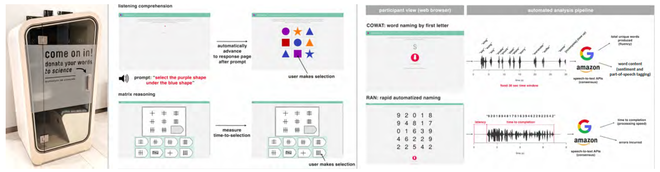

Characteristic	N	Diagnosis		
		Overall, N = 1,094[1]	**ASD**, N = 560[1]	**NASD**, N = 534[1]
sex	1,094			
female		856 (78%)	387 (69%)	469 (88%)
male		238 (22%)	173 (31%)	65 (12%)
age	1,094	38 (32, 44)	34 (28, 41)	41 (36, 46)

[1]n (%); Median (IQR)

[2]Pearson's Chi-squared test; Wilcoxon rank sum test

Table 1. Demographics of SPARK participants included in the analyses

Results

We identified **COWAT-based features**, including derived composite features, that were associated with various ASR **strength**, **syndrome-based**, and **DSM5-oriented** subscales. We found that these ASR-based profiles were most clearly differentiated using a combination of **unique word count**, **atypical vocab**, and other more specific features (e.g., fluency, mean delay time).

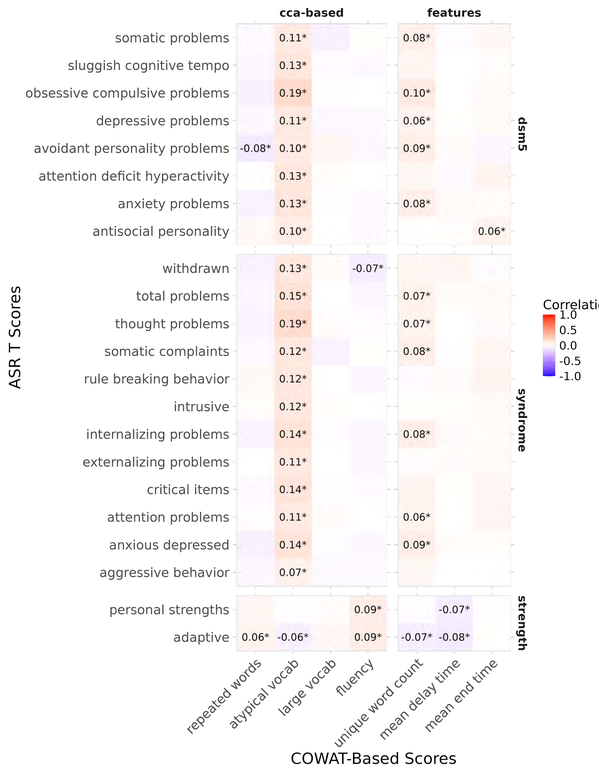

Figure 1. Heat map showing correlations between COWAT-based scores and ASR t scores

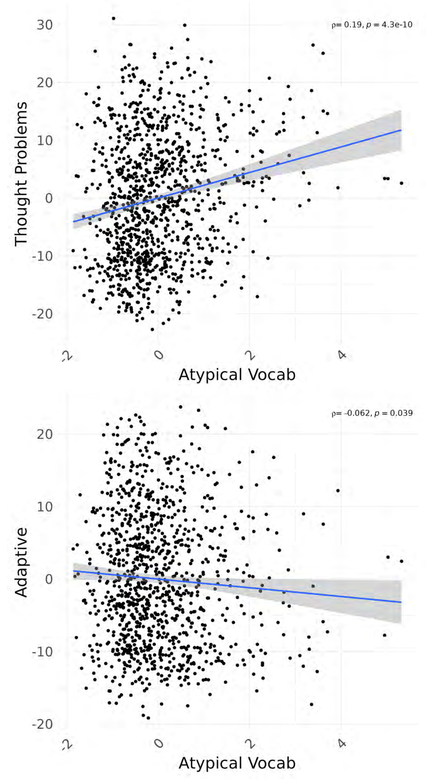

Figure 2. Scatterplots showing relationships between Atypical Vocab and Adaptive versus Thought Problems

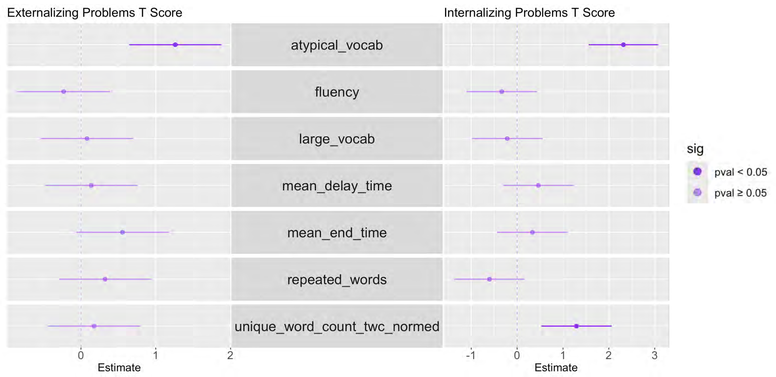

Figure 3. Forest Plot shows the difference in associations of diverse COWAT scores with externalizing and internalizing problems

Conclusion/Future Direction

- Standard psychiatric assessments are time consuming and costly in diagnosing mental disorders (Stein et al., 2022). COWAT takes a minute to complete and may inform psychiatric state in real-time.
- Preliminary characterization suggests that informative COWAT-based language features can be derived and used together to better understand current psychological states.
- Continued development of these language-based features may help us build mental health "vital signs" that can help identify individuals who may be at risk and benefit from intervention.

Acknowledgments

Special thanks to the Michaelson Lab in helping me put this project together. I truly thank the SPARK participants, researchers, and funding for providing valuable data for my research. Thank you to SSTP and the Belin-Blank Center for organizing this summer program.

References

1. Malek-Ahmadi, M., Small, B. J., & Raj, A. (2011). The diagnostic value of controlled oral word association test-fas and category fluency in single-domain amnestic mild cognitive impairment. *Dementia and Geriatric Cognitive Disorders*, *32*(4), 235–240.
2. Rezaii, N., Walker, E., & Wolff, P. (2019). A machine learning approach to predicting psychosis using semantic density and latent content analysis. *Npj Schizophrenia*, *5*(1), 1–12.
3. Stein, D. J., Shoptaw, S. J., Vigo, D. V., Lund, C., Cuijpers, P., Bantjes, J., Sartorius, N., & Maj, M. (2022). Psychiatric diagnosis and treatment in the 21st century: Paradigm shifts versus incremental integration. *World Psychiatry*, *21*(3), 393–414.

SPARK
Simons Powering Autism Research

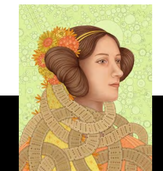

Contact haeeunyun@uiowa.edu michaelson-lab@uiowa.edu

The Effects of CO_2 on Arousal Latency and Seizure Profiles in a Mouse Model of Temporal Lobe Epilepsy

David Zhang[1,2], Rui Li PhD[3,4], and Gordon F Buchanan MD, PhD[3-5]

[1]Johnston High School, Johnston IA, USA, [2]Secondary Student Training Program, [3]Iowa Neuroscience Institute, [4]Department of Neurology, [5]Carver College of Medicine, Iowa City, IA, USA

Introduction

- Epilepsy is characterized by recurring spontaneous seizures.[1]
- Sudden unexpected death in epilepsy (SUDEP) ranks second only to stroke in years of potential life lost among all neurological conditions.[2]
- SUDEP also tends to follow a generalized tonic-clonic seizure which can cause hypercapnia and acidosis.[3]
- CO_2 rises in association with a convulsive seizure, and especially a generalized tonic-clonic seizure.[4]
- Impaired CO_2 arousal is believed to further the risk of SUDEP because an inability to arouse to dangerous CO_2 levels increases the possibility to become acidotic and hypoxic before eventually succumbing to death.[4]
- The serotonergic (5-HT) system also plays a major role in seizure profiles and arousal to CO_2.[5,6]

HYPOTHESIS: CO_2 infusion and the serotonergic (5-HT) system impacts seizure profiles which affects the animal's response to CO_2 and plays a role in the relationship between seizures and arousal ability.

Materials and Methods

Temporal Lobe Epilepsy Model

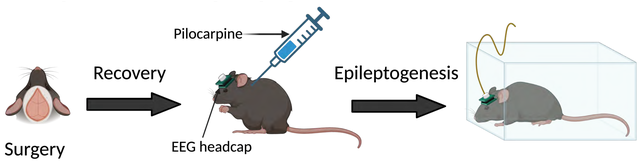

Figure 1. Experimental timeline. *Lmx1b*$^{f/f/p}$ and *Lmx1b*$^{f/f}$ mice were implanted with an EEG/EMG headcap and after 7 days were injected with pilocarpine to induce status epilepticus. After a 45-60 day period the mice were recorded in the closed loop system to collect data.

Closed Loop System

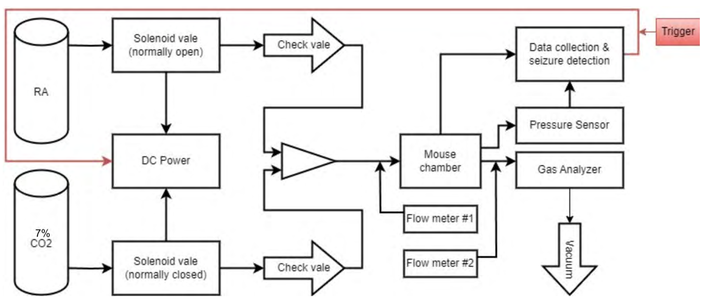

Figure 2. Diagram of the closed loop system utilized for recording data.

Results

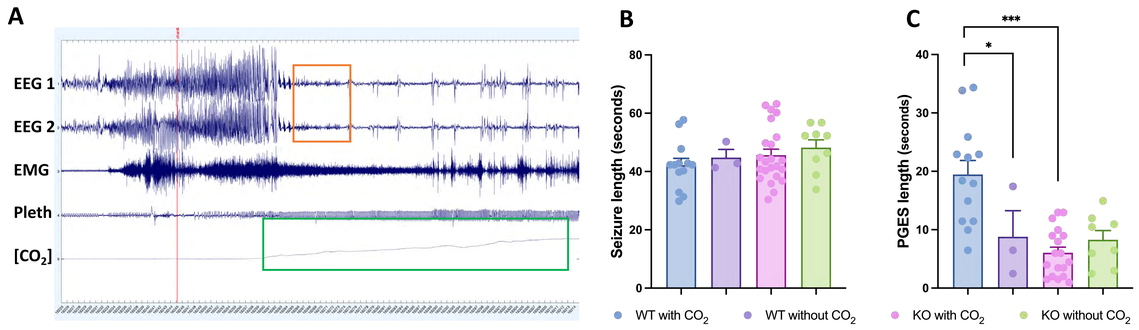

Figure 3. Comparison of seizure profiles with or without CO_2 infusion in the piloTLE model. (A) A generalized tonic-clonic seizure with the red line indicates the opening of the CO_2 gas valve. The orange box indicates *a* period of postictal brain suppression. The green box indicates the rise in CO_2 level which eventually reaches 7%. **(B-C)** The average length for seizures and Postictal Generalized EEG Suppression (PGES). Data was presented as mean ± S.E.M. and was analyzed using two-Way ANOVOA. * indicates p <0.05 and *** indicates p <0.001.

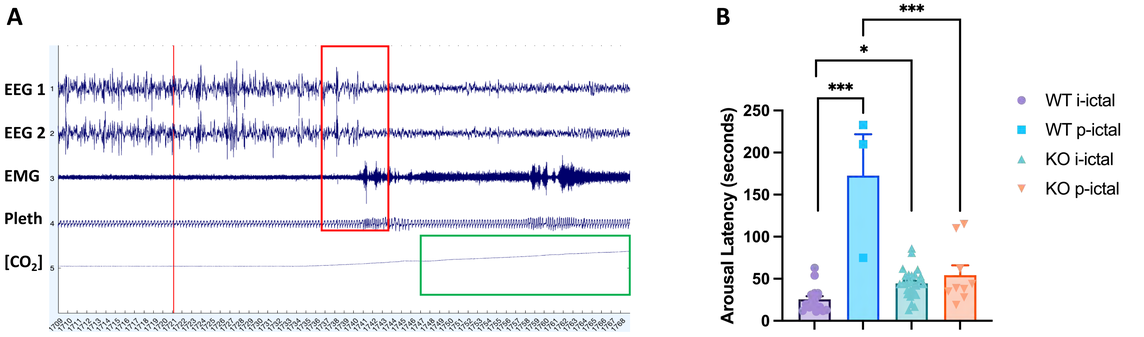

Figure 4. Comparison of CO_2-induced arousal latencies in the piloTLE model. (A) An interictal event with the CO_2 gas valve opening. The red box indicates that the animal arouses at this point. The green box indicates the rise in CO_2 level which eventually reaches 7%. **(B)** The length it took for the animal to arouse to CO_2. Data was presented as mean ± S.E.M. and was analyzed using two-way ANOVA. * indicates p < 0.05 and *** indicates p < 0.001.

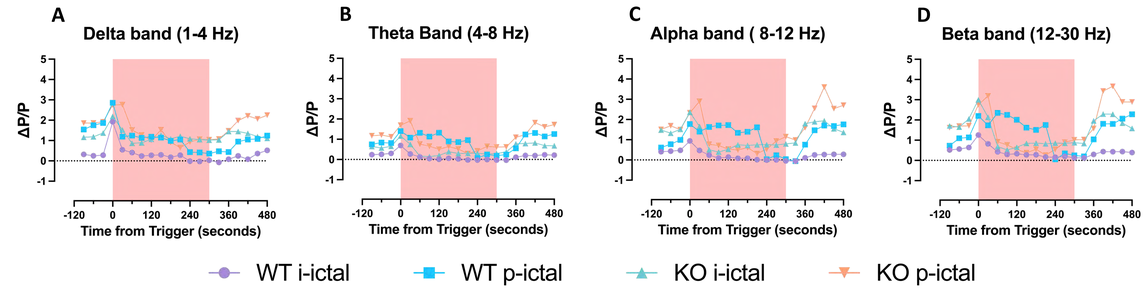

Figure 5. EEG frequency decomposition after CO_2 infusion in the piloTLE model. The graphs **(A-D)** are averages of all trial data for each EEG band. The red filled in space represents the time the CO_2 valve was open. Data was analyzed using three-way ANOVA. In all EEG frequency bands, genotype, event timing, and the interaction between the two contributed significantly to the variance in the data.

Summary

- The seizure length was unaffected by genotype or CO_2 levels, while WT mice with CO_2 influx had the highest PGES length.
- The CO_2-induced arousal latency was higher in KO mice compared to that in WT mice during interictal period.
- The CO_2-induced arousal latency increased significantly in WT mice after a seizure compared to WT mice in the interictal period and KO mice in the postictal period.
- The EEG frequency of the mice across all EEG bands of the brain showed less activity in interictal than postictal phases for both WT and KO mice.

Future Directions

- Increase the sample size of both WT and KO mice to support assertions on arousal latencies and seizure profiles.
- Investigate further the relationship between the serotonin (5-HT) system and CO_2 with PGES and its potential as a biomarker in SUDEP.
- Delve deeper into event classification to provide a concrete timeframe to classify events as interictal or postictal.
- Link the changes in EEG frequencies to certain physiological events.
- Analyze the effects of CO_2 on breathing patterns by utilizing plethysmography.

Acknowledgements

NIH/NINDS R01 NS095842 (to GFB), and the Beth L. Tross Epilepsy Professorship (to GFB).

References

1. Carmant L et al. (2015). Cold Spring Harbor perspectives in medicine.
2. French JA et al. (2014). Epilepsia.
3. Sanju RK et al. (2019) Epilepsia.
4. Buchanan GF. (2019). Trends in neurosciences.
5. Buchanan GF. (2015). Journal of Neurophysiology.
6. Buchanan GF. (2014). The Journal of Physiology.

Harmful Algal Bloom (HAB) Prediction Using Ensemble Machine Learning Models and XAI Technique

Eddie Zhang[1,2] , Omer Mermer[2], Yusuf Sermet[2], İbrahim Demir[2, 3]

[1]The Harker School, [2]IIHR Hydroscience & Engineering, University of Iowa, [3]Electrical and Computer Engineering, University of Iowa

Introduction

- Harmful algal blooms (HABs) present in multiple bodies of water (Saxena, 2017)
- Result of various factors including climate change and agricultural water pollution (Saxena, 2017)
- High amounts of nutrients lead to higher concentrations of algae in water (Patel, 2017)
- Negative Effects on Environments
  - Deplete water of oxygen
  - Contaminate drinking water
  - Threat to biodiversity + animal life in surrounding areas

Algae Bloom Examples (Saxena, 2017; Molinari, 2024)

- Study Area: Lake Erie
  - Multiple harmful algae blooms in last years (Patel, 2017)
  - Important area for fishing and drinking water

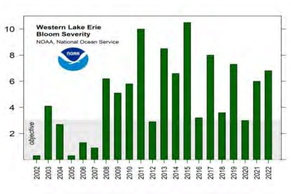

Algal Blooms in Lake Eerie (Patel, 2017; Stumpf, 2024)

Background Information

- Water supply reservoir in South Korea predictions using RF and XGB (Jeong et. al, 2022)
- SHAP values on three different machine learning models to identify relationships between chlorophyll-a concentrations and various water quality factors (Shukla et. al, 2024)
- Use of multiple deep learning and linear models to predict chlorophyll-a values as an index of algae bloom prediction (Busari et. al, 2024)
- Lake Erie algae modeling and prediction using long short term memory networks based off of different features in water quality (Ai et. al, 2024)
- Use of remote sensing images and image processing techniques to detect and forecast algae blooms in Taihu Lake in China (Cao et. al, 2024)

Research Gap

- No **comprehensive and comparative study** of **ensemble** learning and linear machine learning techniques on **algae bloom data**
- Lack of understanding of the effects of using **stronger** and **weaker learners** in **ensemble regressors**
- Lack of **in depth analysis** on most important **features** to a **machine learning model** using **XAI**

Methodology

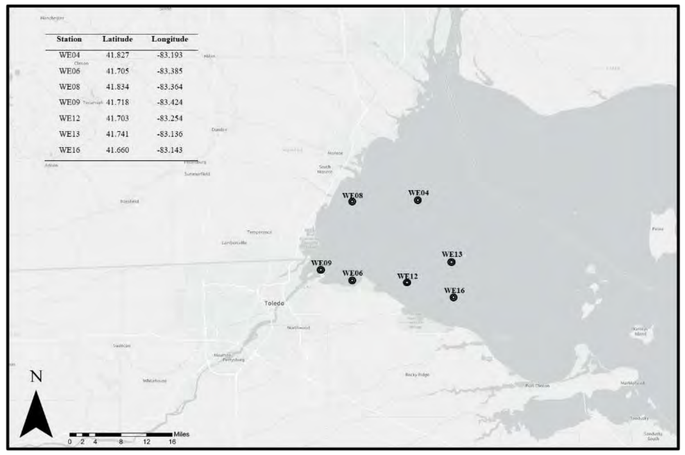

Location Map of Seven Data Collection Stations

Variables	Min	Max	Mean	Median	Standard Deviation
Secchi Depth (m)	0.00	6.50	1.15	0.90	0.917
CTD Temperature (°C)	2.90	29.70	22.02	22.90	0.134
CTD Specific Conductivity (µS/cm)	19.90	583.30	297.77	280.40	2.314
CTD Dissolved Oxygen (mg/L)	4.20	13.04	7.58	7.60	0.039
Turbidity (NTU)	0.68	1148.00	19.77	9.30	55.561
Total Phosphorus (µgP/L)	4.00	2482.24	77.83	48.14	132.919
Total Dissolved Phosphorus (µgP/L)	0.16	273.58	20.42	9.27	28.248
Ammonia (µgN/L)	0.04	2108.70	33.61	12.25	87.502
Nitrate + Nitrite (mgN/L)	0.00	9.45	0.88	0.34	1.341
Particulate Organic Carbon (mg/L)	0.14	219.34	2.53	1.30	10.576
Particulate Organic Nitrogen (mg/L)	0.01	40.93	0.43	0.21	1.895
Total Suspended Solids (mg/L)	0.82	540.80	17.99	10.20	33.228
Chlorophyll-a (µg/L)	0.71	678.40	30.59	16.14	50.701

Characteristics of the Lake Erie Dataset

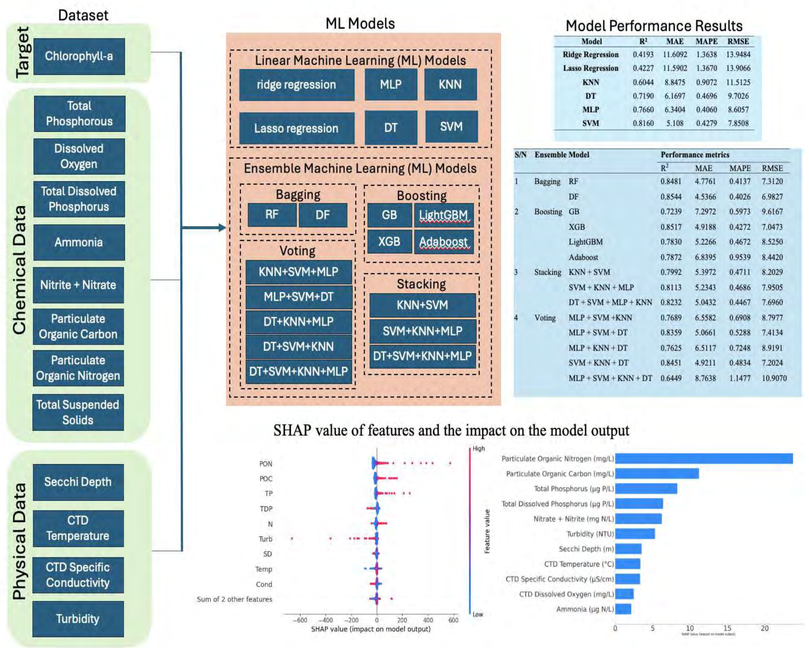

Model Performance Results

Model	R^2	MAE	MAPE	RMSE
Ridge Regression	0.4193	11.6092	1.3638	13.9484
Lasso Regression	0.4227	11.5902	1.3670	13.9066
KNN	0.6044	8.8475	0.9072	11.5125
DT	0.7190	6.1697	0.4696	9.7026
MLP	0.7660	6.3404	0.4060	8.6057
SVM	0.8160	5.108	0.4279	7.8508

S/N	Ensemble Model		Performance metrics			
			R^2	MAE	MAPE	RMSE
1	Bagging	RF	0.8481	4.7761	0.4137	7.3120
		DF	0.8544	4.5366	0.4026	6.9827
2	Boosting	GB	0.7239	7.2972	0.5973	9.6167
		XGB	0.8517	4.9188	0.4272	7.0473
		LightGBM	0.7830	5.2266	0.4672	8.5250
		Adaboost	0.7872	6.8395	0.9539	8.4420
3	Stacking	KNN + SVM	0.7992	5.3972	0.4711	8.2029
		SVM + KNN + MLP	0.8113	5.2343	0.4686	7.9505
		DT + SVM + MLP + KNN	0.8232	5.0432	0.4467	7.6960
4	Voting	MLP + SVM +KNN	0.7689	6.5582	0.6908	8.7977
		MLP + SVM + DT	0.8359	5.0661	0.5288	7.4134
		MLP + KNN + DT	0.7625	6.5117	0.7248	8.9191
		SVM + KNN + DT	0.8451	4.9211	0.4834	7.2024
		MLP + SVM + KNN + DT	0.6449	8.7638	1.1477	10.9070

Overview of Methodology Including ML Models Tested SHAP Diagrams and Model Performances

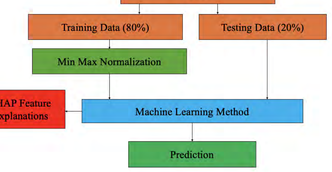

Architecture for Individual Models

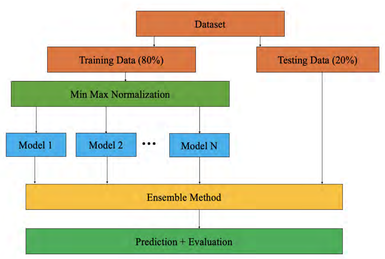

Architecture for Ensembled Models Using the Voting and Stacking Classifiers

Results

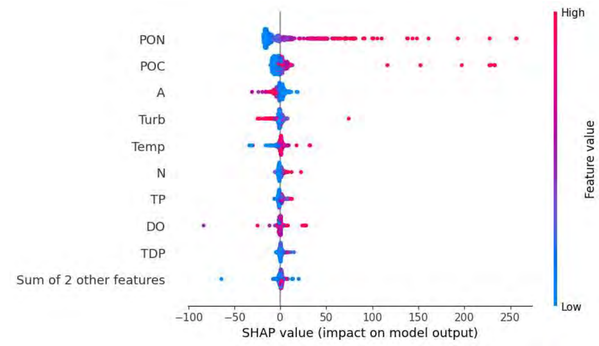

Beeswarm Plot for XGBoost Ensemble Model

ML Model	Input features (mean|SHAP|)				
Lasso	TP (25)	Turb (6.5)	A (2.0)	TDP (1.5)	POC (0.5)
Ridge	TP (35)	Turb (10)	A (2.5)	TDP (2.0)	POC (0.7)
KNN	N (6.0)	TDP (3.5)	DO (2.5)	Temp (2.0)	Cond (1.1)
DT	PON (20.0)	POC (6.0)	A (4.0)	Turb (2.5)	DO (2.0)
MLP	TP (15.0)	Turb (12.2)	A (10.0)	POC (5.3)	PON (2.0)
AdaBoost	PON (14.5)	POC (2.2)	A (1.8)	Temp (0.3)	N (0.1)
LightGBM	PON (17.7)	POC (7.5)	A (2.8)	Turb (2.7)	TP (2.5)
RF	PON (9.5)	POC (6.0)	A (2.5)	Turb (1.8)	Temp (1.5)
SVM	PON (24)	POC (12)	TP (7.5)	TDP (6.0)	N (5.9)
GB	PON (25)	POC (6)	TP (5)	Turb (5)	A (4.5)
XGBoost	PON (18)	POC (7)	A (3)	Turb (2.7)	Temp (2.5)
DF	PON (14)	POC (5)	A (2)	Turb (1.5)	N (1)

SHAP Values for Top 5 Features for Each Model

Model	Training runtime (s)
Lasso	1.0s
Ridge	1.0s
MLP	144.9s
RF	5.2s
LightGBM	7.0s
SVM	12.7s
Adaboost	5.2s
DT	1.0s
KNN	0.5s
DF	561.8s
GB	1.0s
XGBoost	1.0s

Training Time for Each Model

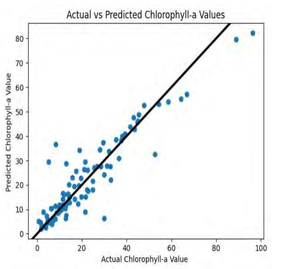

Actual vs Predicted Chlorophyll-a Values

Conclusions

- Most accurate **linear model -> SVM**, achieves **R^2 value** of **0.8160**
- **Ensemble models** more **accurate** than linear models with **DF** and **XGBoost** achieving **R^2** values of **0.851 and 0.854 respectively**
- **Fusion** of **weak learners** using **voting** and **stacking** regressors **improves accuracies**
- **Explainable AI** techniques and **decoding** the **black box** of machine learning models using **SHAP** reveals that the concentrations of **particulate organic carbon** and **particulate organic nitrogen** are **most important** factors in predictions
- Future Works: Developing a real-time monitoring system for algal blooms

Selected References

Ai, H., Zhang, K., Sun, J., & Zhang, H. (2023). Short-term lake erie algal bloom prediction by classification and regression models. *Water Research*, *232*, 119710. https://doi.org/10.1016/j.watres.2023.119710

Busari, I., Sahoo, D., Harmel, R. D., & Haggard, B. E. (2024). Prediction of chlorophyll-a as an index of harmful algal blooms using machine learning models. *Journal of Natural Resources and Agricultural Ecosystems*, *2*(2), 53-61. https://doi.org/10.13031/jnrae.15812

Cao, H., Han, L., & Li, L. (2022). A deep learning method for cyanobacterial harmful algae blooms prediction in taihu lake, china. *Harmful Algae*, *113*, 102189. https://doi.org/10.1016/j.hal.2022.102189

Jeong, B., Chapeta, M. R., Kim, M., Kim, J., Shin, J., & Cha, Y. (2022). Machine learning-based prediction of harmful algal blooms in water supply reservoirs. *Water Quality Research Journal*, *57*(4), 304-318. https://doi.org/10.2166/wqrj.2022.019

Molinari, C. (2024, January 12). *Chilean algae bloom continues to cause salmon mortalities, hitting Blumar with USD 8.5 million loss*. (n.d.). Retrieved July 18, 2024, from https://www.seafoodsource.com/news/premium/aquaculture/chilean-algae-bloom-continues-to-cause-salmon-mortalities-hitting-blumar-with-usd-8-5-million-loss

Patel, J. K., & Parshina-Kottas, Y. (2017, October 3). Miles of Algae Covering Lake Erie. *The New York Times*. https://www.nytimes.com/interactive/2017/10/03/science/earth/lake-erie.html

Saxena, R. (2017, April 29). *Toxic algae on the rise as our oceans warm*. Ars Technica. https://arstechnica.com/science/2017/04/harmful-algal-blooms-occur-more-often-now-that-oceans-are-warming/

Shukla, R. K., Boegman, L., & Kumar, P. (2024). Application of interpretable machine learning and causal discovery to understand chlorophyll-a variation in a large shallow lake. *SSRN*. https://doi.org/10.2139/ssrn.4821781

Stumpf, R. (2022, November 16). *2022 Lake Erie Algal Bloom More Severe than Predicted by Seasonal Forecast*. (2021, November 5). NCCOS Coastal Science Website. https://coastalscience.noaa.gov/news/2022-lake-erie-algal-bloom-more-severe-than-predicted-by-seasonal-forecast/

Acknowledgements

I would like to thank the SSTP program and the Belin Blank Center for giving me this opportunity. I would also like to thank Dr. Demir for mentoring me in his lab and allowing me to gain research experience. Lastly, I would also like to thank Dr. Mermer and Dr. Sermet for their support and mentorship on this project.

Exploring Rgs6's effects on Dopamine Transporter function and its implications in Parkinson's Disease

Larry Zhang[1,2], Jacob Bernholtz[3], Jianqi Yang, PhD[3], Adele Stewart, PhD[3], Rory Fisher, PhD[3]

[1]Belmont High School, Belmont, MA, [2]Secondary Student Training Program, [3]Department of Neuroscience and Pharmacology, Carver College of Medicine, University of Iowa

Introduction

- Dopamine is responsible for reward systems and movement/locomotion
- Parkinson's Disease (PD) results from the loss of dopamine producing neurons in the substantia nigra (SNc) (Luo et al, 2019).
- Mice lacking the RGS6 gene (RGS6-/-) show similar symptoms to human PD patients, and they progressively lose SNc neurons (Luo et al, 2019)
- RGS6 protects SNc neurons, but exactly how is unknown

Dopamine Transporter (DAT) facilitates dopamine transport across the membrane

- RGS6 proteins regulate GPCR's like DAT

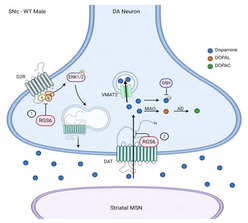

Figure 1: Synapse diagram, showing DAT function clearing synapse DA

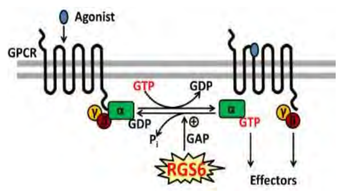

Figure 2: Processes showing RGS6 function for GPCR proteins and DAT function clearing extracellular DA

RGS6 & DAT: Preliminary data from the lab has shown that RGS6 binds to DAT (see below) forming a complex. Likely, RGS6 regulates DAT function.

Hypothesis

We **hypothesize** that RGS6, by negatively regulating DAT, prevents SNc dopamine neuron loss from DAT-dependent DA uptake preventing intracellular accumulation of toxic DA metabolites.

Preliminary Data

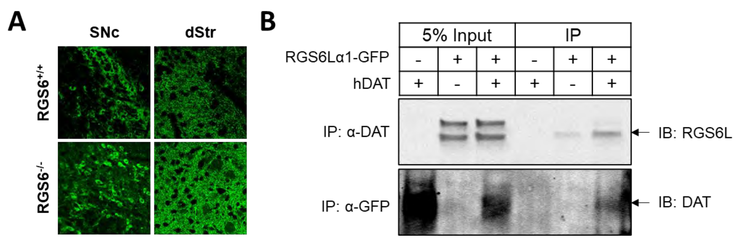

Figure 3: Evidence for DAT regulation by RGS6. (A) Immunostaining for DAT is increased in the SNc and dorsal striatum (dStr) of RGS6 knockout mice. (B) RGS6 and DAT form a co-precipitable complex in transfected HEK293T cells.

Materials and Methods

We compared RGS6's effects on DAT with a fluorescent label uptake assay. Human DAT in culture cells with and without RGS6.

- **ASP+:** Mirrors dopamine
- **GBR-12909:** Specific DAT blocker (measuring effects of other transporters)

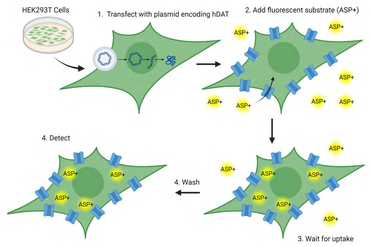

Figure 4: DA uptake protocol with ASP+

Step 1: Counting & Seeding (48 hours before)

- Count cells with a hemocytometer
- Seed ~350,000 cells/well to get 70% confluency for transfection after 24 hours

Step 2: Transfection (24 hours before)

- Transfect cells using lipofectamine with plasmids encoding hDAT and/or RGS6
- To stabilize RGS6 expression, binding partners R7BP and $G\beta_5$ were also introduced

Step 3: Uptake Assay

- Add tagged ASP+ to each well and let incubate for 10 minutes for cells to uptake, measure

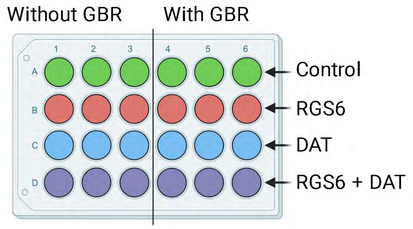

Figure 5: Transfection conditions for each well

Results

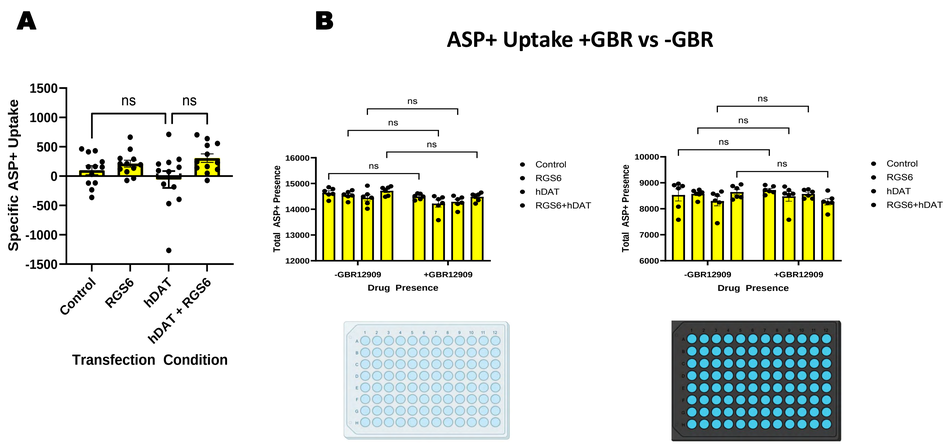

Figure 6: Preliminary ASP+ uptake data from 4 pilot experiments. (A) Uptake by transporters not including DAT (uptake not sensitive to the selective DAT inhibitor GBR). (B) Comparing raw ASP+ uptake values for each transfection condition, both with and without GBR.

Discussion

Pilot experiments yielded very low specific ASP+ uptake regardless of transfection condition. The ASP+ uptake assay requires further optimization to ensure good signal/noise (fluorescence readings with and without GBR blocker).

Future Direction

1. Switch to using radiolabeled DA for uptake assay (more selective for DAT)

2. Perform Western Blot to confirm hDAT expression after transfection

3. Protocol Modification (ASP+ Efflux)

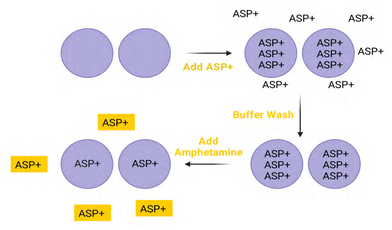

Figure 7: Modified ASP+ Efflux uptake protocol with amphetamine

Adding amphetamine reverses DAT function, removing ASP+ from the cell into the surrounding media. We will compare amphetamine-dependent DA efflux in cells containing or lacking RGS6

4. Use biotinylation to detect DAT surface expression (±RGS6)

Acknowledgements

Thank you to the SSTP program for arranging this opportunity for me and thank you to Dr. Adele Stewart and Dr. Rory Fisher for welcoming me into their research groups and providing me with guidance. Special thanks to Jacob Bernholtz for guiding me with my project, working with me, and teaching me about cell culture and lab techniques.

References

- Bromberg-Martin, E. S., Matsumoto, M., & Hikosaka, O. (2010). Dopamine in motivational control: rewarding, aversive, and alerting. *Neuron*, *68*(5), 815–834. https://doi.org/10.1016/j.neuron.2010.11.022
- Luo, Z., Ahlers-Dannen, K. E., Spicer, M. M., Yang, J., Alberico, S., Stevens, H. E., Narayanan, N. S., & Fisher, R. A. (2019). Age-dependent nigral dopaminergic neurodegeneration and α-synuclein accumulation in RGS6-deficient mice. JCI insight, 5(13), e126769. https://doi.org/10.1172/jci.insight.126769
- Stewart, A., Maity, B., Anderegg, S. P., Allamargot, C., Yang, J., & Fisher, R. A. (2015). Regulator of G protein signaling 6 is a critical mediator of both reward-related behavioral and pathological responses to alcohol. Proceedings of the National Academy of Sciences of the United States of America, 112(7), E786–E795. https://doi.org/10.1073/pnas.1418795112

Dynamic Testing of Energetic Materials Fabricated Through Smart Additive Manufacturing

Steve Zhang, Michael Gearing, Arnold Bangel III MS, Jackson Berlage, Nazanin Tabatabaei, Xuan Song PhD
Department of Industrial and System Engineering, University of Iowa

Introduction

Commonly Used Energetic Materials
- Explosives, Propellants, Protective Composites, etc.
- TNT, RDX, PETN, HMX

Problems
- Unsafe to handle (too sensitive)
- Too generic – might not be optimal for many use cases

Polymer-Bonded Energetic Materials
- Could possibly solve issues of conventional energetic materials
- Composites created using sugar and binders are similar in structure to energetic powders

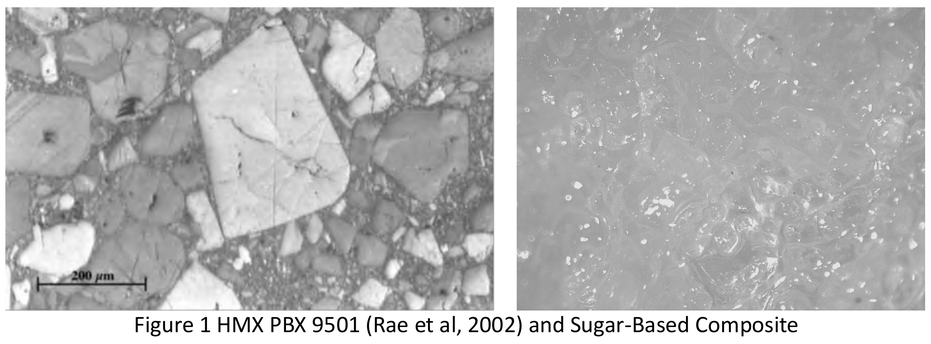

Figure 1 HMX PBX 9501 (Rae et al, 2002) and Sugar-Based Composite

Goals:
- Prove that Pressured-Assisted Binder Jetting Additive Manufacturing can be used to generate voids (empty spaces) in specific places in the composite
- Examine deformation of different void patterns and sugar/binder ratios when under high-speed impact from a Split-Hopkinson Pressure Bar

Methodology

Creating Samples
- Sugar was mixed with Hydroxyl-terminated polybutadiene (HTPB) binder at various ratios
- Samples were made using Pressure-Assisted Binder Jetting Additive Manufacturing (PABJAM)
- This mixture was poured layer by layer into the print bed (Figure 2)
- The press comes down and creates a uniform layer (Figure 3), the excess material is scraped off
- Hydrogen Peroxide is loaded into the piezoelectric printhead and deposited layer by layer into the sample (Figure 4) in a specified pattern (Figure 5)
- Each sample consisted of around 10 layers, each 1 mm
- After printing, samples were cured in a 100° C oven for one day

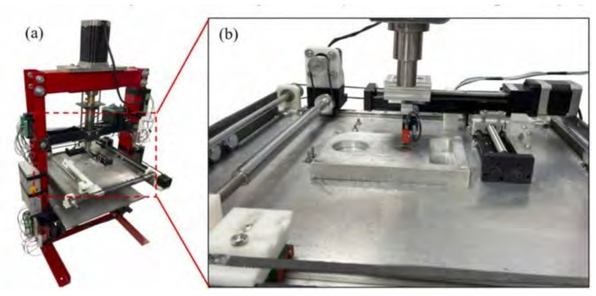

Figure 2 Binder Jet Printer

Figure 3 Press

Figure 4 Printhead

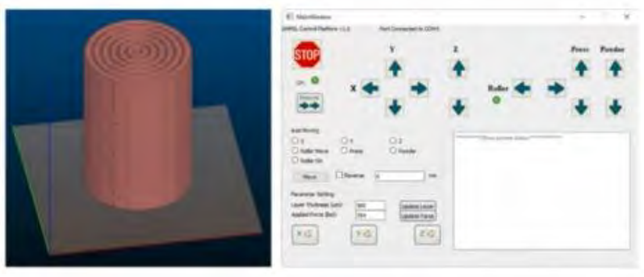

Figure 5 Example of g-code for hydrogen peroxide

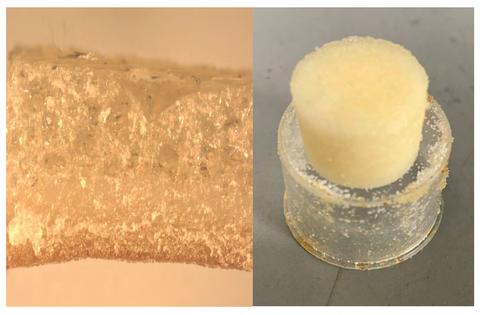

Figure 6 Example of samples

Split-Hopkinson Pressure Bar (SHPB)

Figure 7 Split-Hopkinson Pressure Bar used for impact testing

Testing SHPB: Speed System for Slug
- Teensy 4.1 with IR LEDs and phototransistors
- Two checkpoints, calculate speed using time between detections and distance

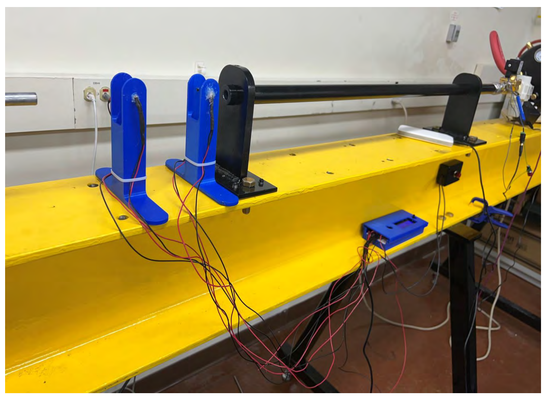

Figure 8 Teensy Speed System

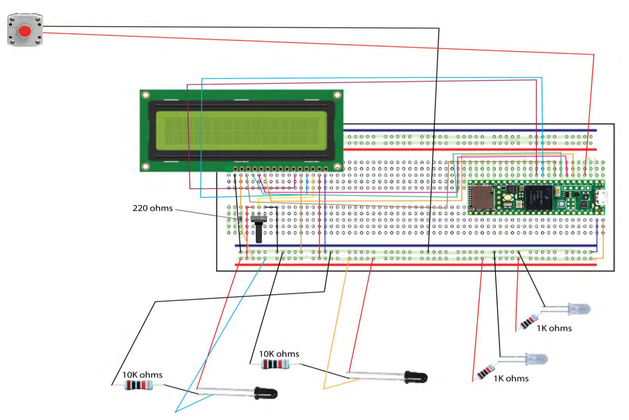

Figure 9 Schematic of Speed System

Estimating Strain Rate

$$\epsilon = \frac{l_f - L}{L} = \frac{\Delta L}{L} \qquad \dot{\epsilon} = \frac{d\epsilon}{dt}$$

Average speed of incident bar over the collision divided by the original length of the sample

High Speed Camera
- Examine deformation of samples during impact at 150,000 frames per second
- Verify speed of incident bar and digital image correlation (DIC)

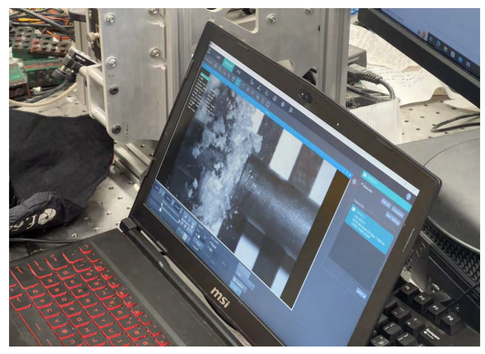

Figure 10 FASTCAM NOVA Highspeed Camera

Results

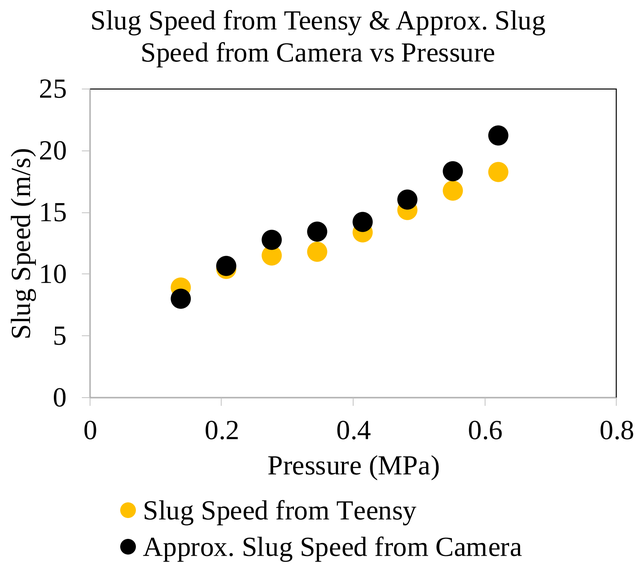

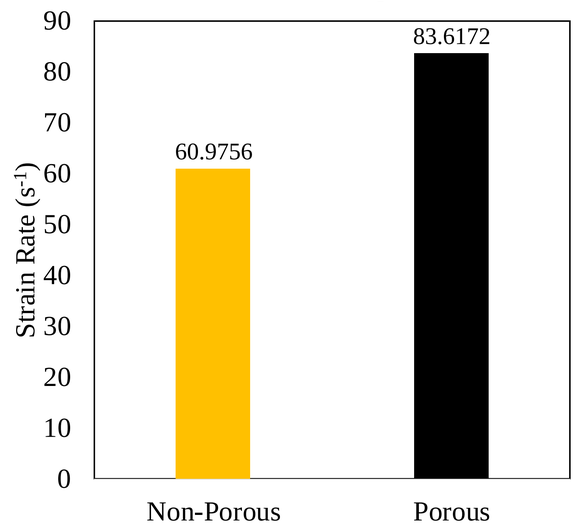

Porous (Mushy) vs Non-Porous (Brittle)
- Non-Porous Sample, 70% fine sugar to 30% HTPB binder (20 psi or 0.14 MPa)

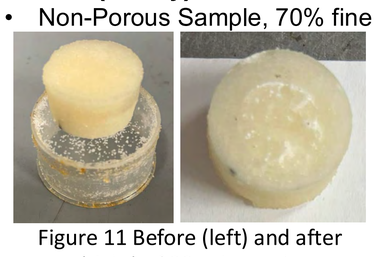

Figure 11 Before (left) and after (right) of 20 psi sample

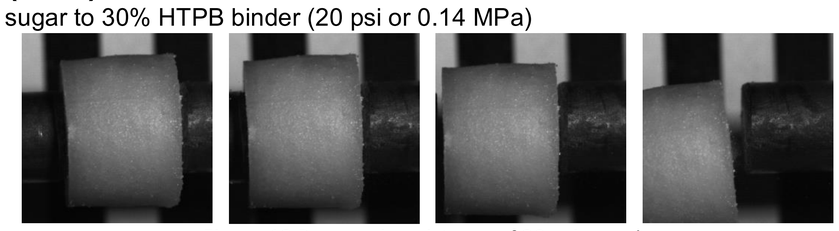

Figure 12 Progressive pictures of 20 psi sample

- Non-Porous Sample, 70% fine sugar to 30% HTPB binder (50 psi or 0.34 MPa)

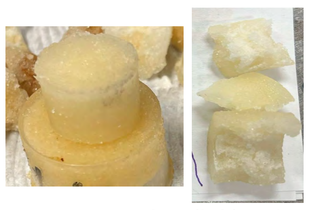

Figure 13 Before (left) and after (right) of 50 psi sample

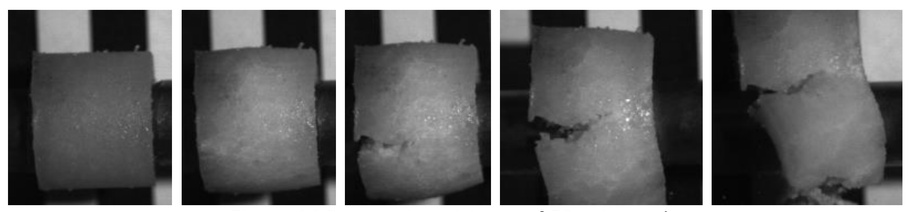

Figure 14 Progressive pictures of 50 psi sample

- Porous Sample, 60% coarse sugar to 40% HTPB binder (30 psi or 0.21 MPa)

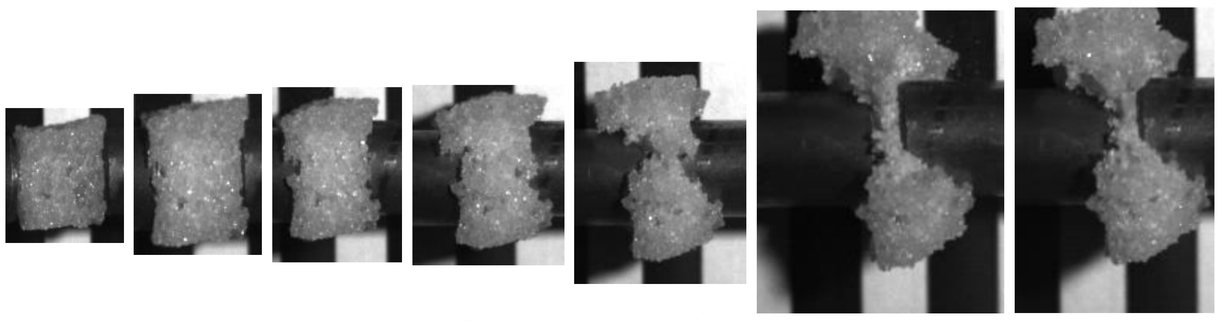

Figure 15 Progressive pictures of 30 psi sample

Conclusion & Future Work

Conclusion
- Successfully developed a method of tailoring voids in sugar-based polymers
- Made a double-checking system for calculating the speed of the slug and incident bar
- Porous samples can deform more and withstand a higher speed impact than non-porous samples
  - Porous samples inherently have more voids than non-porous samples
- Find a relatively correct strain rate value for certain samples
  - Porous samples can withstand a higher strain rate than non-porous samples

Future Work
- Realign and lubricate the bar so that the incident bar doesn't jitter when it hits the sample
- Design and print complex patterns of additive into the samples
  - Possible spatial 3D patterns available (DNA spiral)
- Install strain gauges and an oscilloscope to measure strain rate and deformation of samples

Sources & Acknowledgment

Rae, P. J., Palmer, S. J. P., Goldrein, H. T., Field, J. E., & Lewis, A. L. (2002). Quasi–static studies of the deformation and failure of PBX 9501. *Proceedings of the Royal Society: Mathematical, Physical, and Engineering Sciences, 458(2025).* https://doi.org/10.1098/rspa.2002.0967

Kirby, L., Lawrence, A., Udaykumar, H. S., Sippel, T., & Song, X. (2023). Pressure-assisted binder jet additive manufacturing of solid propellants. *Additive Manufacturing, 77,* 103808. https://doi.org/10.1016/j.addma.2023.103808.

We thank the support from National Science Foundation (Grant No. 2236905) and Air Force Office of Scientific Research (Grant No. FA9550-24-1-0147).